# INFORMATION TO USERS

This manuscript has been reproduced from the microfilm master. UMI films the text directly from the original or copy submitted. Thus, some thesis and dissertation copies are in typewriter face, while others may be from any type of computer printer.

**The quality of this reproduction is dependent upon the quality of the copy submitted.** Broken or indistinct print, colored or poor quality illustrations and photographs, print bleedthrough, substandard margins, and improper alignment can adversely affect reproduction.

In the unlikely event that the author did not send UMI a complete manuscript and there are missing pages, these will be noted. Also, if unauthorized copyright material had to be removed, a note will indicate the deletion.

Oversize materials (e.g., maps, drawings, charts) are reproduced by sectioning the original, beginning at the upper left-hand corner and continuing from left to right in equal sections with small overlaps.

Photographs included in the original manuscript have been reproduced xerographically in this copy. Higher quality 6" x 9" black and white photographic prints are available for any photographs or illustrations appearing in this copy for an additional charge. Contact UMI directly to order.

Bell & Howell Information and Learning
300 North Zeeb Road, Ann Arbor, MI 48106-1346 USA
800-521-0600

# *The Calculation of Accurate Electronic Properties of Biological Radicals*

by

Stacey D. Wetmore

Submitted in partial fulfillment of the requirements
for the degree of Doctor of Philosophy

at

Dalhousie University
Halifax, Nova Scotia
July, 1999

**DALHOUSIE UNIVERSITY**

**FACULTY OF GRADUATE STUDIES**

The undersigned hereby certify that they have read and recommend to the Faculty of Graduate Studies for acceptance a thesis entitled "The Calculation of Accurate Electronic Properties of Biological Radicals"

by Stacey Dawn Wetmore

in partial fulfillment of the requirements for the degree of Doctor of Philosophy.

Dated: July 5, 1999

External Examiner

Research Supervisor

Examining Committee

DALHOUSIE UNIVERSITY

Date: July 16, 1999

Author: Stacey Dawn Wetmore
Title: The Calculation of Accurate Electronic Properties of Biological Radicals
Department or School: Department of Chemistry

Degree: Ph. D. Convocation: October Year: 1999

Permission is herewith granted to Dalhousie University to circulate and to have copied for non-commercial purposes, at its discretion, the above title upon the request of individuals or institutions.

[redacted]
Signature of Author

*To my grandmother.*

Perhaps the most important application of theoretical chemistry is the study of radicals or molecules with one or more unpaired electrons. It is difficult to obtain information about these systems experimentally since radicals are highly reactive, and therefore short-lived, species. Experimental information about radicals can be obtained by measuring the hyperfine coupling constants (HFCCs) of various atoms within the molecule of interest. However, experimental HFCCs yield very little information about the nature of the radical. Through comparison of theoretically calculated HFCCs to those obtained experimentally, the radical structure can be revealed and other electronic properties of the system can be obtained. This thesis concentrates on studies involving accurate calculation of HFCCs and their application to specific chemical and biochemical problems.

The first component of the thesis reports a study of peroxyl radicals, which are of interest due to their involvement in biological and industrial processes. Emphasis was placed on the calculation of accurate oxygen HFCCs. The larger peroxyl radicals were investigated with density-functional theory (DFT), a relatively new theoretical method that allows for the study of large molecules using reduced computational resources (computer time, memory and disk space). The work revealed important information about the electronic structure of these radicals. The smaller peroxyl radicals were investigated via high-level calculations, which require large computer resources. The peroxyl studies elucidated the best method for the calculation of accurate oxygen HFCCs. Since poor agreement was observed with DFT for small inorganic peroxyl radicals, a subset of these species was examined through the use of a combined quantum mechanics and molecular dynamics technique. This method, which accounts for matrix and vibrational effects, cannot correct for the failure of DFT to sufficiently describe the geometry of these radicals.

The accurate methods for the calculation of HFCCs were then applied to an investigation of the radicals formed upon irradiation of DNA, and this study comprises the second component of the thesis. DNA radicals are of interest due to the decrease in the ozone layer and the increase in the use of radiation therapy. Theoretical studies are important since many experimental unknowns exist regarding which radicals are the main radiation products. Studies were performed on all four DNA bases, as well as the sugar moiety. The results for some of the bases (thymine, adenine and guanine) are in good agreement with experiment indicating that a sufficient level of theory was implemented. For cytosine, however, differences were found between the theoretical and experimental results and a new mechanism was proposed for radiation damage to this base. This new mechanism indicates that the surrounding water molecules play an important role in the radiation damage. Based on the good agreement observed for the other DNA bases, this new mechanism seems reasonable, and was tested through an investigation of the various possible reaction mechanisms. All of the calculated data for the DNA bases and the sugar group were then used to generate a model for radiation damage in DNA which encompasses the bases, the sugar-phosphate backbone and the surrounding water molecules. This model provides the basis for future experimental and theoretical studies on DNA since it outlines the main radical products formed upon irradiation.

| | | | |
|---|---|---|---|
| $\Psi$ | wave function | $\hat{H}_{total}$ | total Hamiltonian |
| $E$ | energy | $\hat{T}$ | kinetic energy operator |
| $\hat{V}$ | potential energy operator | $\hat{H}_{elect}$ | electronic Hamiltonian |
| $\Phi$ | trial wave function | $\hat{F}$ | Fock operator |
| $\psi_i$ | $i$th molecular orbital | $\varepsilon_i$ | $i$th orbital energy |
| $\hat{H}_{core}$ | one electron Hamiltonian | $\hat{J}_j$ | Coulomb operator |
| $\hat{K}_j$ | exchange operator | $\varphi_\mu$ | $\mu$th atomic orbital |
| $F_{\mu\upsilon}$ | element of the Fock matrix | $P_{\mu\upsilon}$ | element of the density matrix |
| $S_{\mu\upsilon}$ | element of the overlap matrix | $c_{\mu\upsilon}$ | expansion coefficient |
| $(\mu\upsilon \mid \lambda\sigma)$ | two-electron integral | $T_E$ | configuration selection energy threshold |
| $\hat{H}_0$ | zero-order Hamiltonian | $V$ | perturbation |
| $\rho$ | electron density | $E_{xc}$ | exchange-correlation functional |
| $v_{eff}$ | effective potential | $\phi$ | basis functions |
| $d_{i\mu}$ | contraction coefficients | $h$ | Planck's constant |
| $g_e$ | electronic g-value | $\beta_e$ | electronic Bohr magneton |
| B | field strength | $Z$ | nuclear charge |
| $A_{iso}$ | isotropic hyperfine coupling constant | $T_{ij}^{(N)}$ | $ij$th component of the anisotropic hyperfine coupling tensor |
| $r$ | distance between an electron and nuclei (or electron) | $R$ | nuclear-nuclear distance |

| | | | |
|---|---|---|---|
| **MM** | molecular mechanics | **DFT** | density-functional theory |
| **HF** | Hartree-Fock | **SCF** | self-consistent field |
| **LCAO** | linear combination of atomic orbitals | **RHF** | restricted Hartree-Fock |
| **ROHF** | restricted open-shell Hartree-Fock | **UHF** | unrestricted Hartree-Fock |
| **AUHF** | annihilated UHF | **PUHF** | projected UHF |
| **CI** | configuration interaction | **MRCI** | multi-reference CI |
| **IEPA** | independent electron pair approximation | **CC** | coupled-cluster |
| **QCI** | quadratic CI | **MP** | Møller-Plesset |
| **RSPT** | Rayleigh- Schrödinger perturbation theory | **MBPT** | many-body perturbation theory |
| **LSDA** | local spin density approximation | **S** | Slater's exchange functional |
| **VWN** | Vosko, Wilk and Nusair's correlation functional | **P86** | Perdew's correlation functional |
| **GGA** | generalized gradient approximation | **PW91** | Perdew and Wang's 1991 exchange functional |
| **LYP** | Lee, Yang and Parr's correlation functional | **PW86** | Perdew and Wang's 1986 exchange functional |
| **B** | Becke's 1988 exchange functional | **B3** | Becke's hybrid exchange functional |
| **G96** | Gill's 1996 exchange functional | **STO** | Slater-type orbital |
| **GTO** | Gaussian-type orbital | **CGTO** | contracted GTO |
| **PES** | potential energy surface | **IP** | ionization potential |
| **EA** | electron affinity | **ESR** | electron spin resonance |
| **EPR** | electron paramagnetic resonance | **HFCC** | hyperfine coupling constant |
| **ENDOR** | electron-nuclear double resonance | **ESEEM** | electron spin-echo envelope modulation |
| **QM/MD** | combined quantum mechanics and molecular dynamics | **P(C)** | product (complex) |
| **R(C)** | reactant (complex) | **TS** | transition state |

| | | | |
|---|---|---|---|
| **T** | anhydrous thymine | **1MeT** | 1-methylthymine |
| **dT** | deoxythymidine | **1MeT:9MeA** | co-crystals of 1MeT and 9-methyladenine |
| **Cm** | cytosine monohydrate | **1MeC** | 1-methylcytosine |
| **3'CMP** | cytidine 3'-monophosphate | **5'dCMP** | deoxycytidine 5'-monophosphate |
| **U** | uracil | **1MeU** | 1-methyluracil |
| **rU** | uridine | **1MeU:9EA** | co-crystals of 1MeU and 9-ethyladenine |
| **2'dU** | 2'-deoxyuridine | **9MeA** | 9-methyladenine |
| **dA** | anhydrous deoxyadenosine | **dAm** | deoxyadenosine monohydrate |
| **rA** | adenosine | **rA:5BrU** | co-crystals of adenosine and 5-bromouracil |
| **rI** | inosine | **3'CMP** | cytosine 3'-monophosphate |
| **5CldU** | 5-chlorodeoxyuridine | **5BrdU** | 5-bromodeoxyuridine |
| **Uβaf** | uracil-β-D-arabinofuroside | **5'dGMP** | 2'-deoxyguanosine 5'-monophosphate |
| **A:2HCl** | adenine dihydrochloride | **G:HBr:2H$_2$O** | guanine hydrobromide |
| **G:HBr:H$_2$O** | guanine hydrobromide monohydrate | **A:HCl:½H$_2$O** | adenine hydrochloride hemihydrate |
| **rA:HCl** | anhydrous adenosine hydrochloride | **3'5'cGMP** | guanosine 3',5'-cyclic monophosphate |
| **G:HCl:H$_2$O** | guanine hydrochloride monohydrate | **5'rUMP** | uridine 5'-monophosphate |
| **5'GMP(FA)** | free acid of guanosine 5'-monophosphate | | |

## *Acknowledgments*

I would like to take this opportunity to thank Dr. R. J. Boyd for introducing me to theoretical chemistry. It has been a great honor to start my career under his careful supervision. His encouragement and guidance in both research and life is greatly appreciated. I would also like to thank Dr. L. A. Eriksson who assisted me at great lengths, both through e-mail and in person. The momentous opportunities that he provided to me through visits to Stockholm and Uppsala will not be forgotten. A thanks also goes to Dr. Aatto Laaksonen for allowing me to visit his laboratory and for teaching me about his combined quantum mechanics and molecular dynamics program.

My work in the lab could not have been started without the patience of many people. Dr. Kent Worsnop taught me about the dreaded computers, Dr. Jing Kong introduced me to the dreaded MELDF-X program and Dr. George Heard always provided comic relief. I am also thankful for the company of more recent members of the group. Kathryn Rankin's helpful "conversations" and encouragement over the past couple of years are greatly cherished. Fuqiang Ban's interesting conversations about biological systems, HFCCs and Chapter Seven were extremely helpful. Nelaine Mora-Diez provided encouragement while I was writing with never ending smiles. Sandra Rafai's company was also greatly appreciated, as was her immense patience with me. A distinguished thanks also goes to Dr. Susan Boyd for helpful criticisms on my writing. Outside the lab, I will not forget the company provided by other members of the department over the years, including the Friday "lunch meetings" with Stephanie Mehlman, Mitch Lohnes and Brent Jewett. Jill Hollis also provided much needed support by listening to my complaints day after day.

The financial assistance of the Natural Science and Engineering Research Council (NSERC), the Killam Trust Fund and the Dalhousie Graduate Fellowship Fund was greatly appreciated.

Without the support of my family and friends my work would not have been possible. My family (Mom, Dad and Krista) have always been there for me and provided continuous encouragement. A special thanks goes to Steven who stood by my side during the last four years with unconditional love, encouragement and support.

# *CHAPTER ONE*

# Introduction

## *1.1 General Background*

With the development of computer hardware and new theoretical algorithms, the use of quantum mechanical methods to solve chemical problems is increasing. One of the most important applications of quantum chemistry is the study of species that are extremely reactive and therefore difficult to examine experimentally. These species can include ions, reaction intermediates and radicals. Radicals are especially interesting since they contain one or more unpaired electron(s) despite the fact that electrons prefer to exist as pairs of opposite spin. An unpaired electron has a spin angular momentum that results in unique magnetic properties.

Experimentally, radicals are studied via spectroscopic techniques that utilize their magnetic character, including electron spin resonance (ESR), electron-nuclear double resonance (ENDOR) and electron spin-echo envelope modulation (ESEEM). From these procedures, a property known as the hyperfine coupling constant (HFCC) can be obtained for each atom within the molecule. A HFCC arises from the interaction between the unpaired electron and the magnetic nuclei in the radical. This property leads to information about the distribution of the unpaired spin in the radical, which in turn may lead to clues about the radical's reactivity. However, these experiments yield no direct information about the radical's geometry, charge and atomic composition. In addition, radicals are relatively short-lived species and, hence, experimental conditions required to isolate them are often unattainable. Thus, experimental information about these systems can be difficult to obtain and theoretical calculations provide an attractive alternative approach.

While theoretical calculations on radicals are desirable, the application of quantum chemical methods to these systems is not always straightforward. Very high-levels of theory are required to obtain meaningful information. In addition, an extremely accurate description of the molecular orbitals within the molecule is required and can be achieved only with a large basis set. This thesis is primarily concerned with the calculation of accurate hyperfine coupling constants and the use of these calculations to

obtain information about biochemical systems. A brief description of available quantum chemical methodologies and basis sets used for the determination of molecular structure and other electronic properties will be given in Chapter Two. A detailed discussion of hyperfine coupling constants, including how they are determined experimentally and the theoretical requirements for their calculation, will also be presented. The remainder of this chapter will focus on background information pertaining to the biochemical problems to which these methods and basis sets were applied.

## *1.2 Overview*

### *1.2.1 Peroxyl and Hydroxyl Radicals*

Peroxyl radicals comprise the first class of radicals to be discussed in the present thesis (Chapter Three). Peroxyl radicals have been investigated both experimentally[1,2,3] and theoretically.[4] Attention has been given to these radicals because they are involved in many common processes, such as respiration, combustion and even the drying of paint. Recent interest in peroxyl radicals has also arisen because their lifetime is long enough to enable them to travel long distances in solution and in biological systems. Thus, research has turned to investigating the effects of peroxyl radicals on lipid biomembranes, such as cell membranes. The geometries, electron distributions and various other properties of alkyl peroxyl radicals have been examined through theoretical techniques, including both *ab initio* and semi-empirical methods.[4]

I II

Figure 1.1: Resonance structures of peroxyl radicals.

Two main resonance structures can be written for peroxyl radicals: structure I (Figure 1.1), which involves no formal charges with the unpaired electron located on the terminal oxygen, and structure II, which involves charges with the unpaired electron found on the inner oxygen. The charged resonance structure (II) has previously been used to explain the behavior of peroxyl radicals.[2] These arguments were later questioned in a theoretical study, which concluded that there is a larger negative charge on the inner oxygen and that the spin density is associated almost exclusively with the terminal

oxygen. These properties imply that the behavior of peroxyl radicals can be accounted for without involving charged structures.[4] Experimentally, the HFCCs in peroxyl radicals have been determined in numerous studies and conflicting results were obtained for the unpaired spin distribution.[3] Due to these discrepancies in past research, theoretical calculations would be useful to determine the relative magnitude of the HFCCs on the terminal and inner oxygen atoms, thus revealing information about the location of the unpaired electron, the relative importance of resonance structures and the distribution of spin density.

Oxygen's most abundant isotope, $^{16}O$, does not possess a magnetic moment and, thus, $^{16}O$ must be replaced by $^{17}O$ (natural abundance of 0.037%) if the hyperfine structure of oxygen is to be examined. Experimentally, this technique is known as spin labeling and has been performed with relative ease for a number of years. The most accurate $^{17}O$ experimental data exists for the hydroxyl radical.[5] Among peroxyl radicals that have been examined experimentally, the most complete set of accurate HFCCs exists for *t*-butyl peroxyl radical, which includes a $^{13}C$ coupling for the carbon attached to the inner oxygen.[3d-f]

Hyperfine coupling constants have been studied with a wide variety of theoretical methods and basis sets. Accurate data can now be calculated with a great deal of confidence for hydrogen ($^{1}H$) and carbon ($^{13}C$) nuclei. However, the best method for calculating $^{17}O$ hyperfine coupling constants was unknown prior to the work presented within. The calculations of $^{17}O$ hyperfine coupling constants to be presented in Chapter Three will be discussed according to the size of the radical. First, the HFCCs in large alkyl peroxyl radicals obtained using density-functional theory (DFT) will be compared to accurate experimental results. DFT has been used in the past with varying degrees of success. It is desirable to study large oxygen centered radicals with DFT since this method possesses many of the important theoretical requirements when HFCCs are to be investigated. In addition, DFT requires less computer resources (time, memory, disk space) than other methods, which allows for the study of large species. The oxygen HFCCs obtained with DFT via a systematic study, where several variables in the DFT method (geometry, functional form, basis set) were varied, will be discussed.

The density-functional study of $^{17}O$ hyperfine coupling constants gave results of sufficient accuracy to allow meaningful comparison to experiment. However, the deviation between experimental and theoretical results for oxygen is larger than that observed for other nuclei ($^{1}H$, $^{13}C$). Thus following the DFT study, calculated oxygen HFCCs from very high-level theoretical techniques, such as multi-reference configuration interaction (MRCI), quadratic configuration interaction (QCI) and coupled-cluster (CC) algorithms, will be discussed. These methods all require greater computer resources than DFT, which dramatically increase with the size of the molecule. Hence, the accuracy of these methods will be considered relative to the experimental HFCCs of the hydroxyl radical, the smallest oxygen centered radical.

Differences between theoretical and experimental hyperfine structures can arise for reasons other than the quantum mechanical method employed. Calculations are generally performed on static, gas phase structures in a vacuum at 0 K. Experiments, on the other hand, are performed at a variety of temperatures and the radicals may exhibit vibrational motion that can lead to averaged spectra. In addition, radicals are often trapped in matrices, such as argon, neon, chlorofluorocarbons (CFCs) or zeolites, in order to reduce their reactivity. These differences can be accounted for through the use of a combined quantum mechanics and molecular dynamics approach (QM/MD).[6] In this technique, part of the system (the radical) is treated with highly accurate quantum mechanical methods and the rest of the system (the experimental matrix) is treated classically (methods based on the laws of classical physics). Thus, the radical's motion in terms of the stretching of bonds and bending of angles is simulated and the property of interest is calculated at each time step. This method will be discussed in Chapter Three where it will be implemented in attempts to improve the agreement between theoretical and experimental $^{17}O$ hyperfine coupling constants in small peroxyl radicals.

### *1.2.2 Radicals Formed in Irradiated DNA*

Radicals formed through the exposure of deoxyribonucleic acid (DNA) to radiation form the second class of radicals to be discussed. Within its double-helical structure, DNA stores and transmits genetic information. Nucleotides are the building blocks of DNA, where each nucleotide is composed of a base, a sugar and one or more phosphate groups. The DNA bases are derivatives of either pyrimidine or purine (Figure

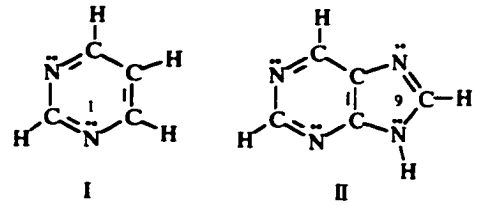

I II

Figure 1.2: Chemical structure of pyrimidine (I) and purine (II), the parent compounds of the nucleobases.

1.2). The most common pyrimidines in DNA are thymine (T) and cytosine (C), and the purines are adenine (A) and guanine (G).

The DNA sugar group, deoxyribose (dR), is a derivative of ribose (R) where the hydroxyl group at the C2' position is removed (Figure 1.3). A nucleoside is formed when a bond is created between the C1' position in the sugar group and the N1 or N9 position

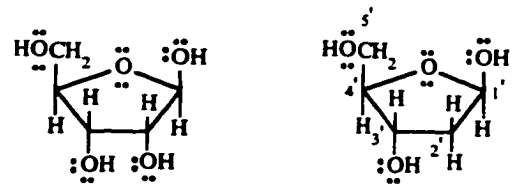

I II

Figure 1.3: Chemical structure of ribose (I) and deoxyribose (II).

in a pyrimidine or purine, respectively. The four DNA nucleosides are denoted deoxyadenosine (dA), deoxyguanosine (dG), deoxythymidine (dT) and deoxycytidine (dC). Nucleotides are phosphate esters of nucleosides, where esterfication occurs at the C5' and C3' positions. Examples of nucleotides include deoxycytidine 5'-monophosphate (5'dCMP) and deoxyguanosine 5'-monophosphate (5'dGMP). The sugar and phosphate groups provide the structural features of DNA and the bases store genetic information. The bases occur in unique hydrogen-bonded pairs, where due to the molecular structure A and T are always paired and similarly C and G are base paired (Figure 1.4).

DNA also plays an important role in protein synthesis along with ribonucleic acid (RNA). RNA has a similar structure to DNA although it is usually present as a single strand. The main differences between RNA and DNA arise in the sugar group and the bases present. The DNA pyrimidine thymine is replaced by uracil (U) in RNA, although the rest of the bases remain unaltered. The main RNA nucleosides, formed through the addition of ribose to one of the four bases, are cytidine (rC), uridine (rU), adenosine (rA)

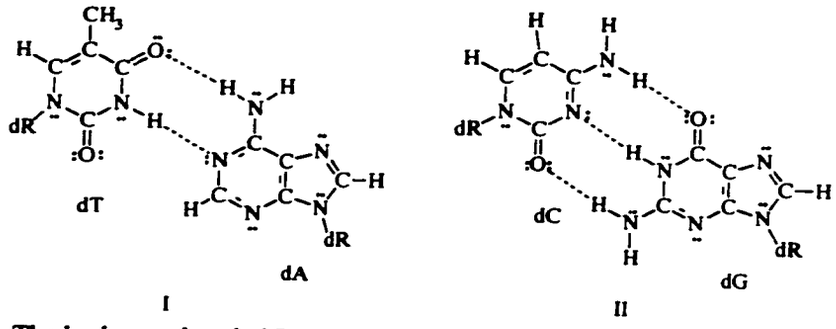


Figure 1.4: The hydrogen-bonded DNA base pairs: deoxythymidine:deoxyadenosine (I) and deoxycytidine:deoxyguanosine (II).

and guanosine (rG), where the *r* indicates that the sugar present is ribose rather than deoxyribose. Examples of RNA nucleotides include adenosine 5'-monophosphate (5'AMP) and cytidine 3'-monophosphate (3'CMP).

The effects of radiation on DNA, as well as RNA, have become increasingly popular topics in the literature. Understanding the radiation chemistry of DNA is important due to increasing radiation exposure to the population as a result of the decrease in the ozone layer, the increase in the number of space flights and the demand for radiation therapy to treat ailments such as cancer. It is accepted that damage to DNA occurs via direct and indirect processes. Direct radiation damage generates base anions and cations which subsequently undergo protonation and deprotonation to form radical products. The primary indirect radiation damage pathway involves reactions of DNA with products from water radiolysis (hydrogen atoms, hydroxyl radicals and $e^-_{(aq)}$). The primary products of DNA radiation damage are base and sugar radicals, which react to form lesions such as DNA-protein cross-links, single-strand breaks and, inevitably, cell death. Numerous experimental studies have been performed to identify these primary base radicals with the hope of preventing the drastic damage that occurs in cells due to these radicals. Experimental studies on full DNA samples are extremely difficult since the spectra of the radiation products are highly similar. Thus, the most reliable experimental information has been obtained through single-crystal ENDOR studies performed on derivatives of the four DNA bases in numerous environments at very low temperatures.[7] In addition, some recent work has examined radiation effects on the DNA base pairs.[8] However, even the spectra of the individual bases are elaborate due to significant hydrogen bonding in the crystal structures. Thus, assignment of these spectra

often requires simulations, assumptions of possible mechanisms and/or other additional arguments. These assumptions can cause debate over the identity of radical products.

Due to the difficulties encountered during experimental studies of DNA radiation products, theoretical calculations may be able to provide important information. In particular, calculation of accurate HFCCs in possible radiation products and comparison to the experimental spectra can elucidate the primary damage sites. It was not until the development of density-functional theory that the study of biological molecules at a meaningful level of theory became feasible. Discussions in Chapters Two and Three show that this technique allows for the determination of accurate HFCCs at a reasonable computational cost. Previous theoretical work has concentrated on the structure of possible radiation products, properties such as ionization potentials and electron affinities, and solvation effects on these properties.[9] Two studies have appeared in the literature that have examined properties of sugar radicals, including the hyperfine couplings.[10] However, these HFCCs were obtained at a theoretical level too low to render any valuable insight.

In order to examine the extent of radiation damage in DNA thoroughly, an initial investigation must be performed to determine the most important reaction products. Chapters Four and Five will present calculations performed on DNA and RNA bases with density-functional theory. Focus will be placed on the HFCCs calculated for all possible radiation products for each base, as well as the relative energetics and geometrical distortions arising due to radical formation. These radiation products include all hydrogenated (net hydrogen atom addition), dehydrogenated (net hydrogen atom removal) and hydroxylated (net hydroxyl radical addition) products, as well as the anion and cation. A discussion comparing calculated hyperfine couplings to ENDOR results obtained from single-crystal studies of base derivatives will be given. Chapter Four will focus on the DNA pyrimidines, thymine and cytosine, as well as the RNA base uracil. The succeeding chapter will offer a similar comparison for the purines, adenine and guanine.

Sugar radicals are also of interest since it is now widely accepted that single-strand breaks in DNA occur via these intermediates.[11] Sugar radicals have not been observed directly in the spectra of full DNA,[12] although many products believed to arise

from mechanisms involving these radicals have been observed. Hole *et al.*[13] were the first to note a large variety of sugar radicals in their study of deoxyguanosine 5'-monophosphate, although numerous sugar radicals were previously observed in studies of different nucleotides and nucleosides. In their ENDOR study, Hole *et al.* characterized nine sugar radicals, indicating that almost every carbon site in the sugar is affected by radiation. A subsequent ENDOR study of deoxyadenosine crystals[14] supported the hypothesis of the formation of sugar radicals upon application of small radiation doses. These studies indicate that the DNA sugar, in addition to the DNA bases, may be the site of significant radiation damage in DNA even though detection of sugar radicals in full DNA is difficult.[12] Chapter Six will report on a comprehensive study of sugar radicals generated in irradiated DNA components. This study focused on the HFCCs of sugar radicals formed through hydrogen atom and hydroxyl radical abstraction from a model sugar group, as well as energetics of the various products.

The discussions in Chapters Four through Six will give a complete picture of the main radiation products in irradiated DNA components. These discussions will be centered only on the relative energies of radiation products and the HFCCs. As will be discussed, good agreement between theoretical and experimental results can be obtained for a wide variety of base and sugar radicals. However, some discrepancies arise, which lead to the proposal of alternative radiation products and damage mechanisms. These mechanisms can be tested through a theoretical investigation of the reaction potential energy surfaces. A more detailed picture of the relative importance of radiation products can thereby be obtained. Chapter Seven will present an investigation of the reactions of DNA bases with water in order to justify proposed radiation reaction mechanisms and clarify reasons why certain products are favored in some bases, but not in others.

The radiation damage model developed in Chapters Four through Seven can be extended by comparing the calculated properties for the primary DNA radiation products to those properties observed experimentally in studies on full DNA. The most accurate results on full DNA have been obtained from studies on orientated fibers.[15] Additional experimental work has considered the effects of the hydration layer on DNA and reactions of the hydration layer with DNA.[16] Consideration of the calculated results, together with the experimental results on single crystals and on full DNA, allow a model

of the radiation damage in DNA to be developed. This model encompasses the damage to water, the bases and the sugar group. Chapter Eight will present this discussion of radiation damage in DNA in order to correlate the work presented in the previous chapters and create a picture of full DNA radiation damage.

Chapter Nine will present global conclusions drawn from the work presented within. The discussion will include potential research topics arising directly from the research presented on hyperfine coupling constants in peroxyl radicals and radicals formed in irradiated DNA.

### *1.3 References*


1. (a) Ingold, K. U. *Acc. Chem. Res.* **1969**, *2*, 1; (b) Barclay, L. R. C. In *Peroxyl Radicals*, Alfossi, Z. B., Ed.; John Wiley & Sons Ltd.: New York, 1997.

2. (a) Pryor, W. A. *Ann. Rev. Physiol.* **1986**, *48*, 657; (b) Halliwell, B.; Gutteridge, J. M. C. *Free Radicals in Biology and Medicine;* Clarendon Press: Oxford, 1985; (c) *Free Radicals in Biology*; Pryor, W. A., Ed.; Academic Press: New York, 1976; (d) Barclay, L. R. C.; Baskin, K. A.; Locke, S. J.; Schaefer, T. D. *Can. J. Chem.* **1987**, *65*, 2529.

3. (a) Fessenden, R. W.; Schuler, R. H. *J. Chem. Phys.* **1966**, *44*, 434; (b) Melamud, E.; Silver, B. L. *J. Phys. Chem.* **1973**, *77*, 1896; (c) Bower, H. J.; Symons, M. C. K.; Tinling, D. J. A. *Radical Ions*; Kaiser, E. T.; Kevan, L., Eds.; Interscience: New York, 1968; (d) Adamic, K.; Ingold, K. U.; Morton, J. R. *J. Am. Chem. Soc.* **1970**, *92* 922; (e) Howard, J. A. *Can. J. Chem.* **1972**, *50*, 1981; (f) Howard, J. A. *Can. J. Chem.* **1979**, *57*, 253.

4. (a) Boyd, S. L.; Boyd, R. J.; Barclay, L. R. C. *J. Am. Chem. Soc.* **1990**, *112*, 5724; (b) Liskow, D. H.; Schaefer, H. F., III; Bender, C. F. *J. Am. Chem. Soc.* **1971**, *93*, 6734; (c) Ohkubo, K.; Fujita, T.; Sato, H. *J. Mol. Struc.* **1977**, *36*, 101; (d) Bair, R. A.; Goddard, W. A., III *J. Am. Chem. Soc.* **1982**, *104*, 2719; (e) Besler, B. H.; Sevilla, M. D.; MacNeille, P. *J. Phys. Chem.* **1986**, *90*, 6446.

5. Leopold, K. R.; Evenson, K. M.; Comben, E. R.; Brown, J. M. *J. Mol. Spectr.* **1987**, *122*, 440.

6. (a) Field, M. J.; Bash, P. A; Karplus, M. *J. Comp. Chem.* **1990**, *11*, 700; (b) Åqvist, J.; Warshel, A. *Chem. Rev.* **1993**, *93*, 2523; (c) Stanton, R. V.; Hartsough, D. S.; Merz, K. M. *J. Comp. Chem.* **1995**, *16*, 113.

7. Close, D. M. *Radiat. Res.* **1993**, *135*, 1.

8. (a) Sagstuen, E.; Hole, E. O.; Nelson, W. H.; Close, D. M. *Radiat. Res.* **1998**, *149*, 120; (b) Sagstuen, E.; Hole, E. O.; Nelson, W. H.; Close, D. M. *Radiat. Res.* **1996**, *146*, 425.

9. Colson, A. -O.; Sevilla, M. D. *Int. J. Radiat. Biol.* **1995**, *67*, 627.

10. (a) Miaskiewicz, K.; Osman, R. *J. Am. Chem. Soc.* **1994**, *116*, 232; (b) Colson, A.-O.; Sevilla, M. D. *J. Phys. Chem.* **1995**, *99*, 3867.

11. (a) von Sonntag, C. In *The Chemical Basis of Radiation Biology*; Taylor and Francis: New York, 1987; (b) Becker, D.; Sevilla, M. D. In *Advances in Radiation Biology*; Academic Press: New York, 1993.

12. Close, D. M. *Radiat. Res.* **1997**, *147*, 663.

13. Hole, E. O.; Nelson, W. H.; Sagstuen, E.; Close, D. M. *Radiat. Res.* **1992**, *129*, 119.

14. Close, D. M.; Nelson, W. H.; Sagstuen, E.; Hole, E. O. *Radiat. Res.* **1994**, *137*, 300.

15. Gatzweiler, W.; Hüttermann, J.; Rupprecht, A. *Radiat. Res.* **1994**, *138*, 151.

16. (a) Hüttermann, J.; Röhrig, M.; Köhnlein, W. *Int. J. Radiat. Biol.* **1992**, *61*, 299; (b) La Vere, T.; Becker, D.; Sevilla, M. D. *Radiat. Res.* **1996**, *145*, 673.

# CHAPTER TWO

## Theoretical Background

### *2.1 Introduction*

Many theoretical methods are available for computational chemists to investigate chemical systems. These techniques fall into two main categories: molecular mechanics and electronic structure methods. Molecular mechanics (MM) techniques are based on classical physics and require few computer resources. The disadvantages of these methods include the fact that they rely on the interactions between nuclei rather than explicitly treating electrons. This implies that properties depending on electronic effects, such as the formation or breaking of bonds, will be poorly described. Alternatively, electronic structure methods are based on the laws of quantum mechanics. From quantum mechanics, it is known that observable properties can be obtained from the wave function. Classes of electronic structure methods differ through the approximations implemented. One class of electronic structure techniques, semi-empirical methods, implements empirical parameters to reduce the number of integrals that must be solved to obtain the wave function. Thus, similar to MM methods, semi-empirical techniques are computationally efficient. However, these electronic structure methods are reliable only for systems similar to those included in the data set used to fit the empirical parameter.

The majority of the techniques implemented in the present thesis fall into two main categories of electronic structure methods: *ab initio* and density-functional theory (DFT). *Ab initio* methods use a small number of physical constants in their derivation, but do not employ empirical parameters. These methods provide quantitative results for a variety of systems and the size of the systems to which these methods can be applied is constantly increasing with developments in computer hardware. *Ab initio* methods differ from one another through the approximations used to obtain the wave function. Alternatively, density-functional methods are based on the electron density and do not explicitly solve for the wave function. These methods possess the accuracy of *ab initio* techniques at a reduced computational cost.

Since a predominant portion of this thesis is concerned with the calculation of hyperfine coupling constants, the present chapter will describe *ab initio* and density-

functional methods that can be used to calculate this property. The goal of this chapter is to leave the non-expert with a concrete idea of how different quantum chemical methods are developed and their relative level of accuracy. In addition, a complete discussion of hyperfine coupling constants will be presented, including a description of experimental techniques and suitable theoretical methods for the calculation of this property.

### *2.2 The Schrödinger Equation*

The energy and many other important properties of a particle are explicitly defined in quantum mechanics by the wave function.[1,2] The wave function ($\Psi(\bar{r},t)$) can be obtained from the time-dependent Schrödinger equation

$$\hat{H}_{total}\Psi(\bar{r},t) = \frac{ih}{2\pi}\frac{\partial\Psi(\bar{r},t)}{\partial t}. \tag{2.1}$$

$\hat{H}_{total}$ is the Hamiltonian expressed as

$$\hat{H}_{total} = \frac{-h^2}{8m\pi}\nabla^2 + V \tag{2.2}$$

where $m$ represents the mass of the particle, $h$ is Planck's constant, and $V$ is the potential field in which the particle is moving. The time-dependent Schrödinger equation can be simplified by writing the wave function as the product of a spatial and a time function. This separation results in one equation dependent only on the position of the particle and another equation dependent only on time. The time-independent Schrödinger equation can be written as an eigenvalue equation,

$$\hat{H}_{total}\Psi(\bar{r}) = E\Psi(\bar{r}). \tag{2.3}$$

The wave function (now dependent only on spatial coordinates) is the eigenfunction and the energy ($E$) is the eigenvalue. Solutions to the above eigenvalue equation correspond to stationary states, where the lowest energy solution is the ground state.

Quantum chemistry involves the application of the time-independent Schrödinger equation to atoms and molecules in order to obtain knowledge about their properties. The total Hamiltonian can be expressed as

$$\hat{H}_{total} = \hat{T}_e + \hat{V}_{ee} + \hat{T}_n + \hat{V}_{ne} + \hat{V}_{nn} \tag{2.4}$$

where $\hat{T}$ and $\hat{V}$ are the kinetic and potential energy operators, the subscripts $n$ and $e$ represent the nuclear and electronic contributions to these operators, respectively, and $\Psi$ becomes the $N$-electron wave function. Since an exact solution to the time-independent Schrödinger equation cannot be obtained except for a few simple cases, approximate solutions are sought through the application of various assumptions. The approximations implemented in *ab initio* and DFT methods will now be discussed.

### *2.3 The Electronic Problem*

The first approximation applied to the time-independent Schrödinger equation is the Born-Oppenheimer approximation.[3,4] This assumption suggests that since the nuclei are more massive and, thus, move more slowly than the electrons, electronic and nuclear motion can be separated. Hence, solving the Schrödinger equation is reduced to solving the electronic eigenvalue equation where the electronic Hamiltonian replaces the total Hamiltonian,

$$\hat{H}_{elect} = \hat{T}_e + \hat{V}_{ee} + \hat{V}_{ne}. \tag{2.5}$$

The electronic energy can be obtained from the electronic Schrödinger equation,

$$\hat{H}_{elect}\Psi(\bar{r}) = E_{elect}\Psi(\bar{r}). \tag{2.6}$$

The total energy is evaluated by adding the classical nuclear energy expression to $E_{elect}$.

In order to solve the electronic Schrödinger equation, more information about $\Psi$ is required. For a system of $2N$ noninteracting electrons, the simplest form of $\Psi$ is a Hartree product of $2N$ spin orbitals (the product of the spin function $\alpha$ or $\beta$ with a spatial one-electron wave function). Mathematically,

$$\Psi(1,2,...,2N) = \psi_1\alpha(1)\psi_1\beta(2)\psi_2\alpha(3)...\psi_N\beta(2N). \tag{2.7}$$

This simple description of the wave function is not adequate since experiment indicates that electrons are fermions, which possess half-integral spin and antisymmetric wave functions described by

$$\Psi(1,2,...,i,j,...,2N) = -\Psi(1,2,...,j,i,...,2N). \tag{2.8}$$

Since the Hartree product wave function does not satisfy the antisymmetry principle, a Slater determinant must be used to express a $2N$-electron wave function as

$$\Psi = [(2N)!]^{-1/2} \begin{vmatrix} \psi_1\alpha(1) & \psi_1\beta(1) & \psi_2\alpha(1) & \cdots & \psi_N\beta(1) \\ \psi_1\alpha(2) & \psi_1\beta(2) & \psi_2\alpha(2) & \cdots & \psi_N\beta(2) \\ \vdots & & & & \\ \psi_1\alpha(2N) & \psi_1\beta(2N) & \psi_2\alpha(2N) & \cdots & \psi_N\beta(2N) \end{vmatrix} \tag{2.9}$$

or $$\Psi(1,2,...,2N) = |\psi_1\alpha(1)\psi_1\beta(2)...\psi_N\beta(2N)| . \tag{2.10}$$

A Slater determinant guarantees that the antisymmetry principle is satisfied since interchanging two rows (electrons) changes the sign of the wave function. Also, if two columns (orbitals) are identical the determinant vanishes, implying that the Pauli principle in orbital theory is satisfied.

The next problem to be addressed is how to obtain the atomic or molecular orbitals ($\psi_i$) used to create the total wave function. Methods commonly used to obtain wave functions will be discussed in subsequent sections. However, before discussing these methods, it is imperative to introduce one of the main theorems of quantum mechanics.

### *2.4 The Variational Principle*

The variational principle states that for any trial wave function ($\Phi$), the energy obtained with $\Phi$ will be greater than the true ground state energy,[1,2]

$$E_\Phi \geq E_o . \tag{2.11}$$

The equality in Equation 2.11 holds only when the trial function is the exact ground state wave function ($\Psi$), implying $E_\Phi$ is an upper bound to the true energy. The closer $\Phi$ is to $\Psi$, the lower the energy. Trial wave functions are written in terms of parameters that are altered to achieve the lowest energy. In particular, a Slater determinant has flexibility through the spin orbitals, indicating that the spin orbitals can be altered until the lowest energy is achieved. The variational principle thereby provides a means to judge the relative quality of wave functions.

### *2.5 The Hartree-Fock Approximation*

The simplest *ab initio* method to obtain the wave function, or more specifically the atomic or molecular orbitals, is the Hartree-Fock (HF) method.[2,3] The HF equations

are the basis of many higher order approximations. From the variational principle, the best wave function, represented by a single Slater determinant, can be obtained by finding the lowest energy through optimizing the spin orbitals. The Hartree-Fock equations were generated by considering this fact and can be written as

$$\hat{F}\psi_i = \varepsilon_i\psi_i \qquad i = 1,2,...2N \tag{2.12}$$

where $\hat{F}$ is the Fock operator defined by

$$\hat{F} = \hat{H}_{core} + \sum_j (2\hat{J}_j - \hat{K}_j)\,. \tag{2.13}$$

$\psi_i$ are the HF orbitals and $\varepsilon_i$ are the orbital energies. $\hat{H}_{core}$ represents the one-electron Hamiltonian and corresponds to the motion of electron $i$ in the field of the bare nuclei. The second term in Equation 2.13 represents the average potential experienced by the $i$th electron due to the presence of the other electrons where $\hat{J}_j$ and $\hat{K}_j$ are the Coulomb and the exchange operators, respectively, defined by

$$\hat{J}_j(1) = \int \psi_j^*(2)\frac{1}{r_{12}}\psi_j(2)d\tau_2 \tag{2.14}$$

$$\hat{K}_j(1)\psi_i(1) = \left[\int \psi_j^*(2)\frac{1}{r_{12}}\psi_i(2)d\tau_2\right]\psi_j(1) \tag{2.15}$$

Since the Fock operator is a function of the spin orbitals, the HF equations must be solved iteratively until the $\psi_i$ no longer change appreciably. At this point, the orbitals are said to be self-consistent with the field that they generate and the iterative technique is known as the self-consistent field (SCF) method.

### *2.6 Restricted Closed-Shell Hartree-Fock*

For systems larger than atoms or diatomic molecules, the Hartree-Fock equations are too complicated to solve numerically. Roothaan and Hall extended the applicability of the HF method to larger, closed-shell systems. The Roothaan-Hall method,[2,3] or the LCAO method, proposed that molecular orbitals ($\psi_i$) can be expanded as a linear combination of atomic orbitals ($\varphi_\mu$),

$$\psi_i = \sum_{\mu=1}^{M} c_{\mu i}\varphi_\mu \,. \tag{2.16}$$

The variational principle leads to the Roothaan-Hall equations

$$\sum_{\nu=1}^{M}(F_{\mu\upsilon} - \varepsilon_i S_{\mu\upsilon})c_{\upsilon i} = 0 \qquad \mu = 1,2,...,M \tag{2.17}$$

where $\varepsilon_i$ is the one-electron orbital energy of the molecular orbital $\psi_i$ and $S_{\mu\upsilon}$ is an element of the overlap matrix which describes the overlap between the orbitals. The elements of the Fock matrix ($F_{\mu\nu}$) are defined as follows

$$F_{\mu\upsilon} = H_{\mu\upsilon} + \sum_{\lambda,\sigma} P_{\lambda\sigma}\left[(\mu\upsilon \mid \lambda\sigma) - \frac{1}{2}(\mu\lambda \mid \upsilon\sigma)\right] \tag{2.18}$$

where $H_{\mu\upsilon}$ is an element of the matrix representing the energy of a single electron in the field of the bare nuclei, $P_{\mu\upsilon} = 2\sum_{i=1}^{occ} c_{\mu i}c_{\upsilon i}$ is an element of the density matrix and $(\mu\upsilon \mid \lambda\sigma)$ is a two-electron repulsion integral defined by

$$(\mu\upsilon \mid \lambda\sigma) = \iint \varphi_\mu^*(1)\varphi_\upsilon(1)\frac{1}{r_{12}}\varphi_\lambda^*(2)\varphi_\sigma(2)d\tau_1 d\tau_2 \,. \tag{2.19}$$

These equations must be solved by the SCF method since the Fock matrix depends on the expansion coefficients ($c_{\mu\nu}$).

The Roothaan-Hall equations provide solutions for closed-shell molecules whose pairs of electrons occupy the same spatial molecular orbital. This method is called restricted HF (RHF) and even for closed-shell molecules it cannot accurately reproduce all molecular properties. For example, RHF dissociation of the hydrogen molecule does not result in two hydrogen atoms since the wave function forces the two electrons to occupy the same region in space. Since not all molecules or states of closed-shell systems can be described by RHF methods, alternate techniques with greater flexibility must be considered.

### *2.7 Open-Shell Hartree-Fock Methods*

There are two main methods, both based on the RHF method, used for open-shell molecules. Open-shell molecules include those possessing one or more unpaired

electron(s). This does not mean that open-shell molecules are necessarily systems with an odd number of electrons, but these systems can also include, for example, a triplet state such as the ground state of oxygen. The first technique to be discussed is called restricted open-shell HF (ROHF). In this method, the orbitals are separated into two classes: those that are doubly occupied and those that are singly occupied. The doubly occupied orbitals are treated under the RHF formalism and the open-shell orbitals are treated separately through more complicated expressions.

The ROHF method is not sufficiently flexible since it does not account for interactions between unpaired and paired electrons. For example, if the unpaired electron has $\alpha$ spin then paired electrons with $\alpha$ spin will have additional repulsion interactions with the unpaired electron that the paired electrons with $\beta$ spin will not have. These interactions between the paired and unpaired electrons imply that $\alpha$ and $\beta$ electrons will occupy orbitals with different spatial components. The unrestricted-HF (UHF) method[3,4] accounts for these alterations by implementing two molecular orbital expansions,

$$\psi_i^{\alpha} = \sum_{i=1}^{M} c_{\mu i}^{\alpha} \varphi_{\mu} \quad \text{and} \quad \psi_i^{\beta} = \sum_{i=1}^{M} c_{\mu i}^{\beta} \varphi_{\mu} \,. \tag{2.20}$$

Thus, two Fock matrices are required and double the number of equations relative to those examined for the Roothaan-Hall method must be solved. These equations are called the Pople-Nesbet equations and the convergence of these equations is slow relative to the closed-shell problem. A pictorial description of the RHF, ROHF and UHF formalisms is given in Figure 2.1 in order to illustrate the difference between these methods.

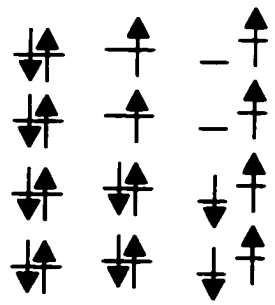


**Figure 2.1: Depiction of the RHF, ROHF and UHF formalisms.**

For reasons outlined above, the UHF method yields a superior description of open-shell systems over the ROHF method. In addition, the ROHF equations are more complicated and the resulting variational energy is high due to the restrictions placed on pairs of electrons. The major drawback of the UHF method over the ROHF method is that solutions to the UHF equations may not be pure spin states, but are often contaminated by higher states. For example, the wave function for a radical with one unpaired electron should be a pure doublet. However, it is possible that the UHF wave function contains higher states such that it could be expressed as

$$\Psi_{UHF}^{Doublet} = c_D \Psi^{Doublet} + c_Q \Psi^{Quartet} + c_S \Psi^{Sextet} + \ldots \tag{2.21}$$

The problem of spin contamination can be resolved by either partial or full annihilation of the major contaminating quartet spin state (AUHF)[5] or by complete projection (PUHF)[6] which eliminates all contaminating spin states.

### *2.8 Beyond Hartree-Fock*

The main deficiency of HF theory is that it assumes the probability of finding two electrons in the same region of space is equal to the product of the individual probabilities. This clearly does not hold for electrons of parallel spin since it is energetically favorable for these electrons to be far apart. Thus, in attempts to stay a reasonable distance away from each other, the motion of the electrons in a molecule is correlated. The energy associated with this property is called the correlation energy[2,3] and is defined as

$$E_{corr} = E_{exact} - E_{HF}\,. \tag{2.22}$$

Although the correlation energy yields only a small contribution to the total energy, it is very important for the calculation of molecular properties. Methods that account for electron correlation are classified as post-HF (post-SCF) techniques. The post-HF methods implemented in the present thesis will be discussed in the following sections.

#### *2.8.1 Configuration Interaction*

Hartree-Fock uses only a single determinant to describe the exact wave function, which proves to be inadequate for the calculation of many electronic properties.

Configuration interaction[3,7] (CI) is a post-HF method which expresses the total wave function ($\Psi$) as a linear combination of numerous Slater determinants ($\Phi_i$)

$$\Psi = \sum_i c_i \Phi_i \tag{2.23}$$

where $c_i$ represents the expansion coefficient for the $i$th determinant. The first determinant ($\Phi_o$) is taken to be the HF determinant and additional determinants are created by moving electrons from occupied orbitals in the HF determinant to virtual (unoccupied) orbitals. This is equivalent to exciting electrons to higher energy orbitals. Thus, the CI wave function could also be written as

$$\Psi = c_o \Phi_o + \sum_{ar} c_a^r \Phi_a^r + \sum_{\substack{a<b \\ r<s}} c_{ab}^{rs} \Phi_{ab}^{rs} + \sum_{\substack{a<b<c \\ r<s<t}} c_{abc}^{rst} \Phi_{abc}^{rst} + \ldots \tag{2.24}$$

where $\Phi_a^r$ represents a single excitation generated by moving an electron from the occupied orbital $a$ to the virtual orbital $r$. Similarly, $\Phi_{ab}^{rs}$ and $\Phi_{abc}^{rst}$ represent double and triple excitations, respectively.

Full CI includes all possible configurations or excitations and represents the most complete non-relativistic treatment of a molecular system. However, full CI is very expensive and time consuming for all but the smallest systems. To overcome this problem, the CI expansion is usually truncated at some level by allowing only certain excitations. For example, CIS includes only single excitations, CISD includes single and double excitations, CISDT includes single, double and triple excitations, and so on. The disadvantage of truncating the CI expansion arises since the resulting wave function is not size consistent. This means the result obtained with a truncated CI wave function for a system of molecules infinitely separated from each other is not equal to the sum of the results calculated for each individual molecule. Size consistency is important for the comparison of results obtained for different systems with the same level of theory.

### *2.8.2 Multi-Reference Configuration Interaction*

Due to demands on computational resources, it is usually impossible to include all quadruple excitations in a CI calculation (CISDTQ), although these excitations have been determined to be important for some molecular properties. The method used to go beyond the inclusion of triple excitations is multi-reference configuration interaction

(MRCI).[7] In this method, all single and double excitations are included from a set of reference configurations. Including more reference configurations than solely the HF determinant guarantees that more of the CI space is covered. More specifically, MRCI is advantageous over CISD since some triple and quadruple excitations are included through single and double excitations with respect to the additional reference configurations.

The problem with MRCI, besides its great demand for computer resources, is developing a method to choose the most important reference configurations and the important excitations with respect to these configurations. A typical MRCI calculation involves the following steps:[8]

1. Transform the virtual orbital space to K-orbitals[9] to improve CI convergence.
2. Select a list of reference configurations, starting with the ROHF determinant.
3. Generate all single and double excitations from each configuration in the reference space and extract the lowest energy eigenvector from the Hamiltonian matrix.
4. Order the CI wave function based on the magnitude of the expansion coefficients or the energy contribution.
5. From the ordered list, choose some set of the most important configurations outside the current reference space to augment the reference space for the next calculation.
6. Repeat the process until convergence has been reached.

The number of single and double excitations generated through this method is very large and thus double excitations with energy contributions less than some threshold ($T_E$) are discarded. All single excitations are included since they have been shown to be essential for the calculation of some molecular properties, in particular spin densities.[10]

Hence, the two main assumptions of this method are that many of the configurations in full CI are not important and that it is possible to determine the important configurations. These are very difficult criteria to investigate and thus the implementation of the MRCI technique can be more intricate than other quantum mechanical methods. In addition, MRCI techniques which choose configurations based on the magnitude of their energy contributions are often criticized since a configuration which contributes little to the energy may be a large contributor to the property of interest.[11]

### *2.8.3 Coupled-Cluster Methods*

The problem of size consistency discussed for truncated CI techniques can be overcome by coupled-cluster methods.[3,7] These techniques extend upon the independent electron pair approximation (IEPA). Within the IEPA, the correlation energy is estimated as the sum of the correlation energy calculated for pairs of electrons,

$$E_{corr}^{IEPA} = \sum_{ab} \varepsilon_{ab} \,. \tag{2.25}$$

The correlation energy for each pair ($\varepsilon_{ab}$) is obtained by assuming that other electrons in the system can be ignored and only allowing the two electrons of interest to correlate. This is accomplished by exciting the electron pair of interest to virtual orbitals and allowing the HF determinant to interact with determinants formed through excitations of only this pair.

The IEPA can be improved upon by accounting for the correlation between pairs of electrons, in other words accounting for coupling of the pairs. This approach leads to methods based on the coupled-cluster (CC) approximation. In addition to including the correlation energy between pairs, this formalism approximates the coefficients of higher order excitations by those of lower order excitations. For example, CCD includes the correlation between pairs of electrons as does the CID method, but extends upon CID by approximating quadruple excitations. The quadruple excitations are included in CCD by approximating the coefficients of these excitations with the coefficients of the double excitations

$$c_{abcd}^{rstu} \cong c_{ab}^{rs} * c_{cd}^{tu} \tag{2.26}$$

It is important to note that Equation 2.26 is not a simple product, but a complex expression that includes all possible products of the coefficients of the double excitations leading to a particular quadruple excitation. Approximation of the quadruple excitations through the CCD technique results in a size consistent method, but this method requires more computer time than CID.

### *2.8.4 Quadratic Configuration Interaction*

The size consistency downfall of truncated CI methods can also be overcome simply by adding supplementary terms to these truncated equations. Examination of the equations describing CID or CISD truncated CI methods indicates that these equations

are not size consistent since they are not purely quadratic. Addition of quadratic terms results in methods known as quadratic CI (QCI).[12] Essentially, QCI methods expand upon truncated CI methods by adding terms to make them size consistent and to approximate higher order excitations, while at the same time neglecting some of the terms included in CC techniques. Through this formalism, QCID and CCD are identical techniques, which improve upon CID by approximating the effects of quadruple excitations. Alternatively, QCISD adds terms to CISD to form a size consistent method. The resulting QCISD method is missing terms included in CCSD and can be considered to be an approximation or simplification of CCSD. Thus, QCISD methods are slightly more computationally efficient than CCSD and therefore are a popular computational technique.

### *2.8.5 Many-Body Perturbation Theory*

All of the methods discussed thus far are based on the variational principle. However, there exists another systematic method for the inclusion of correlation called perturbation theory.[2,3] In this approach, the total Hamiltonian for the system is divided into two parts

$$\hat{H} = \hat{H}_o + \lambda V \tag{2.27}$$

where $\hat{H}_o$ is a zero-order Hamiltonian which has known eigenfunctions and eigenvalues and $V$ is a perturbation. The exact eigenfunctions and eigenvalues are then expanded as a series in $\lambda$

$$E_{total} = E_i^{(0)} + \lambda E_i^{(1)} + \lambda^2 E_i^{(2)} + \cdots \tag{2.28}$$

$$\left|\Psi_{total}\right\rangle = \left|\Psi_i^{(0)}\right\rangle + \lambda\left|\Psi_i^{(1)}\right\rangle + \lambda^2\left|\Psi_i^{(2)}\right\rangle + \ldots \tag{2.29}$$

where $E_i^{(n)}$ is the *n*th order energy. Equations 2.28 and 2.29 are subsequently substituted back into the electronic Schrödinger equation, the products expanded and the coefficients of equal powers of $\lambda$ are equated. These steps result in a series of equations representing progressively higher orders of perturbation. If $\hat{H}_o$ is chosen wisely, $V$ is small and the perturbation expansion will converge quickly, implying that only lower order corrections to the energy must be considered. This type of perturbation theory is most commonly

associated with the names Rayleigh and Schrödinger (RSPT) and is also often referred to as many-body perturbation theory (MBPT).

The most common calculation based on perturbation theory implemented in computational chemistry is Møller-Plesset perturbation theory (MP),[3] which uses the HF Hamiltonian as the zero-order Hamiltonian. Calculation of the total energy to the second order is called MP2, to the third order MP3 and so on. It should be noted that the energy obtained from the first-order equations is equivalent to the HF energy and thus the first-order correction to HF occurs in the second-order expansion (MP2). Since MP techniques are size consistent, they overcome the major disadvantage of variational techniques, such as truncated CI methods. However, since they are not variational techniques, these methods may overestimate the correlation energy.

The most familiar form of Møller-Plesset techniques used in the literature includes only the second-order energy contribution (MP2). In general, including third-order corrections leads to little enhancement in calculated results and often worse agreement with experiment is obtained at an increased computational cost. Thus, MP4 is usually implemented to improve upon the second-order correction. Similarly, MP5 leads to little improvement over results obtained with MP4, which represents the oscillating behavior of the MP series. MP2 has been used to obtain a variety of electronic properties since it includes electron correlation at a reduced computational cost relative to other *ab initio* techniques.

It should be noted that although MP techniques are the most common form of perturbation theory used in the literature, more than one perturbation might be necessary to describe a molecular system. For example, the molecular Hamiltonian may include the HF determinant as the zero-order Hamiltonian, a perturbation to account for electron correlation (similar to MP methods) and a second perturbation to describe the effects of an external electric field.

### *2.8.6 Density-Functional Theory*

Another class of theoretical techniques that includes the effects of electron correlation is based on density-functional theory (DFT).[13] These methods differ from those discussed thus far since they are based on the electron density ($\rho$) defined as

$$\rho(\vec{r}) = \sum_{i}^{occ} |\psi_i(\vec{r})|^2 \tag{2.30}$$

and avoid the direct calculation of the $2N$-electron wave function.

Hohenberg and Kohn[14] devised the two main theorems of DFT. The first theorem states that the energy can be written as a functional of the density, where a functional is a mathematical function whose variable is also a function. In particular, Hohenberg and Kohn provided that the energy can be written as

$$E[\rho] = T[\rho] + V_{ee}[\rho] + V_{ne}[\rho] = F_{HK}[\rho] + \int \rho(r)\upsilon(r)dr \tag{2.31}$$

where $\upsilon(r)$ is the external potential, which is usually described by the nuclear potential. $F_{HK}[\rho]$ is a universal functional since it does not depend on the external potential and can be expressed as

$$F_{HK}[\rho] = T[\rho] + V_{ee}[\rho] = T[\rho] + J[\rho] + nonclassical \tag{2.32}$$

where $J[\rho]$ is the classical electron repulsion energy. The second Hohenberg-Kohn theorem is equivalent to the HF variational theorem and states that the energy obtained with any trial density ($\tilde{\rho}$) is an upper bound to the exact energy of the ground state,

$$E[\tilde{\rho}] \geq E_o . \tag{2.33}$$

Kohn and Sham[15] made the implementation of these equations practical by introducing orbitals such that the major portion of the kinetic energy can be evaluated exactly, leaving only a small contribution to be approximated. The universal functional introduced by Kohn and Sham can be written as

$$F[\rho] = T_s[\rho] + J[\rho] + E_{xc}[\rho] . \tag{2.34}$$

$T_s[\rho]$ is the kinetic energy functional of $2N$ noninteracting electrons and can be evaluated exactly. $E_{xc}[\rho]$ is the exchange-correlation energy functional, which contains the difference between the exact kinetic energy and $T_s[\rho]$, as well as the non-classical

contributions to $V_{ee}[\rho]$. The density can be evaluated by solving the following Kohn-Sham equations

$$\left[-\frac{1}{2}\nabla^2 + v_{eff}(\vec{r})\right]\psi_i = \varepsilon_i\psi_i \qquad i = 1, 2, ..., 2N \tag{2.35}$$

where the effective potential is defined as

$$v_{eff}(\vec{r}) = \upsilon(\vec{r}) + \int\frac{\rho(\vec{r}')}{|\vec{r} - \vec{r}'|}d\vec{r}' + \frac{\delta E_{xc}[\rho]}{\delta\rho(\vec{r})}. \tag{2.36}$$

Since $v_{eff}(\vec{r})$ depends on the density, the Kohn-Sham equations must be solved self-consistently and the energy is subsequently evaluated via Equation 2.31.

If $E_{xc}[\rho]$ is neglected in the above equations, a solution analogous to the HF solution would be obtained. An exact expression for $E_{xc}[\rho]$ would make the above equations an exact method to determine molecular properties. However, such an expression is not available at this time and DFT methods currently used by computational chemists differ by the $E_{xc}[\rho]$ expression employed. The simplest expression for the exchange-correlation energy functional is provided by the local spin density approximation (LSDA)[13]

$$E_{xc}^{LSDA}[\rho^\alpha, \rho^\beta] = \int\varepsilon_{xc}^{LSDA}[\rho^\alpha(\vec{r}), \rho^\beta(\vec{r})]d(\vec{r}). \tag{2.37}$$

$\varepsilon_{xc}^{LSDA}$ represents the exchange-correlation energy per particle of a uniform electron gas of density $\rho$ and can be separated into its individual exchange and correlation components. The most common LSDA functional implemented in the literature consists of the Slater exchange[16] functional (S) in combination with the correlation functional of Vosko, Wilk and Nusair (VWN).[17]

The LSDA is applicable to slowly varying densities but not to atoms or molecules, which are highly inhomogeneous. The nonuniformity of the electron density can be accounted for by including gradients of the density in the exchange and correlation functionals,

$$E_{xc}^{GGA}[\rho^\alpha, \rho^\beta] = \int d(\vec{r})\varepsilon_{xc}[\rho^\alpha(\vec{r}), \rho^\beta(\vec{r}), \nabla\rho^\alpha, \nabla\rho^\beta]. \tag{2.38}$$

Functionals of this form are dependent on the generalized gradient approximation (GGA).[13] GGA functionals are referred to as gradient-corrected or nonlocal. The development of $E_{xc}[\rho]$ is broken into the development of an exchange and a correlation functional. The most popular correlation functionals used in the literature include that of Perdew (P86),[18] Perdew and Wang (PW91)[19] and Lee, Yang and Parr (LYP).[20] The most commonly used exchange functionals are those derived by Perdew and Wang (PW86)[21] and Becke (B or B88).[22]

In order to improve the GGA functionals, Becke believed that part of the exact exchange must be taken into account.[23] Through this realization, Becke developed a hybrid functional, where hybrid implies that these functionals combine DFT and HF methods. The hybrid functional developed by Becke can be expressed as a linear combination of HF, LSDA and B exchange contributions, together with LSDA and non-local correlation contributions (usually P86, PW91 or LYP). For example, the B3PW91 functional can be expressed as

$$E_{xc} = E_{xc}^{LSDA} + a_o\left(E_x^{exact} - E_x^{LSDA}\right) + a_x \Delta E_x^{B88} + a_c \Delta E_c^{PW91} \qquad (2.39)$$

where $a_o$, $a_x$ and $a_c$ are coefficients whose values are determined by fitting $E_{xc}[\rho]$ to experimental data (atomization energies, ionization potentials and proton affinities). All hybrid functionals are denoted B3C, where B3 represents Becke's three parameter functional and C represents the correlation functional.

The major advantage of DFT over the other methods discussed to this point is that it includes electron correlation (even at the lowest levels), but it is computationally efficient (requires few computer resources). The disadvantages of DFT include the fact that there is no systematic way to improve upon a calculation. For example, we can improve upon CIS by including double excitations (CISD) and this can be further improved by including approximate quadruple excitations through CCSD or QCISD. Thus, a lower energy and more reliable properties are expected from CCSD or QCISD. Alternatively, there is no systematic way to improve upon DFT methods. In addition, a lower energy by one DFT method does not guarantee that the functional used leads to more accurate molecular properties. Thus, all functional combinations must be tested to determine the best DFT method for a particular property. Due to the advantages of DFT

and the fact that it would be an exact method if an exact expression for the exchange-correlation functional was known, many books[24,25] and review articles[26,27] have appeared which discuss various aspects of DFT.

### *2.9 Basis Functions*

During the discussion of the Roothaan-Hall equations, it was mentioned that molecular orbitals are best described through a linear combination of atomic orbitals (LCAO). Thus, the problem of describing molecular orbitals ($\psi_i$) reduces to finding an accurate description of atomic orbitals ($\varphi_i$). Similarly, atomic orbitals can be expressed as a linear combination of a set of mathematical functions known as basis functions ($\phi$),

$$\varphi^{AO} = \sum_i c_i \phi_i^{BF} \,. \tag{2.40}$$

Basis sets, a finite group of basis functions, should contain enough functions to provide an accurate description of the atomic orbitals, while at the same time the number of functions should be small enough to maintain the feasibility of molecular calculations. It should be mentioned that expressing the atomic orbitals in terms of a basis set implies that a larger number of two-electron repulsion integrals, used to solve the Roothaan-Hall equations, must be evaluated since these are calculated with basis functions rather than atomic orbitals,

$$(\mu\upsilon|\lambda\sigma) = \iint \phi_\mu(1)\phi_\upsilon(1)\frac{1}{r_{12}}\phi_\lambda(2)\phi_\sigma(2)d\tau_1 d\tau_2 \,. \tag{2.41}$$

Ideally, basis functions should closely resemble atomic orbitals and thus functions of the following form are favorable,

$$\phi^{STO} \propto e^{-\eta|\vec{r}-\vec{R}_A|} \,. \tag{2.42}$$

These basis functions, known as Slater-type orbitals (STOs),[3,28] duplicate the properties of atomic orbitals with great accuracy. However, evaluation of the two-electron repulsion integrals using STOs is complicated. Thus, Gaussian functions or Gaussian-type orbitals (GTOs) are more commonly implemented,[3,28]

$$\phi^{GTO} \propto e^{-\alpha|\vec{r}-\vec{R}_A|^2} \,. \tag{2.43}$$

The advantage of using GTOs is that a product of Gaussians on two different centers is a Gaussian on a third center, implying that integral evaluation is greatly simplified. The disadvantage of GTOs is that they do not accurately describe atomic orbitals at $r = 0$ and at large $r$ they decay too rapidly.

In order to maintain the accuracy of STOs and the computational advantage of GTOs, STOs are commonly represented as a linear combination of GTOs. Pople and coworkers were the first to use this approximation through the following equation[3,28]

$$\phi_{\mu}^{CGTO} = \sum_{i=1}^{L} d_{i\mu} \phi_i^{GTO}(\alpha_{i\mu}, \bar{r} - \bar{R}_A) \tag{2.44}$$

where $L$ is the number of Gaussians in the contraction and the $d_{i\mu}$'s are the contraction coefficients. The atomic orbitals can now be expressed as

$$\varphi_i = \sum_{\mu} c_{\mu i} \phi_i^{CGTO} \tag{2.45}$$

where each $\phi^{CGTO}$ is a contracted GTO with fixed $d_{i\mu}$'s and the $c_{i\mu}$'s are optimized during the calculations. In Pople's basis sets, the GTOs, also known as primitives, are fitted through the optimization of the $d_{i\mu}$'s to best imitate the behavior of Slater orbitals. For example, the STO-3G basis set uses three GTOs ($L = 3$) in a fixed contraction scheme to mimic one STO. Other Gaussian basis sets differ from these by the number of GTOs used and the way they are linearly combined (contracted). In the search of greater accuracy, basis sets are often decontracted. Decontracting a basis set implies that each $\phi^{GTO}$ in Equation 2.44 is used directly in Equation 2.45 and individual coefficients are optimized for each function.

The STO-3G basis set discussed above is an example of the smallest basis set used in molecular calculations, a minimal basis set. Minimal basis sets use the least number of functions possible to describe the occupied atomic orbitals. For example, a minimal basis set on oxygen would consist of only 5 contracted GTOs ($1s$, $2s$, $2p_x$, $2p_y$, $2p_z$). Due to the small number of contracted GTOs and thus the small number of coefficients ($c_{i\mu}$) that can be optimized during a calculation, the variational flexibility of minimal basis sets must be improved upon. This can be accomplished by using a double-zeta split-valence basis set, which divides the description of orbitals into core and valence

orbitals and uses twice the number of functions as a minimal basis set to describe the valence orbitals. An example of this type of basis set commonly used is 6-31G. For atoms Li to F, this basis set uses 6 contracted GTOs to form one basis function to describe the core orbitals (1*s*), 3 contracted GTOs to form the first set of basis functions to describe the valence orbitals (2*s*, $2p_x$, $2p_y$, $2p_z$) and a single GTO to form each additional basis function to describe the valence orbitals. Thus, a double-zeta split-valence basis set of this form for oxygen would consist of 9 functions and 9 variational parameters, which is an improvement over the 5 used in a minimal basis set. Through using two sets of functions to define the valence region, a double-zeta split-valence basis set allows the orbitals to change shape depending on the molecular environment.

Additional flexibility in a basis set can be gained by further dividing the valence region into three (for example, the 6-311G basis set) or more partitions, but this leads to an unbalanced basis set since only the *s* and *p* space is described. The effects of an unbalanced basis set can be drastic. For example, an unbalanced basis set can predict ammonia to be planar. Additional Gaussians can be added to a basis set to extend its accuracy beyond that of a double-zeta split-valence basis set (6-31G). Polarization functions, or functions with a high angular momentum, can be added to account for distortion of the atomic orbitals in the molecular environment. For example, *d* or higher functions can be added to second row atoms (for example, 6-31G*, 6-31G(2df), etc.). Similarly, *p* or higher functions can be added to hydrogen basis sets (for example, 6-31G**, 6-31G(2df,pd), etc.). Alternatively, diffuse functions, or functions with small exponents, can be added to heavy atoms (6-31+G) or hydrogen (6-31++G). These functions account for large electron clouds by allowing the orbitals to occupy larger regions in space. This is particularly useful to describe systems where electrons are loosely bound, such as anions.

The above discussion shows that choosing an appropriate basis set can be challenging. Many research papers have examined the effects of different basis sets on a variety of molecular properties. In order to obtain results that can be compared to accurate experimental data, both the basis set and the theoretical method must be carefully considered. A large portion of the work to be presented within involves a

systematic study of methods and basis sets to determine which combination can provide an accurate prediction of oxygen hyperfine coupling constants.

### *2.10 Determination of Electronic Properties*

The primary goal of quantum chemistry is to use the aforementioned techniques to obtain information about electronic properties such as dipole moments, bond energies and hyperfine couplings to name but a few. In order to calculate these properties, an accurate description of the molecular geometry must first be acquired. Geometry optimizations involve searching the potential energy surface (PES) that describes the energy of a system as a function of its geometrical parameters.[4] Stationary points on this surface are identified by the first derivatives of the energy with respect to nuclear coordinates (the energy gradients) which must all equal zero. These stationary points are in turn characterized through the second derivatives of the energy (the force constants) which are proportional to the square of the vibrational frequencies. A minimum is defined as a point on the PES from which motion in any direction along the surface will lead to higher energy. Thus, at a minimum the surface possesses all positive force constants and consequently all positive frequencies. A transition state occurs at a point with maximum energy on the PES along the path connecting two minima and minimum energy for motion in any other direction on the surface. A transition structure can be identified through one negative force constant or, equivalently, one imaginary frequency. Higher order saddle points are also characterized through the number of imaginary frequencies they possess, however, these species are generally not of chemical interest.

Geometries calculated at low levels of theory are often comparable to those obtained with larger basis sets or more involved computational methods (high level of theory). Thus, geometries are commonly optimized ("best" arrangement of atoms determined) and characterized through a frequency analysis at low theoretical levels. Subsequently, these geometries are held fixed and electronic properties are calculated at a higher level of theory than that used to obtain the geometry. These calculations are called single-point calculations since a single geometry is used rather than optimizing all of the geometrical parameters. Through this technique accurate properties can be obtained at a

reduced computational cost since searching the PES for an optimum geometry is a time consuming process.

### *2.11 Hyperfine Coupling Constants*

Radicals provide one of the best examples of a practical application of the methods discussed in the present chapter since experimental identification of radicals is sometimes difficult. Theoretical difficulties lie in choosing the most appropriate method and basis set. This section will describe important features of experimental techniques used to identify radicals and theoretical methods suitable for the calculation of the property elucidated from experiment. The discussion of experimental methods will include some more detailed techniques used to identify species when interpretation of experimental spectra is complicated. The discussion of theoretical considerations will include the computational requirements for accurate prediction of radical properties in terms of both the theoretical method and the basis set. Additional concerns when comparing experimental and theoretical results will also be considered.

#### *2.11.1 Experimental Prediction*

The key experimental techniques implemented to identify radicals make use of the fact that radicals contain one or more unpaired electron(s) and therefore have a net spin angular momentum associated with them. The most common experimental method is referred to as electron spin resonance (ESR) or electron paramagnetic resonance (EPR) spectroscopy.[29,30]

To illustrate the concept of an ESR experiment the proton spectra of a methyl radical with three equivalent hydrogens will be discussed (Figure 2.2). An electron can possess one of two possible spin states corresponding to $\alpha$ (up or $^1/_2$) or $\beta$ (down or $-^1/_2$) spin. In the absence of a magnetic field these states are degenerate. However, upon application of a magnetic field many interactions arise and the degeneracy is removed. The first interaction to consider is the interaction between the unpaired electron and the magnetic field (electronic Zeeman interaction). This interaction splits the degenerate energy level of the electron into two levels. Next, any magnetic nuclei in the radical can also interact with the magnetic field (nuclear Zeeman interaction). In the proton spectra

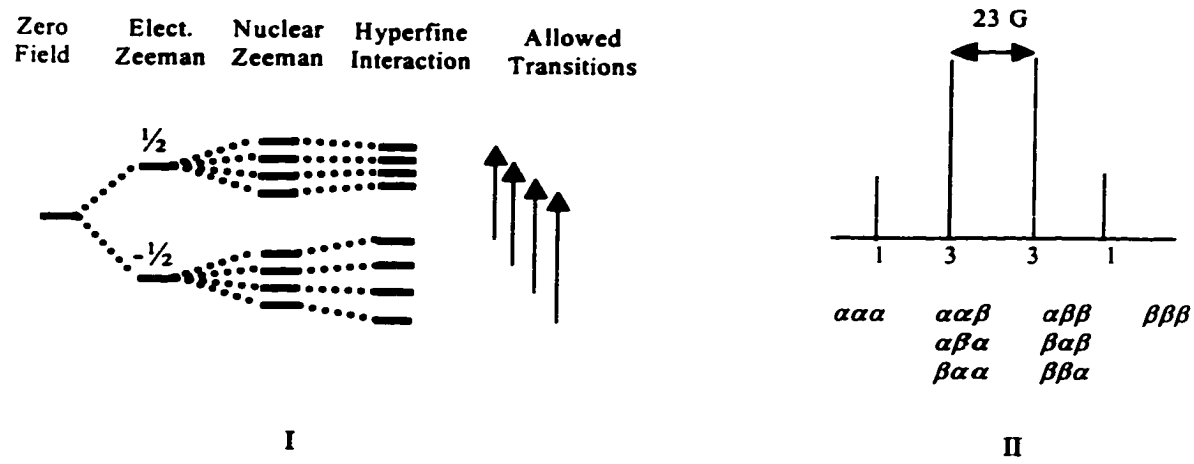


Figure 2.2: The interactions and allowed transitions which occur in the proton spectrum of the methyl radical, assuming all protons are equivalent (I). A model proton ESR spectrum depicting relative peak intensities and hyperfine coupling constant of approximately 23 G (II).

of the methyl radical, each hydrogen can possess spin $^1/_2$ or spin $-^1/_2$ and thus four possible states arise corresponding to all negative, one positive, two positive and three positive spins. Thus, this interaction splits each electronic level into four levels. The final modification of the electronic energy levels occurs due to the interaction between the unpaired electron and the magnetic nuclei (hyperfine interaction). This interaction slightly modifies each of the eight energy levels. Thus, four allowed transitions (those that change the orientation of the electron spin) exist for the methyl radical. The resulting ESR spectrum contains four peaks with relative intensities of 1:3:3:1, which correspond to the ratio of the degeneracy of each level. The hyperfine coupling constant (HFCC) can be obtained from the ESR spectra. The proton HFCC in the methyl radical is approximately 23 G. If it was instead assumed that all protons were inequivalent, then the degeneracy of the electronic levels would be lifted and the spectra would contain eight peaks of equal intensity.

In addition to protons, any nuclei possessing a net spin angular momentum will give rise to a hyperfine interaction. These nuclei include those with an odd mass number or those with an even mass number and odd nuclear charge. Examples of magnetic nuclei include $^{13}C$, $^{14}N$, $^{19}F$ and $^{17}O$. Each magnetic nucleus will split the electronic Zeeman levels into various sublevels depending on its spin. For example, $^{17}O$ possesses a

spin of $^5/_2$ and therefore will split each electronic energy level into six levels ($-^5/_2$, $-^3/_2$, $-^1/_2$, $^1/_2$, $^3/_2$, $^5/_2$).

A typical ESR experiment uses two magnetic fields: one static field and one oscillating field, which is applied perpendicular to the first. The static field splits the electronic energy levels and the oscillating field induces transitions between the levels. The radical will absorb energy from the oscillating magnetic field once the frequency ($\nu$) satisfies the following resonance condition

$$h\nu = g_e\beta_e B \tag{2.46}$$

where $h$ is Planck's constant, $g_e$ is the electronic g-value (2.00232), $\beta_e$ is the electronic Bohr magneton and $B$ is the strength of the applied magnetic field. Typically, the frequency is fixed and the field strength is scanned until resonance occurs.

In addition to ESR, hyperfine coupling constants can also be obtained from a rotational spectrum.[31] HFCCs arise in rotational spectra since the rotational angular momentum of an electron can generate a magnetic moment similar to the spin angular momentum giving rise to the magnetic moment considered in ESR. The magnetic moment can subsequently interact with magnetic nuclei and coupling models are applied to the experimental data to obtain HFCCs. Most of the experimental data to be discussed in this thesis have been obtained through ESR or related methods. Units of gauss (G), which are related to megahertz (MHz) through the conversion factor 2.8025, will be used throughout for the HFCCs.

### *2.11.2 More Detailed Experimental Techniques*

Since radicals are short-lived, extreme experimental conditions are often required to observe these species. For example, radicals are frequently isolated at low temperatures and in an external matrix.[32] Matrices commonly employed include rare gases (Ar, Ne), zeolites, $SF_6$ and chlorofluorocarbons (CFCs). The compound used to generate the radical of interest is mixed in low concentrations with a matrix substance. This mixture is subsequently cooled and the sample irradiated (usually $\gamma$- or X-rays). Upon irradiation, matrix molecules are the primary radiation targets since they are more abundant and the radical site is subsequently transferred to form the desired radical. For example, if a radical cation is desired, a matrix with a higher ionization potential than the

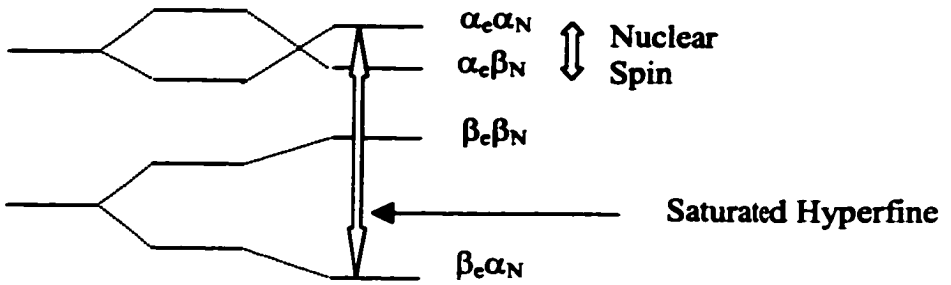


**Figure 2.3: Depiction of the ENDOR experiment, where the interactions between one proton and one electron have been considered.**

molecule under study is used, which allows the radical site to propagate until the radical cation of interest is generated.

The ESR spectra of solid samples can be quite complicated and hence more elaborate techniques must be used to identify radicals. Electron-nuclear double resonance (ENDOR) is a commonly employed method.[30,33] To illustrate this technique the interactions between one proton (spin $^1/_2$) and an electron will be considered. From the discussion of ESR, the interactions between the electron and the proton will result in four modified energy levels (Figure 2.3). During the ENDOR experiment, the population of the $\beta_e\alpha_N$ and $\alpha_e\alpha_N$ levels is made equivalent by applying a strong field that induces transitions between these two levels. Therefore, the electron resonance signal becomes weak and very broad (saturated hyperfine line). Subsequently, a magnetic field of an appropriate frequency is applied to induce transitions between the $\alpha_e\beta_N$ and $\alpha_e\alpha_N$ levels corresponding to a change in the orientation of the nuclear spin. At this instant the populations of the $\alpha_e\alpha_N$ and $\alpha_e\beta_N$ levels interchange. Hence, the populations of the $\beta_e\alpha_N$ and $\alpha_e\alpha_N$ levels are no longer equivalent and a peak in the ENDOR spectrum will appear until saturation is once again achieved at which point the peak falls back to its low value. Similarly, as the frequency is further increased, transitions between the $\beta_e\alpha_N$ and $\beta_e\beta_N$ levels will occur resulting in an additional ENDOR peak separated from the first by a value proportional to the hyperfine coupling constant.

The ENDOR technique has the advantage over traditional ESR that very small hyperfine couplings can be measured in conditions where many spectral lines overlap. Through ENDOR it is possible to observe each radical species independently and the

spectral lines are sharper, closely resembling nuclear resonance lines. In addition, direct information about the nucleus leading to each coupling can be obtained. Thus, this method is favorable if many lines appear in the ESR spectrum, more accurate HFCCs are required or the identity of a magnetic nucleus is desired. Since the radicals generated in biological systems often possess similar characteristics, the resulting ESR spectra are very complicated and the ENDOR technique can be useful to characterize radical sites. For example, this technique can be used to determine the protonation state of a radical.

Another useful technique is called electron spin-echo envelope modulation (ESEEM).[30] During an ESEEM experiment, a magnetic field ($B_1$) is applied perpendicular to the static field ($B_o$) for a short time period and the net magnetization (M) of the system is redirected onto the plane perpendicular to the direction of the original orientation (Figure 2.4, I and II). After the field $B_1$ has been turned off for some time

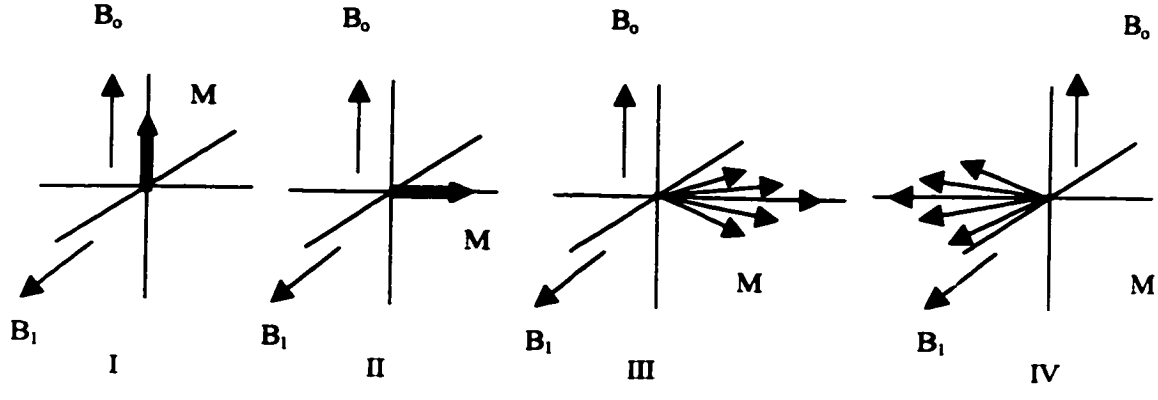


Figure 2.4: Description of the ESEEM technique. A field ($B_1$) is applied perpendicular to the static field (I). As a result of $B_1$, the magnetization is orientated in a plane perpendicular to the original orientation (II). After some time $\Delta t$, the magnetization is dephased (III). The field $B_1$ is reapplied to reverse the orientation of the magnetization (IV). A signal (echo) grows and decays due to the realignment of the spins followed by dephasing.

interval ($\Delta t$), the spins resulting in the net magnetization dephase or spread out in the plane (Figure 2.4, III). The field $B_1$ is applied again for a short time, which has the effect of reversing the orientation of the spins (Figure 2.4, IV). This causes the dephasing to reverse and a net magnetization grows and then dephases again after a time interval $\Delta t$. The growth and decay of the net magnetization results in ESR signal growth and decay (an echo). The amplitude of the echo versus time interval between the applied fields ($\Delta t$) can be plotted as a decay curve. In some systems, complex features are observed on this

decay curve (the envelope), which represent fluctuations (modulations) in the curve. Mathematical manipulation (Fourier transformation) converts this time domain curve to a frequency domain curve. Examination of the frequency domain curve reveals that the fluctuations are a direct result of hyperfine interactions. Through ESEEM experiments, data for nuclei weakly coupled to that possessing spin density can be obtained, thus providing another very powerful experimental tool. ESEEM results are usually more accurate than those obtained from ESR.

### *2.11.3 Theoretical Description*

From experimental ESR spectra, information about the radical such as the multiplicity or the number of equivalent atoms can be obtained. However, a lot of properties are left undetermined such as the geometry, atomic composition, charge distribution, effects of hydrogen bonding, protonation state and reaction mechanisms. Since there exist many experimental unknowns, theory may be able to play an important role. In particular, the hyperfine coupling constant can be determined from theoretical calculations. Through comparison of experimental and theoretical HFCCs more information about the nature of the species detected experimentally can be obtained.

The hyperfine coupling constant is a tensor composed of two main contributions. The first contribution is called the isotropic hyperfine coupling constant ($A_{iso}$).[29] This component can be obtained from theoretical calculations through the following equation

$$A_{iso} = \frac{4\pi}{3} g_e \beta_e g_N \beta_N \langle S_z \rangle^{-1} \rho^{\alpha-\beta}(0) \tag{2.47}$$

where $g$ and $\beta$ are the g-factor and Bohr magneton, the subscripts $e$ and $N$ represent the electronic and nuclear constants, $\langle S_z \rangle$ is the expectation value of the $S_z$ operator (½ for free radicals) and $\rho^{\alpha-\beta}(0)$ is the unpaired spin density at the nucleus. The unpaired spin density is defined by convention to be the difference between the $\alpha$ and $\beta$ spin densities normalized to unity. Thus, if $N_\alpha$ and $N_\beta$ are the number of $\alpha$ and $\beta$ electrons, respectively, then the spin density can be defined as

$$\rho^{\alpha-\beta}(r) = \frac{\rho^{\alpha}(r) - \rho^{\beta}(r)}{N_\alpha - N_\beta}. \tag{2.48}$$

Thus, the isotropic HFCC yields a description of the unpaired spin distribution in the molecule. Since this contribution depends only on the electron density at the nucleus, it is often referred to as the Fermi contact term. This component has no classical counterpart and information about the sign of the isotropic coupling constant is sometimes difficult to obtain experimentally.

The second contribution to the HFCC measures the anisotropy of the spin distribution in a molecule and the *ij*th component of this tensor for nuclei $N$ can be calculated from

$$T_{ij}^{(N)} = \frac{1}{2} g_e \beta_e g_N \beta_N \langle S_z \rangle^{-1} \sum_{\mu\upsilon} P_{\mu\upsilon}^{\alpha-\beta} \left\langle \varphi_\mu \left| \bar{r}_{kN}^{-5} (\bar{r}_{kN}^2 \delta_{ij} - 3\bar{r}_{kN,i}\bar{r}_{kN,j}) \right| \varphi_\upsilon \right\rangle \qquad (2.49)$$

where $P_{\mu\upsilon}^{\alpha-\beta}$ is an element of the spin density matrix and the other variables have been defined previously. This contribution, referred to as the anisotropic HFCC, arises due to the interaction between two dipoles.[29] Experimentally, the anisotropic couplings will average to zero in a spherically symmetric environment or in a situation where molecules can tumble freely, for example in solution.

Experimentally, three basic numerical parameters ($A_{XX}$, $A_{YY}$, $A_{ZZ}$), the principal components of the HFCC matrix, are obtained. These can be obtained in a special set of coordinate axes (the principal-axis system). The principal components arise simply as the sum of the isotropic and the anisotropic coupling tensors,

$$\begin{bmatrix} A_{XX} & 0 & 0 \\ 0 & A_{YY} & 0 \\ 0 & 0 & A_{ZZ} \end{bmatrix} = \begin{bmatrix} A_{iso} & 0 & 0 \\ 0 & A_{iso} & 0 \\ 0 & 0 & A_{iso} \end{bmatrix} + \begin{bmatrix} T_{XX} & 0 & 0 \\ 0 & T_{YY} & 0 \\ 0 & 0 & T_{ZZ} \end{bmatrix}. \qquad (2.50)$$

Sometimes, it is also useful to define the components of the HFCCs perpendicular ($A_\perp$) and parallel ($A_\parallel$) to a particular bond, which is often assumed to be in the direction of the z-axis. The relation of these parameters to those previously defined is

$$A_\perp = A_{iso} + \tfrac{1}{2}(T_{XX} + T_{YY}), \qquad (2.51)$$

$$A_\parallel = A_{iso} + T_{ZZ}. \qquad (2.52)$$

Theoretically, the equation describing the isotropic component is easy to evaluate, but $A_{iso}$ is difficult to calculate accurately since it depends on the spin density at only one point in space and thus an accurate description of this point is required. The anisotropic

HFCCs are more time consuming to evaluate, but can be obtained to a greater degree of accuracy since the integrals are calculated over all space rather than at only one point. Even at the lowest levels of theory, the anisotropic components can be calculated with a great degree of accuracy. Thus, interest lies in the accurate calculation of the isotropic HFCC. The main contributions to the spin density upon which the isotropic coupling is based include:[34]

1. a zero-order (direct) effect arising from the orbital occupied by the unpaired electron;
2. a first-order (indirect or spin polarization) effect arising from interactions between the unpaired electron and the paired electron(s), which leads to a propagation of the spin throughout the molecule;
3. second or higher-order effects arising due to electron correlation.

Considering that the isotropic HFCC depends on the unpaired spin density at the nucleus and interactions between electrons, a very good description of the core and inner-valence regions will be required to calculate this property accurately. This would indicate that basis sets must describe the core region precisely. In addition, since correlation effects become important near the nucleus, it would be expected that the isotropic HFCCs require electron correlation in order to be predicted with any accuracy. Thus, it appears that both the computational method and the basis set should be chosen carefully for the calculation of this property. These computational requirements have been the topic of several review articles[35,36,37] and will be discussed in more detail in the following sections.

### *2.11.4 Survey of Computational Methods*

The simplest *ab initio* techniques that can be used to examine open-shell molecules are the ROHF and UHF methods. ROHF is not a suitable method since it incorrectly predicts the isotropic HFCC in $\pi$-radicals to be zero. This can be understood through consideration of the effects leading to $A_{iso}$. In particular, the unpaired electron is located in a $p$ orbital that has a node at the nucleus and therefore no direct effects will contribute to the HFCC. Indirect effects will also lead to a zero contribution since under the ROHF formalism the paired electrons are forced to occupy the same spatial orbital and hence the contributions from these electrons will cancel. In addition, second or

higher-order effects arising from electron correlation make no contribution since the main portion of electron correlation is not accounted for in ROHF. Thus, $A_{iso}$ is predicted to have a value of zero although experimentally many $\pi$-radicals possess large isotropic couplings.

The failure of the ROHF method can be overcome through the UHF formalism. In this technique, a different spatial arrangement is allowed for spin pairs. Thus, interactions between the unpaired electron and the paired electrons can lead to spin polarization and a net unpaired spin density. However, the downfall of the UHF method is that large spin contamination occurs for many systems. This leads to an overestimation of the isotropic HFCC. The AUHF and PUHF methods can be used in order to eliminate a large portion of the spin contamination and hence lead to improved HFCCs. However, these methods have been shown to be unreliable and there is no theoretical explanation for why these methods perform better than UHF.[37] In particular, PUHF does not always reproduce the correct experimental trends in the magnitude of the couplings.[35] In order to ensure that results obtained from theoretical calculations are trustworthy, higher levels of theory must be used. Specifically, as mentioned earlier, electron correlation is expected to be important when examining isotropic HFCCs.

The simplest method to include electron correlation is through low orders of Møller-Plesset perturbation theory. MP2 up to estimated MP5 techniques have been investigated as possible methods for the calculation of accurate HFCCs. Calculations estimating an infinite order of perturbation have proven adequate for the determination of atomic HFCCs as well as those for the $B_2$ molecule.[38] However, calculations that use lower orders of perturbation are unreliable and do not converge fast enough to make these methods feasible for the calculation of HFCCs.[8] Since MP methods are based on the UHF wave function, spin contamination can occur. Spin-projection of the quartet and sextet contaminants reduces the variation in the MP results, but satisfactory results are difficult to obtain at low orders of perturbation.

Another method to account for electron correlation discussed in the present chapter is through the addition of important configurations to the wave function. As previously discussed, full CI is much too expensive and truncated CI methods must be

used, such as CIS or CISD. In addition, higher-order excitations can be accounted for through coupled-cluster or quadratic CI methods. Studies on these techniques[36] have determined that the inclusion of single excitations is very important and methods that account for only double excitations (CID, CCD, QCID) prove to be inadequate to calculate the HFCCs accurately. It has also been noted that methods which account for only single excitations, such as CIS, yield couplings in very good agreement with experiment. Unfortunately, this good agreement is due to fortuitous cancellation of errors and these methods should not be relied upon if accurate data is desired. In general, it has been concluded that QCISD out performs both CISD and CCSD and results within 10 to 20% of the experimental values can be obtained. Nitrogen HFCCs in the NO molecule have been calculated with the techniques discussed above[8] and the results are compared to experiment in Table 2.1. These results illustrate the quality of HFCCs that can be expected from each method.

Table 2.1: Values of the nitrogen isotropic HFCCs (G) calculated for the NO molecule with a modified form of a triple-zeta basis set.

| Method | $A_{iso}(^{14}N)$ |
|---|---|
| UHF | 21.0 |
| PUHF | 42.8 |
| MP2 | -19.4 |
| PMP2 | 2.2 |
| MP3 | 6.0 |
| PMP3 | 12.2 |
| MP4 | -11.6 |
| PMP4 | 6.8 |
| QCID | -6.9 |
| QCISD | 9.1 |
| QCISD(T) | 8.0 |
| CCD | -6.8 |
| CCSD | 8.6 |
| CCSD(T) | 6.7 |
| Experimental | 8.0 |

Triple excitations are also known to be important for the calculation of accurate isotropic HFCCs. Directly including triple excitations in CI, CC and QCI techniques is very expensive. Alternate techniques have appeared in the literature that approximate the effects of triples through the use of perturbation theory (QCISD(T) and CCSD(T)) and good results for the HFCCs can be obtained.[37] The relative accuracy of these methods to those discussed above is illustrated in Table 2.1. Multi-reference configuration

interaction has also been implemented to calculate HFCCs. This method was first applied to atoms[39] and subsequently to small molecules.[8,40] MRCI is attractive since excitations most important to the calculation of HFCCs can be included with additional reference configurations. For example, triple excitations are directly included through double excitations with respect to some of the additional reference configurations. Thus, this method is expected to yield more reliable results for HFCCs than QCISD(T) or CCSD(T) which only approximate the inclusion of the triple excitations. However, due to difficulties in determining which configurations to include in a calculation (reference space and configuration selection thresholds), the convergence of MRCI results to the experimental values is sometimes slow.

An improvement over traditional MRCI methods can be obtained through methods that correct for excitations not included in the MRCI calculation. One such technique is the MRCI-$B_k$ method.[41] Configurations can affect the wave function directly (through their inclusion into the wave function) or indirectly (through interactions between the additional configurations and configurations already present in the wave function). The MRCI-$B_k$ method uses the fact that indirect effects of triple and quadruple excitations are more important than direct effects. Thus, including the indirect effect of these excitations through second-order perturbation theory should lead to an improved wave function without explicitly including all configurations in the wave function. In the MRCI-$B_k$ method, corrections are made to the MRCI wave function by accounting for important configurations or those with coefficients greater than some threshold value ($B_k$). The improvement upon the MRCI results obtained with this method for the CH radical[36] is displayed in Table 2.2. Both MRCI and MRCI-$B_k$ methods are time consuming and have only been applied to small radicals.[36]

Table 2.2: Comparison of HFCCs (G) obtained with the MRCI and MRCI-$B_k$ methods for the CH radical.

| Method | $A_{iso}(^{13}C)$ | $A_{iso}(^{1}H)$ |
|---|---|---|
| QCISD | 43.7 | -58.5 |
| QCISD(T) | 42.1 | -57.2 |
| MRCI | 37.2 | -56.3 |
| MRCI-$B_k$ | 45.8 | -58.5 |
| Experimental | 46.8 | -57.7 |

The use of density-functional theory to calculate electronic properties, including HFCCs, has increased since the early 1990's. Despite the fact that the lowest level of DFT (LSDA) accounts for electron correlation, unacceptable isotropic couplings are obtained since the density is not localized. GGA functionals lead to improved HFCCs. This arises mainly because these functionals move density from the outer-core and valence regions to the core, the region upon which isotropic HFCCs are most dependent.[37] Since all GGAs were developed independently and thus provide a different description of the density, isotropic HFCCs are very dependent on the functional form. Although DFT methods are based on an unrestricted formalism, spin-contamination is less a concern than it is with UHF based techniques. Due to the design of better DFT functionals and the advantage of small computer requirements, DFT has been applied to numerous systems in the literature. The relative accuracy of functional combinations for two small molecules is displayed in Table 2.3.[42] The B3LYP and PWP86 functional combinations have been shown to calculate HFCCs most accurately,[37] especially for carbon and hydrogen couplings. On a series of hydrocarbons, the PWP86 functional underestimates hydrogen couplings by approximately 5-15%, while the B3LYP functional slightly overestimates some hydrogen couplings.[43] Since results for biological systems are primarily obtained from proton spectra, these functionals are increasingly used to study biological radicals.[44] Two main deficiencies of DFT are $\sigma^{\bullet}$-radicals and transition metal complexes or clusters. Poor HFCCs arise in these systems due to poorly described geometries and inadequate basis sets.[37]

Table 2.3: Comparison of isotropic HFCCs (G) obtained for CN and $HCN^-$ molecules with a variety of density functionals.

| Molecule | Atom | SVWN | BLYP | B3LYP | BP86 | B3P86 | Exp. |
|---|---|---|---|---|---|---|---|
| CN | $^{13}C$ | 177.1 | 181.2 | 196.9 | 174.5 | 201.4 | 210.0 |
| | $^{14}N$ | -1.9 | -2.0 | -6.0 | -4.1 | -7.9 | -4.5 |
| $HCN^-$ | $^{13}C$ | 96.7 | 105.0 | 102.3 | 99.3 | 97.9 | 75.4 |
| | $^{14}N$ | 2.4 | 4.6 | 6.0 | 3.1 | 4.6 | 7.1 |
| | $^{1}H$ | 109.9 | 127.3 | 131.0 | 117.8 | 124.6 | 137.2 |

In summary, the above discussion provides a clear picture of the difficulty in obtaining a wave function accurate enough for reliable calculations of the isotropic HFCCs. The strict demands placed on computational techniques by this property also extend to the basis set requirements.

### *2.11.5 Basis Set Requirements*

The basis sets required to obtain accurate HFCCs are more complicated than those necessary to calculate many electronic properties (for example, geometries or reaction mechanisms). Basis sets no smaller than triple-zeta quality can be used to obtain accurate couplings.[37] For isotropic HFCCs, the region around the nucleus must be described very accurately. Unfortunately, Gaussian functions fail to properly describe this area indicating that many functions should be linearly combined to describe the core region. Specifically, *s*-functions with very large exponents are often added to basis sets or *s*-functions in the outer-core region are decontracted to describe the area close to the nucleus more accurately. Since a delicate portrayal of the core is required, STOs can be considered to be the "best" basis functions for the calculation of isotropic HFCCs. However, due to computational costs these basis sets have mostly been used in conjunction with semi-empirical techniques.[37] Density-functional methods have also implemented STOs to study small molecules.[37]

In addition to describing the core region, a basis set for the calculation of HFCCs must be well balanced. This means that the valence space must also be well represented. Polarization functions are also essential for reliable HFCCs. Diffuse functions can lead to improved results in some cases although these functions drastically increase the computational cost. These demands indicate that appropriate basis sets for the calculation of HFCCs include many functions.

### *2.11.6 Additional Computational Considerations*

One of the main assumptions of electronic structure calculations is that results calculated in the gas phase at zero Kelvin can be compared to experimental results obtained at a variety of temperatures in solution or in crystals. This assumption is generally supported by the good agreement observed between theory and experiment. However, even in experiments performed at low temperatures with radicals isolated in a matrix, vibrational motion and crystal effects can influence the hyperfine coupling constants.

Vibrational effects have been included in electronic structure calculations through a variety of methods. MRCI has been used to obtain a vibronically corrected wave function and HFCCs.[37] Accurate HFCCs can be obtained from this method, but the

process involves searching the entire potential energy surface of a molecule and is therefore very time consuming. A more common approach is to use a Boltzmann population analysis to approximate the relative population of vibrational levels.[37] The HFCCs obtained at the optimized geometry are subsequently adjusted using the values calculated at each vibrational level, where the magnitude of the adjustment depends on the relative population of each level. This method has implemented less demanding methods such as DFT or CIS.

The effects of the local environment have also been accounted for in some calculations. One technique is to use a "supermolecule" approach where, for example, the first shell of rare gas atoms is directly included in every aspect of the calculation (geometry optimization and single-point calculation).[37] Alternatively, the effects of a solvent can be examined with various solvation models. The Onsager model, which estimates interactions with the solvent by describing the molecule of interest as a sphere with a set dipole moment and the solvent through a dielectric constant, has been used on occasion.[37] More complicated solvation models have also been used to estimate the effects of a solvent on HFCCs.

A combined quantum mechanics and molecular dynamics (QM/MD) technique has also been used to investigate both vibrational and matrix effects.[45] This technique uses molecular mechanics to describe the matrix environment and quantum mechanics to describe the molecule of interest. Essentially, a molecular dynamics simulation is performed where a quantum mechanical calculation is carried out at each time step and the temperature is held fixed. Through QM/MD the motion of the molecule and the resulting changes in the HFCCs can be monitored as a function of time. Some studies have implemented MP2 as the QM method, but if HFCCs are desired then DFT is a more promising method since MP techniques are known to be unreliable for this property. This combined technique is favorable over the aforementioned methods since both vibrational and matrix effects are taken into account in the same calculation. The disadvantage is this method is computationally expensive since many time steps are required for averaged results and each time step involves a QM calculation. The temperature and matrix effects on the HFCCs obtained from QM/MD calculations on the ethane radical cation[46] are displayed in Table 2.4. The results show that for the ethane

Table 2.4: HFCCs (G) calculated for the ethane radical cation with the QM/MD method implementing the B3LYP functional as the QM method and the 6-311G(d,p) basis set.

| Method | $A_{iso}(^1H)$ | Method | $A_{iso}(^1H)$ |
|---|---|---|---|
| B3LYP 0 K | 125.4 | B3LYP 60 K | 52.7 |
| B3LYP 4 K | 149.5 | B3LYP 100 K | 53.8 |
| Experimental 4 K | 152.5 | Experimental 70 K | 50.3 |

radical cation, vibrational effects are important even at 4 K where improved results are obtained from simulations performed at this temperature relative to the static, gas phase results at 0 K. In addition, experimental temperature effects on the HFCCs are well reproduced.

### *2.12 Conclusions*

The present chapter outlined many of the approaches (*ab initio* and density-functional) commonly used in theoretical calculations. In addition, experimental and theoretical methods applied to radicals were considered. From these discussions, it is apparent that many theoretical methods and basis sets are available to examine molecular systems. However, not all methods are suitable to investigate radicals. An understanding of the method and basis set requirements to calculate accurate hydrogen, carbon and nitrogen couplings is available from the literature. The direct extension of these results to the calculation of oxygen HFCCs is not apparent. Thus, the present thesis can be divided into two parts. First, a comprehensive survey of many of the methods discussed in this chapter will be presented in order to determine which methods and basis sets yield accurate oxygen hyperfine coupling constants (Chapter Three). Secondly, methods known to yield accurate hydrogen couplings will be used to investigate radicals generated upon irradiation of DNA components (Chapters Four through Six). Consideration of available computational resources, the desired level of accuracy and appropriate methods outlined in the present chapter, indicate that density-functional theory is the most suitable method to examine DNA radicals.

### *2.13 References*

1. McQuarrie, D. A. *Quantum Chemistry*; University Science Books: California, 1983.

2. Levine, I. N.; *Quantum Chemistry*; Prentice Hall: New Jersey, 1991.

3. Szabo, A.; Ostlund, N. S. *Modern Quantum Chemistry: Introduction to Advanced Electronic Structure Theory*; MacMillan Publishing Co., Inc.: New York, 1982.

4. Hehre, W. J.; Radom, L.; Schleyer, P. v. R.; Pople, J. A. *Ab Initio Molecular Orbital Theory*; John Wiley & Sons, Inc.: New York, 1986.

5. (a) Amos, A. T.; Hall, G. G. *Proc. Roy. Soc. A* **1961**, *263*, 483; (b) Amos, A. T.; Hall, G. G. *J. Chem. Phys.* **1964**, *41*, 1773.

6. (a) Harriman, J. E. *J. Chem. Phys.* **1964**, *40*, 2827; (b) Phillips, D. H.; Schug, J. C. *J. Chem. Phys.* **1974**, *61*, 1031.

7. *Methods of Electronic Structure Theory;* Schaeffer, H. F., III, Ed.; Plenum Press: New York, 1977.

8. Feller, D.; Glendening, E. D.; McCullough, E. A., Jr.; Miller, R. J. *J. Chem. Phys.* **1993**, *99*, 2829.

9. Feller, D.; Davidson, E. R. *J. Chem. Phys.* **1981**, *74*, 3977.

10. Chipman, D. M. *J. Chem. Phys.* **1989**, *91*, 5455.

11. Chipman, D. M. *Theor. Chim. Acta* **1989**, *76*, 73.

12. Pople, J. A.; Head-Gordon, M.; Raghavachari, K. *J. Chem. Phys.* **1987**, *87*, 5968.

13. Parr, R. G.; Yang, W. *Density-Functional Theory of Atoms and Molecules*; Oxford University Press: New York, 1989.

14. Hohenberg, P.; Kohn, W. *Phys. Rev. B* **1964**, *136*, 864.

15. Kohn, W.; Sham, L. J. *Phys. Rev. A* **1965**, *140*, 1133.

16. Dirac, P. A. M. *Proc. Cambridge Phil. Soc.* **1930**, *36*, 376.

17. Vosko, S. H.; Wilk, L.; Nusair, M. *Can. J. Phys.* **1980**, *58*, 1200.

18. (a) Perdew, J. P. *Phys. Rev. B* **1986**, *33*, 8822; (b) Perdew, J. P. *Phys. Rev. B* **1986**, *34*, 7406.

19. Perdew, J. P.; Wang, Y. *Phys. Rev. B* **1992**, *45*, 13244.

20. Lee, C.; Yang, W.; Parr, R. G. *Phys. Rev. B* **1988**, *37*, 785.

21. Perdew, J. P.; Wang, Y. *Phys. Rev. B* **1986**, *33*, 8800.

22. Becke, A. D. *Phys. Rev. A* **1988**, *38*, 3098.

23. Becke, A. D. *J. Chem. Phys.* **1993**, *98*, 1372.

24. *Chemical Applications of Density-Functional Theory;* Laird, B. B.; Ross, R. B.; Ziegler, T., Eds.; American Chemical Society: Washington, 1996.

25. *Modern Density Functional Theory. A Tool For Chemistry;* Seminario, J. M.; Politzer, P.; Eds.; Elsevier: Amsterdam, 1995.

26. Ziegler, T. *Chem. Rev.* **1991**, *91*, 651.

27. Kohn, W.; Becke, A. D.; Parr, R. G. *J. Phys. Chem.* **1996**, *100*, 12974.

28. Davidson, E. R.; Feller, D. *Chem. Rev.* **1986**, *86*, 681.

29. Weltner, W., Jr. *Magnetic Atoms and Molecules*; Van Nostrand Reinhold Company Inc.: New York, 1983.

30. Weil, J. A.; Bolton, J. R.; Wertz, J. E. *Electron Paramagnetic Resonance. Elementary Theory and Practical Applications*; John Wiley & Sons, Inc.: New York, 1994.

31. Townes, C. H.; Schawlow, A. L. *Microwave Spectroscopy*; McGraw-Hill: New York, 1955.

32. *Chemistry and Physics of Matrix-Isolated Species;* Andrews, L.; Moskovits, M., Eds.; Elsevier Science Publishers B.V.: Amsterdam, 1989.

33. Carrington, A.; McLachlan, A. D. *Introduction to Magnetic Resonance with Applications to Chemistry and Chemical Physics*; Harper & Row: New York, 1967.

34. Chipman, D. M. *Theor. Chim. Acta* **1992**, *82*, 93.

35. Feller, D.; Davidson, E. In *Theoretical Models of Chemical Bonding, Part 3, Molecular Spectroscopy, Electronic Structure and Intramolecular Interactions;* Maksic, Z. B., Ed.; Springer-Verlag: Berlin, 1991.

36. Engels, B.; Eriksson, L. A.; Lunell, S. *Adv. Quantum Chem.* **1996**, *27*, 297.

37. Eriksson, L. A. In *Encyclopedia of Computational Chemistry*, Schleyer, P. v. R., Ed.; Wiley and Sons: New York, 1998.

38. Carmichael, I. *J. Phys. Chem.* **1989**, *93*, 93.

39. Feller, D.; Davidson, E. R. *J. Chem. Phys.* **1988**, *88*, 7580.

40. Kong, J.; Boyd, R. J.; Eriksson, L. A. *J. Chem. Phys.* **1995**, *102*, 3674.

41. (a) Engels, B. *Chem. Phys. Lett.* **1991**, *179*, 398; (b) Engels, B. *J. Chem. Phys.* **1994**, *100*, 1380.

42. Gauld, J. W.; Eriksson, L. A.; Radom, L. *J. Phys. Chem. A* **1997**, *101*, 1352.

43. Eriksson, L. A. *Mol. Phys.* **1997**, *91*, 827.

44. Eriksson, L. A.; Himo, F. *Trends in Physical Chemistry* **1997**, *6*, 153.

45. Eriksson, L. A.; Laaksonen, A. *Rec. Dev. Phys. Chem.* **1998**, *2*, 369.

46. Wetmore, S. D.; Boyd, R. J.; Eriksson, L. A.; Laaksonen, A. *J. Chem. Phys.* **1999**, *110*, 12059.

# *CHAPTER THREE*

# Hyperfine Structures of Peroxyl and Hydroxyl Radicals

## *3.1 Introduction*

The techniques discussed in Chapter Two for the calculation of accurate hyperfine coupling constants will now be applied to the specific problem of oxygen centered radicals. This chapter focuses on the calculation of accurate oxygen HFCCs in peroxyl radicals, as well as the hydroxyl radical. Calculations on peroxyl radicals will include the determination of the HFCCs in large molecules, where accurate experimental data exists, with density-functional theory. As will be shown, satisfactory agreement can be obtained with DFT for alkyl peroxyl radicals. However, DFT results for an inorganic peroxyl radical (fluoroperoxyl radical) do not coincide with experiment. Attempts will be made to improve upon DFT results using higher levels of theory. A systematic study of a variety of methods will be performed on the hydroxyl radical to elucidate the most accurate method for the calculation of $^{17}O$ HFCCs. Additionally, a combined quantum mechanics and molecular dynamics technique will be discussed. This unique approach will be introduced and applied to the problem of calculating accurate coupling constants in small, inorganic peroxyl radicals.

## *3.2 Examination of Density-Functional Methods*

Experimentally, Fessenden and Schuler obtained the first $^{17}O$ HFCCs for alkyl peroxyl radicals.[1] Later, Melamud *et al.*[2] obtained a ratio of 0.56:0.44 for the terminal to inner oxygen atom spin densities. Alternatively, Bower *et al.*[3] concluded that there exists an equal spin distribution in peroxyl radicals, which is highly unlikely. Adamic *et al.*[4] were the next to examine oxygen labeled peroxyl radicals and the ratio of the spin densities was determined to be 2:1. In these experimental studies, it was speculated that the larger HFCC should be associated with the terminal oxygen. However, it was not until a study that specifically labeled the terminal oxygen in *t*-butyl peroxyl radical with $^{17}O$ was performed that this assignment could be made with confidence.[5] The oxygen HFCC obtained from the $^{17}O$ labeling experiment was in good agreement with the HFCCs assigned to the terminal oxygen in other alkyl peroxyl radicals. Hence, it was

concluded that the terminal oxygen possesses the larger HFCC. As mentioned above and in Chapter One, experimental studies have arrived at different conclusions about the spin distribution in peroxyl radicals and theoretical calculations would be useful to clarify these discrepancies and reveal important information about this class of radicals.

### *3.2.1 Computational Details*

The B3LYP functional combined with the 6-311+G(d,p) basis set was used for the geometry optimizations. Single-point calculations were performed on these geometries with a variety of basis sets including Pople's 6-31G and 6-311G series, up to 6-311+G(2df,p),[6] the IGLO-III basis set of Kutzelnigg *et al.*,[7] and the correlation-consistent polarized-valence triple-zeta basis sets of Dunning *et al.*[8] (CC-PVTZ and aug-CC-PVTZ). Once satisfactory results were obtained from the basis set study, other functionals discussed in Chapter Two were examined including BLYP, BP86, BPW91, B3P86 and B3PW91. These calculations were performed with GAUSSIAN 94.[9] The deMon[10] program was used for the calculation of the anisotropic HFCCs with Perdew and Wang's non-local exchange (PW86) and Perdew's non-local correlation functional (P86), together with the IGLO-III orbital basis set. The H: (5,1;5,1), C-F: (5,2;5,2), and Cl: (5,4;5,4) auxiliary basis sets were used to fit the spin density and the exchange-correlation potential. The anisotropic results deviate from experiment by less than ±2 G. This implies that any discrepancies in the HFCCs reside almost exclusively in the isotropic component and, hence, the discussion within will be concerned only with this component.

The radicals investigated include FOO, OH, $(CH_3)_3COO$, $ClH_2COO$, $HO(CH_2)_3OO$, $CO_2HCH_2OO$, and $HOCHCH_3OO$, with emphasis placed on the peroxyl functional group. The molecules FOO and OH were chosen since they are two of the smallest oxygen centered radicals for which accurate experimental HFCCs exist.[11,12,13]

### *3.2.2 Alkyl Peroxyl Radicals*

#### *3.2.2.1 Basis Set Study*

The results for the basis set study will be discussed in terms of the results obtained for all radicals examined, excluding FOO. The results for *t*-butyl peroxyl radical (Table 3.1) were chosen to illustrate the typical HFCCs obtained for all species

studied.[14] For the alkyl peroxyl radicals, the HFCCs obtained using the 6-31G(d,p) basis set are in good agreement with experiment. Expanding this basis set from double-zeta valence (6-31G(d,p)) to triple-zeta valence (6-311G(d,p)) leads to a uniform deterioration in the results. Improvement upon triple-zeta valence HFCCs is found by adding a set of diffuse functions (6-311+G(d,p)) and further improvement is obtained by including additional polarization functions (6-311+G(2df,p)). Results using the largest triple-zeta valence basis set implemented in this study, 6-311+G(2df,p), are still on average approximately 8.8 G (terminal oxygen) and 3.2 G (inner oxygen) smaller in magnitude than the experimental results.

Table 3.1: Isotropic HFCCs (G) in *t*-butyl peroxyl radical calculated with the B3LYP functional and a variety of basis sets.

| Basis Set | $A_{iso}(^{17}O_{terminal})$ | $A_{iso}(^{17}O_{inner})$ | $A_{iso}(^{13}C)$ |
|---|---|---|---|
| 6-31G(d,p) | -17.9 | -13.0 | -3.4 |
| 6-31+G(d,p) | -20.9 | -14.1 | -3.4 |
| 6-31+G(2df,p) | -21.6 | -14.4 | -3.4 |
| 6-311G(d,p) | -11.0 | -8.4 | -3.7 |
| 6-311+G(d,p) | -11.6 | -8.7 | -3.6 |
| 6-311+G(2df,p) | -12.7 | -9.6 | -3.5 |
| CC-PVTZ | -9.3 | -7.5 | -3.2 |
| aug-CC-PVTZ | -6.9 | -6.3 | -3.4 |
| CC-PCVTZ | -16.9 | -10.2 | -3.3 |
| aug-CC-PCVTZ | -17.0 | -10.1 | -3.3 |
| IGLO-III | -17.5 | -10.3 | -3.5 |
| us-6-31G(d,p) | -14.5 | -10.8 | -3.7 |
| us-6-311G(d,p) | -15.3 | -11.5 | -3.7 |
| us-6-311+G(2df,p) | -16.7 | -12.1 | -3.6 |
| us-CC-PVTZ | -16.1 | -11.9 | -3.7 |
| us-aug-CC-PVTZ | -16.6 | -12.2 | -3.7 |
| us-CC-PCVTZ | -15.9 | -11.9 | -3.6 |
| us-aug-CC-PCVTZ | -16.5 | -12.1 | -3.6 |
| us-IGLO-III | -16.6 | -12.4 | -3.8 |
| Experimental[4,5] | -21.8 | -16.4 | -3.9 |
| | -23.5 | -17.6[a] | |

[a] Inner oxygen coupling obtained from private correspondence with K. U. Ingold, since the ratio between the two HFCCs (1.33) is expected to remain the same as in a previous experimental study.

Considering the size of the 6-31G(d,p) basis set and the fact that it does not satisfy many of the criteria for basis sets to be used in HFCC calculations discussed in Chapter Two (triple-zeta, diffuse and polarization functions), this good agreement is likely due to fortuitous cancellation of errors. Single-point calculations were performed using the 6-31+G(d,p) and 6-31+G(2df,p) basis sets. The addition of diffuse functions to 6-31G(d,p)

increases the magnitude of the HFCC from -17.9 G and -13.0 G to -20.9 G and -14.1 G on the terminal and inner oxygen atoms, respectively (experimental values: -20.4 G and -14.2 G). Inclusion of additional polarization functions also increases the magnitude of the HFCCs (-21.6 G and -14.4 G). The trend of increasing magnitude of the HFCCs upon improving the 6-31G series is very similar to that observed for the 6-311G series, thus supporting the hypothesis that good results obtained with the double-zeta basis set are fortuitous. This is in agreement with work by Cohen and Chong[15] who determined that this basis set does not extend over the orbital space between the 1*s* and 2*s* shells. It was also suggested that cancellation of errors occurs since correlation effects cancel spin density introduced by larger basis sets.

The IGLO-III basis set appears to yield results that are closest to the experimental values. Alternatively, Dunning's correlation-consistent polarized-valence basis set of triple-zeta quality does not perform well. Augmentation of this basis set is expected to improve the results, however worse agreement with experiment is obtained. As previously noted, the contraction scheme of this basis set is not well designed for DFT calculations of HFCCs.[16,17,18,19] A more recent basis set designed by Dunning (CC-PCVTZ)[20] improves upon CC-PVTZ by accounting for core and core-valence correlation. Additional basis functions were added to the original CC-PVTZ basis set, where the exponents were determined by minimizing the difference between all-electron and valence-only correlation energies. The results for both CC-PCVTZ and its augmented form show improvement over the regular CC-PVTZ basis set and are comparable to those obtained with IGLO-III.

Results obtained for $^{1}H$ and $^{13}C$ in OH and $(CH_3)_3{}^{13}COO$, respectively, were not affected to the same extent by the basis sets examined herein.[14] This shows the difficulty in calculating accurate oxygen hyperfine couplings relative to the HFCCs of other atoms. The carbon couplings in *t*-butyl peroxyl radical are displayed in Table 3.1.

The basis set study was further extended by examining the effects of full decontraction of the *s*-shell on the heavy atoms (denoted as u*s*- in the tables) for IGLO-III, aug-CC-PVTZ, 6-311+G(2df,p) and 6-311G(d,p). Decontraction should lead to an improvement in the results through a better description of the core region. Accounting for spin polarization of the 1*s* shell generally provides a large negative contribution to the

spin density. As can be seen from the data (Table 3.1), the basis set decontraction has a positive effect on the HFCCs. The decontraction improves the result obtained with 6-311G(d,p) by on average 3.7 G for all radicals studied. A slightly smaller improvement (on average 3.4 G) is exhibited for the 6-311+G(2df,p) basis set.

The greatest improvement in results upon decontraction occurs for Dunning's augmented correlation-consistent triple-zeta basis set with an average improvement of 8.3 G for all radicals studied. Evidently, the standard contraction schemes used in the aug-CC-PVTZ basis set are unsuitable for HFCC calculations, which is expected since this basis set was designed to recover only valence correlation energy, but HFCCs require a good description of core correlation. Many other studies have also shown the importance of decontracting this basis set in order to calculate accurate HFCCs.[16,17,18,19] Alternatively, decontraction of the CC-PCVTZ and aug-CC-PCVTZ basis sets led to little improvement over the contracted forms. This is not surprising since the CC-PCVTZ series was designed to account for core and core-valence correlation, an important contribution to HFCCs. This further supports the hypothesis that the original CC-PVTZ basis set is not well designed for HFCC calculations. Decontraction of 6-31G(d,p) leads to HFCCs in far worse agreement with experimental results indicating that good results obtained with this basis set are due to its contraction scheme.

Minor changes of less than one gauss resulting from the decontraction of IGLO-III indicate that this basis set is well suited for HFCC calculations on peroxyl radicals. Upon decontraction of the *s*-shell, all bases examined are of comparable accuracy. Analogous results for $^{1}H$ in the hydroxyl radical were obtained for all basis sets implying that decontraction of basis functions on the neighboring atom has negligible effects.[14] As well, the results from $(CH_3)_3{}^{13}COO$ show that the $^{13}C$ HFCC is not affected by decontraction of the *s*-shell on oxygen or carbon. Decontraction of the *p*-shell was not examined in this study since it has previously been shown that even with a poorly behaved basis set prior to *s*-shell decontraction, the decontraction of *p* functions leads to little or no improvement in the HFCC with increased computational resources.[18,19]

Examination of the absolute mean deviation between experimental and B3LYP results (Table 3.2) indicates that IGLO-III, us-IGLO-III, us-6-311+G(2df,p) and us-aug-CC-PVTZ yield similar results. The mean deviations for the $^{13}C$ and $^{1}H$ HFCCs in *t*-

butyl peroxyl and the hydroxyl radical were extremely small and on average the basis sets employed recover 92 and 88 percent of the experimental value, respectively.[14] Since it was already stated that changes in HFCCs obtained with IGLO-III upon decontraction were small and IGLO-III is the smallest, most computationally time efficient basis set of those which gave promising results, it was chosen as the basis set to be used in a functional study. The success of IGLO-III for HFCC calculations has also been observed in several other studies.[18] It should be noted that even though the 6-31G series gave results comparable to experiment it was not used in the functional study since the reason for its success remains unclear.

Table 3.2: Absolute mean deviation between experimental and B3LYP isotropic HFCCs (G) for the alkyl peroxyl radicals and the hydroxyl radical.

| Basis Set | $\lvert\Delta A_{iso}(^{17}O_{terminal})\rvert$ | $\lvert\Delta A_{iso}(^{17}O_{inner})\rvert$ |
|---|---|---|
| 6-31G(d,p) | 3.1 | 1.0 |
| 6-311G(d,p) | 10.5 | 4.6 |
| 6-311+G(d,p) | 9.7 | 4.1 |
| 6-311+G(2df,p) | 8.8 | 3.2 |
| CC-PVTZ | 13.6 | 5.6 |
| aug-CC-PVTZ | 15.0 | 6.7 |
| IGLO-III | 4.5 | 1.8 |
| us-6-311G(d,p) | 6.3 | 1.6 |
| us-6-311+G(2df,p) | 4.6 | 1.4 |
| us-aug-CC-PVTZ | 4.8 | 1.3 |
| us-IGLO-III | 4.8 | 1.2 |

### *3.2.2.2 Functional Study*

The results obtained using six functional combinations with the IGLO-III basis set are displayed in terms of absolute mean deviations and the spread of the deviation in Table 3.3 for all alkyl peroxyl radicals and the hydroxyl radical. Examination of the results indicates that Becke's hybrid exchange functional (B3) is superior to the "pure" gradient-corrected DFT exchange functional (B) for both determining results in agreement with experiment and determining results with a greater certainty. This is reasonable due to the added degree of flexibility in the hybrid functional and the results support previous findings.[18] The P86 and PW91 correlation corrections gave highly similar results which were inferior to those obtained with the LYP functional. The spread in the deviations in the terminal oxygen HFCC for all functionals is nearly equal, while the spread in the deviations in the inner oxygen HFCC is smallest for the B3LYP

functional. The $^{13}C$ and $^{1}H$ HFCCs in $(CH_3)_3{}^{13}COO$ and OH, respectively, are not as sensitive to changes in the functional form.

Table 3.3: Absolute mean deviation in experimental and calculated isotropic HFCCs (G) obtained with various functionals and the IGLO-III basis set for the alkyl peroxyl and the hydroxyl radicals.

| Functional | $\lvert\Delta A_{iso}(^{17}O_{terminal})\rvert$ | $\lvert\Delta A_{iso}(^{17}O_{inner})\rvert$ |
|---|---|---|
| BLYP | 10.4 (±4.5) | 5.2 (±2.2) |
| BP86 | 14.7 (±3.3) | 7.4 (±2.2) |
| BPW91 | 15.0 (±2.5) | 7.5 (±2.3) |
| B3LYP | 4.7 (±2.0) | 2.4 (±1.4) |
| B3P86 | 8.5 (±1.9) | 3.7 (±2.3) |
| B3PW91 | 8.3 (±1.8) | 3.6 (±2.3) |

From Table 3.3, it is clear that the B3LYP functional predicts HFCCs in peroxyl radicals with the greatest degree of accuracy and precision, which is in accord with previous studies.[15,17,18,21] Hence, it appears that the B3LYP/ IGLO-III approach provides one of the best methods to determine the HFCCs in large peroxyl radicals. Similar results could be obtained with *us*-IGLO-III, *us*-6-311+G(2df,p) and *us*-aug-CC-PVTZ, but considering the size of these basis sets relative to IGLO-III and the size of the molecules being examined, B3LYP/IGLO-III would be the most reasonable choice for the calculation of $^{17}O$ HFCCs in large molecules.

### *3.2.2.3 Spin Density*

New information about the location of the unpaired electron in peroxyl radicals can be obtained directly from the examination of HFCCs, since the isotropic component provides a direct measure of the unpaired spin density at the nucleus. The results show that the unpaired electron is primarily located on the terminal oxygen. From the B3LYP/IGLO-III hyperfine splittings, the average predicted ratio for terminal to inner oxygen atom spin density is 0.61:0.39.

The spin densities obtained from the Mulliken population analysis, calculated at various levels of theory, yield very consistent results. The values obtained indicate that there is a net spin density of 0.7 electrons on the terminal oxygen and 0.3 electrons on the inner oxygen for all of the alkyl peroxyl radicals. Table 3.4 displays the results for *t*-butyl peroxyl radical, which are representative of those obtained for all alkyl peroxyl radicals.

Table 3.4: Spin densities obtained for *t*-butyl peroxyl radical with a variety of methods.

| Functional | Basis Set | Spin Density ($^{17}O_{terminal}$) | Spin Density ($^{17}O_{inner}$) |
|---|---|---|---|
| B3LYP | 6-31G(d,p) | 0.690 | 0.306 |
| B3LYP | 6-311G(d,p) | 0.695 | 0.299 |
| B3LYP | 6-311+G(d,p) | 0.691 | 0.305 |
| B3LYP | 6-311+G(2df,p) | 0.687 | 0.297 |
| B3LYP | CC-PVTZ | 0.693 | 0.300 |
| B3LYP | aug-CC-PVTZ | 0.703 | 0.291 |
| B3LYP | us-6-311G(d,p) | 0.693 | 0.302 |
| B3LYP | us-6-311+G(2df,p) | 0.684 | 0.300 |
| B3LYP | us-aug-CC-PVTZ | 0.696 | 0.293 |
| B3LYP | us-IGLO-III | 0.692 | 0.317 |
| B3LYP | IGLO-III | 0.710 | 0.296 |
| B3PW91 | IGLO-III | 0.656 | 0.345 |
| B3P86 | IGLO-III | 0.714 | 0.291 |
| BLYP | IGLO-III | 0.656 | 0.345 |
| BPW91 | IGLO-III | 0.661 | 0.340 |
| BP86 | IGLO-III | 0.658 | 0.342 |

Thus, it is evident that whether the isotropic HFCCs or the spin densities from the Mulliken population analysis are examined, the valence bond structure in which the terminal oxygen possesses the lone electron is favored. However, some unpaired spin density is also located on the inner oxygen. It should be noted that the values estimated for the spin density distribution in the $p_z$ orbitals by Sevilla *et al.*[22] (0.3-0.39 for the inner oxygen and 0.70-0.61 for the outer oxygen) are in excellent agreement with both of our predicted values.

### *3.2.3 Fluoroperoxyl Radical*

The isotropic HFCCs in the fluoroperoxyl radical (Table 3.5) are more sensitive to the basis set and the functional form than the HFCCs in alkyl peroxyl radicals. The isotropic component for the inner oxygen is predicted with the wrong sign in all calculations. In addition, the $^{19}F$ HFCC is highly erroneous, whereas the value of the isotropic HFCC on the terminal oxygen displays the same functional and basis set dependence observed for alkyl peroxyl radicals. These factors indicate significant problems in the description of the F-$O_{inner}$ part of the molecule. It should be noted that the spin contamination for all but the pure DFT functionals is very high.

#### *3.2.3.1 Evaluation of Calculated Geometries*

Results for the calculated geometry of FOO obtained in this study are compared

Table 3.5: Isotropic HFCCs (G) for FOO calculated at the B3LYP/6-311+G(d,p) geometry with various methods and basis sets.

| Basis Set | $A_{iso}(^{17}O_{terminal})$ | $A_{iso}(^{17}O_{inner})$ | $A_{iso}(^{19}F)$ | $\langle S^2 \rangle$ |
|---|---|---|---|---|
| B3LYP/6-31G(d,p) | -26.8 | 8.1 | -41.0 | 1.207 |
| B3LYP/6-311G(d,p) | -15.9 | 24.2 | -28.6 | 1.203 |
| B3LYP/6-311+G(d,p) | -15.9 | 23.4 | -29.7 | 1.176 |
| B3LYP/6-311+G(2df,p) | -18.2 | 21.1 | -28.7 | 1.170 |
| B3LYP/CC-PVTZ | -13.2 | 24.2 | 7.9 | 1.183 |
| B3LYP/aug-CC-PVTZ | -10.4 | 26.7 | -20.3 | 1.164 |
| B3LYP/us-6-311G(d,p) | -22.5 | 17.5 | -40.9 | 1.203 |
| B3LYP/us-6-311+G(2df,p) | -23.7 | 15.9 | -24.2 | 1.172 |
| B3LYP/us-aug-CC-PVTZ | -23.5 | 16.3 | -61.3 | 1.166 |
| B3LYP/us-IGLO-III | -23.2 | 16.8 | -55.9 | 1.155 |
| BLYP/IGLO-III | -10.4 | 2.2 | -8.3 | 0.797 |
| BP86/IGLO-III | -6.2 | 4.4 | -0.8 | 0.789 |
| BPW91/IGLO-III | -6.2 | 5.6 | -0.8 | 0.799 |
| B3LYP/IGLO-III | -23.6 | 17.6 | -60.0 | 1.164 |
| B3P86/IGLO-III | -18.8 | 21.1 | -39.1 | 1.159 |
| B3PW91/IGLO-III | -19.1 | 21.3 | -41.6 | 1.176 |
| Experimental | -22.2[a] | -14.5[a] | \|10.8\|-\|17.6\|[b] | 0.75 |

[a] References (1) and (12). [b] Reference (13).

to other calculated[23,24,25,26] and experimental[27] results in Table 3.6. The wide range of values obtained for the geometrical parameters indicates that complications occur when the geometry of this molecule is calculated. Even high-level perturbation methods have great difficulty describing the molecular geometry, which is predominantly shown by a drastically underestimated FO bond length. DFT methods using the B3LYP functional compensate for this error and yield results closer to experiment, however these geometries are dependent upon the basis set used for the calculation.

The geometry obtained with B3LYP/6-311+G(d,p) overestimates the FO bond by approximately 0.2 Å. Inclusion of additional polarization functions (6-311++G(3df,3pd)) leads to a reduction in the FO bond length[27] and better agreement with experiment. This information would lead to the conclusion that a large basis set is required to describe the FOO geometry with DFT. However, the geometry obtained from a smaller basis set (6-31G(d)) was also determined to be in excellent agreement with experiment.[24] It is tempting once again to blame this on fortuitous cancellation of errors, but further optimizations were performed at the B3LYP/6-31+G(2df,p) and the B3LYP/6-311+G(2df,p) levels (Table 3.6) to achieve a greater understanding of the basis set dependence of this property. The geometries obtained with both basis sets are comparable to those obtained with the 6-31G(d) and 6-311+G(3df,3pd) bases. Similar

Table 3.6: The bond lengths (Å) and bond angle (degrees) for FOO calculated with various methods.

| Method | r(FO) | r(OO) | ∠(FOO) |
|---|---|---|---|
| HF/6-31G(d)[a] | 1.380 | 1.437 | 107.6 |
| MP2/6-31G(d)[b] | 1.383 | 1.250 | 109.6 |
| MP2/6-311G(d)[b] | 1.377 | 1.236 | 109.8 |
| MP3/6-311G(d)[b] | 1.375 | 1.235 | 109.4 |
| MP3/6-311+G(d)[b] | 1.377 | 1.233 | 109.5 |
| MP3/6-311+G(2d)[b] | 1.381 | 1.238 | 109.4 |
| MP4SDTQ/6-311++G(2d)[b] | 1.389 | 1.245 | 110.6 |
| B3LYP/6-31+G(d)[c] | 1.625 | 1.200 | 111.2 |
| B3LYP/6-31+G(2df)[d] | 1.621 | 1.190 | 111.2 |
| B3LYP/6-311+G(d)[d] | 1.815 | 1.181 | 112.0 |
| B3LYP/6-311+G(2df)[d] | 1.625 | 1.187 | 111.3 |
| B3LYP/6-311++G(3df)[e] | 1.626 | 1.184 | 111.1 |
| B3LYP/IGLO-III[d] | 1.636 | 1.189 | 111.2 |
| Experimental[f] | 1.649 | 1.200 | 111.2 |

[a] Reference (26). [b] Reference (25). [c] Reference (23). [d] This work. [e] Reference (24). [f] Reference (27).

results were also obtained with the B3LYP/IGLO-III combination. Thus, the reason for the poor agreement with experiment when the 6-311+G(d,p) basis set is implemented remains to be resolved. A possible explanation is spin contamination. The eigenvalues of $\langle S^2 \rangle$ calculated with various methods for FOO range from 0.752 to 1.207, where the value of a pure doublet is 0.75. For all basis sets that yield an FO bond length of approximately 1.62 Å, the eigenvalue of $\langle S^2 \rangle$ is 0.81. However, the eigenvalue of $\langle S^2 \rangle$ obtained with the implementation of the 6-311+G(d,p) basis set is 1.17. Alternatively, it could be speculated that the state of the radical with the long FO bond length is different from that in the other calculations. This arises since it is known that peroxyl radicals can be in two states: $^2A''$ or $^2A'$, where the latter results in longer bond lengths due to a decrease in the $\pi$ character. This fact does not explain the long FO bond length calculated with B3LYP/6-311+G(d), however, since all calculations were performed on the $^2A''$ state.

### *3.2.3.2 Geometry Effects on the HFCCs*

The dependence of the HFCCs in FOO on the geometry (Table 3.7) was examined through single-point calculations performed using a representative set of geometries (Table 3.6), the IGLO-III basis set and a variety of functionals. The HFCCs calculated for FOO vary drastically with geometry and the results are not logical. Concentrating on only the B3LYP results, the HFCC of the terminal oxygen is calculated to the greatest

degree of accuracy with the B3LYP/6-311+G(d,p) geometry. However, this geometry fails to even reproduce the correct sign for the inner oxygen coupling. The same conclusions can be reached when the experimental geometry is implemented in a single-point calculation. On the other hand, the MP2/6-31G(d) geometry gives a much better description of the HFCC for the inner oxygen despite the fact that the FOO bond length differs from the experimental value by approximately 0.27 Å. The terminal oxygen HFCCs obtained using the MP2 geometry display greater deviations from experiment.

Once again, the degree of spin contamination must be examined. The largest eigenvalue of $\langle S^2 \rangle$ occurs for the calculation using the B3LYP/6-311+G(d,p) geometry. $\langle S^2 \rangle$ eigenvalues closest to the value for a pure doublet state were obtained using the MP2/6-31G(d) geometry, the geometry with the greatest deviations from experiment. Explanations for the cause of high contamination or the resulting poor HFCCs are not available at this time.

Table 3.7: Comparison of FOO hyperfine coupling constants (G) calculated using various optimized geometries, functionals and the IGLO-III basis set.

| Functional | Geometry | $A_{iso}(^{17}O_{terminal})$ | $A_{iso}(^{17}O_{inner})$ | $A_{iso}(^{19}F)$ | $\langle S^2 \rangle$ |
|---|---|---|---|---|---|
| B3LYP | MP2/6-31G(d) | -16.3 | -10.5 | -4.9 | 0.755 |
| | B3LYP/6-311+G(d,p) | -23.6 | 17.6 | -60.0 | 1.164 |
| | Experimental | -19.5 | 13.3 | -40.7 | 0.853 |
| B3PW91 | MP2/6-31G(d) | -13.0 | -8.6 | -4.7 | 0.755 |
| | B3LYP/6-311+G(d,p) | -19.1 | 21.3 | -41.6 | 1.176 |
| | Experimental | -15.8 | 16.7 | -31.8 | 0.859 |
| B3P86 | MP2/6-31G(d) | -12.8 | -8.7 | -4.1 | 0.754 |
| | B3LYP/6-311+G(d,p) | -18.8 | 21.1 | -39.1 | 1.159 |
| | Experimental | -15.3 | 14.9 | -28.4 | 0.844 |
| BLYP | MP2/6-31G(d) | -9.7 | -7.0 | -3.9 | 0.752 |
| | B3LYP/6-311+G(d,p) | -10.4 | 2.2 | -8.3 | 0.797 |
| | Experimental | -9.5 | -2.0 | -6.9 | 0.759 |
| BPW91 | MP2/6-31G(d) | -5.8 | -4.6 | -4.9 | 0.752 |
| | B3LYP/6-311+G(d,p) | -6.2 | 5.6 | -0.8 | 0.799 |
| | Experimental | -5.7 | 0.9 | -4.9 | 0.758 |
| BP86 | MP2/6-31G(d) | -6.0 | -4.8 | -4.3 | 0.752 |
| | B3LYP/6-311+G(d,p) | -6.2 | 4.4 | -0.8 | 0.789 |
| | Experimental | -5.9 | 0.6 | -5.1 | 0.758 |
| Experimental | | -22.2[a] | -14.5[a] | \|10.8\| - \|17.6\|[b] | 0.75 |

[a] References (1) and (12). [b] Reference (13).

### *3.2.4 Summary of DFT Study*

In this section, the geometries and hyperfine coupling constants of a variety of oxygen centered radicals were determine through the use of DFT. For the alkyl peroxyl

radicals, the IGLO-III basis set proves to be superior for DFT calculation of oxygen HFCCs as it does not require decontraction of the *s*-shell for converged results. Satisfactory results were also obtained with decontracted forms of Pople's 6-311+G(2df,p) and Dunning's aug-CC-PVTZ basis sets. A functional study was subsequently performed using the IGLO-III basis set and it was concluded that the B3LYP functional yields $^{17}O$ hyperfine couplings in best agreement with experiment. Through the calculated HFCCs, it was concluded that the terminal oxygen possesses the main fraction of the lone electron. This conclusion is supported by the Mulliken spin densities where the ratio of the spin distribution on the terminal and inner oxygen atoms is predicted to be 0.7:0.3.

The results for the alkyl peroxyl radicals and the hydroxyl radical follow a clear pattern. The results for FOO did not conform and an incorrect sign for the inner oxygen HFCC was often predicted. It was concluded that spin contamination could be leading to poor results for this molecule. Other possible explanations for the apparent failure of DFT include vibrational, multi-reference and matrix effects. Multi-reference effects can be examined through the use of additional determinants (MRCI). This avenue will be discussed in more detail in the subsequent section. Furthermore, the matrix used in ESR experiments could be leading to the discrepancy between theory and experiment since the geometry may change, even in the presence of rare gas atoms, and drastic effects on the coupling constants would be observed. Investigations of matrix, as well as vibrational, effects can be achieved through the implementation of a combined quantum mechanics and molecular dynamics technique, which was briefly discussed in Chapter Two.

### *3.3 Evaluation of* Ab Initio *Methods*

As mentioned in Chapter Two, multi-reference CI has been used with great success for the calculation of HFCCs in atoms and small molecules. Since this method provides a greater degree of flexibility through the use of additional determinants, an improvement over DFT results for $^{17}O$ HFCCs is expected. The hydroxyl radical was chosen for preliminary investigations of the limitations of this method (rather than fluoroperoxyl radical) since MRCI techniques are very time consuming. The hydroxyl radical has been investigated extensively with theoretical techniques[17a,18b,28,29] due to its

size relative to other molecules for which accurate experimental $^{17}O$ couplings exist.[11] Previous theoretical studies have shown that the calculation of accurate $^{17}O$ HFCCs in the hydroxyl radical is extremely difficult. In particular, calculated oxygen HFCCs vary between -9.8 and -23.5 G (experimental value: -18.3 G). The calculated hydrogen couplings also vary between -16.2 and -31.9 G (experimental value: -26.1 G). Since hydrogen couplings can be calculated accurately, the range of hydrogen HFCCs reflects the variety of basis sets and methods previously tested. Within this section, MRCI results will be presented, where the basis set, the number of configurations included in the reference space and the selection threshold ($T_E$) for including configurations will be systematically improved. These results will be compared to those obtained from DFT (discussed previously), as well as values obtained from QCI and CC methods. These calculations will provide a systematic study of methods suitable for the calculation of oxygen couplings.

### *3.3.1 Computational Details*

The difficulty of MRCI is determining how to select the most important reference configurations and the important excitations from these configurations. The method used for the calculations to be presented was discussed in detail in Chapter Two (Section 2.8.2). In the work to be discussed, the CI wave function was ordered according to the magnitude of the expansion coefficients. A variety of basis sets and alternate modifications to the configuration selection scheme were implemented. Additional details will be presented in the discussion section. All MRCI calculations were carried out with the MELDF-X program.[30] The MP2/6-31G(d) bond length of 0.979 Å was used throughout (experimental bond length: 0.969 Å).[31]

### *3.3.2 Multi-Reference Configuration Interaction Study*

#### *3.3.2.1 Basis Set Study*

The first basis set to be examined is based on Huzinaga's Gaussian basis set (9s5p/5s)[32] augmented with diffuse *sp* functions on oxygen,[33] diffuse *s* functions on hydrogen[34] and polarization functions.[34] A contraction scheme of the resulting (10s6p1d/6s1p) basis set, suggested by Chipman for the accurate determination of spin densities,[34] was tested. In the contraction scheme, only the innermost primitives are contracted resulting in a basis set of the form (511111,411,1/3111,1) which indicates the

number of Gaussians used in each contraction. The uncontracted and contracted basis sets will be referred to as (10s6p1d/6s1p) and [6s3p1d/4s1p], respectively.

The best value of the oxygen isotropic HFCC obtained with the contracted basis set is -16.8 G (experimental value: -18.3 G). In addition, converged results are obtained for calculations with $T_E$ smaller than $10^{-7}$ hartrees and more than 59 reference configurations with this basis set. These convergence trends are not observed for the (10s6p1d/6s1p) basis set. For the uncontracted basis set, the convergence of $A_{iso}(^{17}O)$ is much slower and the result closest to experiment is -14.6 G. Conversely, $A_{iso}(^{1}H)$ is overestimated with the [6s3p1d/4s1p] basis set (-28.2 G compared to the experimental value of -26.1 G), but a value in good agreement with experiment is obtained when the uncontracted basis set is used (-25.8 G). In addition, overall converged results were obtained for $T_E = 10^{-8}$ hartrees within a given size of the reference space through the use of the uncontracted basis set. The contracted and uncontracted forms of the modified Huzinaga's basis set provide a good example of the great difficulty of calculating HFCCs and the sensitivity of this property to different variables, such as the form of the basis set.

The basis set study was further extended by using the basis set applied by Kong *et al.*,[35] which consists of a set of diffuse *s* and *p* functions added to the (10s6p/6s) basis set

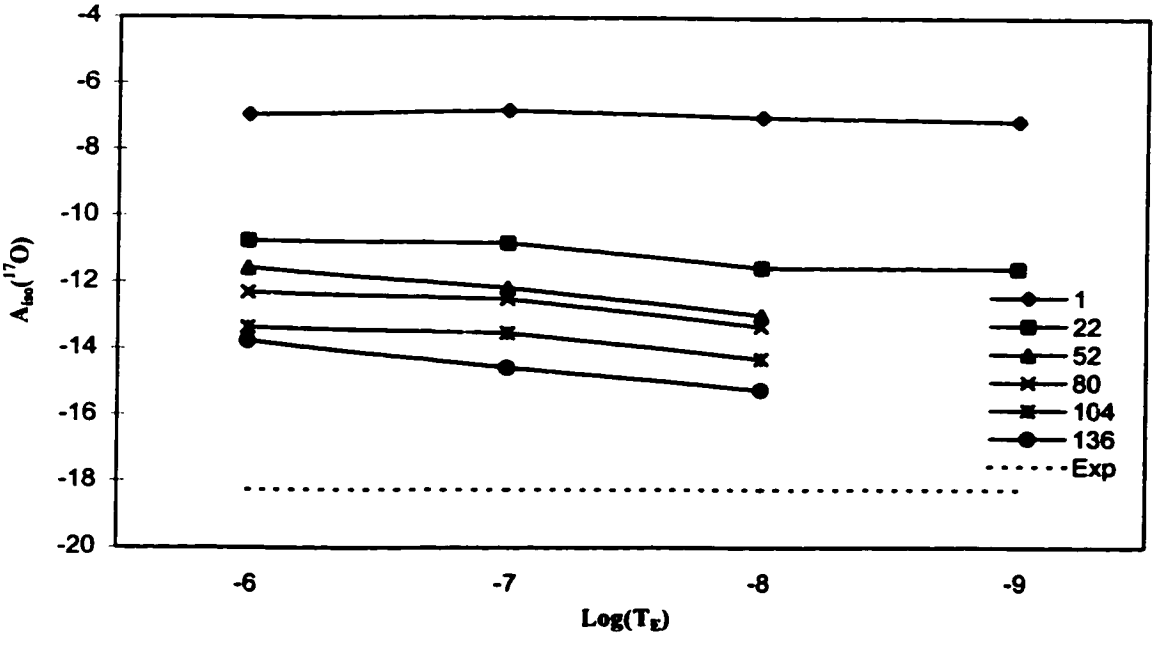


Figure 3.1: Oxygen isotropic HFCC in the hydroxyl radical versus log(energy selection threshold).

of van Duijneveldt,[36] plus two additional polarization functions (*d*-type on oxygen and *p*-type on hydrogen) from Dunning.[8c] This basis set will be denoted as (11s7p2d/7s2p). The calculated $A_{iso}(^{17}O)$ values are consistent with changes in the selection energy threshold (Figure 3.1), but change more rapidly with the size of the reference space (Figure 3.2). However, for the sizes of the reference space and the energy selection thresholds examined, the calculated results are not in agreement with experimental data.

The (11s7p2d/7s2p) basis set was further improved upon by the addition of one *f* function to oxygen and calculations were done with energy thresholds of $10^{-6}$ and $10^{-8}$ hartrees (represented as 1*f*-6 and 1*f*-8, respectively, in the legend of Figures 3.1 and 3.2). The addition of one *f* function does not improve the convergence of the property at hand to the experimental results.

Results for $A_{iso}(^{1}H)$ (graphs not shown, but can be found in reference 37) indicate that convergence is faster for this property, but results are not as good as expected (the best value for the (11s7p2d/7s2p) basis set is -25.0 G). The addition of one *f* function to the oxygen basis set causes only a slight alteration in $A_{iso}(^{1}H)$, resulting in a shift away from the experimental value by approximately 0.5 G.

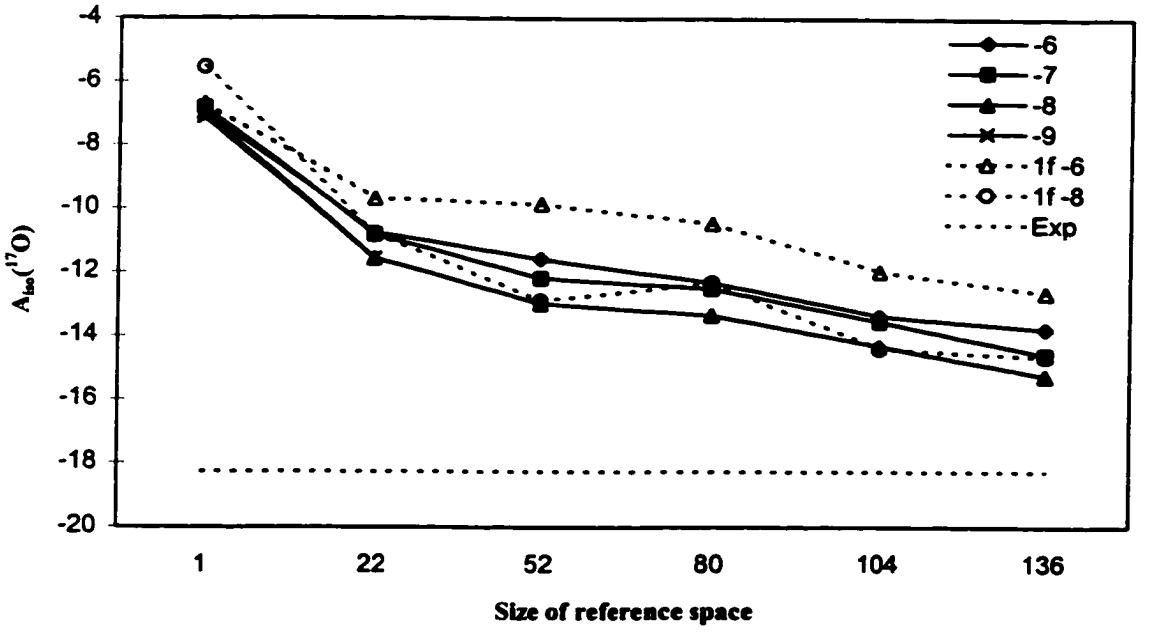


Figure 3.2: Oxygen isotropic HFCC in the hydroxyl radical versus the size of the reference space.

Additional modifications of the (11s7p2d/7s2p) basis set were also investigated in attempts to improve the agreement of the calculated $A_{iso}(^{17}O)$ values with experiment. In addition to the *f* function, one more *d* function was also implemented and was shown to have little effect on the results. An *s* function with a very high exponent was added to the oxygen basis set. This did not change the results either since cusp functions are not expected to be important unless the singly-occupied molecular orbital directly contributes to the HFCC. In the hydroxyl radical the unpaired electron occupies a *p* orbital with a node at the nucleus and therefore does not directly contribute to $A_{iso}$. A (13s8p2d/8s2p) basis set, created from the (11s7p/7s) basis set of van Duijneveldt[36] in a manner analogous to that used to obtain the previously discussed (11s7p2d/7s2p) basis set, was also examined. Although this basis set is larger than (11s7p2d/7s2p), they are very similar in structure and little to no improvement was obtained for the oxygen HFCCs (results not shown since they deviate only slightly from those obtained with (11s7p2d/7s2p)).

The excellent agreement with experiment obtained for the $NH_2$ molecule by Kong *et al.*[35] compared to the poor results obtained for the hydroxyl radical indicate that an extra degree of difficulty is present when calculating HFCCs for oxygen nuclei. Since the various basis sets failed to yield converged MRCI results, despite the efforts put forth to improve upon such basis sets, other methods must be examined to improve CI convergence.

#### *3.3.2.2 Attempts to Improve CI Convergence*

One solution to the problem of poor convergence of the MRCI results is the transformation of the MOs to natural orbitals.[38] Natural orbitals are defined as the orbitals that diagonalize the first-order reduced density matrix. The K-orbitals, which were used to obtain the MRCI results discussed thus far, are chosen only to mimic the frozen natural orbitals.[39] Thus, the use of the true natural orbitals may lead to some improvement in convergence, since in previous studies they have been shown to improve CI convergence.[38]

The (11s7p2d/7s2p) basis set was used to investigate the effects of natural orbitals on the convergence of the oxygen isotropic HFCC. This basis set was chosen since it gave nice results in previous studies on small molecules and, as seen in the preceding

section, modifications to this basis set are unlikely to improve the results for the hydroxyl radical. As discussed, results for hydrogen converge relatively quickly and consistently and, thus, the results and discussion presented within will be confined to the $^{17}O$ isotropic HFCCs. Table 3.8 displays the results for the $^{17}O$ HFCCs obtained using K-orbitals and natural orbitals with the (11s7p2d/7s2p) basis set and a variety of configuration selection thresholds and reference spaces. From the results, it can be seen that the natural orbitals improve the convergence of $A_{iso}(^{17}O)$. For example, at a configuration energy selection threshold of $10^{-6}$ hartrees, 136 reference configurations are required when K-orbitals are used, while only 114 reference configurations are required if natural orbitals are implemented. This reduction increases upon implementation of smaller configuration energy selection thresholds. For $T_E = 10^{-7}$ or $10^{-8}$ hartrees, only 75 reference configurations are required to obtain convergence with natural orbitals, compared to the 136 reference configurations required when K-orbitals are used. Although the use of natural orbitals improves the convergence rate of the $^{17}O$ HFCCs, the calculated results are not converged to the experimental value. The best value obtained for $A_{iso}(^{17}O)$ is -15.2 G compared to the experimental value of -18.3 G. Thus, other methods to obtain better convergence must be examined.

The effects of various excitation classes on the isotropic hyperfine coupling constants obtained from CI calculations have been previously investigated.[38] As discussed in Chapter Two, it has been concluded that the indirect influences of triple and quadruple excitations on the isotropic hyperfine coupling constants are more important than their direct contribution.[40] This arises since single excitations contribute the most to the isotropic HFCCs. In turn, the double excitations with respect to these single excitations, or the triple excitations with respect to the main reference configuration, significantly influence the HFCCs. Inclusion of important triples is most easily accomplished through the addition of single configurations that contribute to large off-diagonal elements in the spin density matrix to the reference space.[38]

Table 3.8: The effects of natural orbitals and the inclusion of important single excitations from the spin density matrix on the oxygen isotropic HFCCs (G) in the hydroxyl radical.*

| $T_E$ | K-Orbitals | | Natural Orbitals | | Spin Density | |
|---|---|---|---|---|---|---|
| (hartrees) | No. Refs. | $A_{iso}$ | No. Refs. | $A_{iso}$ | No. Refs. | $A_{iso}$ |
| $10^{-6}$ | 1 | -7.0 | 1 | -7.6 | 1 | -7.6 |
| | 22 | -10.8 | 29 | -10.8 | 35 | -13.3 |
| | 52 | -11.6 | 44 | -12.3 | 50 | -13.8 |
| | 80 | -12.3 | 75 | -13.3 | 85 | -13.8 |
| | 104 | -13.4 | 110 | -13.3 | 118 | -13.8 |
| | 136 | -13.8 | 114 | -13.8 | | |
| | 180 | -14.3 | 149 | -14.0 | | |
| $10^{-7}$ | 1 | -6.8 | 1 | -7.1 | 1 | -7.1 |
| | 22 | -10.8 | 26 | -11.7 | 35 | -14.8 |
| | 52 | -12.2 | 44 | -12.9 | 50 | -15.2 |
| | 80 | -12.5 | 75 | -14.5 | 85 | -15.1 |
| | 104 | -13.5 | 110 | -14.5 | | |
| | 136 | -14.6 | 114 | -14.8 | | |
| | | | 149 | -15.1 | | |
| $10^{-8}$ | 1 | -7.0 | 1 | -7.6 | 1 | -7.6 |
| | 22 | -11.6 | 29 | -12.2 | 35 | -15.2 |
| | 52 | -13.0 | 44 | -13.8 | | |
| | 80 | -13.3 | 75 | -15.2 | | |
| | 104 | -14.3 | | | | |
| | 136 | -15.2 | | | | |
| Exp.[11] | | -18.3 | | -18.3 | | -18.3 |

*The number of reference configurations corresponds to the number of spin-adapted configurations.

The $A_{iso}(^{17}O)$ obtained by selecting additional single excitations based on the spin density matrix were obtained through the use of natural orbitals and the (11s7p2d/7s2p) basis set (Table 3.8). The results for hydrogen did not change substantially from those previously discussed and therefore are not included in the table or the present discussion. Faster convergence for $A_{iso}$ is once again obtained with this selection scheme. For example, at a configuration selection energy threshold of $10^{-6}$ hartrees, only 50 reference configurations are required under the new selection scheme. Once again, as the configuration selection energy threshold is decreased, even smaller numbers of reference configurations are required. For example, at a selection energy threshold of $10^{-7}$ hartrees, only 35 reference configurations are required compared to 75 when the spin density matrix is not examined. Thus, a drastic decrease in the required number of reference configurations is obtained, compared to the 136 required if K-orbitals are used and the spin density matrix is not analyzed to select important reference configurations. Although faster convergence is obtained for the $^{17}O$ HFCCs by examining the spin

density matrix, the values are still not converging to the experimental result. The value in best agreement with experiment is -15.2 G (experimental value: -18.3 G).

One further consideration is the bond length used in the single-point calculations. Examination of the effects of bond length on the HFCCs was accomplished through calculations performed with a variety of bond lengths, natural orbitals, a configuration energy selection threshold of $10^{-7}$ hartrees and 35 reference configurations (Table 3.9). This set of restrictions was chosen based on the results displayed in Table 3.8. The isotropic $^{17}O$ HFCCs do not change appreciably upon alteration of the OH bond length.

Since a large basis set, a large number of reference configurations, a small configuration selection threshold and an accurate MP2/6-31G(d) geometry were implemented in the present study, the poor results obtained with MRCI remain puzzling. The quality of the reference space used in these calculations can be roughly judged through the examination of the sum of the squares of the CI coefficients. If the calculations were carried out to the limit of full CI, the sum of the squares of the coefficients would be 1.0. A plot of $A_{iso}(^{17}O)$ versus the sum of the squares of the reference coefficients is given in Figure 3.3 for the results obtained using the (11s7p2d/7s2p) basis set and natural orbitals. From the graph, it can be seen that a large part of the reference space is covered, where the largest sum of the coefficients is 0.9910, 0.9891 and 0.9810 for calculations performed with $T_E$ equal to $10^{-6}$, $10^{-7}$ and $10^{-8}$ hartrees, respectively. It appears that convergence is almost linear over the range studied.

Table 3.9: The effects of bond length (Å) on isotropic HFCCs (G) in the hydroxyl radical.*

| Bond Length | $A_{iso}(^{1}H)$ | $A_{iso}(^{17}O)$ |
|---|---|---|
| 0.929 | -24.8 | -13.9 |
| 0.969 | -25.1 | -14.7 |
| 0.979 | -25.3 | -14.8 |
| 0.989 | -25.4 | -14.5 |
| 1.009 | -25.9 | -14.2 |
| 1.029 | -26.4 | -14.3 |
| 1.069 | -27.2 | -14.0 |
| 1.109 | -27.9 | -13.7 |
| Exp.[11] | -26.1 | -18.3 |

*Results were obtained using natural orbitals, $T_E = 10^{-7}$ hartrees and 35 reference configurations.

Similar graphs obtained by Feller *et al.*[16] for the NO molecule indicate that convergence is exponential at very tight selection thresholds ($10^{-8}$ or $10^{-9}$ hartrees). Due to the number of points obtained in the present study for $T_E = 10^{-8}$ hartrees, it is difficult to determine whether convergence is linear or exponential. If convergence is linear, then a linear regression can be performed for each set of data and the results are displayed as open symbols for each data set in Figure 3.3. From the regression results, $A_{iso}(^{17}O)$ at the full CI limit is approximately -20 G. If however the curve should be more exponential, then $A_{iso}(^{17}O)$ is approximately -18 G. On either account, it is apparent that the full CI limit is approximately -19 ± 1 G, which is in good agreement with the experimental value (-18.3 G).

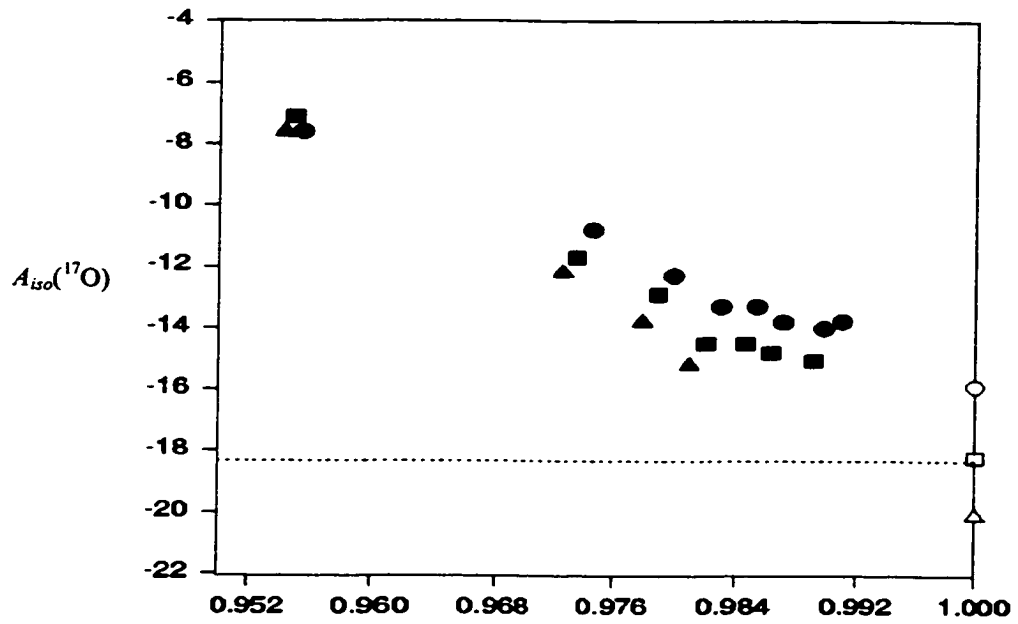


Figure 3.3: Oxygen isotropic HFCCs (G) in the hydroxyl radical versus the sum of the squares of the CI coefficients with $T_E = 10^{-6}$ (●), $10^{-7}$ (■) and $10^{-8}$ (▲).

Since full CI is only limited by the basis set implemented, Figure 3.3 indicates that a large enough basis set was used in the present study. Thus, the failure of the MRCI approach to accurately describe the HFCCs in the hydroxyl radical must be due to the expansion of the reference space. In particular, the failure of this method lies in the slow

convergence of the isotropic $^{17}O$ HFCCs. Feller and Davidson[41,42] noted that for the $H_2CO^+$ radical, there exists a single excitation whose importance was not established until a very large scale calculation was performed. However, similar to the NO radical studied by Feller *et al.*,[16] no single configuration could be identified as solely resulting in the slow convergence of the HFCCs in the hydroxyl radical. Thus, discrepancies between theory and experiment must be due to the neglect of many different excitations. Since converged results cannot be obtained for $A_{iso}(^{17}O)$ with MRCI using reasonable computational resources, even for a small molecule such as the hydroxyl radical, other theoretical techniques must be considered.

### *3.3.3 Comparison of MRCI, DFT and QCISD Hyperfine Structures*

Despite the efforts put forth, the best value obtained for the isotropic oxygen HFCC in the hydroxyl radical with high-level MRCI (-15.2 G) is not in any better agreement with experiment than the value obtained with B3LYP and the IGLO-III basis set (-15.3 G). This is rather curious considering the levels of theory used in each study. Previously, results in the best agreement with experiment were obtained by Carmichael[29] through extensive QCISD(T) calculations in which the effects of up to the fifth order triples were included and a very large, contracted basis set was implemented ((14s9p4d1f/9s3p1d)/[8s5p4d1f/6s3p1d]). This indicates that a closer look at the QCI method may be required. Full QCISD calculations were implemented in which all electrons were correlated. The results from these calculations are compared to those obtained from DFT (analogous to calculations discussed in the previous section for *t*-butyl peroxyl radical) and MRCI calculations in Table 3.10. All QCI and DFT calculations were performed using the GAUSSIAN 94 program.[9]

The QCISD isotropic HFCCs display a typical basis set dependence. The "best" value observed in the current study through the implementation of QCISD was obtained with *s*-shell decontraction of Dunning's augmented correlation consistent core and valence polarization triple zeta basis set (-18.5 G versus -18.3 G for the calculated and experimental $^{17}O$ HFCCs, respectively). However, very reliable results are also obtained with Pople's 6-311+G(2df,p) basis set (-17.3 G) which does not require *s*-shell decontraction for improved results. This is promising since this basis set is much smaller

Table 3.10: Comparison of MRCI, QCISD and B3LYP results for the HFCCs (G) in the hydroxyl radical.

| Basis Set | QCISD $A_{iso}(^{17}O)$ | B3LYP $A_{iso}(^{17}O)$ | MRCI $A_{iso}(^{17}O)$ | QCISD $A_{iso}(^{1}H)$ | B3LYP $A_{iso}(^{1}H)$ | MRCI $A_{iso}(^{1}H)$ |
|---|---|---|---|---|---|---|
| 6-311G(d,p) | -15.0 | -10.0 | | -28.7 | -24.3 | |
| 6-311+G(d,p) | -16.2 | -11.3 | | -28.6 | -23.9 | |
| 6-311+G(2df,p) | -17.3 | -11.4 | -16.4 | -26.6 | -22.6 | -25.8 |
| us-6-311G(d,p) | -13.2 | -13.7 | | -28.8 | -24.1 | |
| us-6-311+G(d,p) | -15.6 | -13.7 | | -28.6 | -24.1 | |
| us-6-311+G(2df,p) | -17.1 | -16.1 | -15.0 | -26.6 | -22.6 | -25.4 |
| CC-PVTZ | 1.5 | -2.7 | | -26.9 | -23.2 | |
| aug-CC-PVTZ | -2.0 | -3.4 | | -25.8 | -22.1 | |
| aug-CC-PCVTZ | -17.8 | -15.6 | | -25.7 | -22.1 | |
| us-CC-PVTZ | -15.1 | -14.3 | | -26.9 | -22.9 | |
| us-aug-CC-PVTZ | -17.7 | -15.8 | -14.0 | -25.7 | -22.1 | -24.9 |
| us-aug-CC-PCVTZ | -18.5 | -15.4 | | -25.7 | -22.1 | |
| [6s4p1d/4s1p] | -16.0 | -15.0 | -14.6 | -27.2 | -22.9 | -25.8 |
| (10s6p1d/6s1p) | -17.4 | -13.4 | -16.8 | -29.1 | -24.5 | -28.2 |
| (11s7p2d/7s2p) | -17.0 | -15.6 | -15.2 | -26.7 | -22.6 | -25.0 |
| Experimental[11] | -18.3 | -18.3 | -18.3 | -26.1 | -26.1 | -26.1 |

in magnitude than Dunning's basis set or the basis set used by Carmichael, indicating a reduction in computational cost. The effects of triple excitations on the QCISD HFCCs in the hydroxyl radical will be discussed in the following section.

The B3LYP results display a similar basis set dependence to QCISD. An exception is *s*-shell decontraction of Pople's basis sets where QCISD values are decreased in magnitude while DFT HFCCs are increased in magnitude. The "best" value observed for the $^{17}O$ HFCC calculated with DFT is -16.1 G (experimental: -18.3 G), which was obtained using Pople's *s*-shell decontracted 6-311+G(2df,p) basis set. This result is approximately 1 G further away from the experimental value than the results obtained with the identical basis set and QCISD. The values obtained with the same basis set for the hydrogen HFCCs are -26.6 G and -22.6 G for QCISD and DFT methods, respectively (experimental value: -26.1 G).

In order to ensure observed differences in MRCI and QCISD methods are not due to differences in the basis sets, calculations were performed on a subset of basis sets with each method (Table 3.10). QCISD indicates that the good results obtained with the contracted [6s3p1d/4s1p] basis set for $^{17}O$ HFCCs are due to the contraction scheme as the results deteriorate upon decontraction. In addition, the $A_{iso}(^{1}H)$ QCISD results obtained with the contracted basis set are overestimated as previously discussed for

MRCI. Overall poor results were obtained with B3LYP for both the contracted and uncontracted (10s6p1d/6s1p) basis sets. The (11s7p2d/7s2p) basis set, which yields the most reliable $A_{iso}(^{17}O)$ HFCCs for MRCI (-15.2 G), gave very similar results when used in combination with the B3LYP functional (-15.6 G). Results in much better agreement with experiment were obtained with QCISD (-17.0 G). As for the oxygen couplings, QCISD gave better results (-26.7 G) than either DFT (-22.6 G) or MRCI (-25.0 G) for the hydrogen HFCCs with this basis set (experimental coupling: -26.1 G). Similarly, comparison of the results obtained with all three methods and the basis sets previously used for QCISD and B3LYP indicates that QCISD outperforms B3LYP and MRCI for both the oxygen and the hydrogen isotropic HFCCs.

Thus, more evidence appears to exist to support the previous statements that the poor results obtained with MRCI are not due to the basis set implemented, since the same basis sets yield acceptable results with QCISD. It is also evident that QCISD is the best method discussed thus far for the calculation of the $^{17}O$ HFCC in the hydroxyl radical. A possible explanation for the failure of the MRCI technique, but the success of the QCISD technique is that the importance of the HF configuration in the hydroxyl radical outweighs the importance of the other configurations. Hence, when implementing MRCI, convergence of the HFCCs is very slow since each additional configuration yields only a small contribution, whereas QCISD appears to represent the effects of subsequent contributions more accurately.

### *3.3.4 Comparison of UHF and ROHF Based Methods*

One problem with the comparison of QCISD and MRCI results arises due to differences in reference determinants. QCISD uses UHF as the reference determinant whereas MRCI uses ROHF as the reference determinant. This poses a problem since, as discussed in Chapter Two, the unpaired electron in the hydroxyl radical is located in a *p*-orbital and therefore ROHF predicts a value of zero for the isotropic HFCCs. Thus, electron correlation methods implementing ROHF as the reference determinant must increase the magnitude of $A_{iso}$. Alternatively, UHF overestimates isotropic HFCCs. In the hydroxyl radical on average values of -33.2 G and -37.9 G are obtained for the oxygen and hydrogen HFCCs with UHF (Table 3.11), respectively, through the implementation of those basis sets previously discussed for QCISD and MRCI. Thus,

electron correlation must decrease the magnitude of the isotropic HFCC for UHF based methods. From this discussion it is evident that differences may arise in the basis set requirements for methods based on the UHF wave function rather than the ROHF wave function.

This difficulty can be tested through the implementation of the coupled-cluster (CC) method. In particular, Bartlett and coworkers have devised a computational scheme in which either the UHF or ROHF reference determinants can be used for the coupled-cluster singles and doubles (CCSD) method.[43,44] In addition, analytical energy derivatives to approximate triple excitations (CCSD(T)) have been implemented.[45,46] The effects of the nature of the reference determinant on HFCCs have been investigated through the use of CCSD and CCSD(T) for the second row elements and the $BH_2$ radical,[47] as well as for a number of organic radicals.[48] However, $^{17}O$ HFCCs in small molecules have not been investigated. Calculations were performed using a variety of basis sets previously discussed for QCI and MRCI with the ACES II program.[49]

Results obtained with the QCISD and CCSD methods based on the UHF wave function are in very good agreement with one another (Table 3.11). In addition, the MRCI (Table 3.10) and ROHF-CCSD isotropic HFCCs are in good agreement. This indicates that perhaps the ROHF based methods do not sufficiently compensate for the neglect of spin polarization in the ground state wave function. If one considers the

Table 3.11: Comparison of the isotropic HFCCs (G) in the hydroxyl radical obtained with UHF and ROHF based methods.

| Basis Set | UHF | UHF-QCISD | UHF-QCISD(T) | UHF-CCSD | UHF-CCSD(T) | ROHF | ROHF-CCSD | ROHF-CCSD(T) |
|---|---|---|---|---|---|---|---|---|
| $A_{iso}(^{17}O)$ | | | | | | | | |
| 6-311+G(2df,p) | -33.0 | -17.3 | -17.0 | -17.3 | -16.9 | 0.0 | -16.1 | -16.8 |
| us-6-311+G(2df,p) | -34.0 | -17.1 | -16.7 | -17.1 | -16.6 | 0.0 | -15.9 | -16.6 |
| us-aug-CC-PVTZ | -33.5 | -17.7 | -17.5 | -17.6 | -17.4 | 0.0 | -16.4 | -17.4 |
| (10s6p1d/6s1p) | -32.6 | -16.0 | -15.9 | -16.3 | -15.8 | 0.0 | -15.4 | -15.7 |
| [6s3p1d/4s1p] | -32.3 | -17.4 | -17.1 | -17.3 | -16.9 | 0.0 | -16.4 | -16.8 |
| (11s7p2d/7s2p) | -33.7 | -17.0 | -16.6 | -17.0 | -16.6 | 0.0 | -15.9 | -16.5 |
| $A_{iso}(^{1}H)$ | | | | | | | | |
| 6-311+G(2df,p) | -37.7 | -26.6 | -25.7 | -26.4 | -25.7 | 0.0 | -26.0 | -25.6 |
| us-6-311+G(2df,p) | -37.8 | -26.6 | -25.7 | -26.3 | -25.6 | 0.0 | -26.0 | -25.6 |
| us-aug-CC-PVTZ | -36.8 | -25.7 | -24.8 | -25.5 | -24.7 | 0.0 | -25.1 | -24.8 |
| (10s6p1d/6s1p) | -37.7 | -27.2 | -26.2 | -26.8 | -26.1 | 0.0 | -26.4 | -26.1 |
| [6s3p1d/4s1p] | -40.1 | -29.1 | -28.4 | -29.0 | -28.3 | 0.0 | -28.6 | -28.3 |
| (11s7p2d/7s2p) | -37.4 | -26.7 | -25.6 | -26.4 | -25.6 | 0.0 | -26.0 | -25.6 |

inclusion of triples through the CCSD(T) method, then the UHF and ROHF based methods yield identical results (Table 3.11). This indicates that the HFCCs are independent of the reference determinant once enough electron correlation has been taken into account. The effects of triple excitations have been examined by Feller *et al.*[16] and determined to be less than 1 G for both atoms in the NO molecule. The effect of triples on the QCISD HFCCs in the hydroxyl radical (Table 3.11) indicate that HFCCs slightly smaller in absolute magnitude than the QCISD results are obtained with QCISD(T). In addition, the QCISD(T) HFCCs are in excellent agreement with those obtained with CCSD(T) using both UHF and ROHF reference determinants. Thus, converged results are obtained if a high enough level of electron correlation is included.

Excluding the [6s3p1d/4s1p] basis set due to its deficiencies discussed earlier, the UHF-CCSD(T), ROHF-CCSD(T) and QCISD(T) methods recover, on average, approximately 92% of the experimental oxygen isotropic HFCC for the basis sets examined (Table 3.11). UHF based CCSD and QCISD also recover a large amount of the experimental value (approximately 93%). The slightly better results obtained with these methods, compared to those which include noniterative triples, indicates that a cancellation of errors may prevail in methods which do not account for triple excitations. In particular, UHF-CCSD and QCISD do not sufficiently compensate for the overestimation of the HFCCs by UHF, thus leading to values larger in magnitude than those obtained through the corresponding methods accounting for triple excitations. ROHF-CCSD and MRCI, on the other hand, recover on average only 88% and 82% of the oxygen coupling, respectively. It should be noted that all methods recover approximately 98% of the experimental hydrogen isotropic HFCC.

Once again, the results indicate that it is not the basis sets implemented which are leading to the poor results obtained with MRCI. It appears that the MRCI wave function inadequately accounts for the additional polarization required when the ROHF reference determinant is implemented. Although the ROHF-CCSD method recovers only 88% of the experimental oxygen coupling, this result is improved upon through the inclusion of the effects of triple excitations. These effects are very difficult to describe through the use of MRCI. Thus, even though a great number of reference configurations and a small configuration energy selection threshold were implemented in the present study, the

MRCI wave function is not easily adjusted to accurately predict $^{17}O$ HFCCs in the hydroxyl radical.

### *3.3.5 Summary of MRCI Study*

In the present section, the hyperfine coupling constants in the hydroxyl radical were investigated through comparison of results obtained with MRCI, DFT, QCI and CC methods. The results obtained from MRCI were studied through variations in the basis set, the configuration selection energy threshold and the size of the reference space. The results obtained from the basis set study converged well within themselves, but not to the experimental value for the isotropic $^{17}O$ HFCC. Alternatively, the calculated hydrogen HFCCs agree well with experiment.

The use of natural orbitals increases the rate of convergence, although results do not converge with respect to the experimental value. Additional attempts to improve convergence of $^{17}O$ HFCCs were made by augmenting the reference space with additional configurations chosen through examination of the spin density matrix. The rate of convergence within the results was improved, but deviations from experimental data were still observed. Variations in the bond length used for single-point calculations led to no improvement in the results, implying vibrational effects on the HFCCs are small.

Results obtained with QCISD are in better agreement with experiment than results obtained with MRCI and DFT (B3LYP functional), despite the extreme computational demands of the former. UHF and ROHF based CCSD and CCSD(T) methods were examined to ensure that QCISD did not yield improved results over MRCI due to differences in the reference determinant. It was concluded that once a high enough level of correlation is implemented, oxygen HFCCs are independent of the nature of the reference determinants and results in good agreement with experiment are obtained. The UHF and ROHF-CCSD(T) methods, with a variety of basis sets, recover on average 92% of the experimental oxygen HFCC, whereas MRCI recovers on average only 82%. Approximately 98% of the experimental hydrogen HFCC is recovered by all methods.

It was concluded that the basis sets implemented are not responsible for the poor results obtained with MRCI. Rather, the MRCI method implemented, which included a large number of reference configurations and a small configuration selection energy threshold, is not easily adjusted to account for the inadequacies of the ROHF reference

determinant to describe couplings in the hydroxyl radical. Thus, additional configurations cannot be accounted for by using MRCI. If DFT $^{17}O$ HFCCs require improvement through the use of techniques which implement multi-determinants, then either the QCISD(T) or CCSD(T) methods are recommended.

### *3.4 The Combined Quantum Mechanics and Molecular Dynamics Technique*

As mentioned in Chapters One and Two, combined quantum mechanics and molecular dynamics techniques (QM/MD) allow for the inclusion of vibrational and matrix effects in calculations. The hybrid QM/MD method consists of treating part of the system (the "solute") through highly accurate QM methods and treating the rest of the system (the "solvent") classically with MD techniques. The solute could be a fraction of a macromolecule, a cluster or a chemically interesting target molecule. The QM/MD method has been used previously on numerous occasions for computational problems such as the study of reaction schemes,[50] solvation phenomena,[51] the simulation of enzyme reactions and various other biochemical problems,[52] and the calculation of radical properties such as HFCCs,[53] to name but a few. In the case of calculating radical properties, the molecule whose HFCCs are desired is treated quantum mechanically and the surrounding matrix environment is treated classically. In this section, the QM/MD method will be described and subsequently applied to small inorganic peroxyl radicals. This study will attempt to improve upon the HFCCs calculated with DFT for FOO in the gas phase at 0 K.

#### *3.4.1 The Methodology of QM/MD*

The molecular system to be examined can be separated into three parts: a QM region, an MD region and a boundary region (Figure 3.4).[50,52,54] The QM particles are represented as nuclei and electrons and the potential energy surface for these atoms is obtained under the Born-Oppenheimer approximation. In the MD region, the particles are represented as atoms and their interactions are determined from empirical potential energy functions, a variety of which are available in the literature. The boundary region is included to account for the surroundings that are neglected in the other two regions.

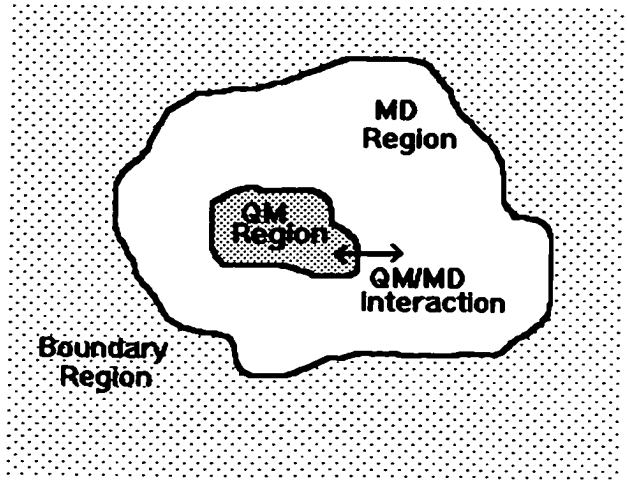


Figure 3.4: Division of the QM/MD system.

During a simulation, the molecular trajectories, which describe the position and molecular momenta, are obtained. The trajectories are calculated by solving Newton's equations of motion

$$F_i(t) = m_i a_i(t) \qquad i = 1, 2, ..., N \tag{3.1}$$

where $N$ represents the number of atoms under consideration. Integration of Equations 3.1 once yields velocity and twice yields the position of the atoms. According to Newton's laws, the forces acting on the body are required. In the QM/MD method, the forces are obtained by differentiating the system's energy expression (the expectation value of an effective Hamiltonian) with respect to the nuclear ($\alpha$) or atomic ($M$) coordinates,

$$F_\alpha = -\frac{\partial E}{\partial R_\alpha} \quad \text{and} \quad F_M = -\frac{\partial E}{\partial R_M}. \tag{3.2}$$

The energy and forces of the entire system are obtained by solving the time-independent Schrödinger equation with an effective Hamiltonian and a wave function. Hence, the problem is reduced to writing an expression for the Hamiltonian of the entire system. Figure 3.4 indicates that an effective Hamiltonian can be written as the sum of four terms

$$\hat{H}_{eff} = \hat{H}_{QM} + \hat{H}_{MD} + \hat{H}_{QM/MD} + \hat{H}_{Boundary} \tag{3.3}$$

The wave function is thus a function of the position of the electrons and parametrically depends on the positions of the nuclei of the QM and MD atoms.

The first term in Equation 3.3 represents the Hamiltonian describing the interactions between the electrons and nuclei of the QM particles. Mathematically,

$$\hat{H}_{QM} = -\frac{1}{2}\sum_i \nabla_i^2 + \sum_{ij}\frac{1}{r_{ij}} - \sum_{i\alpha}\frac{Z_\alpha}{r_{i\alpha}} + \sum_{\alpha\beta}\frac{Z_\alpha Z_\beta}{R_{\alpha\beta}} \tag{3.4}$$

where $i$, $j$ and $\alpha$, $\beta$ are the electronic and nuclear coordinates respectively, $r$ is the distance between an electron and either another electron or a nucleus, $R$ is a nuclear-nuclear distance and $Z_\alpha$ is the nuclear charge.

The long-range interactions of the MD particles are obtained by representing the atoms by partial charges and van der Waals spheres centered at the atoms. The short-range interactions linking the atoms are represented by harmonic bonds and other internal coordinate terms. The Hamiltonian for the MD particles can be represented as

$$\hat{H}_{MD} = \sum_M \frac{P_M^2}{2m_M} + V_{MD} \tag{3.5}$$

where $P_M$ and $m_M$ are the momentum and mass of the MD particles and $V_{MD}$ is the potential energy function between the MD particles (the force field). A typical MD force field can be expressed as

$$V_{MD} = V_{bonds} + V_{angles} + V_{dihedrals} + V_{improper} + V_{non-bonded} \tag{3.6}$$

or

$$V_{MD} = \sum_{All-bonds}\frac{1}{2}k_B(r-r_{eq})^2 + \sum_{All-angles}\frac{1}{2}k_\theta(\theta-\theta_{eq})^2 + \sum_{All-dihedrals}\frac{1}{2}k_\phi[1+\cos(n\phi-\delta)]$$
$$+ \sum_{All-impropers}\frac{1}{2}k\varphi(\varphi-\varphi_{eq})^2 + \sum_{All-(ij)pairs}4\varepsilon_{ij}\left[\left(\frac{\sigma_{ij}}{r_{ij}}\right)^{12} - \left(\frac{\sigma_{ij}}{r_{ij}}\right)^{6}\right] + \sum_{All-(ij)pairs}\frac{q_i q_j}{r_{ij}}$$

One of the simplest representations of the interactions between the QM and MD regions is as follows

$$\hat{H}_{QM/MD} = -\sum_{iM}\frac{q_M}{r_{iM}} + \sum_{\alpha M}\frac{Z_\alpha q_M}{R_{\alpha M}} + \sum_{\alpha M}\left\{\frac{A_{\alpha M}}{R_{\alpha M}^{12}} - \frac{B_{\alpha M}}{R_{\alpha M}^{6}}\right\} \tag{3.7}$$

where the subscripts $i$ and $\alpha$ correspond to the QM electrons and nuclei respectively and $M$ corresponds to the MD atoms. The first two terms in Equation 3.7 represent the interactions between the MD atoms and the QM electrons or nuclei, respectively. The

third term represents the van der Waals interactions between the QM nuclei and the MD atoms. This term must be included since if a molecule has no charge, then the first two terms will not account for its influence on the QM atoms. Additionally, the first terms are equivalent for atoms with the same charge and, thus, the third term provides a distinction between different atom types. The electrostatic and van der Waals interactions are truncated at some point to save computational time. For example, a typical cutoff includes only the interactions between atoms within 8 to 15 Å of each other.

It is also necessary to account for the boundary, since not all of the atoms in the real system are included in a simulation. The most popular method to account for the neglected area is called the periodic boundary condition. In this method, the system is surrounded in three dimensions by exact duplicates (images) of itself. The energy and forces of the atoms in the image are summed into the total energy and forces for the system. The MD atoms in the images are treated the same as the MD atoms in the box and they have similar interactions with the QM electrons and nuclei. One problem is that the images also contain QM atoms which must be taken into account. However, these atoms cannot be treated similarly to the MD particles since their charges change as the simulation proceeds. The preferred method to deal with this problem is to keep the QM atoms in the duplicate boxes far enough away from the original QM atoms so that they do not interact and, therefore, do not need to be included in the calculation. Alternatively, the image QM atoms can be treated as point charges, where the charge on each atom must be determined by a population analysis at each time step during the simulation.

Many different QM methods have been used including semi-empirical, DFT, valence bond and HF methods.[55] In particular, DFT is attractive since it includes electron correlation at a lower computational cost than *ab initio* methods. Computational speed is a very important consideration for the QM/MD method since the time required for each simulation step is slightly more than the time required to perform a single-point calculation at the same level of theory. This implies that it is not practical to use, for example, full CI as the QM method.

When DFT is chosen to calculate the forces for the QM/MD technique, Equation 3.4 for each electron becomes

$$H_{DFT} = -\frac{1}{2}\nabla^2 + \sum_A \frac{Z_A}{|R_A - r_1|} + \int \frac{\rho(r_2)}{|r_1 - r_2|} dr_2 + V_{xc} . \quad (3.8)$$

The first term in Equation 3.8 represents the kinetic electronic energy, the second term accounts for the nuclear-electron interactions, the third term is the interelectronic repulsion and the fourth term is the exchange-correlation potential, which is defined by the chosen DFT functional. Thus, the components of the energy can be obtained by solving the Kohn-Sham equations, and the remainder of the procedure is as discussed.

As with any theoretical method, the QM/MD technique possesses some shortcomings. Limitations are clearly imposed by the QM method implemented, which is constrained by available computer resources and time. The simulations describe the experimental matrix through an assigned value for its density. The density value used in the calculations can have an effect on the geometry of the radical under consideration and thus the chosen density can lead to differences between the experimental and modeled environment. Fractional atomic charges for the QM atoms are obtained from the QM calculation through a Mulliken population analysis. This is controversial since the charge in the molecule would be distributed differently if an alternative method for a population analysis was implemented. Treating the matrix atoms classically is also a downfall since it is well known that quantum mechanics must be employed to accurately describe atoms. The description of bond stretching and bending through harmonic wells is also a disadvantage since although this is a good approximation at bond lengths close to the equilibrium value, it deteriorates when larger deviations are considered. Finally, due to computer constraints, short-time spans (1 ps) are usually considered in the simulation, which may not be sufficient to obtain reliable averaged properties. Despite the downfalls discussed within, the QM/MD method provides a means to examine matrix, vibrational and temperature effects on the HFCCs of small radicals.

### *3.4.2 Computational Details*

Results from the QM/MD method were obtained with a modified version of the McMoldyn simulation package.[56] The B3LYP functional was implemented due to good results observed in the past.[53] The basis set used was Pople's 6-311G(d,p). In order to obtain improvements on the results obtained from the B3LYP/6-311G(d,p) method,

larger basis sets and more involved computational techniques such as QCISD must be implemented. Since a single-point calculation is performed at each MD time step and improvements in either the basis set or method drastically increase the computational time required, the B3LYP/6-311G(d,p) combination is the most feasible QM method. Additionally, the MP2/6-31G(d,p) combination was used to obtained the QM forces. A smaller basis set was implemented for the MP2 simulations due to the increased computational time required over DFT. MP2 was used in addition to the B3LYP functional to examine differences in geometrical fluctuations calculated with these two methods. The QM calculations were carried out using GAUSSIAN 94.[9]

The geometry of each radical under investigation was optimized and the force constants calculated at the B3LYP/6-311G(d,p) level. A classical simulation was then performed including both the radical and the matrix. The radicals were embedded in an matrix consisting of 255 argon atoms. A rare gas matrix was implemented in order to concentrate on temperature and steric hindrance effects imposed by a rigid matrix system rather than effects imposed by, for example, a more polar matrix. The temperature was held constant at 4 K throughout the simulation. A time step of $10^{-16}$ s was implemented and a classical simulation was performed to allow for equilibration. The geometrical variables in the molecule of interest are used as a gauge for equilibration. Next, the quantum mechanical forces were applied and the system was allowed to re-establish equilibrium. Once equilibration occurred, the system was monitored and the data collected for an additional few thousand time steps.

### *3.4.3 The HOO Radical*

The first radical to be discussed in terms of results obtained from the DFT/MD method is HOO. This species was not discussed in the previous sections since no experimental data is available for the oxygen nuclei. However, it is the smallest inorganic peroxyl radical, which is a benefit when using a computationally demanding method such as QM/MD. Additionally, this species is the main radical involved in biological processes and therefore a complete understanding about this system is desirable. The results from static MP2 and B3LYP calculations, along with those obtained using the respective force fields in an MD simulation, are displayed in Table 3.12.

Table 3.12: The geometry and HFCCs obtained for the HOO radical from static and molecular dynamics (Ar, 4K) calculations at various levels of theory.

| | | r(HO) | r(OO) | ∠(HOO) | $A_{iso}(^1H)$ | $A_{iso}(^{17}O)$ | $A_{iso}(^{17}O)$ |
|---|---|---|---|---|---|---|---|
| B3LYP/6-311G(d,p) | Static | 0.975 | 1.328 | 105.5 | -9.1 | -7.2 | -11.4 |
| B3LYP/6-311G(d,p) | Ar, 4K | 0.977 | 1.330 | 105.5 | -9.1 | -7.2 | -11.4 |
| MP2/6-31G(d,p) | Static | 0.975 | 1.326 | 104.4 | -8.2 | -15.0 | -39.2 |
| MP2/6-31G(d,p) | Ar, 4K | 0.976 | 1.327 | 104.4 | -8.2 | -15.0 | -39.0 |
| QCISD/6-311G(d,p) | Static | 0.969 | 1.333 | 104.3 | | | |
| QCISD/6-311+G(2d,p)[a] | Static | | | | -10.2 | -11.6 | -22.4 |
| B3LYP/6-311+G(2d,p)[a] | Static | | | | -8.8 | -7.7 | -13.0 |
| Experimental[b] | | | | | -10.2 | | |

[a]Results obtained from a single-point calculation at the QCISD/6-311G(d,p) geometry.
[b]Reference (57).

The geometries calculated at both the MP2 and B3LYP levels in the gas phase are very similar (Static, Table 3.12). However, the HFCCs calculated at the respective levels are very different. This reflects the fact that MP2 overestimates the isotropic HFCC as discussed in Chapter Two. The oxygen HFCCs calculated at the B3LYP level (-7.2 and -11.4 G) do not resemble those obtained experimentally for other small peroxyl radicals. For example, the inner and outer couplings obtained experimentally for FOO ($ClH_2COO$) are -14.5 (-11.1) and -22.2 (-22.3) G, respectively. The time-averaged geometries obtained from the MD simulations (Ar, 4K; Table 3.12) are very similar to the static results. The fluctuations in the HO and OO bond lengths observed with both the MP2 and B3LYP force fields are relatively small. More precisely, deviations from the average results were approximately ±0.02 and ±0.025 Å, respectively. Deviations in the HOO bond angle from the average value obtained with the MP2 force fields (±2°) are much smaller than those obtained with the B3LYP forces (±6.5°), despite the fact that the frequency of the oscillations is similar. This supports data in the literature indicating that DFT transition barriers are much lower than those predicted by MP2. Similar to the geometries, the averaged HFCCs obtained from the simulations are nearly identical to those obtained at the same level of theory in static calculations. Larger changes in the HFCCs have been observed in many other radicals once molecular vibration is taken into account (for example, see Table 2.4, Chapter Two).

Since the calculated HFCCs do not change upon inclusion of matrix and vibrational effects, it is of interest to examine the HFCCs in HOO with a high-level of theory. From the work presented on the hydroxyl radical, it is known that either QCI or

CC methods are required to improve upon DFT results for oxygen HFCCs. Thus, the geometry of HOO was calculated at the QCISD/6-311G(d,p) level and HFCCs obtained through a single-point calculation with a larger basis set (6-311+G(2d,p)). From the results (Table 3.12) it can be seen that the geometry calculated with QCISD is very similar to those obtained from B3LYP and MP2. However, the QCISD HFCCs are much different from those previously obtained. Additionally, the hydrogen isotropic coupling is in excellent agreement with available experimental data and the oxygen couplings closely resemble those obtained for other small peroxyl radicals. The HFCCs calculated with B3LYP at the QCISD geometry with a slightly larger basis set (6-311G+(2d,p)) are not much different from those obtained from the simulations.

These results indicate that the inclusion of matrix and vibrational effects are not sufficient to yield HFCCs for the HOO radical in agreement with a value expected from experimental studies on other peroxyl radicals. Additionally, couplings that are more reasonable can be obtained for this species if QCISD is examined. This reemphasizes one of the main sources of error outlined in the previous section. More specifically, the QM/MD method cannot overcome the main deficiencies of the QM method employed.

### *3.4.4 The FOO Radical*

The uncertainty of the FO bond length in FOO has been discussed in Section 3.2.3.1. This peroxyl radical, as well as its peroxide analogue (FOOF), is well known to be a difficult test for current computational methods.[25,58] From the data presented earlier, the experimental FO bond length in FOO (1.649 Å) is drastically underestimated with MP2 (1.38 Å), while many DFT methods yield a value (1.62 Å) close to that observed from experimental gas phase studies. However, if a high degree of spin contamination is observed in the DFT calculation, then the predicted bond length (1.82 Å) is much longer than the experimental value. Regardless of the geometry employed, the calculated HFCCs are in poor agreement with experimental data.

In a recent CCSD(T) study of FOO, the HFCCs were investigated as a function of increasing FO bond length.[59] Nine single-point calculations were performed and it was determined that the best agreement with experimental data could be obtained with an FO bond length of approximately 1.58 Å, which is shorter than predicted experimentally (1.649 Å). The great dependence of the HFCCs in FOO on the FO bond length, and the

differences between the experimental bond length and that required to calculate accurate couplings, indicate that the FO bond length is in reality shorter than reported experimentally. Thus, a reexamination of the experimental results was suggested. An alternative explanation is that the matrix used to study the HFCCs experimentally influences the radical's geometry. For example, the matrix could compress the elongated FO bond length measured in gas phase experiments to yield HFCCs in good agreement with those calculated at shorter bond lengths. This seems unlikely, however, since identical isotropic $^{19}F$ couplings were obtained in both Ar and $CF_4$ matrices. Alternatively, the experimental HFCCs could be modified through a vibrational averaging of the long and short FO bond lengths.

The possibility that the FO bond length is shortened in the experimental matrix or that the HFCCs are dependent upon vibrational effects can be investigated with the QM/MD method. The geometries and HFCCs obtained with both the MP2 and B3LYP force fields are displayed in Table 3.13. As discussed above, differences exist between the MP2 and B3LYP geometries for this radical. However, the results obtained from static, gas phase calculations for a particular method and the averaged data obtained with the same QM method from simulations in Ar at 4 K are very similar. The deviations from the averaged r(FO), r(OO) and ∠(FOO) values at the MP2 level are ±0.01, ±0.06 and ±2°, while the deviations in the B3LYP results are ±0.15, ±0.04 and ±9°, respectively. As opposed to the HOO radical, a great deal of motion is exhibited for FOO under the B3LYP force field. Despite these large oscillations, the HFCCs obtained with the B3LYP/MD method are nearly identical to those obtained from static calculations. Neither the B3LYP nor the MP2 HFCCs are in good agreement with experimental data. Since no difference was observed between DFT HFCCs in the gas phase and in an Ar matrix, the inconsistencies between experimental and theoretical geometries must not be due to matrix effects, but perhaps the theoretical method employed.

To investigate HFCCs obtained from high-level calculations, the geometry of FOO was optimized at the QCISD/6-311G(d,p) level (Table 3.13). The QCISD r(OO) and ∠(FOO) parameters are in good agreement with the experimental data. However, the calculated FO bond length (1.588 Å) is shorter than the experimental value (1.649 Å).

Table 3.13: The geometry and HFCCs obtained for the FOO molecule from static and molecular dynamics (Ar, 4K) calculations at various levels of theory.

| | | r(FO) | r(OO) | ∠(FOO) | $A_{iso}(^{19}F)$ | $A_{iso}(^{17}O)$ | $A_{iso}(^{17}O)$ |
|---|---|---|---|---|---|---|---|
| B3LYP/6-311G(d,p) | Static | 1.791 | 1.185 | 111.6 | -26.7 | 25.3 | -15.6 |
| B3LYP/6-311G(d,p) | Ar, 4K | 1.788 | 1.188 | 111.4 | -27.0 | 21.6 | -15.1 |
| MP2/6-31G(d,p) | Static | 1.383 | 1.251 | 109.6 | 13.3 | -18.1 | -44.6 |
| MP2/6-31G(d,p) | Ar, 4K | 1.382 | 1.253 | 109.5 | 12.6 | -8.2 | -44.4 |
| QCISD/6-311G(d,p) | Static | 1.588 | 1.203 | 110.6 | | | |
| QCISD/6-311+G(2d,p)[a] | Static | | | | -13.5 | -13.5 | -21.5 |
| B3LYP/6-311+G(2d,p)[a] | Static | | | | -17.9 | -6.2 | -13.0 |
| Experimental[b] | | 1.649 | 1.200 | 111.2 | -12.8 | -14.4 | -22.1 |

[a]Results obtained from a single-point calculation at the QCISD/6-311G(d,p) geometry.
[b]References (1), (12), (13) and (27).

The HFCCs calculated by a single-point calculation with QCISD/6-311+G(2d,p) are in very good agreement with the experimental couplings (Table 3.13). Additionally, HFCCs calculated at the QCISD geometry with B3LYP/6-311+G(2d,p) are in much better agreement with the experimental values than those obtained at the B3LYP geometry or the time-averaged geometry from the simulations. However, the B3LYP HFCCs are still far from the experimental values. It should be noted that the optimized QCISD FO bond length is close to the value predicted by scanning the FO bond length and comparing CCSD(T) HFCCs to experimental results.

In summary, poor agreement is observed between experimental HFCCs and geometries and those calculated at 0 K in the gas phase. Theoretical data in better agreement with experiment are not obtained upon inclusion of vibrational and matrix effects, which indicates that these effects are small and not responsible for the discrepancies. However, when geometries with FO bond lengths shorter than the experimental value are used to calculate the HFCCs, good agreement between theoretical and experimental HFCCs is obtained. Since HFCCs are highly dependent on geometry, deviations between experimental and theoretical FO bond lengths must be explained by possible errors in the experimental data. Thus, a reexamination of the experimental geometry for FOO is necessary to help clarify these inconsistencies.

### *3.4.5 The ClOO Radical*

A molecule closely related to FOO is the chloroperoxyl radical (ClOO). This species has also been under both theoretical and experimental investigation. It is primarily of interest due to its long ClO bond length (similar to that observed for FOO).

This radical has been identified as an important radical in ozone depletion and its lifetime is too short to allow for detailed studies of its properties. The most accurate geometry calculated for this radical has been obtained with MRCI.[60] The R(ClO), R(OO) and ∠(ClOO) values determined with this method are 2.139 Å, 1.201 Å and 115.7°, respectively. These values were verified through comparison with experimental data obtained in both argon and neon matrices.[61] Experimental studies of ClOO embedded in a $KClO_4$ matrix,[62] concluded that the matrix cavity into which the radical must be embedded is small. Therefore, it was predicted that a compressed geometry is present in this matrix. The r(ClO), r(OO) and ∠(ClOO) values were estimated to be equal to 2.0 Å, 1.20 Å and 112°, respectively.

Despite the geometrical differences predicted when ClOO is placed in argon versus $KClO_4$, the chlorine isotropic hyperfine coupling constant has been measured in both matrices and determined to be nearly identical. This implies that either the HFCCs are insensitive to the geometry or that the geometries observed in Ar and $KClO_4$ matrices are very similar despite the available experimental data. In a previous theoretical study, the HFCCs in ClOO were calculated at both experimental geometries through single-point calculations at the CCSD(T) level. Naturally, it was determined that the HFCCs depend on the geometry employed. This implies that the latter explanation for the experimental discrepancies must be true. More specifically, the geometry in both argon and $KClO_4$ matrices must be the same in order to obtain similar couplings in both experiments. Thus, once again it appears that more detailed experimental work must be performed on this radical.

### *3.4.6 Summary of QM/MD Study*

The hyperfine coupling constants in small inorganic peroxyl radicals have been discussed in the present section. It has been shown that DFT (the B3LYP functional) cannot adequately calculate the HFCCs in these systems. Through the investigation of time-averaged properties it was hoped that data in better agreement with experiment would be obtained. This was examined through the combined QM/MD technique, where the radical of interest was placed in an argon matrix and simulations were performed at a temperature of 4 K. Neither the time-averaged geometrical properties nor the HFCCs

obtained from the simulations were drastically different from those obtained from static, gas phase calculations, despite the fact that large oscillations were observed in some instances. The results indicate that neither the Ar matrix nor the vibrational averaging affects the HFCCs in HOO and FOO. Thus, differences between experiment and theory must lie entirely in the quantum mechanical method employed. This illustrates one of the main sources of error for the combined QM/MD method, namely the QM method implemented.

High-level *ab initio* methods (QCISD) must be used to improve upon the results obtained from DFT for both HOO and FOO. Once QCISD was implemented, HFCCs in good agreement with experimental data for FOO were obtained. Additionally, the couplings calculated for HOO with QCISD were in good agreement with the experimental hydrogen coupling and oxygen couplings observed for other small peroxyl radicals. The geometry obtained with QCISD for FOO consists of a shorter FO bond length than the experimental value, even though the experimental and calculated HFCCs are in good agreement and calculated HFCCs have been previously shown to be very dependent on the geometry. This provides evidence that the experimentally reported geometry may not be reliable and further experimental work would be very useful. The discussion presented for ClOO lends more credibility to this conclusion. In particular, it can clearly be understood that more detailed experimental work must be performed on ClOO to determine an accurate geometry. Due to the similar nature between these two species, it is not surprising that a reinvestigation of both radicals is desirable.

### *3.5 Conclusions*

An in-depth investigation of oxygen hyperfine coupling constants was undertaken in the present chapter. Large alkyl peroxyl radicals were investigated through the use of density-functional theory. The calculated couplings were in fair agreement with experimental results. However, it was noted that couplings which agree much better with experiment have been obtained for nuclei different than oxygen in other theoretical investigations. Despite the disagreements between theory and experiment for the oxygen centered couplings, information about the location of the unpaired spin density in alkyl

peroxyl radicals was obtained. The fluoroperoxyl radical was also investigated with DFT and the couplings for this species are in very poor agreement with experimental results.

In order to improve upon the DFT results for oxygen couplings, the MRCI technique was investigated by examining the couplings in the hydroxyl radical. It was determined, after great computational efforts, that this method is not adequate to calculate the property at hand for the hydroxyl radical. The faults in this method lie mainly in the difficulties encountered when choosing the reference space. It was concluded that additional reference configurations provide only small contributions to the oxygen isotropic hyperfine coupling constant and therefore convergence of the MRCI results is slow. It was also determined that the MRCI wave function for the hydroxyl radical cannot be easily adjusted to recover effects neglected by the ROHF reference determinant (spin polarization). Other *ab initio* methods were also examined including QCI and CC based techniques. It was determined that once enough electron correlation is included in a calculation, it does not matter whether UHF or ROHF is used as a reference determinant. Additionally, it was concluded that either QCISD(T) or CCSD(T) is required to accurately calculate oxygen couplings in small molecules. Thus, these methods can account for the deficiencies in the UHF and ROHF reference determinants more efficiently than MRCI. These methods were able to recover approximately 92% of the experimental $^{17}O$ HFCCs, whereas MRCI recovers only 82%.

Besides the direct faults of the DFT method, the extremely poor results observed for fluoroperoxyl radical may be due to geometrical effects imposed by the experimental matrix or molecular vibration. These two possibilities were investigated for the HOO and FOO molecules through a combined QM/MD method. Both MP2 and DFT were used as the QM method. It was determined that neither the geometries nor the HFCCs in HOO and FOO changed drastically upon inclusion of matrix or vibrational effects. This indicates that DFT is to blame for the poor agreement between theory and experiment. Through the use of QCISD, accurate couplings were obtained for both molecules. The FO bond distance calculated with QCISD is shorter than that determined experimentally, despite the fact that the HFCCs are in good agreement with experimental data. This information, in addition to experimental and theoretical discrepancies observed for the ClOO radical, was used to speculate that the available experimental geometries for both

fluoro and chloroperoxyl radicals are inadequate and reexamination of this property is necessary.

Thus, the present chapter clearly shows the difficulty encountered when calculating accurate hyperfine coupling constants. It was illustrated that DFT will yield couplings in fair agreement with experiment for large molecules, however a deviation as large as 80% from the experimental value must be accepted when implementing this method for the calculation of oxygen coupling constants. For small molecules, QCI appears to be a wise choice to determine accurate couplings.

### *3.6 References*

1. Fessenden, R. W.; Schuler, R. H. *J. Chem. Phys.* **1966**, *44*, 434.

2. Melamud, E.; Silver, B. L. *J. Phys. Chem.* **1973**, *77*, 1896.

3. Bower, H. J.; Symons, M. C. K.; Tinling, D. J. A. In *Radical Ions;* Kaiser, E. T.; Kevan, L.; Eds.; Interscience: New York, 1968.

4. Adamic, K.; Ingold, K. U.; Morton, R. J. *J. Am. Chem. Soc.* **1970**, *92*, 922.

5. (a) Howard, J. A. *Can. J. Chem.* **1972**, *50*, 1981; (b) Howard, J. A. *Can. J. Chem.* **1979**, *57*, 253.

6. Ditchfield, R.; Hehre, W. J.; Pople, J. A. *J. Chem. Phys.* **1971**, *54*, 724; Hehre, W. J.; Ditchfield, R.; Pople, J. A. *J. Chem. Phys.* **1972**, *56*, 2257; Hariharan, P. C.; Pople, J. A. *Mol. Phys.* **1974**, *27*, 209; Gordon, M. S. *Chem. Phys. Lett.* **1980**, *76*, 163; Hariharan, P. C.; Pople, J. A. *Theor. Chim. Acta* **1973**, *28*, 213; McLean, A. D.; Chandler, G. S. *J. Chem. Phys.* **1980**, *72*, 5639; Krishnan, R.; Binkley, J. S.; Seeger, R.; Pople, J. A. *J. Chem. Phys.* **1980**, *72*, 650; Clark, T.; Chandrasekhar, J.; Spitznagel, G. W.; Schleyer, P. v. R. *J. Comput. Chem.* **1983**, *4*, 294; Frisch, M. J.; Pople, J. A.; Binkley, J. S. *J. Chem. Phys.* **1984**, *80*, 3265.

7. Kutzelnigg, W.; Fleischer, U.; Schindler, M. In *NMR - Basic Principles and Progress;* Springer-Verlag: Heidelberg, 1990; Vol. 23. The IGLO-III basis set consists of an (11s7p2d/6s2p) primitive set contracted to [7s6p2d/4s2p].

8. (a) Woon, D. E.; Dunning, T. H. *J. Chem. Phys.* **1993**, *98*, 1358; (b) Kendall, R. E.; Dunning, T. H.; Harrison, R. J. *J. Chem. Phys.* **1992**, *96*, 6796; (c) Dunning, T. H. *J. Chem. Phys.* **1989**, *90*, 1007.

9. Frisch, M. J.; Trucks, G. W.; Schlegel, H. B.; Gill, P. M. W.; Johnson, B. G.; Robb, M. A.; Cheeseman, J. R.; Keith, T. A.; Petersson, G. A.; Montgomery, J. A.; Raghavachari, K.; Al-Laham, M. A.; Zakrzewske, V. G.; Ortiz, J. V.; Foresman, J. B.; Cioslowski, J.; Stefanov, B. B.; Nanayakkara, A.; Challacombe, M.; Peng, C. Y.; Ayala, P. Y.; Chen, W.; Wong, M. W.; Andres, J. L.; Replogle, E. S.; Gomperts, R.; Martin, R. L.; Fox, D. J.; Binkley, J. S.; Defrees, D. J.; Baker, J.; Stewart, J. P.; Head-Gordon, M.; Gonzalez, C.; Pople, J. A. *Gaussian 94* (Revision B.2); Gaussian, Inc.: Pittsburgh, PA, 1995.

10. St-Amant, A.; Salahub, D. R. *Chem. Phys. Lett.* **1990**, *169*, 387; St-Amant, A. PhD. thesis, Université de Montréal, 1991; Salahub, D. R.; Fournier, R.; Mlynarski, P.; Papai, I.; St-Amant, A.; Ushio, J. In *Density Functional Methods in Chemistry;* Labanowski, J., Andzelm, J., Eds.; Springer: New York, 1991.

11. Leopold, K. R.; Evenson, K. M.; Comben, E. R.; Brown, J. M. *J. Mol. Spectr.* **1987**, *122*, 440.

12. Adrian, F. J. *J. Chem. Phys.* **1967**, *46*, 1543.

13. Morton, J. R.; Preston, K. F. Landolt-Börnstein, New Series. Vol. 9.; Fisher, H.; Hellwege, K.-H.; Eds.; Springer-Verlag, 1977; Part a.

14. Wetmore, S. D.; Boyd, R. J.; Eriksson, L. A. *J. Chem. Phys.* **1997**, *106*, 7738.

15. Cohen, M. J.; Chong, D. P. *Chem. Phys. Lett.* **1995**, *234*, 405.

16. Feller, D.; Glendening, E. D.; McCullough, E. A., Jr.; Miller, R. J. *J. Chem. Phys.* **1993**, *99*, 2829.

17. (a) Barone, V. *Theor. Chim. Acta* **1995**, *91*, 113; (b) Barone, V. *J. Chem. Phys.* **1994**, *101*, 6834; (c) Barone, V.; Adamo, C.; Russo, N. *Chem. Phys. Lett.* **1993**, *212*, 5; (d) Adamo, C.; Barone, V.; Fortunelli, A. *J. Chem. Phys.* **1995**, *102*, 384.

18. (a) Gauld, J. W.; Eriksson, L. A.; Radom, L. *J. Phys. Chem. A* **1997**, *101*, 1352; (b) Eriksson, L. A.; Malkina, O. L.; Malkin, V. G.; Salahub, D. R. *J. Chem. Phys.* **1994**, *100*, 5066; (c) Austen, M. A.; Eriksson, L. A.; Boyd, R. J. *Can. J. Chem.* **1994**, *72*, 695; (d) Kong, J.; Eriksson, L. A.; Boyd, R. J. *Chem. Phys. Lett.* **1994**, *217*, 24; (e) Eriksson, L. A.; Wang, J.; Boyd, R. J.; Lunell, S. *J. Phys. Chem.* **1994**, *98*, 792; (f) Martell, J. M.; Boyd, R. J.; Eriksson, L. A. *J. Phys. Chem.* **1995**, *99*, 623.

19. (a) Chipman, D. M.; Carmichael, I.; Feller, D. *J. Phys. Chem.* **1991**, *95*, 4702; (b) Feller, D. *J. Chem. Phys.* **1990**, *93*, 579; (c) Beck, S. N.; McCullough, E. A., Jr.; Feller, D. *Chem. Phys. Lett.* **1990**, *175*, 629; (d) Fernández, B.; Jørgensen, P.; Simons, J. *J. Chem. Phys.* **1993**, *98*, 7021.

20. Woon, D. E.; Dunning, D. H., Jr. *J. Chem. Phys.* **1995**, *103*, 4572.

21. Barone, V.; Adamo, C.; Mele, F. *Chem. Phys. Lett.* **1996**, *249*, 290.

22. Sevilla, M. D.; Becker, D.; Yan, M. *J. Chem. Soc. Faraday Trans.* **1990**, *86*, 3279. The numbers reported in Table 3.1 were obtained by converting the $A_{||}$ values to $A_{iso}$ through the use of the calculated anisotropic data. The values for all of the alkyl peroxyl radicals were very similar and on average can be reported as (-74.5 ± 0.9, 36.9 ± 0.5, 37.6 ± 0.4 G) for the terminal oxygen and (-44.5 ± 0.3, 21.2 ± 0.3, 23.3 ± 0.5 G) for the inner oxygen representing the anisotropic $T_{ZZ}$, $T_{YY}$ and $T_{XX}$ components, respectively.

23. McKee, M. L.; Webb, T. R. *J. Phys. Chem.* **1996**, *100*, 11292.

24. Ventura, O. N.; Kieninger, M. *Chem. Phys. Lett.* **1995**, *245*, 488.

25. Francisco, J. S.; Zhao, Y.; Lester, W. A., Jr.; Williams, I. H. *J. Chem. Phys.* **1992**, *96*, 2861.

26. Francisco, J. S.; Goldstein, A. N.; Lin, Z.; Zhao, Y.; Williams, I. H. *J. Phys. Chem.* **1990**, *94*, 4791.

27. Yamada, C.; Hirota, E. *J. Chem. Phys.* **1984**, *80*, 4694.

28. (a) Bender, C. F.; Davidson, E. R. *Phys. Rev.* **1969**, *183*, 23; (b) Rodgers, J. E.; Lee, T.; Das, T. P.; Ikenberry, D. *Phys. Rev. A* **1973**, *7*, 51; (c) Kristiansen, P.; Veseth, L. *J. Chem. Phys.* **1986**, *84*, 2711; (d) Kristiansen, P.; Veseth, L. *J. Chem. Phys.* **1986**, *84*, 6336; (e) Chipman, D. M. *J. Chem. Phys.* **1989**, *91*, 5455; (f) Chong, D. P.; Langhoff, S. R.; Bauschlicher, C. W., Jr. *J. Chem. Phys.* **1991**, *94*, 3700; (g) Momose, T.; Yamaguchi, M.; Shida, T. *J. Chem. Phys.* **1990**, *93*, 7284; (h) Nakatsuji, H.; Ehara, M.; Momose, T. *J. Chem. Phys.* **1994**, *100*, 5821; (i) Suter, H. U.; Pleβ, V.; Ernzerhof, M.; Engels, B. *Chem. Phys. Lett.* **1994**, *230*, 398; (j) Barone, V. *Chem. Phys. Lett.* **1994**, *226*, 392; (k) Ishii, N.; Shimizu, T. *Chem. Phys. Lett.* **1995**, *235*, 614.

29. Carmichael, I. *J. Phys. Chem.* **1990**, *94*, 5734.

30. MELDF-X, McMurchie, L.; Elbert, S.; Langhoff, S.; Davidson, E. R.; Feller, D. The University of Washington, Indiana University, and the Molecular Science Research Center, 1993.

31. Herzberg, G. *Spectra of Diatomic Molecules*; Van Nostrand: Princeton, 1950.

32. Huzinaga, S. *J. Chem. Phys.* **1965**, *42*, 1293.

33. Chipman, D. M. *Theor. Chim. Acta* **1989**, *76*, 73.

34. Chipman, D. M. *J. Chem. Phys.* **1989**, *91*, 5455.

35. Kong, J.; Boyd, R. J.; Eriksson, L. A. *J. Phys. Chem.* **1995**, *102*, 3674.

36. van Duijneveldt, F. B. IBM Research Report RJ 945, 1971.

37. Wetmore, S. D.; Boyd, R. J.; Eriksson, L. A. *J. Chem. Phys.* **1998**, *109*, 9451.

38. Engels, B.; Eriksson, L. A.; Lunell, S. *Adv. Quantum Chem.* **1997**, *27*, 297.

39. Feller, D.; Davidson, E. R. *J. Chem. Phys.* **1981**, *74*, 3977.

40. Engels, B. *Theor. Chim. Acta* **1993**, *86*, 429.

41. Feller, D.; Davidson, E. R. *J. Chem. Phys.* **1984**, *80*, 1006.

42. Feller, D.; Davidson, E. R. *Theor. Chim. Acta* **1985**, *68*, 57.

43. Gauss, J.; Stanton, J. F.; Bartlett, R. J. *J. Chem. Phys.* **1991**, *95*, 2639.

44. Gauss, J.; Lauderdale, W. J.; Stanton, J. F.; Watts, J. D.; Bartlett, R. J. *Chem. Phys. Lett.* **1991**, *182*, 207.

45. Watts, J. D.; Gauss, J.; Bartlett, R. J. *Chem. Phys. Lett.* **1992**, *200*, 1.

46. Watts, J. D.; Gauss, J.; Bartlett, R. J. *J. Chem. Phys.* **1993**, *98*, 8718.

47. Perera, S. A.; Watts, J. D.; Bartlett, R. J. *J. Chem. Phys.* **1994**, *100*, 1425.

48. Perera, S. A.; Salemi, L. M.; Bartlett, R. J. *J. Chem. Phys.* **1997**, *106*, 4061.

49. Aces II program is a product of the Quantum Theory Project, University of Flordia, Stanton, J. F.; Gauss, J.; Watts, J. D.; Nooijen, M.; Oliphant, N.; Perera, S. A.; Szalay, P. G.; Lauderdale, W. J.; Gwaltney, S. R.; Beck, S.; Balková, A.; Bernholdt, D. E.; Baeck, K. K.; Sekino, H.; Rozyczko, P.; Huber, C.; Bartlett, R. J.; integral packages included are VMOL (Almlöf, J.; Tayler, P. R.); VPROPS (Taylor, P. R.); A modified version of ABACUS intergral derivative package (Helgaker, T. U.; Aa, H. J.; Jensen; Olsen, J.; Jørgensen, P.; Taylor, P. R.).

50. Field, M. J.; Bash, P. A.; Karplus, M. *J. Comp. Chem.* **1990**, *11*, 700.

51. Wang, J.; Boyd, R. J.; Laaksonen, A. *J. Chem. Phys.* **1996**, *104*, 7261.

52. Åqvist, J.; Warshel, A. *Chem. Rev.* **1993**, *93*, 2523.

53. Eriksson, L. A.; Laaksonen, A. *Rec. Dev. Phys. Chem.* **1998**, *2*, 369.

54. Stanton, R. V.; Hartsough, D. S.; Merz, K. M., Jr. *J. Comp. Chem.* **1995**, *16*, 113.

55. Bakowies, D.; Thiel, W. *J. Phys. Chem.* **1996**, *100*, 10580 *and references therein.*

56. Laaksonen, A. *Comp. Phys. Commun.* **1986**, *42*, 271.

57. Adrain, F. J.; Cochran, E. L.; Bowers, V. A. *J. Chem. Phys.* **1967**, *47*, 5441.

58. Lee, T. J.; Rice, J. E.; Dateo, C. E. *Mol. Phys.* **1996**, *89*, 1359.

59. Fernández, B.; Christiansen, O.; Jørgensen, P.; Byberg, J.; Gauss, J.; Ruud, K. *J. Chem. Phys.* **1997**, *106*, 1847.

60. Peterson, K. A.; Werner, H. J. *J. Chem. Phys.* **1992**, *96*, 8948.

61. Müller, H. S. P.; Willner, H. *J. Phys. Chem.* **1993**, *97*, 10589.

62. Byberg, J. R. *J. Phys. Chem.* **1995**, *99*, 13392.

# CHAPTER FOUR

## Elucidation of the Main Radiation Products in Prymidine Components

### *4.1 Introduction*

The structure and chemical numbering of the three major pyrimidine bases are displayed in Figure 4.1. Thymine is an important target for radiation damage and, thus, is the DNA base for which the most experimental literature exists.[1,2] An assortment of electron spin resonance (ESR) work has been done on this base and many debates exist in the literature over possible radiation products, such as the protonation state of the anion.[3,4,5] A lot of experimental work on cytosine has also appeared in the literature and it has been under dispute whether thymine or cytosine is the primary site of electron gain upon irradiation of full DNA.[6] It is also of interest to investigate uracil, since it replaces thymine when RNA is investigated rather than DNA, although limited experimental work is available. Many theoretical calculations have been performed previously to obtain a variety of properties, excluding the HFCCs, of the pyrimidines.[7]

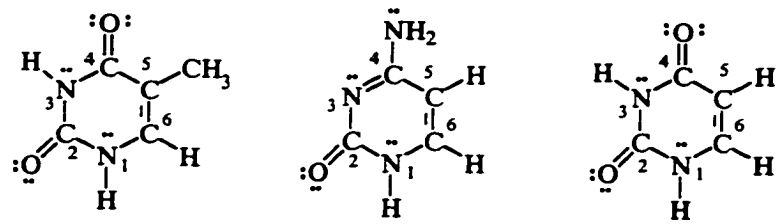

I II III

Figure 4.1: The chemical structure and numbering of thymine (I, 5-methyl-2,4-dioxypyrimidine), cytosine (II, 2-oxy-4-aminopyrimidine) and uracil (III, 2,4-dioxypyrimidine).

In order to examine the extent of radiation damage in DNA thoroughly, an initial investigation must be performed to determine the most important reaction products. Some of the mechanisms that give rise to the various forms of radiation damage will be the subject of a subsequent chapter. Thus, in the present chapter, the possible hydrogenation (net ·H addition), dehydrogenation (net ·H removal) and hydroxylation products (net ·OH addition), as well as the anion and the cation, of thymine, cytosine and uracil will be discussed. In particular, density-functional theory (DFT) has been used to calculate the HFCCs in potential radical radiation products and these results will be

compared to those obtained from single-crystal ENDOR studies on base derivatives. It should be noted that the calculation of accurate isotropic HFCCs requires both a good description of electron correlation and a well defined basis set, as discussed in Chapter Two. On the other hand, accurate anisotropic HFCCs can be calculated more easily. Thus, comparison of anisotropic hyperfine tensors can be used as an accurate guide to identify radical sites even when less satisfactory agreement is obtained for the isotropic component.

### *4.2 Computational Details*

The potential energy surfaces for possible radiation products were explored using Becke's three-parameter exchange functional (B3)[8] in combination with Lee, Yang and Parr's correlation expression (LYP)[9] and Pople's 6-31G(d,p) basis set.[10] It should be noted that for thymine at least two main conformers were obtained corresponding to eclipsed and staggered methyl conformations relative to the C5C6 double bond as determined in an investigation of thymine tautomers.[11] The minimum energy conformations were located for each potential radiation product and frequency analyses were performed to ensure these to be local minima. The zero-point vibrational energy can be accounted for through the use of a scale factor of 0.9804.[12]

Two sets of single-point calculations were performed on the global minima. First, the B3LYP hybrid functional and Pople's 6-311G(2df,p) basis set[10] were used to obtain relative energies and spin densities. The geometry optimizations and this set of single point calculations were carried out using GAUSSIAN 94.[13] Secondly, HFCCs were obtained using Perdew and Wang's nonlocal exchange (PW),[14] Perdew's nonlocal correlation functional (P86)[15] and Pople's 6-311G(2d,p) basis set.[10] In some cases, the isotropic HFCCs were obtained using the B3LYP single-point calculations described above, but it should be noted that nearly identical results were obtained with both functional forms. The present combination of methods has previously been employed in studies of model $\pi$-radicals.[16] These calculations were carried out with the deMon program,[17] using the (5,4;5,4) family of auxiliary basis sets for the fitting of the charge density and the exchange correlation potential.

### *4.3 Thymine*

#### *4.3.1 Previous Experimental Work*

Perhaps the most accurate data available for the hyperfine coupling constants (HFCCs) in thymine (Table 4.1) are from Sagstuen *et al.* who performed careful ENDOR studies on anhydrous thymine (T),[18] 1-methylthymine (1MeT)[19] and deoxythymidine (dT).[3,19] The major components identified in irradiated crystals of deoxythymidine[19] include the O4 and C6-hydrogenated radicals, the radical formed through hydrogen abstraction from the methyl group and a sugar group alkoxyl radical. Minor products

Table 4.1: Experimental HFCCs (G) obtained in thymine derivatives.

| Radical | Molecule | | $A_{iso}$ | $T_{XX}$ | $T_{YY}$ | $T_{ZZ}$ |
|---|---|---|---|---|---|---|
| O4-hydrogenated | T[18] | "C6H" | -14.2 | -8.2 | 1.0 | 7.2 |
| | | "O4H" | 12.3 | -2.6 | -2.5 | 5.1 |
| | | "C5-CH" (3) | -2.6 | -0.6 | -0.4 | 1.1 |
| | | "N3H" | -2.1 | -2.5 | -0.7 | 3.1 |
| | 1MeT[19] | "C6H" | -13.5 | -8.3 | 1.4 | 6.9 |
| | | "N3H" | -2.3 | -1.2 | -0.4 | 2.5 |
| | | "C5-CH" (3) | -2.1 | -0.6 | -0.4 | 1.1 |
| | dT[19] | "C6H" | -11.8 | -8.1 | 1.0 | 7.1 |
| | | "O4H" | 11.8 | 3.4 | -1.4 | -2.0 |
| | | "C5-CH" (3) | -2.4 | -0.7 | -0.4 | 1.1 |
| | | "N3H" | -1.9 | -2.3 | -0.8 | 3.1 |
| $CH_3$-dehydrogenated | T[18] | "C6H" | -10.7 | -4.8 | -0.4 | 5.3 |
| | | "C5-CH" | -15.7 | -8.1 | 0.3 | 7.9 |
| | | "C5-CH" | -16.4 | -9.0 | 0.6 | 8.4 |
| | | "N3H" | -1.0 | -0.9 | -0.8 | 1.7 |
| | 1MeT[19] | "C6H" | -9.2 | -4.1 | -0.4 | 4.6 |
| | | "C5-CH" | -15.7 | -8.4 | 0.2 | 8.3 |
| | | "C5-CH" | -16.6 | -9.2 | 0.8 | 8.4 |
| | dT[19] | "C6H" | -10.2 | -4.7 | -0.4 | 5.2 |
| | | "C5-CH" | -15.3 | -8.0 | 0.0 | 8.0 |
| | | "C5-CH" | -16.1 | -9.0 | 0.8 | 8.2 |
| C5-hydrogenated | T[18] | "C5H" | 48.6 | -1.7 | -0.7 | 2.4 |
| | | "C6H" | -19.2 | -11.2 | 1.0 | 10.2 |
| | 1MeT[19] | "C5H" | 49.0 | -1.7 | -0.5 | 2.2 |
| | | "C6H" | -19.9 | -11.2 | 0.9 | 10.4 |
| | dT[19] | "C5H" | 47.4 | -1.7 | -0.9 | 2.7 |
| C6-hydrogenated | T[18] | "C6H" | 45.3 | -1.6 | -0.9 | 2.5 |
| | | "C6H" | 32.0 | -1.6 | -1.1 | 2.6 |
| | | "C5-CH" (3) | 20.0 | -1.0 | -0.9 | 1.9 |
| | dT[19] | "C6H" | 41.7 | -1.6 | -0.9 | 2.4 |
| | | "C6H" | 39.5 | -1.7 | -2.9 | 2.7 |
| N1-methyl dehydrogenated | 1MeT:9MeA[20] | "N1-CH" | -20.7 | -10.9 | 1.2 | 9.7 |
| | | "N1-CH" | -19.1 | -10.8 | 0.3 | 10.4 |
| | 1MeT:9MeA[20] | "N1-CH" | -19.9 | -11.1 | 1.1 | 10.0 |
| | | "N1-CH" | -19.8 | -10.8 | 0.2 | 10.5 |
| not assigned | 1MeT[19] | | 19.3 | -0.9 | -0.8 | 1.7 |

observed in deoxythymidine include the C5-hydrogenated radical and a sugar radical formed through abstraction of the C1' hydrogen. The main products determined to be formed in 1-methylthymine[19] include the O4 and C5-hydrogenated and the C5-methyl dehydrogenated radicals. One coupling was left unassigned in these crystals. Examination of the co-crystals of 1-methylthymine and 9-methyladenine (1MeT:9MeA)[20] led to the elucidation of the products formed through abstraction of hydrogen from the C5 and N1-methyl groups as the major products and the O4, C5 and C6-hydrogenated radicals as the minor products. An investigation of anhydrous thymine[18] identified the radicals formed through hydrogen addition to the O4, C5 and C6 positions and those formed through hydrogen abstraction at the C5-methyl group as the major radiation products. The N1-dehydrogenated species was also observed as a minor product. In addition, a radical pair formed by linking two C5-methyl dehydrogenated radicals was also identified. Since calculations were performed on T rather than substituted analogues, the calculated results within this chapter will be discussed predominantly through comparison to the experimental work on anhydrous thymine.

### *4.3.2 Anion and Cation*

Base anion and cation radicals are of interest since theories of direct radiation effects are centered on the formation of these radicals, which are thought to subsequently lose or gain a proton to become neutral radicals. The calculated data for the thymine anion and cation are displayed in Table 4.2. The calculated values for the adiabatic ionization potential (IP) and the adiabatic electron affinity (EA) are 196.0 kcal/mol and -14.8 kcal/mol, respectively. The IP is slightly lower than the value determined experimentally[21,22] (204.6 kcal/mol) and that calculated at the MP2 level[23] (204.1 kcal/mol). Unlike the IP, experimental gas phase electron affinities have not been reported for the DNA bases.[24] The adiabatic electron affinity of thymine in dimethyl sulfoxide was reported to be 18.2 kcal/mol,[24] which is slightly larger in magnitude and opposite in sign than our computed value. Sevilla *et al.*[23] computed the adiabatic EA at the SCF level (with scaling) to be 7.2 kcal/mol. Comparison of the computed HFCCs and the experimental values obtained from the various thymine derivatives indicates that even at low temperatures, the cationic species is not observed.

Table 4.2: Calculated electron affinity, ionization potential and HFCCs (G) for the thymine anion and cation.

| Radical | Atom | $A_{iso}$ | $T_{XX}$ | $T_{YY}$ | $T_{ZZ}$ |
|---|---|---|---|---|---|
| $C_1$ Anion | N1H | 2.3 | -1.6 | -1.3 | 2.9 |
| (EA = -14.8 kcal/mol) | N3H | -1.6 | -1.6 | -0.7 | 2.2 |
| | C6H | 4.9 | -7.4 | -0.1 | 7.5 |
| | C5-CH (1) | 2.8 | -0.9 | -0.5 | 1.4 |
| | C5-CH (1) | 3.3 | -1.1 | -0.5 | 1.6 |
| | C5-CH (1) | -0.3 | -0.9 | -0.6 | 1.5 |
| $C_s$ Anion | N1H | -1.9 | -1.6 | -1.2 | 2.8 |
| | N3H | -2.2 | -1.9 | -0.8 | 2.7 |
| | C6H | -15.5 | -8.9 | 1.1 | 7.8 |
| | C5CH (2) | 1.0 | -0.9 | -0.5 | 1.4 |
| | C5CH (1) | -0.4 | -0.8 | -0.7 | 1.5 |
| Cation | N1H | -7.8 | -5.4 | -1.6 | 7.1 |
| (IP = 196.0 kcal/mol) | C6H | -1.7 | -1.9 | -1.4 | 3.4 |
| | C5-CH (2) | 35.7 | -1.7 | -0.8 | 2.5 |
| | C5-CH (1) | -0.1 | -1.0 | -0.1 | 1.7 |

Many conflicting reports regarding the protonation state of the thymine anion exist in the literature. For example, Sagstuen *et al.*'s ENDOR measurements on single crystals at low temperatures[3,18,19] and pulse radiolysis studies on aqueous solutions[2] indicate that the anion is protonated. However, Bernhard and Patrzalek's ESR work on oligomers in aqueous low temperature glasses suggests that the anion is not protonated.[5] The geometry of the thymine anion was calculated to be severely puckered and the resulting HFCCs (Table 4.2) are quite different from those assigned experimentally to the O4-protonated radical. If it is assumed that a planar geometry exists experimentally due to crystal effects, a different set of isotropic coupling constants is obtained (Table 4.2, $C_s$ anion). The isotropic HFCCs obtained for the planar thymine anion are much closer to those assigned experimentally to the O4-protonated form and B3LYP/6-311G(2df,p) single-point calculations indicate that the planar geometry is only 1.9 kcal/mol higher in energy than the nonplanar anion. Despite the fair agreement with experiment for the planar anion, the calculated results for the O4-protonated radical confirm the experimental assignment to the O4-hydrogenated product in T. The hypothesis that the anion exists in an O4-protonated form in single-crystals will be discussed in more detail in the following section.

### *4.3.3 Net Hydrogen Atom Addition Radicals*

From the relative energies displayed in Table 4.3, it can be observed that the C6-hydrogen addition product is the lowest lying species in this radical class. The C5-

Table 4.3: Calculated relative energies (kcal/mol) and HFCCs (G) for thymine hydrogenated radicals.

| Radical | Relative Energy | Atom | $A_{iso}$ | $T_{XX}$ | $T_{YY}$ | $T_{ZZ}$ |
|---|---|---|---|---|---|---|
| C6-hydrogenated | 0.0 | N1H | 0.6 | -0.6 | -0.5 | 1.1 |
| | | N3H | -1.6 | -1.4 | -0.8 | 2.2 |
| | | C6H | 33.9 | -1.5 | -1.1 | 2.6 |
| | | C6H | 33.9 | -1.5 | -1.1 | 2.6 |
| | | C5-CH (2) | 28.8 | -1.5 | -1.1 | 2.6 |
| | | C5-CH (1) | 0.8 | -1.4 | -1.1 | 2.5 |
| C5-hydrogenated | 2.9 | N1H | -3.08 | -2.6 | -1.5 | 4.2 |
| | | C6H | -15.9 | -11.2 | -0.2 | 11.4 |
| | | C5-CH (1) | 0.2 | -0.7 | -0.5 | 1.2 |
| | | C5-CH (1) | 0.7 | -1.4 | -0.7 | 2.1 |
| | | C5-CH (1) | 0.6 | -0.9 | -0.9 | 1.7 |
| | | C5H | 41.9 | -1.5 | -1.1 | 2.5 |
| O4-hydrogenated | 12.6 | N1H | -3.4 | -2.9 | -1.3 | 4.2 |
| | | N3H | -3.4 | -2.9 | -1.0 | 3.9 |
| | | C6H | -15.1 | -8.5 | -0.4 | 8.1 |
| | | C5-CH (2) | -4.5 | -0.7 | -0.3 | 1.1 |
| | | C5-CH (1) | -0.9 | -0.7 | -0.7 | 1.4 |
| | | O4H | -1.6 | -1.7 | -1.6 | 3.3 |
| O2-hydrogenated | 28.2 | N1H | -1.8 | -2.3 | -1.9 | 4.1 |
| | | N3H | -2.3 | -3.2 | -2.1 | 5.3 |
| | | C6H | 1.2 | -0.9 | -0.2 | 1.1 |
| | | C5-CH (2) | 5.8 | -0.5 | -0.3 | 0.8 |
| | | C5-CH (1) | 0.1 | -0.4 | -0.4 | 0.8 |
| | | O2H | 7.6 | -4.9 | -2.4 | 7.3 |

hydrogen addition product lies only 2.9 kcal/mol above the C6H product, while the products formed by H-addition to the O4 and O2 positions lie 12.6 and 28.2 kcal/mol higher in energy, respectively. From the energetics, it can be concluded that the product formed by H-addition to the O2 position is a minor species, which is confirmed by the absence of its assignment experimentally. It should be noted that conclusions based on these energetics regarding which radiation products are most predominant are solely dependent upon thermodynamics. Kinetic effects and reaction intermediates may also be important. Such information can be obtained through careful investigations of the reaction mechanisms for the formation of the various products.

Comparison of the experimental and calculated HFCCs in the O4-hydrogenated product indicates that good agreement between the two sets of data is obtained for all of the HFCCs except for the O4H coupling. The spin density in this molecule was concluded from experimental data to exist predominantly on C6 (0.50) and C4 (0.40), with a small amount on C5 (0.08). This is in good agreement with calculated results, obtained from a Mulliken population analysis (0.56, 0.36 and -0.12 on C6, C4 and C5,

respectively) indicating that an accurate description of the spin distribution in this radical is obtained with the level of theory implemented. The question remains as to why the O4H couplings do not correspond.

Experimentally, the relatively large coupling (12.3 G) assigned to the O4-hydrogen was speculated to be due to an out-of-plane position for this atom. Semi-empirical calculations performed by Sagstuen *et al.*[18] support the initial predictions of an out-of-plane hydrogen configuration. The present study indicates that at a higher level of theory the O4-hydrogen moves back into the molecular plane resulting in a very small HFCC (-1.6 G). Effects of an out-of-plane position on the O4H HFCCs were investigated through single-point calculations performed by fixing the ring geometry, as this is expected not to change considerably, and varying the HO4C4C5 dihedral angle ($\theta$) in steps of ten degrees out of the molecular plane. These single-point calculations (Table 4.4, left columns) indicate that the isotropic O4H HFCC is very dependent on the dihedral angle and a maximum HFCC ($\approx$ 22 G) is obtained at an angle of 90° out of the molecular plane. The rotational barrier is very small, approximately a 2 kcal/mol difference between the in-plane position and the position 90° out of the plane, and a 5 kcal/mol difference when the hydrogen is *cis* relative to the C4N3 bond. Comparing experimental and theoretical HFCCs, it can be predicted that the hydrogen is located at an angle of approximately 50° out of the molecular plane ($\theta$ = 50 or 130°) in the experimental environment. The rotation of this dihedral angle does not modify the spin distribution in the radical which as previously mentioned is primarily located on C6 (0.55±0.02) and C4 (0.36±0.06).

Table 4.4: The relative energy (kcal/mol) and change in the O4H HFCCs (G) upon rotation of the HO4C4C5 dihedral angle (deg.) and the methyl group.

| Dihedral Angle | Methyl group optimized | | Methyl group rotated | |
|---|---|---|---|---|
| | $A_{iso}$(O4H) | Relative Energies | $A_{iso}$(O4H) | Relative Energies |
| 0 | -1.6 | 0.0 | -1.7 | 1.6 |
| 20 | 0.7 | 0.2 | 0.6 | 1.3 |
| 40 | 7.2 | 0.6 | 7.2 | 1.0 |
| 60 | 15.1 | 1.2 | 15.6 | 0.6 |
| 80 | 21.6 | 1.7 | 21.7 | 0.3 |
| 100 | 23.4 | 2.0 | 22.8 | 0.1 |
| 120 | 19.2 | 2.5 | 18.3 | 0.0 |
| 140 | 11.0 | 3.3 | 10.1 | 0.4 |
| 160 | 2.3 | 4.6 | 1.9 | 1.1 |
| 180 | -1.7 | 5.2 | -1.7 | 1.5 |

The difference between theory and experiment for the molecular geometry of this radical arises due to the rapid rotation of the methyl group in the experimental environment, which is characterized by the presence of three equivalent methyl group protons in the ENDOR spectra. Accounting for the rotation of the methyl group, the O4-hydrogen and the in-plane methyl hydrogen positions are only separated by 1.62 Å in the calculated geometry. The effects of this unfavorable interaction[18] and the unfavorable interaction with the N3-hydrogen are expected to result in an out-of-plane position for the O4H in the crystals. This hypothesis is confirmed by additional single-point calculations performed by rotating the HO4C4C5 dihedral angle as before, but fixing the methyl group in a staggered orientation with respect to the C5C6 double bond (Table 4.4, right columns). In this case, the lowest energy orientation for the O4H is at an angle of approximately 50-60° out of the molecular plane ($\theta \approx$ 120-130°), the same position that yields the experimentally determined O4H HFCC.

Sagstuen *et al.*[5] suggested that the anion and its O4-protonated form could be distinguished through anisotropic data. Comparison of the couplings calculated for the anion (both $C_1$ and $C_s$ forms) and the O4-hydrogenated radical to those obtained experimentally indicates that this may be true. In particular, the anion and its O4-protonated form could be identified by differences in the anisotropic data for the nitrogen-bonded protons provided sufficient experimental resolution is achieved.

The results obtained for the thymine O4-hydrogenated radical can be extended to 1-methylthymine and deoxythymidine since geometric and electronic changes are expected to be small upon substitution at the N1 position. Comparison of calculated and experimental HFCCs indicates that the O4-hydrogen remains in the molecular plane and at an angle of approximately 60° out of the molecular plane in 1MeT and dT crystals, respectively. The differences in these systems relative to unsubstituted thymine arise due to the characteristic hydrogen bonding patterns in the crystals.

The radical generated through net H atom addition to C5 displays interesting geometrical effects. When a hydrogen atom is added to this position, the molecule becomes distorted at C5 while the rest of the ring remains planar leading to two possible orientations — pseudo-axial and pseudo-equatorial. The radical with hydrogen in the

pseudo-axial position, almost perpendicular to the molecular plane, is lower in energy by 0.7 kcal/mol. This agrees with the most stable conformation observed for 5,6-dihydrothymine.[25] A spin density of 0.79 at C6 leads to a large isotropic coupling for the out-of-plane C5H (41.9 G) and a smaller coupling for C6H (-15.9 G). These calculated couplings (Table 4.3) match well with the experimental predictions (Table 4.1) where a large coupling was assigned to a $\beta$-hydrogen orientated in a position perpendicular to the thymine base.[18] A second coupling was experimentally assigned to the hydrogen at the C6 position, and the spin density at C6 was predicted to be 0.75.

It was previously concluded that C6-hydrogen addition predominates over C5-hydrogen addition (59.5% versus 37%).[1] The calculated energy difference between these two products (2.9 kcal/mol) accounts for the slight preference of hydrogen addition to the C6 site. The HFCCs for the C6-hydrogenated product do not match as well as those for the C5 product. Experimentally, the hyperfine coupling tensors for two $\beta$-methylene protons could be clearly extracted in anhydrous thymine.[18] The isotropic coupling constants for the two protons are remarkably different from one another (45.3 versus 32.0 G) indicating a locally distorted structure. An additional coupling (20.0 G), assigned to the C5-methyl protons, was also observed. Theoretically, the geometry for this radical was optimized to a near-planar structure resulting in equivalent C6H couplings (33.9 G) and a rotationally averaged C5-methyl proton coupling of approximately 19 G. Since the calculated and experimental anisotropic data for the C6-hydrogenated radical are in good agreement and no other set of couplings calculated for all possible radiation products are closer to those assigned experimentally to the C6-hydrogenated radical, it can be concluded that the calculations support the experimental assignment of this radical.

It can be speculated that some external influence causes the C6 position to be slightly puckered in the experimental setting, hence rendering two different experimental HFCCs. In ENDOR studies of deoxythymidine, the C6-hydrogenated radical was also observed. In these crystals, the two C6H HFCCs differ by only 2.2 G rather than 13.3 G as in thymine. This supports our hypothesis that crystal effects lead to great puckering. This proposal does not agree with the work of Dulcic and Herak[26] who examined both anhydrous and monohydrate thymine crystals. In their study, both crystals exhibited

different couplings for the C6-hydrogens and they concluded that it is an internal property of the molecule that leads to inequivalent C6-hydrogens.

### *4.3.4 Net Hydrogen Atom Abstraction Radicals*

The C5-methyl dehydrogenated product is the lowest lying species for the radicals formed by net hydrogen atom abstraction. The N1, C6 and N3-dehydrogenated radicals lie 8.9, 24.4 and 34.3 kcal/mol higher in energy, respectively, than the lowest lying species (Table 4.5). The C6 and N3 dehydrogenated radicals are expected to be minor species based on the energetics which is confirmed since neither of these radicals were observed in the ENDOR spectrum of anhydrous thymine.[18]

Table 4.5: Calculated relative energies (kcal/mol) and HFCCs (G) for thymine dehydrogenated radicals.

| Radical | Relative Energy | Atom | $A_{iso}$ | $T_{XX}$ | $T_{YY}$ | $T_{ZZ}$ |
|---|---|---|---|---|---|---|
| $CH_3$-dehydrogenated | 0.0 | N1H | -2.5 | -1.8 | -1.1 | 2.9 |
| | | N3H | 0.1 | -0.4 | 0.1 | 0.4 |
| | | C6H | -11.4 | -5.4 | -0.7 | 6.1 |
| | | C5-CH (1) | -15.1 | -8.9 | -0.1 | 9.0 |
| | | C5-CH (1) | -14.1 | -8.1 | -0.5 | 8.6 |
| N1-dehydrogenated | 8.9 | C6H | 2.5 | -1.5 | 0.0 | 1.5 |
| | | C5-CH (2) | 26.0 | -1.3 | -0.7 | 1.9 |
| | | C5-CH (1) | 0.4 | -0.9 | -0.8 | 1.7 |
| C6-dehydrogenated | 24.4 | N1H | 13.4 | -2.7 | -2.0 | 4.7 |
| | | N3H | 0.7 | -0.7 | -0.6 | 1.3 |
| | | C5-CH (2) | 2.2 | -0.7 | -0.6 | 1.3 |
| | | C5-CH (1) | 0.7 | -0.6 | -0.9 | 2.5 |
| N3-dehydrogenated | 34.3 | N1H | 0.6 | -1.0 | -0.2 | 1.2 |
| | | C6H | 1.0 | -0.9 | -0.4 | 1.3 |
| | | C5-CH (2) | 1.3 | -0.8 | 0.0 | 0.8 |
| | | C5-CH (1) | 0.4 | -0.9 | -0.8 | 1.7 |

The C5-methyl dehydrogenated product has been observed in almost every ESR study on thymine to date.[2] Experimentally,[18] this radical is characterized in thymine crystals by two methyl hydrogen isotropic HFCCs (-15.7 and -16.4 G) and a small C6H isotropic coupling (-10.7 G). The corresponding theoretical isotropic couplings are -14.1, -15.1 and -11.4 G, respectively. In addition, the anisotropic HFCCs agree closely for all three allylic protons. An additional weak coupling ($A_{iso}$ = -1.0 G) was assigned to N3H and an estimated spin density of 0.04 was assigned to N3. The calculated spin densities indicate a smaller amount of spin on N3 (-0.01) and a greater amount on N1 (0.08). Although the calculated isotropic couplings are small in both cases, it can be suggested that the experimental coupling arises due to the hydrogen at N1 (-2.5 G) rather than at N3

(0.1 G). The experimentally derived anisotropic HFCCs fall in-between those calculated for N1H and N3H, and thus assignment to either of these atoms is not facilitated through the examination of the anisotropic HFCCs.

The N1-dehydrogenated radical is important since most of the cation chemistry of thymine is expected to be dominated by the removal of this hydrogen atom.[27,28] ENDOR spectra revealed that the N1-dehydrogenated species is present in small concentrations in anhydrous thymine, but no further information about the couplings in this radical could be obtained. From the calculated values, it can be seen that this radical's spectrum would be composed of a relatively large isotropic coupling (17.3 G) due to the rotating methyl group, obtained simply as the average of the three calculated values, and a smaller coupling (2.5 G) due to C6H. An ESR study by Dulcic and Herak[29] observed what was thought to be the N1-dehydrogenated radical. They reported a coupling assigned to a rotating methyl group ($A_{iso}$= 19.1, $A_{||}$ = 20.1 and $A_{\perp}$ = 18.6 G) and a nitrogen coupling assigned to the N1 position ($A_{iso}$= 6.4, $A_{||}$ = 14.0 and $A_{\perp}$ = 2.6 G). This is in good agreement with the calculated results for the methyl ($A_{iso}$= 17.3 G, $A_{||}$ = 19.1 and $A_{\perp}$ = 16.4 G) and N1 ($A_{iso}$= 4.2 G, $A_{||}$ = 14.8 and $A_{\perp}$ = -1.1 G) HFCCs in the N1-dehydrogenated radical. This comparison will facilitate the elucidation of the N1-dehydrogenated product in subsequent solid state studies.

### *4.3.5 Hydroxyl Radical Addition Products*

The reaction between hydroxyl radicals, generated through water radiolysis, and DNA bases has been speculated to be a predominant pathway for indirect radiation damage. Although hydroxyl radicals will be absent in anhydrous thymine crystals, the C5 and C6-hydroxylated radicals were examined in the present work and the results displayed in Table 4.6. The geometries obtained for both of these radiation products were distorted at the site of OH radical addition. Colson and Sevilla also observed nonplanar structures for these radicals at a lower level of theory.[30]

There exists some disagreement in the literature concerning the favored product of OH radical addition. Many papers[4,31,32] indicate that the C6 position in thymine is preferred over the C5 position for hydroxyl radical addition due to the methyl group. On the other hand, studies have shown that the C5-OH addition product is favored in a 2:1

ratio.[1] The calculated energies of these two products indicate that the C6-hydroxylated product is lower in energy by approximately 6 kcal/mol.

Table 4.6: Calculated relative energies (kcal/mol) and HFCCs (G) for thymine hydroxyl radical addition products.

| Radical | Relative Energy | Atom | $A_{iso}$ | $T_{XX}$ | $T_{YY}$ | $T_{ZZ}$ |
|---|---|---|---|---|---|---|
| C6-hydroxylated | 0.0 | N3H | -1.1 | -0.9 | -0.8 | 1.7 |
| | | C6H | 9.8 | -1.7 | -1.0 | 2.7 |
| | | C5-CH (1) | 34.1 | -1.6 | -1.1 | 2.7 |
| | | C5-CH (1) | 28.6 | -1.6 | -1.0 | 2.6 |
| | | C5-CH (1) | 1.0 | -1.4 | -0.9 | 2.3 |
| | | C6-OH | 1.5 | -2.7 | 0.1 | 2.7 |
| C5-hydroxylated | 6.2 | N1H | -2.5 | -2.4 | -1.5 | 3.9 |
| | | C6H | -17.0 | -11.2 | -0.2 | 11.4 |
| | | C5-CH (1) | 6.0 | -1.0 | -0.4 | 1.4 |
| | | C5-CH (1) | -1.0 | -1.5 | -0.5 | 2.0 |
| | | C5-CH (1) | -0.8 | -1.5 | -0.3 | 1.8 |
| | | C5-OH | -0.4 | -0.7 | -0.7 | 1.5 |

Two different groups have studied reactions of hydroxyl radicals with pyrimidines in solution.[33,34] T and 1MeT C6-hydroxylated radicals were characterized by a C6H coupling of 15.3 and 15.1 G and a C5-methyl coupling of 22.3 and 22.6 G, respectively. The corresponding deoxythymidine radical was characterized by a slightly smaller C6H coupling of approximately 11 G and a C5-methyl coupling of 23 G. The calculated C5-methyl hydrogen coupling averaged over all three hydrogens is 21.2 G, which agrees well with the experimental values. The calculated C6H coupling (9.8 G) is smaller than that assigned to T and 1MeT, but in agreement with dT results. Like the C6-hydrogenated radical, these results indicate that theory inadequately describes the puckering at the C6 position relative to that observed experimentally for T and 1-MeT. Experimentally, a large C6H coupling (approximately 18.7 G) was assigned to the T and dT C5-hydroxylated radicals. The calculated value for this coupling is similar in magnitude, but opposite in sign.

The calculated results indicate that a distinction between the two hydroxylated radicals can be made based on the C6H couplings, which possess a value of approximately -17 G and 10 G in the C5 and C6-hydroxylated radicals, respectively. In addition, there is a considerable difference in $\alpha$ and $\beta$-hydrogen anisotropic HFCCs that would facilitate the identification of these radicals.

### *4.3.6 Summary of Thymine Results*

The lowest energy dehydrogenated and hydrogenated thymine products are the C5-methyl hydrogen abstraction and the C6-hydrogen addition radicals. Experimental and theoretical couplings for the thymine O4-hydrogenated radical are in good agreement except for the coupling assigned to O4H. Through analysis of changes in the HFCCs relative to the dihedral angle, it can be concluded that this hydrogen lies out of the molecular plane at an angle of 50, 0 and 60 degrees in T, 1MeT and dT crystals, respectively. In thymine, the out-of-plane position is the lowest energy orientation when interactions between the added O4H, and the N3 and freely rotating methyl hydrogens are considered.

It was noted that considerable geometry alterations accompany hydrogen addition to the C5 position in thymine. In addition, both the C5 and the C6 hydroxyl radical addition products exhibit similar puckering. It should also be noted that although distortions were observed at the C5 and C6 positions, the geometry on the other side of the ring was not altered. Since the unaltered portion of the ring is involved in base pairing, the location of distortion could be important information when transferring the results from studies of individual thymine crystals to irradiated full DNA samples.

All other calculated couplings for thymine are in good agreement with those obtained experimentally and support the experimental assignment of the proposed radicals. The 1-methylthymine radiation products were also examined with similar theoretical techniques and the good agreement with experimental results obtained for thymine is maintained upon methyl substitution at N1.[35] This indicates that the level of theory chosen for these studies can adequately describe the effects of radiation in thymine DNA components, even when a larger model system is used.

Through these theoretical and experimental investigations of thymine derivatives, a clear picture of radiation effects on thymine can be obtained. It is postulated that when thymine is irradiated, a hydrogen atom is lost from the C5-methyl group. This produces a supply of hydrogen atoms that can add to the base, predominantly at C6 and to a lesser extent at C5 and O4.

## *4.4 Cytosine*

### *4.4.1 Previous Experimental Work*

The most complete experimental study on cytosine derivatives has been performed on cytosine monohydrate (Cm) crystals by Sagstuen *et al.*[36] The crystal structure of this derivative is composed of an extensive hydrogen bonding network.[37] Sagstuen *et al.*[36] concluded that two major radical products are formed upon irradiation, namely the N3-hydrogenated and N1-dehydrogenated radicals. Minor products include the C5 and C6 hydrogen addition radicals. In addition, one large coupling was left unassigned. The C5, C6 and N3 net hydrogen addition radicals were observed in crystals of 1-methylcytosine (1MeC).[38] The cytosine anion was assigned to a spectra observed from cytidine 3'-monophosphate (3'CMP) crystals.[39] This assignment was questioned by Close[2] who proposed that the net N3-hydrogenated radical would be more likely to yield the observed spectrum. In monohydrate crystals of deoxycytidine 5'-monophosphate (5'dCMP) the radical cation and the net N3 hydrogen addition product were assigned.[40]

Table 4.7: Experimental HFCCs (G) obtained in various cytosine derivatives.

| Radical | Molecule | | $A_{iso}$ | $T_{XX}$ | $T_{YY}$ | $T_{ZZ}$ |
|---|---|---|---|---|---|---|
| Anion | 3'CMP[39] | "C6H" | -12.8 | -8.3 | 0.7 | 7.6 |
| Cation | 5'dCMP[40] | "C5H" | -15.1 | -7.6 | -0.9 | 8.5 |
| | | "C1'H" | 14.8 | -1.0 | -0.4 | 1.4 |
| N1-dehydrogenated | Cm[36] | "N4H" | -5.1 | -3.3 | -0.6 | 4.0 |
| | | "N4H" | -4.6 | -2.2 | -1.3 | 3.5 |
| | | "C5H" | -14.8 | -7.5 | -0.3 | 7.8 |
| N3-hydrogenated | Cm[36] | "N3H" | -2.0 | -2.1 | -0.5 | 2.6 |
| | | "N4H" | -1.6 | -1.7 | -0.8 | 2.4 |
| | | "C6H" | -13.5 | -8.8 | 0.8 | 8.0 |
| | 1MeC[38] | "C6H" | -13.8 | -8.5 | 1.4 | 7.1 |
| | 5'dCMP[40] | "C6H" | -14.0 | -8.7 | 2.1 | 6.6 |
| C5-hydrogenated | Cm[36] | "C5H" | 47.1 | | | |
| | | "C5H" | 31.0 | | | |
| | | "C6H" | -18.7 | -11.3 | -0.5 | 10.8 |
| | 1MeC[38] | "C5H" | 45.1 | -1.5 | -1.1 | 2.7 |
| | | "C5H" | 30.8 | -1.4 | -1.2 | 2.6 |
| | | "C6H" | -17.4 | -11.5 | 0.9 | 10.6 |
| C6-hydrogenated | Cm[36] | "C5H" | -18.5 | -10.1 | 0.0 | 10.1 |
| | 1MeC[38] | "C5H" | -17.8 | -10.7 | 1.1 | 9.6 |
| | | "C6H" | 47.7 | -2.1 | -0.9 | 3.0 |
| | | "C6H" | 51.3 | -1.4 | -0.9 | 2.3 |
| Not assigned | Cm[36] | "C6H" | -18.2 | -9.6 | 0.9 | 8.6 |

The calculated results presented within will be compared foremost to the experimental work on cytosine monohydrate (Table 4.7). The suggested mechanism for

radical formation in cytosine monohydrate involves net hydrogen removal from the N1 position of one cytosine and hydrogen addition to the N3 position of a neighboring cytosine. The couplings assigned to the cation in monohydrate crystals of 5'dCMP are similar to those assigned to the N1-dehydrogenated radical in cytosine monohydrate. However, the N1-dehydrogenated product is not possible in 5'dCMP since a sugar group replaces hydrogen at this position. This is the first indication that the assignment of the couplings in cytosine monohydrate may be incorrect and theoretical calculations should prove fruitful.

### *4.4.2 Anion and Cation*

The calculated adiabatic EA and IP of cytosine equal -13.8 and 194.2 kcal/mol, respectively (Table 4.8). The IP is in good agreement with the results obtained experimentally[21] (200.1 kcal/mol) and those calculated at the MP2 level[7] (194.4 kcal/mol). Both the EA and IP are slightly smaller in magnitude than the values calculated for thymine. The largest components of the calculated spin distribution in the cation are located on O2 (0.45), N3 (0.24) and C5 (0.33), whereas in the anion over half of the spin is concentrated on C6 (0.55). This spin distribution reflects the calculated planar cation and distorted anion geometries and agrees well with experimental spectra where the largest HFCCs were obtained for C5 and C6 in the anion and cation, respectively. However, experimental (Table 4.7) and theoretical HFCCs (Table 4.8) for

Table 4.8: Calculated electron affinity, ionization potential and HFCCs (G) for the cytosine cation and anion.

| Radical | Atom | $A_{iso}$ | $T_{XX}$ | $T_{YY}$ | $T_{ZZ}$ |
|---|---|---|---|---|---|
| $C_1$ Anion | N1H | 2.1 | -3.4 | -1.6 | 5.1 |
| (EA = -13.8 kcal/mol) | N4H | 2.0 | -0.9 | -0.4 | 1.3 |
| | N4H | 4.2 | -0.9 | -0.5 | 1.4 |
| | C5H | -0.4 | -1.5 | -0.2 | 1.7 |
| | C6H | 0.3 | -8.0 | 0.0 | 8.0 |
| $C_s$ Anion | N1H | -3.8 | -3.7 | -1.3 | 4.9 |
| | N4H | -1.6 | -1.2 | -0.7 | 1.9 |
| | N4H | -1.4 | -1.1 | -0.8 | 1.9 |
| | C6H | -14.3 | -9.2 | 1.0 | 8.2 |
| Cation | N1H | -3.9 | -2.1 | -1.6 | 3.7 |
| (IP = 194.2 kcal/mol) | N4H | 0.2 | -0.8 | -0.5 | 1.3 |
| | N4H | 0.2 | -0.7 | -0.5 | 1.1 |
| | C5H | -8.1 | -4.7 | -0.6 | 5.3 |
| | C6H | -0.5 | -1.0 | -0.7 | 1.7 |

these two species are in poor agreement. A calculated isotropic C6H coupling in better agreement with the experimental value assigned to the cytosine anion is obtained if a planar geometry for this radical is considered (Table 4.8, $C_s$ anion). From B3LYP/6-311G(2df,p) single-point calculations, this planar anion is only 4.4 kcal/mol higher in energy than the nonplanar form. However, the anisotropic couplings are further from the experimental results. Hence, it can be concluded that the cytosine anion and cation were more than likely not observed directly in the experimental studies.

### *4.4.3 Net Hydrogen Atom Addition Products*

The N3-hydrogenated radical is the lowest energy radical in this class (Table 4.9), which is in agreement with experimental observations that this radical is formed in the highest yield. The C5, C6 and O2-hydrogenated radicals lie 8.2, 10.2 and 13.8 kcal/mol higher in energy than the N3 radical, respectively. The calculated spin density in the N3-hydrogenated radical indicates that significant spin resides on C6 (0.53) and O2 (0.37) with lesser amounts on N3 (0.09) and N4 (0.03). This agrees well with the experimental spin distribution (0.52, 0.07 and 0.06 on C6, N3 and N4). The calculated C6H HFCCs in this radical (Table 4.9) are in very good agreement with those obtained experimentally in cytosine monohydrate. One of the N4H couplings is also well reproduced through the calculations. On the contrary, the N3H coupling was calculated to be smaller than that determined experimentally, while a large coupling (19.6 G) was obtained from the calculations for the second amino hydrogen.

Differences in the experimental and calculated couplings for the N3-hydrogenated radical could arise due to a rotation about the C4N4 bond in the optimized geometry relative to that present experimentally, where hydrogen-bonding effects may be important. More specifically, due to crystal interactions a planar radical may predominate over one with a distorted amino group. This is confirmed through the optimization of a radical constrained to $C_s$ symmetry. From B3LYP/6-311G(2df,p) single-point calculations, the planar radical is only 3.6 kcal/mol higher in energy than the nonplanar form. The two small N4H, the anisotropic C6H and the isotropic N3H couplings obtained for the planar radical (Table 4.9, $C_s$ N3-hydrogenated) are in much better agreement with experiment than those discussed above for the nonplanar form.

The calculated geometry of the C5-hydrogenated radical displays significant ring puckering resulting in the aforementioned pseudo-axial and equatorial positions for hydrogen. The C6 adduct retains a planar geometry with the two hydrogens distributed equally on opposite sides of the molecular plane. The spin density in these systems is confined to the carbon adjacent to the hydrogen addition center (0.74 and 0.75 on C6 and C5 in the C5 and C6-hydrogenated radicals, respectively). The couplings calculated for the C6 adduct are in good agreement with the experimental results obtained in Cm[36] and 1MeC,[38] the largest deviation existing for the two C6H isotropic couplings. It should be noted that although the absolute magnitude of the calculated results is smaller than those observed experimentally, the difference between the two C6H couplings (approximately 3 G) is well reproduced by the calculations. The failure to reproduce the difference in these couplings in the corresponding T radical was previously discussed. On the other hand, the experimental anisotropic tensors for the two hydrogens are different in magnitude, a trait not reproduced by the calculated results which lie between the two experimental values. Despite this small deviation from experiment, the assignment of the C6-hydrogenated radical is supported by the calculations.

The anisotropic C5H couplings obtained in Cm and 1MeC crystals and assigned to the C5-hydrogenated radical agree well with calculated results, but the isotropic components do not concur. In particular, the two calculated isotropic C5H couplings (44.6 and 14.0 G) deviate substantially from those observed in Cm (47.1 and 31.0 G) and 1MeC (45.1 and 30.8 G). One possible explanation is that the calculations inadequately describe the ring puckering, as observed for thymine radicals. Since the two experimental HFCCs are more similar in magnitude (deviate by 15 G) than the calculated values for this radical (deviate by 30.6 G), the effects of ring puckering on the HFCCs must be investigated. If a planar geometry (obtained through a constrained optimization) is considered, the HFCCs of the two C5 hydrogens possess equivalent values (35.3 and 35.4 G from Table 4.9, $C_s$ C5-hydrogenated). The anisotropic tensors calculated for the planar radical are in better agreement with the experimental couplings than those calculated for the distorted radical. Through comparison of the calculated and experimental couplings for the C5-hydrogenated radical, it can be concluded that the geometrical distortion in the crystal environment must lead to a nonplanar radical with

Table 4.9: Calculated relative energies (kcal/mol) and HFCCs (G) for cytosine hydrogenated radicals.

| Radical | Relative Energy | Atom | $A_{iso}$ | $T_{XX}$ | $T_{YY}$ | $T_{ZZ}$ |
|---|---|---|---|---|---|---|
| N3-hydrogenated | 0.0 | N1H | -3.0 | -2.8 | -1.2 | 4.1 |
| | | N3H | 0.6 | -2.5 | -1.0 | 3.5 |
| | | N4H | 19.6 | -1.0 | -1.0 | 2.0 |
| | | N4H | -1.1 | -1.5 | -0.5 | 2.0 |
| | | C5H | 1.7 | -1.6 | 0.6 | 1.0 |
| | | C6H | -13.7 | -8.3 | 0.2 | 8.2 |
| $C_s$ N3-hydrogenated | | N1H | -2.7 | -2.5 | -1.2 | 3.7 |
| | | N3H | -2.9 | -2.6 | -0.9 | 3.5 |
| | | N4H | -2.7 | -2.3 | -0.7 | 3.0 |
| | | N4H | -2.4 | -2.0 | -1.0 | 3.0 |
| | | C6H | -14.8 | -8.9 | 0.5 | 8.5 |
| C5-hydrogenated | 8.2 | N1H | -3.5 | -3.2 | -1.6 | 4.8 |
| | | C5H | 44.6 | -1.2 | -1.1 | 2.3 |
| | | C5H | 14.0 | -1.6 | -1.3 | 2.9 |
| | | C6H | -14.2 | -10.8 | -0.3 | 11.1 |
| $C_s$ C5-hydrogenated | | N1H | -3.7 | -2.9 | -1.8 | 4.7 |
| | | C5H | 35.4 | -1.4 | -1.2 | 2.6 |
| | | C5H | 35.3 | -1.4 | -1.2 | 2.6 |
| | | C6H | -18.3 | -11.3 | 0.2 | 11.1 |
| C6-hydrogenated | 10.2 | N1H | -1.2 | -0.9 | -0.8 | 1.7 |
| | | N4H | -1.0 | -0.7 | -0.5 | 1.3 |
| | | N4H | -1.0 | -1.1 | -0.5 | 1.6 |
| | | C5H | -16.4 | -10.2 | -0.5 | 10.6 |
| | | C6H | 45.1 | -1.6 | -0.9 | 2.5 |
| | | C6H | 42.0 | -1.5 | -0.9 | 2.5 |
| O2-hydrogenated | 13.8 | N1H | -0.9 | -3.1 | -1.3 | 4.4 |
| | | O2H | -0.1 | -0.5 | -0.5 | 1.0 |
| | | N4H | 4.0 | -1.6 | -0.8 | 2.4 |
| | | N4H | 2.4 | -1.5 | -0.9 | 2.4 |
| | | C5H | 0.8 | -1.5 | 0.5 | 1.0 |
| | | C6H | -12.2 | -8.8 | 0.4 | 8.5 |

less puckering than initially discussed in the present study. The energy difference between the planar and nonplanar forms for this radical is only 0.4 kcal/mol, which indicates that interconversion between conformations is energetically feasible. The comparison of calculated and experimental anisotropic tensors confirms the experimental assignment to the C5-hydrogenated radical.

The O2-hydrogenated radical has not been assigned in any recent ENDOR studies of cytosine derivatives. However, Herak *et al.*[41] assigned a room-temperature coupling ($A_{iso}$ = -9.6 G; $T_{ii}$ = -5.4, 0.7, 5.0 G) to this radical. This set of experimental couplings is quite different from that calculated for the O2-hydrogenated radical. The only HFCCs resembling these experimental values are those calculated for C5H in the cation, but it is

unlikely that the cation would remain stable at this temperature. The calculated C6H coupling for the O2-hydrogenated radical is similar to that assigned to the anion in 3'CMP crystals, as well as the main component assigned to the N3-hydrogenated radical in a variety of cytosine derivatives. Since the assignment of the N3-hydrogenated radical in Cm crystals was supported by the calculated couplings in this radical, it can be concluded that the O2 adduct was not generated in these irradiated crystals.

### *4.4.4 Net Hydrogen Atom Abstraction Radicals*

The N1-dehydrogenated radical is the lowest lying radical in this class (Table 4.10), which is in agreement with experimental results for cytosine monohydrate where this radical was determined to be the major dehydrogenated species. The N4, C5 and C6-dehydrogenated radicals lie 2.3, 8.1 and 12.6 kcal/mol above the N1 adduct. The calculated spin density in the N1-dehydrogenated radical displays an alternating pattern with the main components situated on C5 (0.49), O2 (0.35) and N1 (0.29). This distribution is quite different from that obtained experimentally (0.57 and 0.17 at C5 and N4, respectively). In addition, the calculated and experimental HFCCs deviate substantially. In particular, the calculated anisotropic couplings for the amino hydrogens are extremely small compared to experimental values. Since it is known that the anisotropic component can be calculated with a great degree of accuracy using many theoretical techniques, the deviations observed for this radical are too great to be ascribed to the method employed.

Table 4.10: Calculated relative energies (kcal/mol) and HFCCs (G) for cytosine dehydrogenated radicals.

| Radical | Relative Energy | Atom | $A_{iso}$ | $T_{XX}$ | $T_{YY}$ | $T_{ZZ}$ |
|---|---|---|---|---|---|---|
| N1-dehydrogenated | 0.0 | N4H | -0.7 | -0.5 | -0.4 | 0.9 |
| | | N4H | -0.5 | -0.7 | -0.4 | 1.1 |
| | | C5H | -11.2 | -6.9 | -0.4 | 7.2 |
| | | C6H | 1.6 | -1.4 | 0.2 | 1.2 |
| N4-dehydrogenated | 2.3 | N1H | -2.1 | -1.9 | -0.6 | 2.4 |
| | | N4H | -15.5 | -12.5 | -2.8 | 15.3 |
| | | C5H | -2.2 | -1.0 | -0.5 | 1.5 |

One possible explanation for deviations from experimental couplings could be that a rotation occurs about the C4N4 bond in the experimental environment. This could lead to significant N4H couplings compared to those calculated for the nearly planar

structure. Variation in the HFCCs with rotation about the C4N4 bond was examined and the agreement between the experimental and theoretical HFCCs was not improved.[42] Another rationalization of the results could be that a net hydrogen atom is lost at N4 rather than N1. The calculated isotropic coupling for the remaining amino hydrogen in the N4-dehydrogenated species is similar to the coupling assigned experimentally to C5H in the N1-dehydrogenated radical. However, the anisotropic couplings are in poor agreement. In attempts to improve the agreement between these data sets, a study of the dependence of the N4H coupling on rotation about the C4N4 bond was performed. However, the couplings in the N4-dehydrogenated radical did not change appreciably and the possibility that the observed couplings assigned to the N1-dehydrogenated radical arise due to the N4-dehydrogenated radical can also be dismissed. The HFCCs for the C5 and C6-dehydrogenated radicals (not shown) were also in poor agreement with experiment.

### *4.4.5 Hydroxyl Radical Addition Products*

Two radicals formed through addition of hydroxyl radicals to the C5C6 double bond were investigated. The radical formed through addition to the C5 position is lower in energy than the C6 adduct by 2.4 kcal/mol. An additional conformation of the C5-hydroxylated radical (C5OH-2) involving an alternative orientation of the amino group was also obtained, which lies 0.6 kcal/mol above the C6 product. Analogous to the thymine residues, these hydroxylated radicals exhibit a great degree of ring puckering resulting in most of the unpaired spin being located on the site neighboring that of hydroxyl addition (0.70 and 0.78 on C6 and C5 in the C5 and C6-hydroxylated radicals, respectively).

The differences in the couplings obtained for the C5OH-1 and C5OH-2 conformations are quite large (Table 4.11) given the small geometrical discrepancies. Among the entire set of computed couplings, the N1H couplings obtained in each conformation of the C5-hydroxylated product are in best agreement with the experimental couplings assigned to the amino hydrogens in the N1-dehydrogenated radical. One large, negative isotropic coupling, obtained for C6H in these radicals, is not unlike that assigned to C5H in the N1-dehydrogenated radical, although the anisotropic results deviate more substantially. In addition, a coupling left unassigned in cytosine

Table 4.11: Calculated relative energies (kcal/mol) and HFCCs (G) for cytosine hydroxyl radical addition products.

| Radical | Relative Energy | Atom | $A_{iso}$ | $T_{XX}$ | $T_{YY}$ | $T_{ZZ}$ |
|---|---|---|---|---|---|---|
| C5-hydroxylated (C5OH-1) | 0.0 | N1H | -4.2 | -3.5 | -1.7 | 5.3 |
| | | C5H | 33.0 | -1.6 | -0.5 | 2.1 |
| | | C6H | -10.6 | -9.6 | -0.3 | 9.9 |
| C6-hydroxylated | 2.4 | N4H | -1.3 | -0.8 | -0.6 | 1.4 |
| | | N4H | -1.0 | -1.4 | -0.6 | 2.0 |
| | | C5H | -17.6 | -10.7 | -0.5 | 11.2 |
| | | C6H | 13.1 | -1.6 | -1.0 | 2.7 |
| | | C6-OH | 4.8 | -1.1 | -0.6 | 1.7 |
| C5-hydroxylated (C5OH-2) | 3.0 | N1H | -3.8 | -3.2 | -1.7 | 4.9 |
| | | C5H | 37.4 | -1.5 | -0.8 | 2.3 |
| | | C6H | -13.3 | -10.2 | -0.3 | 10.6 |

monohydrate resembles those calculated for C5H and C6H in the C6 and C5-hydroxylated radicals, respectively. The large isotropic coupling (33.0 or 37.4 G) calculated for C5H in the C5-hydroxylated radical could be used as a fingerprint for the identification of this radical in future studies. Alternatively, this coupling may have gone undetected in the experiments due to its similarity to the coupling assigned to the C5-hydrogenated radical.

### *4.4.6 Summary of Cytosine Results*

Comparison of experimental and theoretical HFCCs indicates that the cytosine anion and cation were more than likely observed in a protonated or deprotonated state rather than directly in the experimental studies. The calculated energetics agree with the experimental results for cytosine monohydrate. In particular, the N3-hydrogenated and N1-dehydrogenated radicals were calculated to be the lowest energy radicals in their respective classes and were determined experimentally to be present in the highest yield. The calculated HFCCs for the N3-hydrogenated radical supported the experimental assignment to this product, as did the computed couplings for the C5 and C6-hydrogenated radicals.

The calculated couplings for the N1-dehydrogenated radical did not correspond to those experimentally assigned to this species. Thus it appears that the suggested mechanism for radiation damage in cytosine monohydrate encompassing hydrogen migration from one cytosine to another is unlikely. This statement was further verified through the calculation of the couplings of the N1-dehydrogenated radical surrounded

with up to four water molecules or additional neighboring cytosine fragments to simulate the experimental hydrogen-bonding scheme.[42] Even a cytosine dimer was studied to model the N1-dehydrogenated, N3-hydrogenated diradical pair. None of these investigations lead to a clear theoretical description of the experimental results. Ionization of cytosine, followed by electron capture by another cytosine, was calculated to cost 207 kcal/mol. Subsequent deprotonation of the cation and protonation of the anion leading to the suggested major products is exothermic by 139 kcal/mol. Hence, this proposed mechanism (Equation 4.1) is overall endothermic by 68 kcal/mol.

$$\mathbf{C} + \mathbf{C} \rightarrow \mathbf{C}^{\bullet+} + \mathbf{C}^{\bullet-} \rightarrow \mathbf{C}(\textit{N1-dehydrogenated}) + \mathbf{C}(\textit{N3-hydrogenated}) \qquad (4.1)$$

The C6H couplings in the two conformers of the C5-hydroxylated product match those experimentally assigned to C5H in the N1-dehydrogenated radical and a coupling left unassigned. In addition, the experimental N4H couplings can be attributed to the N1H couplings in these two conformers. Thus, through comparison of experimental and calculated hyperfine data, it appears that the two major products in irradiated cytosine monohydrate are the N3-hydrogenated and C5-hydroxylated products.

At least two different mechanisms can be considered which yield the N3-hydrogenated and C5-hydroxylated products and both involve water molecules. In the first postulated mechanism (Equation 4.2), ionization and electron uptake are initially assumed to occur on cytosine. This step, which leads to the formation of the cytosine anion and cation, costs 207 kcal/mol. Next, water can add to the cation which is followed by deprotonation and proton transfer to N3 of a second cytosine. This second step leads to an energy gain of 149 kcal/mol and, hence, the net energy cost for this reaction is 58 kcal/mol.

$$\mathbf{H_2O} + \mathbf{C} + \mathbf{C} \rightarrow \mathbf{H_2O} + \mathbf{C}^{\bullet+} + \mathbf{C}^{\bullet-} \rightarrow \mathbf{C}(\textit{C5-hydroxylated}) + \mathbf{C}(\textit{N3-hydrogenated}) \quad (4.2)$$

The second postulated reaction mechanism (Equation 4.3) involves ionization of a water molecule followed by electron uptake at cytosine, resulting in a water cation and a cytosine anion. This reaction costs 298 kcal/mol. The water cation subsequently decomposes into a proton and a hydroxyl radical, which add to the anion and neutral cytosine units, respectively. Since identical products are obtained in the two mechanisms, the net energy cost of this reaction is the same as that mentioned above and

it can be concluded that the second step releases 240 kcal/mol.

$$H_2O + C + C \rightarrow H_2O^{\bullet+} + C + C^{\bullet-} \rightarrow C(\textit{C5-hydroxylated}) + C(\textit{N3-hydrogenated}) \quad (4.3)$$

Of the mechanisms discussed, the path involving cytosine ionization and water addition is most likely to occur. Reasons for this include the fact that approximately 85% of all ionization processes will occur on cytosine since it possesses a greater number of electrons relative to water. In addition, this reaction has lower energy costs for the initial step (relative to the mechanism involving ionization of water) and the overall process (relative to the proposed mechanism involving hydrogen addition and abstraction products). However, the reaction mechanism involving radiolysis of water to produce hydroxyl radicals and hydroxyl radical adducts is a commonly used ESR technique.[43,44] In addition, Sevilla and coworkers have investigated the presence of hydroxyl radicals in the DNA hydration layer.[44] Hydroxyl radicals were found in the intermediate hydration shell, but not in the closest hydration layer. This was speculated to occur due to reactions of the hydroxyl radicals with DNA. The present work indicates that this option should be examined more closely. In addition, Wala *et al.*[45] have reported that strand-breaks in DNA occur due to hydroxyl radical addition to the DNA bases. Reactions of DNA and hydroxyl radicals have also been reported to lead to 5-hydroxycytosine.[46]

The proposal that water is also involved in the radiation damage mechanism in cytosine monohydrate crystals is controversial.[47,48] Critisms raised against this proposal include the fact that ENDOR studies predict that the C5 hydrogen remains in the molecular plane and that the low temperatures of the experiments may prevent the hydroxyl radical from migrating to the C5 position in cytosine. However, more recent experiments indicate that radical yield in monohydrate crystals is greater than the yield in anhydrous crystals of cytosine derivatives,[49] which provides more evidence that water may be involved in the damage mechanism.

Through these theoretical and experimental investigations of cytosine derivatives, a picture of radiation damage in cytosine monohydrate crystals can be obtained. It is postulated that when these crystals are irradiated, a net supply of hydrogen atoms and hydroxyl radicals are generated, most probably from water. Through one of two

proposed mechanisms, net hydrogen atom addition occurs predominantly at N3, and to a lesser extent at C5 and C6, and net hydroxyl radical addition occurs predominantly at C5.

### *4.5 Uracil*

#### *4.5.1 Previous Experimental Work*

The RNA base uracil (U) is of interest since it resembles thymine, where the methyl group in thymine is replaced by hydrogen. Since the thymine methyl group is one of the main sites of net hydrogen removal, the radical chemistry of uracil will differ from that discussed for thymine. Relatively few single-crystal ENDOR studies on uracil derivatives have been performed recently. Herak and McDowell studied single-crystals of 1-methyluracil[50] (1MeU) and identified the N1-methyl dehydrogenated and C5-hydrogenated radicals. Zehner and co-workers[51] examined irradiated single-crystals of uracil. In their study, the N1-dehydrogenated and O4, C5 and C6-hydrogenated radicals were identified, although the C6 adduct was thought to be protonated at O4. More recently, Sagstuen *et al.*[52] studied the co-crystals of 1-methyluracil and 9-ethyladenosine (1MeU:9EA). In addition to adenine radicals, the uracil anion, N1-methyl dehydrogenated and C5-hydrogenated radicals were assigned.

#### *4.5.2 Radical Product Energetics*

From the relative energies of uracil radicals, it can be speculated that hydrogen removal occurs primarily at N1 in U and at C6 in uridine and U in full RNA. The C5-dehydrogenated species is also possible in U but not in T derivatives and this radical lies 18.6 kcal/mol above the N1-dehydrogenated species. The relative energy of the hydroxyl radical addition products is reversed from that predicted from solely the experimental radical yield[1] (4:1 for C5:C6). The relative stability of the hydroxylated uracil radicals is similar to that previously discussed for thymine, although the energy difference is 1 kcal/mol smaller in uracil than in thymine. Thus, through sole consideration of thermodynamics, the hypothesis that the methyl group is leading to a favored C6 hydroxyl radical addition product in thymine (compared to uracil) cannot be supported. The kinetics of these reactions will be discussed in Chapter Seven.

The primary difference in the stability of U and T products is the relative energy of the hydrogen addition products. The uracil C5-hydrogenated radical is 2.2 kcal/mol

lower in energy than the corresponding C6 radical. In thymine, the C6 adduct is 2.9 kcal/mol lower in energy than the C5 radical. The uracil energetics agree with experimental results which indicate a 2:1 ratio for the C5 to C6 addition products.[1]

### *4.5.3 Discussion of Uracil Results*

Sagstuen *et al.*[52] speculated that the uracil anion is formed upon irradiation of 1MeU:9EA, however, the ESR/ENDOR spectra was weak and the protonation state could not be determined. Significant isotropic (-14.0 G) and anisotropic (-7.4, 1.4, 6.0 G) hyperfine couplings were assigned to C6H. The anisotropic couplings are smaller than those obtained for C6H in the uracil anion, while the isotropic component is much larger in magnitude (Table 4.12). Among the uracil radicals investigated in the present study, the only radical with comparable C6H couplings is the O4-hydrogenated radical. However, it should be noted that a nonplanar geometry was calculated for the anion and it is possible that better agreement would be obtained with a planar anion as discussed for thymine and cytosine. This avenue was not investigated in the present work since the experimental signal was weak and hence the extracted couplings are prone to errors.

Table 4.12: Calculated results for the uracil anion and cation HFCCs (G).

| Radical | Atom | $A_{iso}$ | $T_{XX}$ | $T_{YY}$ | $T_{ZZ}$ |
|---|---|---|---|---|---|
| Anion | N1H | 2.3 | -1.6 | -1.4 | 3.0 |
| | N3H | -1.6 | -1.6 | -0.7 | 2.4 |
| | C6H | 5.9 | -7.8 | -0.2 | 8.0 |
| | C5H | -1.8 | -2.0 | -1.1 | 3.1 |
| Cation | N1H | -2.4 | -5.7 | -1.6 | 7.3 |
| | C6H | -0.3 | -1.5 | -1.1 | 2.6 |
| | C5H | -13.4 | -7.3 | -1.2 | 8.6 |

Zehner and co-workers[51] observed a radical, with the unpaired electron density located mainly on a nitrogen atom (0.30) and C5 (0.65), suggested to be the N1-dehydrogenated radical. A set of C5H isotropic (-16.2 G) and anisotropic (-9.8, 1.2, 8.7 G) couplings was obtained, as well as a $^{14}N$ coupling of 15.0 G. The assignment to the N1-dehydrogenated radical is supported by the calculated C5H HFCCs (Table 4.13) and the N1 nitrogen isotropic coupling (calculated value: 15.5 G).

Unlike the C5-hydrogenated radical in thymine, the geometry of the uracil radical optimized to a nearly planar structure which supports the hypothesis that the large distortion in T is a result of the methyl group. Zehner *et al.*[51] assigned a C6H coupling

consisting of large isotropic (-18.5 G) and anisotropic components (-11.0, 0.5 10.5 G) and two C5H couplings of 35.5 G to the C5-hydrogenated radical. Herak and McDowell[50] obtained similar results from single-crystals of 1MeU (C6H: $A_{iso}$ = -19.4 G; -11.4, 0.8, 10.6 G and C5H: $A_{iso}$ = 35.3/35.7 G). Sagstuen *et al.*[52] also speculated that the C5-hydrogenated radical was formed in irradiated 1MeU:9EA, but accurate coupling tensors could not be isolated. These couplings are in excellent agreement with the calculated values (Table 4.13).

Similar to T and C, the optimized geometry of the C6-hydrogenated U radical shows no signs of distortion due to the additional hydrogen. This radical product possesses an experimental[51] C5H coupling of -18.0 G, with an anisotropic tensor of (-10.0, 0.0, 9.9 G), which is supported by the calculated results. The two C6H couplings

Table 4.13: Calculated results for uracil dehydrogenated and hydrogenated radical HFCCs (G).

| Radical | Relative Energy | Atom | $A_{iso}$ | $T_{XX}$ | $T_{YY}$ | $T_{ZZ}$ |
|---|---|---|---|---|---|---|
| N1-dehydrogenated | 0.0 | C6H | 2.7 | -1.6 | 0.1 | 1.5 |
| | | C5H | -13.1 | -7.7 | -0.6 | 8.4 |
| C6-dehydrogenated | 11.9 | N1H | 13.8 | -2.7 | -2.0 | 4.7 |
| | | N3H | 0.9 | -0.7 | -0.1 | 0.8 |
| | | C5H | 18.3 | -2.4 | -1.7 | 4.0 |
| C5-dehydrogenated | 18.6 | N1H | 5.0 | -1.2 | -0.5 | 1.8 |
| | | N3H | 8.2 | -1.2 | -0.7 | 1.8 |
| | | C6H | 19.7 | -2.2 | -1.8 | 4.0 |
| N3-dehydrogenated | 24.4 | N1H | -0.1 | -0.9 | 0.0 | 0.9 |
| | | C6H | 1.6 | -0.6 | 0.0 | 0.6 |
| | | C5H | -1.3 | -2.0 | -0.8 | 2.8 |
| C5-hydrogenated | 0.0 | N1H | -3.2 | -2.3 | -1.7 | 4.1 |
| | | C6H | -20.2 | -11.8 | 0.2 | 11.6 |
| | | C5H | 34.5 | -1.5 | -1.1 | 2.7 |
| | | C5H | 34.5 | -1.5 | -1.1 | 2.7 |
| C6-hydrogenated | 2.2 | N1H | -0.6 | -0.6 | -0.6 | 1.2 |
| | | N3H | -1.6 | -1.4 | -0.8 | 2.2 |
| | | C6H | 40.5 | -1.8 | -1.1 | 2.8 |
| | | C6H | 40.5 | -1.8 | -1.1 | 2.8 |
| | | C5H | -17.9 | -11.1 | -0.7 | 11.8 |
| O4-hydrogenated | 13.6 | N1H | -3.2 | -2.2 | -1.3 | 4.2 |
| | | N3H | -3.3 | -2.9 | -1.0 | 3.8 |
| | | C6H | -15.4 | -8.9 | 0.4 | 8.6 |
| | | C5H | 3.3 | -1.6 | 0.8 | 0.8 |
| | | O4H | -1.8 | -1.6 | -1.5 | 3.1 |
| O2-hydrogenated | 27.9 | N1H | -1.8 | -2.2 | -1.7 | 3.9 |
| | | N3H | -2.0 | -3.4 | -2.1 | 5.5 |
| | | C6H | 1.0 | -0.9 | -0.3 | 1.2 |
| | | C5H | -2.7 | -2.7 | -0.2 | 2.9 |
| | | O2H | 4.6 | -4.9 | -2.4 | 7.2 |

have different experimental isotropic components (45 and 51 G), whereas the calculations render two identical couplings (40.5 G) due to the planar geometry. Zehner *et al.*[51] suggested that in order to obtain these large couplings, the C6H product must be protonated at the O4 position. This avenue was not investigated in this work, as it seems unlikely that a charged radical would predominate and large couplings were calculated for the nonprotonated radical. Thus, the calculations support the conclusion that the observed radical was not protonated. It is interesting to note that the difference between the two experimental C6H couplings in uracil (6 G) and in cytosine (3.6) is smaller than the difference observed in thymine (13 G). This further indicates that the C5-methyl group causes greater geometric distortions in T crystals than in either U or C crystals.

Uracil hydroxylated radicals have been identified upon studying the reaction of hydroxyl radicals with pyrimidines in solution.[33,34] Couplings in the C5-hydroxylated radical were assigned in uracil, uridine (rU) and 2'-deoxyuridine (2'dU). The C5H and C6H couplings obtained in these molecules are very similar (approximately 21.5 and 18.6 G, respectively). The predicted C6H coupling is not unlike the calculated value (-16.1 G). However, the calculated C5H coupling (39.9 G) is much larger than that observed experimentally.

The assignment of these couplings to the C5-hydroxylated radical can be rationalized by considering the radical geometry. Upon hydroxyl radical addition, considerable distortion occurs at the damaged site leading to two local minima (Table 4.14). The radical with hydrogen in an axial position (C5OH-1) is 2.9 kcal/mol more stable than the radical with hydrogen in an equatorial position (C5OH-2). The C5H couplings in the axial and equatorial positions are 39.9 G and 8.7 G, respectively. The agreement between theory and experiment becomes evident once vibrational averaging between these two conformers is considered. The average couplings for the axial and equatorial conformers are -16.7 G and 24.3 G for C6H and C5H, respectively. These couplings are very similar to those obtained experimentally and it can be concluded that in solution considerable molecular motion occurs within this radical.

Experimental couplings have also been assigned to the C6-hydroxylated radical in uridine and 2'-deoxyuridine.[33,34] The values for the C5H couplings in rU and 2'dU are 20.0 and 10.4 G, respectively. The C6H couplings assigned in these two compounds also

Table 4.14: Calculated results for the HFCCs (G) in uracil hydroxylated radicals.

| Radical | Relative Energy | Atom | $A_{iso}$ | $T_{XX}$ | $T_{YY}$ | $T_{ZZ}$ |
|---|---|---|---|---|---|---|
| C6-hydroxylated (C6OH-1) | 0.0 | N3H | -1.0 | -0.9 | -0.8 | 1.6 |
| | | C6H | 12.6 | -1.9 | -0.9 | 2.8 |
| | | C5H | -17.9 | -10.9 | -0.8 | 11.8 |
| | | C6-OH | -1.8 | -3.3 | 0.2 | 3.2 |
| C6-hydroxylated (C6OH-2) | 2.5 | C6H | 9.9 | -1.8 | -1.2 | 3.0 |
| | | C5H | -18.9 | -11.3 | -0.8 | 12.2 |
| | | C6-OH | 5.5 | -1.3 | -0.7 | 2.0 |
| C5-hydroxylated (C5OH-1) | 4.8 | N1H | -2.6 | -2.4 | -1.5 | 3.9 |
| | | C6H | -16.1 | -11.2 | -0.3 | 11.5 |
| | | C5H | 39.9 | -0.9 | 0.4 | 0.5 |
| | | C5-OH | 0.5 | -1.7 | -0.7 | 2.4 |
| C5-hydroxylated (C5OH-2) | 7.7 | N1H | -3.2 | -2.8 | -1.6 | 4.4 |
| | | C6H | -16.6 | -10.5 | -0.3 | 10.8 |
| | | C5H | 8.7 | -1.9 | -0.9 | 2.8 |
| | | C5-OH | -2.1 | -3.2 | -0.4 | 3.2 |

differ (26.1 and 13.3 G in rU and 2'dU, respectively). The calculated C5H and C6H couplings for the lowest energy conformer of this radical (C6OH-1) are -17.9 and 12.6 G, respectively. An alternative arrangement of the hydrogen and hydroxyl group (C6OH-2) at C6, which is 2.5 kcal/mol higher in energy than the C6OH-1 conformer, leads to a C5H and C6H coupling of -18.9 and 9.9 G, respectively. Thus, vibrational arguments used in the discussion of the C5-hydroxylated radical cannot be used here. Due to the disagreement between all data sets, further investigation of these couplings is mandatory.

The HFCCs calculated in additional radical products obtained through irradiation of uracil are displayed in Tables 4.12 to 4.14. These have been included to prompt a more detailed experimental study of radiation products in uracil which may lead to a clearer picture of radiation damage in the crystals of uracil derivatives.

### *4.6 Conclusions*

In this chapter, the net hydrogenated, dehydrogenated and hydroxylated products formed in single-crystal studies of thymine, cytosine and uracil derivatives were investigated. The thymine results show that overall good agreement with experimental HFCCs can be obtained for all observed radicals. In cases where this agreement is initially poor, various arguments can be made to clarify the discrepancies. For example, all couplings in the O4-hydrogenated radical were in agreement with experiment except

that due to the additional hydrogen at the O4 position. Coherence between experiment and theory was obtained through studying the effects of rotation about the C4O4 bond on the O4H HFCCs. The reason for the failure of the calculations to reproduce the experimental results for this radical was concluded to be due to the rapidly rotating methyl group not explicitly accounted for in the calculations. Additionally, the poor isotropic couplings obtained for the C6-hydrogenated radical were justified through crystal effects, where experimentally a geometry exhibiting greater distortion is expected. The general conclusion of good agreement between theory and experiment observed for thymine can be extended to 1-methylthymine and uracil.

The calculated couplings for cytosine, on the other hand, were in overall poor agreement with those assigned in the spectrum of cytosine monohydrate. Once crystal interactions were taken into account and a planar radical was considered, experimental assignment to the N3-hydrogenated radical was supported by the calculations. Good agreement between theory and experiment was also observed for the C6-hydrogenated radical. Unlike the corresponding T and U radical, the difference in the two C6H couplings in C was well reproduced by the calculations. Additional arguments concerning the degree of puckering observed in the cytosine C5-hydrogenated radical were required to support assignment to this product. Deviations between experimental and calculated results were not observed for the analogous T and U radicals. The poorest agreement with experiment was obtained for the N1-dehydrogenated radical, where calculations could not reconstruct the anisotropic tensors. Agreement between theory and experiment could not even be achieved through investigations of bond rotation and crystal effects. In addition, the assigned couplings could not be linked to an alternative dehydrogenated product.

From the discussion within, it was concluded that no dehydrogenated products could be assigned to the spectra in cytosine monohydrate. Thus, the question "Where do the hydrogens used to generate net hydrogenated products come from?" must be addressed. Through comparison of experimental and calculated HFCCs, it was concluded that the only set of calculated couplings among possible cytosine radiation products close in magnitude to those assigned experimentally to the N1-dehydrogenated radical arise from the C5-hydroxylated radical. This result indicates that water must also

play an important role in the radiation damage to DNA. In particular, it stands to reason that net hydrogenated products could obtain hydrogen from the water molecules. Thus, it was concluded that the major radiation products in cytosine monohydrate are the N3-hydrogenated and C5-hydroxylated products.

Assigning the N3-hydrogenated and C5-hydroxylated radicals as the major radiation products in cytosine monohydrate crystals would also explain the absence of the Cm couplings assigned to the N1-dehydrogenated radical in the larger cytosine systems. Previously it was assumed that these couplings were not observed since a methyl or sugar group replaces the hydrogen at N1 preventing the N1-dehydrogenated radical from forming. A new explanation uses the fact that water was not present in previous crystal studies and, thus, the C5-hydroxylated product was not possible. Monohydrate crystals of 5'dCMP were studied, however, and the similarity of the couplings observed in these crystals (assigned to the cation) to those experimentally assigned to the N1-dehydrogenated radical in Cm was previously discussed. Since experimental evidence exists that hydroxyl radicals will react with cytosine in full DNA,[46] it seems reasonable that the C5-hydroxylated product is formed in crystalline cytosine monohydrate. It should be noted that couplings have been assigned to hydroxylated products in aqueous crystals of deoxyadenosine[53] and crystals of guanine hydrobromide monohydrate.[54]

The good agreement between experimental and theoretical couplings in thymine makes the newly proposed assignment of the observed radiation products in cytosine monohydrate trustworthy. However, no accurate studies have been performed on monohydrate single-crystals of thymine derivatives. In attempts to gain a greater understanding of the radiation effects on DNA components and the role water plays in this damage, the following chapter will discuss the main radiation products in the purines, adenine and guanine. The credibility of the mechanisms for radiation damage in cytosine monohydrate crystals proposed herein will be discussed in more detail in Chapter Seven.

### *4.7 References*

1. von Sonntag, C; Schuchmann, H.-P. *Int. J. Radiat. Biol.* **1986**, *49*, 1.

2. Close, D. M. *Radiat. Res.* **1993**, *135*, 1.

3. Sagstuen, E.; Hole, E. O.; Nelson, W. H.; Close, D. M. *J. Phys. Chem.* **1989**, *93*, 5974.

4. Fujita, S.; Steenken, S. *J. Am. Chem. Soc.* **1981**, *103*, 2540.

5. Bernhard, W. A.; Patrzalek, A. Z. *Radiat. Res.* **1989**, *117*, 379.

6. Cullis, P. M.; Evans, P.; Malone, M. E. *Chem. Commun.* **1996**, 985.

7. Colson, A.-O., Sevilla, M. D. *Int. J. Radiat. Biol.* **1995**, *67*, 627.

8. Becke, A. D. *J. Chem. Phys.* **1993**, *98*, 1372.

9. Lee, C.; Yang, W.; Parr, R. G. *Phys. Rev. B* **1988**, *37*, 785.

10. Ditchfield, R.; Hehre, W. J.; Pople, J. A. *J. Chem. Phys.* **1971**, *54*, 724; Hehre, W. J.; Ditchfield, R.; Pople, J. A. *J. Chem. Phys.* **1972**, *56*, 2257; Hariharan, P. C.; Pople, J. A. *Mol. Phys.* **1974**, *27*, 209; Gordon, M. S. *Chem. Phys. Lett.* **1980**, *76*, 163; Hariharan, P. C.; Pople, J. A. *Theor. Chim. Acta* **1973**, *28*, 213; McLean, A. D.; Chandler, G. S. *J. Chem. Phys.* **1980**, *72*, 5639; Krishnan, R.; Binkley, J. S.; Seeger, R.; Pople, J. A. *J. Chem. Phys.* **1980**, *72*, 650; Clark, T.; Chandrasekhar, J.; Spitznagel, G. W.; Schleyer, P. v. R. *J. Comput. Chem.* **1983**, *4*, 294; Frisch, M. J.; Pople, J. A.; Binkley, J. S. *J. Chem. Phys.* **1984**, *80*, 3265.

11. Ha, T.-K.; Gunthard, H. H. *J. Am. Chem. Soc.* **1993**, *115*, 11939.

12. Bauschlicher, Jr., C. W.; Partridge, H. *J. Chem. Phys.* **1995**, *103*, 1788.

13. Frisch, M. J.; Trucks, G. W.; Schlegel, H. B.; Gill, P. M. W.; Johnson, B. G.; Robb, M. A.; Cheeseman, J. R.; Keith, T. A.; Petersson, G. A.; Montgomery, J. A.; Raghavachari, K.; Al-Laham, M. A.; Zakrzewske, V. G.; Ortiz, J. V.; Foresman, J. B.; Cioslowski, J.; Stefanov, B. B.; Nanayakkara, A.; Challacombe, M.; Peng, C. Y.; Ayala, P. Y.; Chen, W.; Wong, M. W.; Andres, J. L.; Replogle, E. S.; Gomperts, R.; Martin, R. L.; Fox, D. J.; Binkley, J. S.; Defrees, D. J.; Baker, J.; Stewart, J. P.; Head-Gordon, M.; Gonzalez, C.; Pople, J. A. *Gaussian 94* (Revision B.2); Gaussian, Inc.: Pittsburgh, PA, 1995.

14. Perdew, J. P.; Wang, Y. *Phys. Rev. B* **1986**, *33*, 8800.

15. (a) Perdew, J. P. *Phys. Rev. B* **1986**, *33* 8822; (b) Perdew, J. P. *Phys. Rev. B* **1986**, *34*, 7406.

16. Eriksson, L. A. *Mol. Phys.* **1997**, *91*, 827.

17. St-Amant, A.; Salahub, D. R.; *Chem. Phys. Lett.* **1990**, *169*, 387; St-Amant, A. PhD.

thesis, Université de Montréal, 1991; Salahub, D. R.; Fournier, R.; Mlynarski, P.; Papai, I.; St-Amant, A.; Ushio, J. In *Density Functional Methods in Chemistry;* Labanowski, J., Andzelm, J., Eds.; Springer: New York, 1991.

18. Sagstuen, E.; Hole, E. O.; Nelson, W. H.; Close, D. M. *J. Phys. Chem.* **1992**, *96*, 1121.

19. Hole, E. O.; Sagstuen, E.; Nelson, W. H.; Close, D. M. *J. Phys. Chem.* **1991**, *95*, 1494.

20. Sagstuen, E.; Hole, E. O.; Nelson, W. H.; Close, D. M. *Radiat. Res.* **1996**, *146*, 425.

21. Orlov, V. M.; Smirnov, A. N.; Varshavsky, Y. M. *Tet. Lett.* **1976**, *48*, 4377.

22. Hush, N. S.; Cheung, A. S. *Chem. Phys. Lett.* **1975**, *34*, 11.

23. Sevilla, M. D.; Besler, B.; Colson, A.-O. *J. Phys. Chem.* **1995**, *99*, 1060.

24. Wiley, J. R.; Robinson, J. M.; Ehdaie, S.; Chen, E. C. M.; Chen, E. S. D.; Wentworth, W. E. *Biochem. Biophys. Res. Commun.* **1991**, *180*, 841.

25. Miaskiewicz, K.; Miller, J.; Osman, R. *Int. J. Radiat. Biol.* **1993**, *63*, 677.

26. Dulcic, A.; Herak, J. N. *Radiat. Res.* **1971**, *47*, 573.

27. Bansal, K. M.; Fessenden, R. W. *Radiat. Res.* **1978**, *75*, 497.

28. Novais, H. M.; Steenken, S. *J. Phys. Chem.* **1987**, *91*, 426.

29. Dulcic, A.; Herak, J. N. *J. Chem. Phys.* **1972**, *57*, 2537.

30. Colson, A.-O.; Sevilla, M. D. *J. Phys. Chem.* **1995**, *99*, 13033.

31. Deeble, D. J.; Das, S.; von Sonntag, C. *J. Phys. Chem.* **1985**, *89*, 5784.

32. Wagner, J. R.; Cadet, J.; Fisher, G. J. *Photochem. Photobiol.* **1990**, *52*, 333.

33. Hildenbrand, K.; Behrens, G.; Schulte-Frohlinde, D.; Herak, J. N. *J. Chem. Soc. Perkin. Trans.* **1989**, *2*, 283.

34. Catterall, H.; Davies, M. J.; Gilbert, B. C. *J. Chem. Soc. Perkin Trans.* **1992**, *2*, 1379.

35. Wetmore, S. D.; Boyd, R. J.; Eriksson, L. A. *J. Phys. Chem. B* **1998**, *102*, 5369.

36. Sagstuen, E.; Hole, E. O.; Nelson, W. H.; Close, D. M. *J. Phys. Chem.* **1992**, *96*, 8269.

37. Weber, H. P.; Craven, B. M.; McMullan, R. K. *Acta Cryst. B* **1980,** *36,* 645; McClure, R. J.; Craven, B. M. *Acta Cryst. B* **1973,** *29,* 1234.

38. (a) Rustgi, S. N.; Box, H. C. *J. Chem. Phys.* **1974,** *60,* 3343; (b) Close, D. M.; Bernhard, W. A. *Bull. Am. Phys. Soc.* **1980,** *25,* 416.

39. Box, H. C.; Potter, W. R.; Budzinski, E. E. *J. Chem. Phys.* **1975,** *62,* 3476.

40. Close, D. M.; Bernhard, W. A. *J. Chem. Phys.* **1979,** *70,* 210.

41. Herak, J. N.; Lenard, D. R.; McDowell, C. A. *J. Magn. Reson.* **1977,** *26,* 189.

42. Wetmore, S. D.; Himo, F.; Boyd, R. J.; Eriksson, L. A. *J. Phys. Chem. B* **1998,** *102,* 7484.

43. Hiraoka, W.; Kuwabara, M.; Sato, F.; Matsuda, A.; Ueda, T. *Nucl. Acids Res.* **1990,** *18,* 1217.

44. (a) Becker, D.; La Vere, T.; Sevilla, M. D. *Radiat. Res.* **1994,** *140,* 123; (b) LaVere, T.; Becker, D., Sevilla, M. D. *Radiat. Res.* **1996,** *145,* 673.

45. Wala, M.; Bothe, E.; Görner, H.; Shulte-Frohlinde, D. *J. Photochem. Photobiol. A, Chemistry* **1990,** *53,* 87.

46. (a) Chapman, D.; Gillespie, C. J. *Adv. Radiat. Biol.* **1981,** *9,* 143; (b) Téoule, R. *Int. J. Radiat. Biol.* **1987,** *51,* 573.

47. Close, D. M.; Sagstuen, E.; Hole, E. O.; Nelson, W. H. *J. Phys. Chem. B* **1999,** *103,* 3049.

48. Wetmore, S. D.; Boyd, R. J.; Himo, F.; Eriksson, L. A. *J. Phys. Chem.* **1999,** *103,* 3051.

49. Information obtained through private correspondence between D. M. Close and L. A. Eriksson.

50. Herak, J. N.; McDowell, C. A. *J. Chem. Phys.* **1974,** *61,* 1129.

51. Zehner, H.; Flossmann, W.; Westhof, E.; Müller, A. *Mol. Phys.* **1976,** *32,* 869.

52. Sagstuen, E.; Hole, E. O.; Nelson, W. H.; Close, D. M. *Radiat. Res.* **1998,** *149,* 120.

53. Gregoli, S.; Olast, M.; Bertinchamps, A. *Radiat. Res.* **1974,** *60,* 388.

54. Hole, E. O.; Sagstuen, E.; Nelson, W. H.; Close, D. M. *Radiat. Res.* **1991,** *125,* 119.

# *CHAPTER FIVE*

## Characterization of Purine Radiation Products

### *5.1 Introduction*

The results obtained for thymine presented in Chapter Four were very promising. Conversely, the results discussed for cytosine were puzzling. Through comparison of experimental and theoretical HFCCs a new mechanism was proposed for radiation damage in cytosine monohydrate crystals. A similar mechanism for thymine could not be investigated due to the lack of accurate experimental data on thymine monohydrate crystals. The newly proposed mechanism for radiation damage probes an important question regarding the significance of water in radiation damage. Several experimental studies have appeared in the literature which investigate monohydrate crystals of derivatives of the purines, adenine and guanine. Comparison of theoretical and experimental HFCCs in these bases is important to understand the role water plays in DNA radiation damage. The present chapter will discuss experimental and theoretical (DFT) results obtained for adenine and guanine. Net hydrogenation, dehydrogenation and hydroxylation products will be considered. The computational techniques applied to these systems are identical to those previously employed for the pyrimidines in Chapter Four and the discussion will not be repeated in the present chapter.

It is important to study both radicals generated from neutral base crystals as well as those formed in protonated crystals to better understand the dependence of radical formation on the environment. Environmental effects are of interest when transferring results obtained from single-crystal studies to full DNA samples. In particular, the importance of understanding proton transfer in DNA has been discussed. Nelson *et al.*[1] have suggested that experimental studies on different crystalline environments will aid in gaining a better understanding of the environmental effects on protonation and deprotonation behaviors in adenine molecules. In addition, detailed ESR/ENDOR studies on single crystals of guanine hydrobromide monohydrate[2] were used to render information about the importance of "bound" water to radical formation. Similarily, the examination of 2'-deoxyguanosine 5'-monophosphate crystals[3] supplied information about the influences of the sugar moiety and the phosphate group on radical formation.

The present chapter primarily focuses on radicals generated from the neutral adenine and guanine molecules. However, some of the radicals proposed to be generated in protonated base crystals will be discussed when experimental data is available.

## *5.2 Adenine*

### *5.2.1 Previous Experimental Work*

Even though new experimental data is constantly appearing in the literature, the various adenine derivatives have been investigated experimentally to a lesser extent than the derivatives of any other base. This is due to the fact that early ESR investigations indicated that thymine and guanine are affected by radiation to a greater extent than the other bases, forming thymine (or cytosine) anions and guanine cations. In addition, due to solubility problems, few single-crystal studies on adenine derivatives have been performed since they are extremely difficult to prepare.[4] The chemical numbering of adenine used throughout this study is indicated in Figure 5.1, structure I.

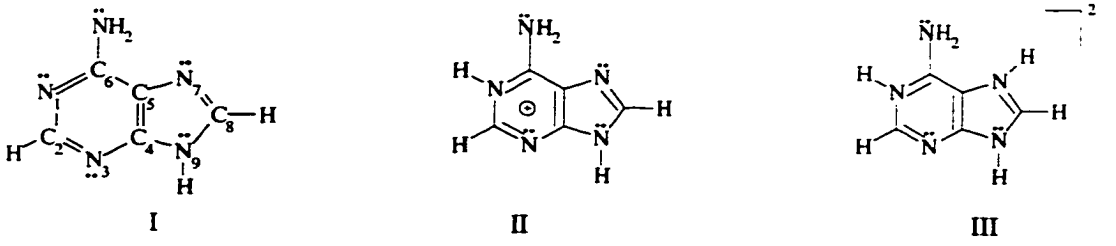

I II III

Figure 5.1: Structure and chemical numbering of adenine (I, 6-aminopurine), singly protonated adenine (II) and doubly protonated adenine (III).

Various adenine radicals have been identified and the HFCCs extracted (Table 5.1). Crystals examined include 9-methyladenine[5] (9MeA), anhydrous deoxyadenosine[1] (dA), deoxyadeonsine monohydrate[6,7,8] (dAm) and adenosine[9,10] (rA). In addition, co-crystals of adenosine and 5-bromouracil have also been investigated (rA:5BrU).[11] Radicals characterized in crystals of 9MeA include the C8 and N3-hydrogenated adducts. In addition to these two radicals, the C2-hydrogenated and N6-dehydrogenated products were identified in crystals of dA. The N6-dehydrogenated radical was not determined to be formed upon irradiation of dAm although three hydrogenated radicals were identified

Table 5.1: Experimental HFCCs (G) in adenine radicals.

| Radical | Molecule | Atom | $A_{iso}$ | $T_{XX}$ | $T_{YY}$ | $T_{ZZ}$ |
|---|---|---|---|---|---|---|
| Cation | A:HCl:½$H_2O$[12] | "N6H" | -7.0 | -4.5 | -1.3 | 5.8 |
| | | "N6H" | -7.3 | -5.2 | -1.1 | 6.3 |
| | | "C8H" | -4.9 | -2.5 | -0.4 | 2.9 |
| C2-hydrogenated | dAm[6] | "C2H" | 32.8 | -1.5 | -0.5 | 2.0 |
| | | "C2H" | 54.3 | -1.4 | 0.0 | 1.4 |
| | | "C8H" | -6.4 | -3.5 | -0.1 | 3.6 |
| | dAm[7] | "C2H" (2) | 43.7 | | | |
| | dAm[8] | "C2H" (2) | 42.0 | | | |
| | | "C8H" | 9.5 | | | |
| | rA[9] | "C2H" (2) | 44.0 | | | |
| | | "C8H" | 10.0 | | | |
| | rA:5BrU[11] | "C2H" (2) | 40 | | | |
| | dA[1] | "C2H" | 38.9 | | | |
| | | "C2H" | 47.5 | | | |
| | | "C8H" | -6.4 | -3.4 | 0.0 | 3.4 |
| N3-hydrogenated | rA[10] | "C2H" | 10.6 | -5.0 | -0.7 | 5.8 |
| | | "N3H" | 3.5 | -4.0 | 0.6 | 3.4 |
| | | "C8H" | 4.1 | -2.1 | -0.4 | 2.5 |
| | dAm[6] | "C2H" | -10.5 | -7.4 | 0.6 | 6.8 |
| | | "C8H" | -3.4 | -2.1 | 0.3 | 1.8 |
| | rA:5BrU[11] | "C2H" | -10.6 | -5.9 | 0.2 | 5.7 |
| | | "N3H" | -3.9 | -3.1 | -0.9 | 4.0 |
| | | "C8H" | -4.4 | -2.4 | 0.3 | 2.1 |
| | dA[1] | "C2H" | -10.9 | -6.8 | 0.9 | 5.9 |
| | | "C8H" | -4.0 | -2.5 | 0.3 | 2.2 |
| | 9MeA[5] | "C2H" | -11.1 | -6.6 | 0.8 | 5.9 |
| | | "C8H" | -4.0 | -2.4 | 0.4 | 2.0 |
| C8-hydrogenated | dAm[6] | "C2H" | -4.8 | -2.6 | 0.0 | 2.6 |
| | | "C8H" | 36.3 | -1.5 | -0.4 | 1.9 |
| | | "C8H" | 41.6 | -1.1 | -0.7 | 1.8 |
| | dAm[8] | "C8H" (2) | 38.0 | | | |
| | rA[9] | "C8H" (2) | 39.0 | | | |
| | dA[1] | "C2H" | -4.8 | -2.7 | 0.1 | 2.6 |
| | | "C8H" | 36.7 | -1.9 | -0.3 | 2.2 |
| | | "C8H" | 40.9 | -1.6 | -0.6 | 2.2 |
| | 9MeA[5] | "C2H" | -4.6 | -2.5 | 0.1 | 2.5 |
| | | "C8H" | 38.4 | -1.2 | -0.4 | 1.6 |
| | | "C8H" | 41.0 | -1.2 | -0.4 | 1.6 |
| N6-dehydrogenated | rA[10] | "N6H" | 12.1 | -9.1 | 1.2 | 7.9 |
| | | "C8H" | 4.4 | -2.1 | -0.1 | 2.3 |
| | rA:5BrU[11] | "N6H" | -10.1 | -11.7 | 4.7 | 6.9 |
| | dA[1] | "N6H" | -11.5 | -8.3 | -1.2 | 9.4 |
| | | "C8H" | -4.6 | -2.4 | -0.2 | 2.6 |

including those formed via net hydrogen addition to C2, N3 and C8. Since no net hydrogen removal radical was observed, but hydrogen addition products were identified, water may also be playing an important role in the radiation damage of these crystals through supplying hydrogen atoms. In two studies of adenosine crystals, the C2 and C8-hydrogenated, as well as the N6-dehydrogenated, radicals were observed. Studies on co-

crystals of adenosine and 5-bromouracil identified the N3 and C2-hydrogenated and the N6-dehydrogenated radicals. The formation of the N3-hydrogenated and the N6-dehydrogenated species in these crystals indicates that these radicals can be formed regardless of the hydrogen-bonding scheme in the crystals.

As discussed in the introduction, various crystalline samples have been used to investigate the effects of radiation on adenine. In some crystals, the parent adenine molecule is protonated at N1 (Figure 5.1, II) or doubly protonated at N1 and N7 (Figure 5.1, III). Upon irradiation of adenine hydrochloride hemihydrate crystals ($A{:}HCl{:}\frac{1}{2}H_2O$),[12] which are protonated at N1, a radical was observed which was postulated to be formed via removal of a hydrogen atom from N1. This radical is structurally equivalent to the cation of the neutral adenine molecule. Additional radicals identified in protonated crystals will be discussed in a later section.

### *5.2.2 Anion and Cation*

In a review of *ab initio* studies on DNA bases, Colson and Sevilla[13] report a negative value for the EA of adenine (-7.2 kcal/mol), which was obtained by scaling the vertical EAs to experimental data on related systems.[14] Direct (DFT) calculation of the adiabatic EA yields a value of -17.7 kcal/mol (Table 5.2). The calculated geometry of the adenine anion indicates that considerable distortion occurs upon addition of an electron. The pyrimidine (six-membered) ring remains planar with the amino group located out of the molecular plane, while the imidazole (five-membered) ring is puckered at C8 and N9H is also located out of the molecular plane. This puckering leads to a concentration of the spin density on C8 (0.43), C6 (0.25), C2 (0.18) and N3 (0.09). The adenine anion has not been proposed to exist as a radiation product in experiments to date. Calculations indicate that this radical could be identified through a large C8H isotropic coupling (10.0 G), as well as substantial couplings for C2H (-5.3 G) and the two amino hydrogens (4.1 G).

The puckered geometry obtained for the anion in the present study may not be possible in crystals due to hydrogen bonding. For this reason, a planar geometry for the anion, which lies 4.7 kcal/mol higher in energy than the non-planar radical anion, was obtained through a constrained optimization. The magnitude of the spin density on C2 (0.28), N3 (0.13) and C6 (0.30) in the planar radical is larger than in the non-planar form,

Table 5.2: Calculated HFCCs (G) in the adenine anion and cation radicals.

| Radical | Atom | $A_{iso}$ | $T_{XX}$ | $T_{YY}$ | $T_{ZZ}$ |
|---|---|---|---|---|---|
| Anion | C2H | -5.3 | -3.0 | -0.2 | 3.2 |
| (EA = -17.7 kcal/mol) | N6H | 4.1 | -0.8 | -1.0 | 0.9 |
| | N6H | 4.1 | -0.8 | -0.5 | 1.3 |
| | C8H | 10.0 | -5.6 | -0.4 | 5.9 |
| | N9H | 1.2 | -1.5 | -1.2 | 2.7 |
| $C_s$ Anion | C2H | -7.7 | -4.4 | 0.0 | 4.4 |
| | N6H | -1.6 | -1.1 | -0.6 | 1.6 |
| | N6H | -1.3 | -1.4 | -0.6 | 2.0 |
| | C8H | -10.5 | -6.2 | 0.9 | 5.4 |
| | N9H | -1.8 | -1.3 | -0.9 | 2.3 |
| Cation | N6H | -6.3 | -4.7 | -1.5 | 6.2 |
| (IP = 182.3 kcal/mol) | N6H | -6.6 | -5.2 | -1.4 | 6.6 |
| | C8H | -5.5 | -3.0 | -0.7 | 3.7 |

whereas the spin density on C8 (0.39) is slightly smaller. The major difference between the couplings in the two forms of the anion is the sign of the C8H isotropic component (Table 5.2). Comparison of the calculated HFCCs of the planar and non-planar radical anion with future experimental spectra will be useful to eliminate the possibility of the anion being formed but its spectra left undetected.

The adiabatic IP was calculated to be 182.3 kcal/mol in the present study (Table 5.2), which is smaller than the experimental value (190.4 kcal/mol)[15] and the value obtained with MP2 (199.6 kcal/mol).[13] Unlike the anion, the adenine cation remains planar, and the major components of the spin density reside on N3 (0.19), C5 (0.20), N6 (0.27) and C8 (0.18). As previously mentioned, a radical equivalent to the adenine cation was assigned in a spectra of A:HCl:½$H_2O$.[12] The spin density distribution in this radical was determined to be located primarily on N6 (0.25) and C8 (0.17/0.21) which is in excellent agreement with the calculated values. The calculated and experimental HFCCs are also in excellent agreement. In particular, the calculated and experimental anisotropic HFCCs for all hydrogens are in extraordinary agreement and the isotropic HFCCs differ by less than 1 G. Thus, our results strongly support the assignment of the experimental couplings in A:HCl:½$H_2O$ to the net radical cation.

### *5.2.3 Net Hydrogen Atom Addition Radicals*

Relative energies of hydrogenated adenine radicals indicate that the radical formed by addition of a hydrogen atom to C8 is the lowest energy radical of this form (Table 5.3). The C2-hydrogenated radical lies 8.7 kcal/mol higher in energy than the

Table 5.3: Calculated HFCCs (G) in adenine hydrogenated radicals.

| Radical | Relative Energy | Atom | $A_{iso}$ | $T_{XX}$ | $T_{YY}$ | $T_{ZZ}$ |
|---|---|---|---|---|---|---|
| C8-hydrogenated | 0.0 | C2H | -5.6 | -3.0 | -0.1 | 3.1 |
| | | N6H | -2.6 | -1.8 | -1.1 | 2.8 |
| | | N6H | -2.7 | -2.9 | -0.8 | 3.7 |
| | | C8H | 38.9 | -1.0 | -0.5 | 1.5 |
| | | C8H | 39.1 | -1.0 | -0.5 | 1.5 |
| | | N9H | -3.7 | -3.0 | -1.0 | 4.0 |
| C2-hydrogenated | 8.7 | C2H | 45.5 | -1.4 | -0.5 | 1.9 |
| | | C2H | 43.3 | -1.4 | -0.5 | 1.9 |
| | | C8H | -6.7 | -3.9 | -0.2 | 4.1 |
| | | N9H | -1.2 | -1.0 | -0.6 | 1.6 |
| N7-hydrogenated | 14.2 | N6H | 1.8 | -0.6 | 0.1 | 0.5 |
| | | N6H | -0.2 | -0.6 | -0.4 | 1.0 |
| | | C8H | 22.5 | -8.2 | -1.3 | 9.5 |
| | | N7H | 13.4 | -3.1 | -2.2 | 5.3 |
| | | N9H | 1.2 | -2.3 | -1.6 | 3.9 |
| N3-hydrogenated | 15.7 | C2H | -12.9 | -7.3 | 0.4 | 6.9 |
| | | N3H | 15.2 | -2.9 | -1.5 | 4.4 |
| | | N6H | 1.3 | -2.0 | -0.6 | 2.6 |
| | | N6H | -1.5 | -1.8 | -0.9 | 2.8 |
| | | C8H | -3.0 | -1.9 | -0.2 | 2.1 |
| $C_s$ N3-hydrogenated | | C2H | -14.0 | -7.9 | 0.2 | 7.7 |
| | | N3H | -3.6 | -3.3 | -1.1 | 4.5 |
| | | N6H | -2.8 | -2.3 | -0.7 | 2.9 |
| | | N6H | -2.4 | -2.0 | -0.9 | 2.9 |
| | | C8H | -5.1 | -2.9 | 0.2 | 2.7 |
| N1-hydrogenated | 16.1 | N1H | -2.1 | -2.2 | -1.4 | 3.6 |
| | | N6H | 16.4 | -1.7 | -1.3 | 3.0 |
| | | N6H | 29.0 | -1.4 | -1.0 | 2.4 |
| | | C8H | -4.4 | -2.5 | 0.0 | 2.5 |
| C5-hydrogenated | 18.2 | C2H | -11.6 | -6.5 | -0.3 | 6.8 |
| | | C5H | 51.2 | -0.7 | -0.1 | 0.8 |
| C4-hydrogenated | 23.0 | C4H | 62.9 | -0.9 | -0.5 | 1.4 |
| | | C8H | -6.0 | -3.7 | -0.6 | 4.3 |
| | | N9H | -3.3 | -3.2 | -1.2 | 4.4 |

corresponding C8 radical. Radicals formed through addition of hydrogen to any of the nitrogens are much higher in energy, on average 15.3 kcal/mol above the C8-hydrogenated radical. The C4 and C5 hydrogen addition radicals are the highest energy products in this class.

#### *5.2.3.1 Nitrogen Hydrogenated Radicals*

The radicals formed through addition of hydrogen to N1 or N7 have not been reported in the experimental spectra of nonprotonated adenine crystals. Upon formation of the N1-hydrogenated radical, C6 is displaced slightly to one side of the molecular plane and the amino group is rotated, resulting in the nitrogen and one hydrogen being

located on one side of the plane and the second hydrogen on the opposite side. These distortions force a large amount of the spin density to be localized on C6 (0.60). Due to the non-planar amino group, the calculated HFCCs consist of two large, N6H isotropic couplings (29.0 and 16.4 G). Upon hydrogen addition to N7, the parent adenine molecule significantly distorts at C8 and N6. The majority of the spin density resides on C8 (0.64) and the remaining spin density is distributed between N7 (0.11) and N9 (0.10). The HFCCs reflect this spin density distribution in that there exists a large isotropic C8H coupling (22.5 G) that has considerable anisotropy (largest component of the tensor: 9.5 G). A smaller, yet significant, coupling was also obtained for N7 (13.4 G).

The radical formed by net hydrogen addition to N3 undergoes significant geometrical alterations upon formation. The N3 hydrogen is located out of the molecular plane and the amino group is puckered with both hydrogens displaced out of the plane. Roughly half of the spin density is located on C2 (0.49) with the rest distributed about the pyrimidine ring (N3 (0.11) and C6 (0.32)). The calculated HFCCs (Table 5.3) indicate that the large spin density at C2 leads to a significant isotropic C2H coupling (-12.9 G) which has considerable anisotropy, ($T_{zz}$ = 6.9 G). Substantial couplings were also calculated for N3H (15.2 G), as well as for both of the hydrogens at N6 (1.3/-1.5 G) and C8H (-3.0 G). All the latter couplings have relatively small anisotropic tensors.

The N3-hydrogenated radical has been observed experimentally in various adenine crystals, such as dA,[1] rA,[10] dAm,[6] rA:5BrU[11] and 9MeA.[5] Experimentally, the spin was determined to be located mainly on C2 (0.4), N3 (0.1) and C8 (0.1), which agrees with the calculations discussed above, although significant spin was determined to reside on C6 rather than C8. The hyperfine coupling constants elucidated from all experimental studies are similar. A major difference is the anisotropic couplings in earlier studies on rA and rA:5BrU are much smaller in magnitude than those determined more recently. In addition, comparison of the experimental results indicates that the sign of the C2H experimental isotropic couplings in rA should be negative. The experimental results reveal significant C2H and C8H couplings (approximately -10 and -4 G, respectively). These isotropic components, as well as the anisotropic tensors, are in good agreement with the calculated results for this radical (-12.9 and -3.0 for C2H and C8H, respectively.)

It should be noted that N3H HFCCs are not observed in all of the experimental studies of adenine crystals. This has been speculated to occur since very strong signals are required for the detection of this coupling. The major difference between theoretical and experimental HFCCs in the N3-hydrogenated radical occurs in the magnitude of the N3H isotropic coupling. Experimentally, a small coupling was observed for this radical (-3.9 G in the most recent study). Alternatively, a large HFCC (15.2 G) was calculated due to distortions at N3. It is possible that hydrogen bonding in the crystal structure forces the N3 hydrogen to remain in the molecular plane, thus leading to a small isotropic HFCC. This hypothesis can be tested through examination of a fully optimized $C_s$ structure, which lies only 1.7 kcal/mol above the non-planar arrangement and possesses two imaginary frequencies. The spin distribution in the planar radical is very similar to that calculated for its puckered form. The calculated C2 and C8 hydrogen HFCCs (Table 5.3) are also very similar for both radical forms with an average deviation of 1.6 and 0.8 G in the isotropic and anisotropic components, respectively. The main difference in the computed couplings is in the magnitude of the N3H isotropic HFCC. In the $C_s$ N3-hydrogenated radical, the N3H isotropic component was calculated to be -3.6 G compared to 15.2 G in the puckered form. Experimentally this coupling was determined to be on average -3.7 G. Hence, it can be concluded that in crystals where the N3H coupling was detected, the N3-hydrogenated radical is likely to remain in a planar form. Through comparison of the couplings in the planar radical with the remainder of the experimental results, it is difficult to determine whether or not the observed radicals were planar. In particular, the C8H and C2H couplings are in better agreement with those values calculated in the distorted radical.

#### *5.2.3.2 Carbon Hydrogenated Radicals*

The radical formed through addition of hydrogen to C2 has been detected on numerous occasions. It has been proposed that the couplings in this radical depend on the protonation state of the parent molecule. In dAm, Lichter and coworkers[7] determined that the C2-hydrogenated radical was present rather than the corresponding C8 radical. The spin density was determined to reside mainly on N1 (0.17) and N3 (0.37), which is in agreement with the calculated results (N1 (0.20) and N3 (0.43)). In crystals of dAm,[7,8] rA[9] and rA:5BrU,[11] two equivalent C2H couplings were recorded (on average

approximately 42 G). In two of these studies, a C8H coupling was also detected (approximately 10 G). These couplings are in fair agreement with the calculated results (Table 5.3), although the C8H coupling was calculated to be negative and anisotropic couplings were not elucidated experimentally.

In a recent ESR/ENDOR study of deoxyadenosine monohydrate by Close *et al.*,[6] a very accurate set of full couplings was assigned to the C2-hydrogenated radical. The experimental isotropic (-6.4 G) and anisotropic (-3.5, -0.1, 3.6 G) C8H couplings are in excellent agreement with those calculated in the present study ($A_{iso}$ = -6.7 G; $T_{ii}$ = -3.9, -0.2, 4.1 G), as well as with the values obtained by the same group in a recent study of anhydrous deoxyadenosine[1] ($A_{iso}$ = -6.4 G; $T_{ii}$ = -3.4, 0, 3.4 G). However, these experimental studies[1,6] and the theoretical results differ in the magnitude of the C2H isotropic HFCCs. The molecular geometry was determined to remain planar upon radical formation and the C2 hydrogens distributed equally on either side of the molecular plane. This arrangement results in two nearly equivalent (43.3 and 45.5 G) isotropic couplings. Alternatively, in the careful ESR/ENDOR studies[1,6] the difference between these couplings is larger [32.8 (38.9) and 54.3 (47.5) G in deoxyadenosine monohydrate (anhydrous deoxyadenosine)].

The experimental results indicate that the distribution of the hydrogens at C2 is more unsymmetric than modeled by gas phase DFT calculations. Difficulties describing ring puckering resulting from the addition of hydrogen to thymine was discussed in Chapter Four. It is possible that insufficient ring puckering is also responsible for the disagreement between theory and experiment in the adenine C2-hydrogenated radical. The disagreement between the most recent experimental studies and those which appeared in the earlier literature indicating equal hydrogen couplings can be understood through the use of a more detailed experimental technique or a reduced vibrational averaging in the later studies. Note that the average value of the two unequal C2H couplings generated from the most recent experiments (~43.6 G) is equal to the couplings obtained in earlier experiments and highly similar to the computed average (44.4 G). Despite discrepancies in isotropic couplings, the anisotropic HFCCs support the experimental assignments to the C2-hydrogenated radical.

The C4-hydrogenated radical has not been assigned in spectra of nonprotonated adenine crystals, although it has been detected in protonated crystals (discussed in a succeeding section). The addition of hydrogen to C4 leads to considerable geometrical distortions, as previously observed by Colson and Sevilla.[16] The geometry in these types of radicals is described as a "butterfly" conformation, where the pyrimidine and imidazole rings remain planar, but are tilted about the C4C5 bond towards each other. A higher energy conformer, not examined herein, has been discussed in the literature in which the rings are tilted to opposite sides of the C4C5 bond. Even though the molecule is distorted upon radical formation, the calculated spin density is distributed throughout both rings with the majority of the spin density located at C5 (0.44), N1 (0.14), N3 (0.10), C8 (0.20) and N9 (0.12). The calculated HFCCs consist of a very large isotropic C4H coupling (62.9 G) and significant couplings for C8H (-6.0 G) and N9H (-3.3 G). The C5-hydrogenated radical also displays a "butterfly" conformation. A large part of the spin density was calculated to be shared between C2 (0.44) and C4 (0.31), with considerable spin density also located on C6 (0.23), N3 (-0.10) and N6 (0.10). The coupling constants calculated for this radical include a large C5H coupling (51.2 G) and a smaller C2H coupling (-11.6 G). No experimental couplings have been isolated for this radical.

The final carbon hydrogenated radical to be discussed is the radical formed through addition of hydrogen to C8. This radical has been observed in numerous studies in the literature and the couplings in this radical, similar to the C2-hydrogenated radical, have been shown to depend on the protonation state of the parent molecule. The HFCCs in the C8 and C2-hydrogenated radicals have been determined to be almost identical and, thus, discussions have appeared in the literature disputing to which position the hydrogen will primarily attach.

The C8-hydrogenated radical was determined to be present in dAm[8] and rA[9] and equivalent C8H couplings of 38.0 and 39.0 G were recorded, respectively. These couplings are in excellent agreement with the calculated values (38.9/39.1 G). A significant C2H coupling was also calculated (-5.6 G). In more recent studies, Close and coworkers detected the C8-hydrogenated radical in dAm,[6] 9MeA[5] and dA.[1] A C2H hyperfine tensor was extracted in these studies consisting of a small isotropic (-4.8 G) and a significant anisotropic coupling (-2.6, 0.0, 2.6 G), which is in good agreement with

the calculations ($A_{iso}$ = -5.6 G; $T_{ii}$ = -3.0, -0.1, 3.1 G). The main difference between the theoretical results or previous experimental results and the more recent experimental work is the magnitude of the isotropic C8H couplings. Experimentally, two unique couplings were obtained in dAm (36.3/41.6 G),[6] dA (36.7/40.9 G)[1] and 9MeA (38.4/41.0 G).[5] Theoretically, radical formation leads to a symmetrical distribution of the two hydrogens at C8. From the more recent experimental results, alteration of the ring at C8 is likely, thus leading to an unsymmetric orientation of the two hydrogens and different couplings. This is an identical situation to that observed for the corresponding C2 radical. Once again the experimental and theoretical anisotropic couplings are in good agreement and, thus, it can be concluded that the theoretical results support the experimental assignment of the C8-hydrogenated radical. It is interesting to note that the two experimental couplings in the C8-hydrogenated radical are closer in magnitude than those obtained in the C2 adduct, indicating smaller geometrical alterations upon formation of the C8 hydrogen addition radical.

### *5.2.4 Net Hydrogen Atom Abstraction Radicals*

The relative energies of the dehydrogenated radicals (Table 5.4) suggest that the radical formed via removal of hydrogen from N9 is the lowest lying radical in this class. The radical formed through abstraction of hydrogen from the amino group lies 2.7 kcal/mol higher in energy. The two radicals formed through hydrogen abstraction from a carbon (C2 or C8) are 9.2 and 16.9 kcal/mol higher in energy than the lowest energy radical. In DNA, a sugar group replaces the N9 hydrogen. This implies that in full DNA samples, the N9-dehydrogenated radical is not possible and the lowest energy dehydrogenated radical would be formed through removal of hydrogen from the amino

Table 5.4: Calculated HFCCs (G) in adenine dehydrogenated radicals.

| Radical | Relative Energy | Atom | $A_{iso}$ | $T_{XX}$ | $T_{YY}$ | $T_{ZZ}$ |
|---|---|---|---|---|---|---|
| N9-dehydrogenated | 0.0 | C2H | -5.2 | -3.0 | -0.6 | 3.5 |
| | | N6H | -4.1 | -2.8 | -1.1 | 3.9 |
| | | N6H | -4.1 | -3.5 | -0.9 | 4.4 |
| | | C8H | -3.7 | -2.2 | -0.8 | 3.0 |
| N6-dehydrogenated | 2.7 | N6H | -11.8 | -9.7 | -2.0 | 11.8 |
| | | C8H | -4.0 | -2.3 | -0.3 | 2.6 |
| C2-dehydrogenated | 9.2 | N6H | 1.3 | -0.4 | -0.3 | 0.8 |
| C8-dehydrogenated | 16.9 | N9H | -1.8 | -3.0 | -1.9 | 4.9 |

group. In co-crystals of thymine and adenine derivatives, both of the amino hydrogens take part in hydrogen bonding and amino hydrogen abstraction radicals have not been observed. However, in DNA only one of the amino hydrogens is involved in hydrogen bonding which permits the formation of the N6-dehydrogenated radical.

The C2 or C8-dehydrogenated radicals have not been identified in experiments to date and the energetics discussed above provide a possible explanation why these radicals have gone undetected. The majority of the spin density in these radicals is located on the radical center (C2 (0.84) and C8 (0.83) in the C2 and C8-dehydrogenated radicals, respectively). In addition, the HFCCs in these radicals (Table 5.4) indicate that the only hydrogen coupling which could possibly be detected is due to N6H (1.3 G) in the C2 centered radical or N9H (-1.8 G) in the C8-dehydrogenated radical. However, these couplings are very small and, hence would probably be difficult to detect even if the radicals are generated.

The lowest lying dehydrogenated radical (N9 centered) has not been detected in experimental studies, which is not surprising since most studies have been performed on adenosine crystals where a sugar group replaces N9H. The optimized geometry of this radical indicates that the molecule remains planar upon formation. The spin density is evenly distributed around both molecular rings. The HFCCs (Table 5.4) indicate that the nuclei with the largest isotropic couplings are C2H (-5.2 G), C8H (-3.7 G) and both of the N6 hydrogens (-4.1 G). In addition, all of these couplings have significant anisotropic character (the largest average component of the anisotropic tensor is approximately 3 to 4 G).

Nelson and coworkers[1] indicated that the N6-dehydrogenated radical has not been observed in many of the adenine samples investigated in the literature. This radical has been identified in co-crystals of rA:5BrU[11] and an isotropic coupling (-10.0 G) was assigned to the remaining N6 hydrogen. The large anisotropy associated with this coupling (-11.7, 4.7, 6.9 G) was speculated to arise due to hydrogen-bonding interactions where the remaining N6 hydrogen is hydrogen bonded to O2 in uracil. Close indicated that the N6H hyperfine tensor obtained in this study is not expected for these interactions.[4] In rA crystals,[10] the spin density in this radical was determined to reside primarily on C8 (0.16) and N6 (0.42) and speculated to exist on cyclic nitrogens (N1 and

N3). A large degree of anisotropy for the N6H coupling was also identified in these crystals (-9.1, 1.2, 7.9 G). A smaller C8H coupling (4.4 G), with an anisotropic tensor of (-2.1, -0.1, 2.3 G), was also isolated. More recently, dA crystals were investigated and the magnitude of the couplings detected are similar to those discussed previously, although through the use of ENDOR the sign of the isotropic components was determined to be negative.[1] Upon careful consideration of the crystal structure it was concluded that the N6-dehydrogenated radical is formed via a concerted proton transfer where the hydrogen is "shuffled" away from the charged site. In addition, it was concluded that hydrogen bonding could control the deprotonation site providing a possible explanation for the lack of detection of this radical in many adenine crystals.

The geometry of the N6-hydrogenated radical was calculated to be planar with the remaining amino hydrogen also located in the molecular plane. The calculations indicate that the N6-dehydrogenated radical indeed possesses a large isotropic coupling (-11.8 G) with significant anisotropy (-9.7, -2.0, 11.8 G). Differences from experimental results may arise due to hydrogen bonding in the crystal structures, although it is clear from the present calculations that the magnitude of the N6H coupling tensor is also significant without hydrogen-bonding effects. In addition, the calculations confirm that the isotropic couplings are negative. Overall, however, it can be concluded that the calculated results support the experimental assignment of this radical.

### *5.2.5 Hydroxyl Radical Addition Products*

Little experimental evidence, besides an ESR study that identified only one isotropic coupling,[19] exists for the formation of hydroxylated radicals in adenine samples. However, as discussed in Chapter Four, studies on DNA bases in the liquid phase have appeared in the literature indicating the possibility of OH radical addition to the parent base molecule. Furthermore, crystal studies on guanine derivatives have detected net hydroxyl radical addition products[2,17] and the calculations presented in Chapter Four indicate that hydroxyl addition to cytosine is also possible. The most likely site for hydroxyl radical addition to adenine is at one of the carbons involved in a double bond (C2, C4, C5 or C8). The relative energies of the hydroxylated radicals (Table 5.5) indicate that the relative stability of the hydroxylated and hydrogenated (Table 5.4) radicals is very similar. The C8-hydroxylated radical is the lowest energy species in this

Table 5.5: Calculated HFCCs (G) in adenine hydroxylated radicals.

| Radical | Relative Energy | Atom | $A_{iso}$ | $T_{XX}$ | $T_{YY}$ | $T_{ZZ}$ |
|---|---|---|---|---|---|---|
| C8-hydroxylated | 0.0 | C2H | -5.6 | -3.0 | -0.1 | 3.2 |
| | | N6H | -4.0 | -1.4 | -1.2 | 2.6 |
| | | N6H | -3.7 | -2.8 | -0.1 | 2.9 |
| | | C8H | 28.8 | -0.8 | -0.4 | 1.2 |
| | | N9H | -3.0 | -2.6 | -0.9 | 3.5 |
| C2-hydroxylated | 12.4 | C2H | 40.0 | -1.1 | -0.4 | 1.6 |
| | | C8H | -6.7 | -4.0 | -0.3 | 4.3 |
| | | N9H | -1.2 | -1.0 | -0.6 | 1.6 |
| C4-hydroxylated | 21.0 | N6H | -1.1 | -1.1 | -0.4 | 1.4 |
| | | C8H | -7.3 | -5.0 | 2.2 | 2.8 |
| | | N9H | -2.4 | -2.4 | -1.0 | 3.4 |
| C5-hydroxylated | 21.5 | C2H | -9.9 | -5.6 | -0.4 | 6.0 |
| | | C8H | -2.2 | -1.3 | -0.5 | 1.8 |

class, which is followed by the C2 centered radical (12.4 kcal/mol higher in energy). The C4 and C5-hydroxylated adducts are the highest energy radicals lying 21.0 and 21.5 kcal/mol above the C8-hydroxylated radical, respectively. The only difference from the energetics discussed for the hydrogenated radicals is the relative order of the C4 and C5 radicals.

The formation of the C4 and C5-hydroxylated radicals results in the same types of "butterfly" conformers previously discussed for the hydrogenated species. The degree of distortion observed for both the C4 and C5 hydrogen and hydroxyl radical addition products is highly similar.[18] This distortion causes a significant amount of the spin density to be localized at C5 (C2/C4) for the C4(C5)-hydroxylated radical. Alternatively, the C2 and C8-hydroxylated radicals undergo only slight geometrical alterations upon hydroxyl radical addition, whereby the addition center is displaced slightly out of the molecular plane.

Perhaps the most interesting feature of the HFCCs in these radicals (Table 5.5) is the magnitude of the C2H (40.0 G) and C8H (28.8 G) couplings in the C2 and C8 adducts, respectively. In particular, the C2H coupling is very similar to those calculated for the C2-hydrogenated radical, while the C8H coupling is much smaller in magnitude than those determined for the C8-hydrogenated radical. Early ESR studies of frozen aqueous solutions of deoxyadenosine 5'-monophosphate[19] revealed one isotropic coupling (29 G) which was believed to be due to a radical formed through addition of a hydroxyl radical to C8. Comparison with the calculated results for the C8-hydroxylated radical

(Table 5.5) indicates that this coupling is indeed due to the C8H in the C8-hydroxylated radical (calculated value: 28.8 G). The calculations also show that a better resolved spectra would yield experimental couplings for C2H, N9H and both of the amino hydrogens. The calculated couplings in hydroxylated radicals are useful to determine whether these radicals are easily formed in adenine crystals.

### *5.2.6 N1-Protonated Radicals*

As previously discussed, it is important to gain a better understanding of factors that affect the formation of DNA base radicals. The present section will discuss select radicals protonated at N1, for which there exists accurate experimental data (Table 5.6). The majority of the experimental studies performed on protonated systems involve adenine hydrochloride crystals, where a chlorine ion participates in a hydrogen bond with N1H. The relative energies of the N1-protonated radicals (Table 5.7) indicate that the C2-hydrogenated radical is slightly lower in energy (0.3 kcal/mol) than the C8-hydrogenated species. In the nonprotonated radicals, the C2-hydrogenated radical was determined to lie 8.7 kcal/mol above the C8-hydrogenated radical. The influence of the protonation state of the parent adenine base on the HFCCs in the C2 and C8-hydrogenated radicals will be discussed in the following section.

The N1-protonated N3-hydrogenated radical has been observed in crystals of adenine hydrochloride hemihydrate (A:HCl:½$H_2O$).[12] The spin density on C2 was determined to vary between 0.55 and 0.65 depending on whether it is calculated from the

Table 5.6: Experimental HFCCs (G) for N1-protonated adenine radicals.

| Radical | Molecule | Atom | $A_{iso}$ | $T_{XX}$ | $T_{YY}$ | $T_{ZZ}$ |
|---|---|---|---|---|---|---|
| N3-hydrogenated | A:HCl:½$H_2O$[12] | "C2H" | -14.2 | -10.0 | 1.0 | 9.0 |
| N6-dehydrogenated | A:HCl:½$H_2O$[12] | "N6H" | -9.4 | -6.4 | -1.4 | 7.9 |
| | | "α-CH" | -6.2 | -3.3 | -0.1 | 3.4 |
| | rA:HCl[12] | "N6H" | -11.4 | -7.9 | -1.3 | 9.2 |
| | | "C8H" | -5.8 | -2.8 | -0.1 | 2.9 |
| N7-hydrogenated | rA:2HCl[20] | "C8H" | -8.7 | -5.8 | 0.8 | 4.9 |
| C2-hydrogenated | rA:HCl[12] | "N1H" | -2.6 | -2.0 | -0.3 | 2.3 |
| | | "C2H" | 40.5 | -1.4 | -0.7 | 2.1 |
| | | "C2H" | 39.1 | -1.6 | -0.8 | 2.4 |
| | | "C8H" | -5.5 | -2.8 | -0.2 | 3.0 |
| C4-hydrogenated | rA:HCl[12] | "C4H" | 9.0 | -4.3 | 0.1 | 4.3 |
| C8-hydrogenated | rA:HCl[12] | "C2H" | -4.3 | -2.4 | 0.0 | 2.4 |
| | | "C8H" | 43.0 | -2.1 | 0.7 | 1.5 |
| | | "C8H" | 40.9 | -1.3 | -0.6 | 2.0 |

isotropic or the anisotropic couplings, respectively (calculated value: 0.71). The discrepancy between the experimental spin densities obtained via the two experimental couplings was suggested to arise due to one of two reasons. First, it was proposed that there may exist significant spin density at N3 that would be accounted for in the dipolar couplings for C2H. Secondly, it was speculated that since net hydrogen addition removes the double bond between N3 and C2, the C2 center may become more pyramidal leading to a smaller isotropic value. The geometry optimization in this study indicated that the radical is distorted at C2, where this position is located out of the molecular plane. In addition, the calculated spin density distribution in this radical indicates that there exists significant spin density at N3 (0.13). Thus, the spin density at N3 and the distortion at C2 could be jointly responsible for the discrepancies in the experimental spin densities.

A large isotropic C2H coupling (-14.2 G) was extracted from the experimental spectrum, which possesses significant anisotropy (-10.0, 1.0, 9.0 G). The anisotropic couplings are in excellent agreement with the calculated values (-9.4, -0.9, 10.3 G), while only a small isotropic HFCC was calculated (2.2 G). The calculated isotropic coupling for the nonprotonated N3-hydrogenated radical (-12.9 G) is in better agreement with the experimental isotropic coupling, however, the anisotropic couplings calculated for the nonprotonated radical are too small (-7.3. 0.4, 6.9 G). The main difference between the protonated and nonprotonated radicals is the geometrical distortion at C2 (the nonprotonated radical is not distorted). It is possible that crystal interactions lead to a planar radical experimentally and a larger isotropic C2H coupling. A $C_s$ N1-protonated N3-hydrogenated radical was optimized which lies only 1.1 kcal/mol higher in energy than the equivalent nonplanar radical, although it possesses multiple imaginary frequencies. The spin density distribution varies only slightly between the planar and nonplanar radical forms and the HFCCs (Table 5.7) are also similar with the exception of the isotropic C2H coupling. In the planar radical, a C2H coupling of -18.5 G was calculated, which is in much better agreement with the experimental coupling (-14.2 G). Since the anisotropic couplings for the protonated planar radical also agree well with experiment, the observed radical most probably possesses a planar form in the crystalline environment.

Table 5.7: Calculated HFCCs (G) in adenine N1-protonated radical cations.

| Radical | Relative Energy | Atom | $A_{iso}$ | $T_{XX}$ | $T_{YY}$ | $T_{ZZ}$ |
|---|---|---|---|---|---|---|
| C2-hydrogenated | 0.0 | N1H | -2.6 | -2.0 | -0.8 | 2.8 |
| | | C2H | 36.7 | -1.4 | -0.7 | 2.1 |
| | | C2H | 36.2 | -1.4 | -0.7 | 2.1 |
| | | C8H | -5.8 | -3.2 | -0.5 | 3.7 |
| | | N9H | -1.5 | -1.0 | -0.9 | 1.9 |
| C8-hydrogenated | 0.3 | C2H | -5.2 | -2.8 | -0.3 | 3.0 |
| | | N6H | -2.9 | -1.4 | -1.1 | 2.6 |
| | | N6H | -2.9 | -2.7 | -0.8 | 3.5 |
| | | C8H | 40.6 | -1.3 | -0.7 | 1.9 |
| | | C8H | 40.5 | -1.3 | -0.7 | 1.9 |
| | | N9H | -3.1 | -2.7 | -0.9 | 3.6 |
| N7-hydrogenated | 6.1 | N1H | -3.2 | -2.8 | -1.1 | 3.9 |
| | | N6H | 18.8 | -1.1 | -0.9 | 2.0 |
| | | N6H | 18.9 | -1.1 | -0.9 | 2.0 |
| | | N7H | -1.8 | -1.2 | -1.0 | 2.2 |
| | | C8H | -10.4 | -5.7 | 0.2 | 5.5 |
| $C_s$ N7-hydrogenated | | N1H | -2.4 | -2.0 | -0.8 | 2.8 |
| | | N6H | -2.8 | -2.5 | -0.7 | 3.2 |
| | | N6H | -2.6 | -1.9 | -0.9 | 2.9 |
| | | N7H | -3.7 | -2.8 | -1.4 | 4.2 |
| | | C8H | -12.8 | -7.2 | 0.4 | 6.8 |
| N3-hydrogenated | 6.8 | N1H | -1.8 | -2.1 | -1.4 | 3.5 |
| | | C2H | 2.2 | -9.4 | -0.9 | 10.3 |
| | | N3H | -3.2 | -3.9 | -1.8 | 5.8 |
| | | C8H | -2.7 | -1.6 | -0.2 | 1.7 |
| $C_s$ N3-hydrogenated | | N1H | -1.2 | -1.6 | -1.1 | 2.7 |
| | | C2H | -18.5 | -10.7 | 0.4 | 10.4 |
| | | N3H | -4.7 | -4.1 | -1.6 | 5.7 |
| | | C8H | -3.4 | -1.9 | -0.1 | 2.0 |
| C4-hydrogenated | 14.6 | N1H | -1.6 | -1.5 | -0.6 | 2.1 |
| | | C4H | 49.2 | -0.9 | -0.4 | 1.4 |
| | | N6H | -2.9 | -1.6 | -1.3 | 2.9 |
| | | N6H | -2.9 | -2.9 | -0.8 | 3.7 |
| | | C8H | -3.9 | -2.5 | -0.9 | 3.4 |
| | | N9H | -3.8 | -3.4 | -1.1 | 4.5 |
| N6-dehydrogenated | | N1H | -1.8 | -1.1 | -0.9 | 2.0 |
| | | C2H | -2.2 | -1.3 | -0.7 | 2.0 |
| | | N6H | -9.6 | -8.0 | -1.7 | 9.7 |
| | | C8H | -6.5 | -3.5 | -0.5 | 4.0 |

The doubly protonated adenine molecule (hydrogens at N1 and N7) was investigated in the crystals of adenine dihydrochloride (A:2HCl)[20] and an anion of the doubly protonated base was identified. This radical is equivalent to the N1-protonated N7-hydrogenated adenine radical. The spin density at C8 was determined to be 0.292/0.311, similar to the calculated value (0.32). The experimental C8H hyperfine tensor is composed of an isotropic component of -8.7 G and an anisotropic component of

(-5.8, 0.8, 4.9 G). The calculations yield isotropic (-10.4 G) and anisotropic (-5.7, 0.2, 5.5 G) couplings, for the C8 hydrogen, in excellent agreement with experiment. In addition, large couplings were calculated for both hydrogens at N6 (18.8/18.9 G) and significant couplings were also calculated for N1H (-3.2 G) and N7H (-1.8 G). The large couplings calculated for the N6 hydrogens arise since in the optimized geometry the amino group is twisted such that one hydrogen atom is above the molecular plane and the other is located below the plane. Hydrogen bonding in the crystal may force these hydrogens to remain in the molecular plane and, hence, these couplings would not be experimentally observable. A planar radical, which lies 2.8 kcal/mol above the nonplanar form, was obtained through a constrained optimization. As predicted, the couplings for both amino hydrogens are very small (approximately 3 G). However, the isotropic and anisotropic C8H couplings for the planar N1-protonated N7-hydrogenated radical are in poorer agreement with experiment and, thus, the nature of the geometry in this radical is difficult to determine. Future experimental studies that measure the N6H couplings in this radical would be beneficial for a description of its geometrical properties.

The next system to be discussed is the N1-protonated N6-dehydrogenated radical, the geometry of which was calculated to be planar. This radical has been identified in crystals of both A:HCl:½$H_2O$ and anhydrous adenosine hydrochloride (rA:HCl).[12] The couplings extracted in irradiated adenine hydrochloride hemihydrate were of poor quality and assignment to the N6-dehydrogenated radical was stated to be tentative. Experimentally, a spin density of 0.33 was determined to be located on a nitrogen atom (probably N6) in A:HCl:½$H_2O$ and on C8 (0.21) and N6 (0.39) in rA:HCl. The calculated spin density was distributed throughout the molecule with significant amounts located at N6 (0.47), N3 (0.10), C4 (0.10), C5 (0.24) and C6 (-0.14). The experimental N6H couplings in A:HCl:½$H_2O$ consist of a substantial isotropic coupling (-9.4 G) with significant anisotropy (-6.4, -1.4, 7.9 G). An additional coupling assigned to an $\alpha$H nucleus was also identified which consists of an isotropic component of -6.2 G and an anisotropic tensor of (-3.3, -0.1, 3.4 G). The couplings in rA:HCl differ somewhat from those identified in A:HCl:½$H_2O$. In particular, larger N6H and smaller $\alpha$H (C8H) couplings were obtained in these crystals.

The calculated N6H isotropic coupling (-9.6 G) matches that obtained in A:HCl:½$H_2O$ crystals. However, the calculated anisotropic couplings differ from these experimental values by on average 1.5 G. This difference could be due to the poorly resolved spectra and, hence, better agreement between theory and experiment is not expected. Support for the assignment of the N6-dehydrogenated radical can be obtained by examining the $\alpha$H coupling which corresponds very well with that calculated for C8H ($A_{iso}$ = -6.5 G; -3.5, -0.5, 4.0 G). The C8H couplings obtained in rA:HCl crystals are in better agreement with those calculated for the deprotonated radical than its protonated form. However, the N6H couplings support the assumption that the radical is protonated, since the largest component of the experimental N6H anisotropic coupling (9.2 G) resembles that calculated for the protonated radical (9.7 G) more closely than that obtained for the nonprotonated form (11.8 G).

The protonated C4-hydrogenated radical was identified in rA:HCl crystals.[12] The spin density at C8 was estimated to be 0.31 (calculated value: 0.11). Only one coupling was obtained experimentally and assigned to C4H ($A_{iso}$ = 9.0; $T_{ii}$ = -4.3, 0.1, 4.3 G). However, the calculated results (Table 5.7) indicate that the C4 hydrogen would possess a much larger isotropic coupling (49.2 G) and a smaller degree of anisotropy (-0.9, -0.4, 1.4 G). Moreover, the experimental couplings obtained in the adenine radical would be expected to be close to those obtained for cytosine or thymine when hydrogen is located perpendicular to the C5C6 double bond. The experimental authors are correct in their prediction that upon radical formation the C4 position becomes pyramidal, but the experimental and calculated C4H couplings do not match. It can be concluded that the C4-hydrogenated radical is unlikely to be responsible for the observed coupling. The assignment of the observed coupling to another radical is difficult in this case since neither of the computed sets gives a clear match for both isotopic and anisotropic data.

### *5.2.7 Protonated C2 and C8-Hydrogenated Radicals*

Surprising results were obtained in a study of the co-crystals of 1-methylthymine and 9-methyladenine.[21] Specifically, no products formed through oxidation of adenine were observed. The only adenine radicals observed were the C2 and C8-hydrogenated radicals. Zehner and co-workers have performed an in-depth experimental study on

properties of the C2 and C8-hydrogenated radicals.[9] The couplings in these two radicals were investigated, in a variety of crystals which represent different protonation states of the parent adenine molecule, and it was determined that the HFCCs depend strongly on the protonation state of the adenine base. It was also determined that the relative yields of the two radicals depends on the crystalline environment. More specifically, in crystals of 9-methyladenine, where the crystal interactions depend on van der Waals forces, only the C8 hydrogen addition radicals were observed, whereas in crystals that involve small polar molecules or extensive hydrogen bonding (singly protonated crystals), both C2 and C8 hydrogen addition radicals were observed. Alternatively, in A:2HCl crystals (doubly protonated), the concentration of the C8 radicals is much larger than the concentration of C2 adduct. The computed relative energies of these species explain these results perfectly. For the free base, the C8 addition radical lies 8.7 kcal/mol below the C2 radical, while the energy difference in the N1-protonated systems is only 0.3 kcal/mol and in the doubly protonated system C8 is lower in energy than C2 by 5.8 kcal/mol.

The relative abundance of the C2 and C8-hydrogenated radicals in different crystals was rationalized by the hypothesis that the C2-hydrogenated radical requires a specific environment to be stabilized.[9] In particular, it was determined from semi-empirical calculations that the dipole moment of the C2-hydrogenated radical (2.7 D) is larger than that of the corresponding C8 radical (1.7 D) and, thus, C2-hydrogenated radicals will be stabilized to a greater extent in ionic environments. Dipole moments calculated with DFT indicate that for the nonprotonated radicals the C2 radical's dipole moment (2.8 D) is larger than the C8 radical's dipole moment (2.3 D), but not to the extent calculated previously. Similarly, the dipole moments calculated for the N1-protonated radical indicate that the C8 radical possesses only a slightly larger dipole moment and the N1,N7-protonated C2 and C8 radicals have identical dipole moments. A more promising explanation can be found in the relative energies as discussed previously.

The HFCCs calculated for C2 and C8-hydrogenated radicals (Table 5.8) indicate that the disagreement between theory and experiment increases with the number of protons added to the parent molecule. This could arise since the surrounding counterions were not included in the calculations. However, even though the absolute magnitude of the results may not agree with experiment, the trend in the couplings is clearly described.

Table 5.8: Calculated and experimental isotropic HFCCs (G) and calculated dipole moments (D) in protonated C2 and C8-hydrogenated adenine radicals.

| Radical | | C2H | C2H | C8H | C8H | Dipole Moment |
|---|---|---|---|---|---|---|
| | | C2-hydrogenated Radical | | | | |
| Free Base | Calculated | 43.3 | 45.5 | -6.7 | | 2.8 |
| | Experimental[9] | 44.0 | 44.0 | 10.0 | | |
| N1-protonated | Calculated | 36.7 | 36.2 | -5.8 | | 3.1 |
| | Expermental (HCl)[9] | 39.0 | 39.0 | 6.5 | | |
| | Experimental ($HCl \cdot \frac{1}{2}H_2O$)[9] | 40.0 | 40.0 | 6.5 | | |
| | Experimental (HCl)[12] | 39.1 | 40.5 | -5.5 | | |
| N1,N7-protonated | Calculated | 50.0 | 50.4 | -2.5 | | 4.9 |
| | Experimental[9] | 45.0 | 45.0 | | | |
| | | C8-hydrogenated Radical | | | | |
| Free Base | Calculated | | -5.6 | 38.9 | 39.1 | 2.3 |
| | Experimental[9] | | | 39.0 | 39.0 | |
| N1-protonated | Calculated | | -5.2 | 40.6 | 40.5 | 3.5 |
| | Expermental (HCl)[9] | | | 40.0 | 40.0 | |
| | Experimental ($HCl \cdot \frac{1}{2}H_2O$)[9] | | 6.0 | 42.0 | 42.0 | |
| | Experimental (HCl)[12] | | -4.3 | 43.0 | 40.9 | |
| N1,N7-protonated | Calculated | | -2.5 | 46.5 | 46.6 | 4.9 |
| | Experimental[9] | | | 41.0 | 41.0 | |

For example, the magnitude of the C2H couplings in the C2-hydrogenated radical increases moving from the N1-protonated radical, to the free base, to the doubly-protonated radical. Similarly the magnitude of the C8H couplings in the C8-hydrogenated radical increases from the free base, to the N1 protonated and to the N1,N7-protonated radicals. The relative magnitudes of the C2H and C8H couplings in the C2 and C8 radicals are also well described by the calculations. For example, the C2H couplings in the C2-hydrogenated radical are larger than the C8H couplings in the C8-hydrogenated radical for the free base, but not for the protonated form. Comparison of calculated and experimental couplings for C2H and C8H in C8 and C2 adducts, respectively, indicates that these isotropic HFCCs are most probably negative.

Perhaps the most complete set of HFCCs for N1-protonated C2 and C8-hydrogenated radicals has been obtained in adenosine hydrochloride (Table 5.6).[12] The values obtained for the N1-protonated C2-hydrogenated radical indicate that the two C2 hydrogens have slightly different couplings (40.5/39.1 G). These isotropic values are a little larger than those calculated for this radical (36.7/36.2 G). However, the anisotropic C2H couplings, as well as the full tensors obtained for C8H and the N1H HFCCs are in remarkable agreement. In addition to differences in the magnitude of the calculated C2H coupling tensors of the nonprotonated C2-hydrogenated radical (45.5/43.3 G) and of the

N1-protonated form (36.7/36.2 G), the two couplings in the nonprotonated radical were calculated to be different from each other. As well, the average of the calculated isotropic HFCCs obtained for the protonated and the nonprotonated radicals (40.4 G) is in astonishing agreement with the magnitude of the couplings obtained experimentally for the singly protonated system (40.5/39.1 G). Thus, it is possible that experimentally an averaging of the protonated and nonprotonated HFCCs is observed or the N7H bond length is longer than that calculated for the protonated radical.

The values obtained in rA:HCl by Close *et al.*[12] for the complete C2H HFCC tensor, as well as the anisotropic couplings for C8H, in the C8-hydrogenated radical (Table 5.6) are in excellent agreement with the calculated values for the singly protonated systems. The calculated isotropic C8H HFCCs (40.6/40.5 G) are also in fair agreement with the experimental values (43.0/40.9 G), even though both couplings are calculated to be of equal magnitude, whereas experiment indicates that there is a slight difference between the two couplings. The calculations clearly indicate, unlike for the C2-hydrogenated radical, that the observed C8-hydrogenated radical is protonated at N1.

### *5.2.8 Summary of Adenine Results*

Calculations confirm that the adenine cation has been observed experimentally, although this radical was only identified in crystals initially protonated at N1. This indicates that more extreme conditions are required for the formation of this radical and if the cation is formed upon irradiation of other adenine derivatives then it quickly deprotonates to form neutral radicals. The N9-dehydrogenated radical was shown to be the lowest energy radical in its class. However, this radical is not possible in full DNA and hydrogen abstraction would primarily occur at N6. The N6-dehydrogenated radical has been identified in adenine crystals and the calculations support the experimental assignment of this species.

The C2 and C8 hydrogen addition radicals were determined to be the lowest energy radicals in this class. Geometrical effects due to the formation of these radicals (local puckering at the addition site) are difficult to describe theoretically and the HFCCs of the two C2 (C8) hydrogens were calculated to differ by only 2 G (0 G), while experimentally these couplings deviate by approximately 10 G (4 G). Other hydrogenated radicals undergo significant geometrical alterations upon formation, with

great distortion noted for the radical formed by addition of hydrogen to N3, C4 and C5. The distortion in the N3-hydrogenated radical results in an out-of-plane position for the N3 hydrogen and, hence, a large isotropic HFCC. Experimentally, this hydrogen yields only a small HFCC and, thus, it is speculated that interactions must be occurring in the crystals that lead to an in-plane position for the N3 hydrogen and a subsequently small HFCC. Calculations on a constrained, planar geometry for this radical confirmed this hypothesis as the HFCCs are in better agreement with experiment.

The C2 and C8 hydroxyl addition radicals are lower in energy than those radicals formed via addition of hydroxyl to either C4 or C5. In addition, the C2 and the C8 addition radicals undergo only slight geometrical alterations, while the radicals formed by hydroxyl addition to C4 and C5 adopt puckered conformations. Only the C8 hydroxyl addition radical has been observed in adenine crystals. The one isotropic coupling identified in this experiment agrees with the calculations. The elucidation of more complete HFCC tensors would be useful for identifying this radical. Comparison of the calculated HFCCs with the experimental spectra will make it easier to determine whether or not these radicals are formed in future experimental studies on base crystals or full DNA.

The HFCCs in a few N1-protonated and N1,N7-diprotonated radicals were also compared to experimental results. The energetics of these radicals were similar to the nonprotonated forms, the only difference being the relative stabilities of the C2 and C8 hydrogen addition radicals. The experimental assignment of the protonated N6-dehydrogenated and N3-hydrogenated radicals is supported by the calculations, although a planar structure was required to obtain good agreement for the latter radical. The differences in the HFCCs of various protonated forms of the C2 and C8-hydrogenated radicals observed experimentally were well reproduced with DFT. Alternatively, comparison of theoretical and experimental results leads to the conclusion that the protonated C4-hydrogenated radical was not detected in the experimental study. In addition, more studies are required to support the formation of the N7-hydrogenated radical.

Through comparison of theoretical and experimental couplings, a comprehensible illustration of the radiation damage in adenine crystals is accessible. It is proposed that

upon irradiation of adenine derivatives, hydrogen is lost from the N6 position. This will produce an abundance of hydrogen atoms that will subsequently add to C2, C8 and N3. Results from protonated crystals indicate that the N6-dehydrogenated and C2, C8 and N3 hydrogenated radicals are formed. These radicals are identical to those elucidated through comparison of calculated HFCCs and those obtained in nonprotonated crystals indicating that protonation at N1 in adenine crystals has little effect on the net radiation products. Although only one experimental isotropic HFCC was elucidated, comparison of the calculated results to the experimental couplings obtained in irradiated frozen aqueous solutions of deoxyadenosine 5'-monophosphate indicates that a net hydroxyl radical addition product is formed in this derivative. This provides promising support for the proposal of a similar cytosine product in Chapter Four.

## *5.3 Guanine*

### *5.3.1 Previous Experimental Work*

Guanine is important to investigate since it has been proposed to be the main site of electron loss upon irradiation of DNA. The chemical structure and numbering of guanine to be used in the present discussions is displayed in Figure 5.2 (structure I). Many guanine crystals have been examined in the literature (Table 5.9) including 2'-deoxyguanosine 5'-monophosphate (5'dGMP),[3,22,23] and guanosine 3',5'-cyclic monophosphate (3'5'cGMP).[17,24] In separate studies of 5'dGMP, the N2-dehydrogenated[22] and C8-hydrogenated[23] radicals were identified. A more recent study provides an enhanced picture of the radicals generated in 5'dGMP crystals[3] through the identification of the guanine anion, the N2-dehydrogenated and the C5 and C8-hydrogenated radicals. One set of couplings was also left unassigned in these crystals. In

I II

Figure 5.2: Structure and chemical numbering of guanine (I, 2-amino-6-oxypurine) and singly protonated guanine (II).

Table 5.9: Experimental HFCCs (G) in guanine radicals.

| Radical | Molecule | Atom | $A_{iso}$ | $T_{XX}$ | $T_{YY}$ | $T_{ZZ}$ |
|---|---|---|---|---|---|---|
| anion | 5'dGMP[3] | "C8H" | -3.0 | -2.5 | 0.0 | 2.5 |
| cation | G:HCl:$H_2O$[25] | "N2H" | 4.3 | -3.8 | 0.7 | 3.2 |
| | | "N2H" | 4.3 | -3.8 | 0.7 | 3.2 |
| | | "C8H" | 5.2 | -2.2 | -0.2 | 2.3 |
| | G:HCl:$H_2O$[26] | "C8H" | -4.0 | -2.0 | -0.4 | 2.5 |
| | 3'5'cGMP[24] | "C8H" | -4.5 | -2.7 | -0.8 | 3.4 |
| | G:HBr:$H_2O$[2] | "C8H" | -4.6 | -2.4 | -0.4 | 2.8 |
| N2-dehydrogenated | 5'dGMP[3] | "N2H" | -9.5 | -6.9 | -0.9 | 7.7 |
| | | "C8H" | -5.0 | -2.5 | -0.1 | 2.6 |
| | 3'5'cGMP[17] | "N2H" | -9.5 | -6.9 | -1.0 | 7.9 |
| | | "C8H" | -4.7 | -2.4 | -0.2 | 2.7 |
| | 5'dGMP[22] | "N2H" | -9.6 | -6.9 | -0.9 | 7.8 |
| | | "C8H" | -4.9 | -2.6 | -0.2 | 2.9 |
| C5-hydrogenated | 5'dGMP[3] | "C5H" | 54.0 | -1.0 | -0.5 | 1.7 |
| C8-hydrogenated | 5'dGMP[3] | "C8H" | 39.3 | -1.4 | -0.8 | 2.1 |
| | | "C8H" | 37.2 | -1.4 | -0.8 | 2.2 |
| | 5'dGMP[23] | "C8H" (2) | 37.8 | -0.8 | -0.5 | 1.4 |
| C4-hydroxylated | 3'5'cGMP[17] | "C8H" | -6.7 | -3.4 | -0.2 | 3.6 |
| unassigned | 5'dGMP[3] | "C8H" | -7.2 | -3.7 | -0.3 | 4.0 |
| | | "NH" | -3.4 | -2.6 | -0.5 | 2.9 |
| | | "NH" | -3.0 | -1.9 | -0.5 | 2.4 |

one study of 3'5'cGMP crystals, the guanine anion was identified.[24] In another study of similar crystals, the N2-dehydrogenated and C4-hydrogenated radicals were characterized.[17]

Similar to adenine, experimental ESR/ENDOR studies on guanine derivatives have evolved around a variety of crystalline environments in which the parent guanine molecule is protonated at N7 (Figure 1, II). For example, Hole *et al.*[2] performed a study on guanine hydrobromide monohydrate (G:HBr:$H_2O$) crystals in which the N7 position is protonated. Examination of protonated guanine model systems, such as the one studied by Hole *et al.*, is important since in nonprotonated crystals the guanine cation is readily deprotonated even at low temperatures. Investigation of the radical thought to be predominantly formed in full DNA, namely the guanine cation, is extremely difficult in nonprotonated samples. However, in N7-protonated crystals, deprotonation primarily occurs at N7 after loss of an electron. The spectrum of this product is hence very similar to that assigned to the guanine cation observed in DNA.[17] In addition to G:HBr:$H_2O$ crystals, the guanine cation has been assigned in crystals of guanine hydrochloride monohydrate.[25,26]

Due to the importance of the N7-protonated radicals, some of these will also be discussed in the current chapter when experimental data is available. Protonated crystals investigated in the literature include guanine hydrochloride monohydrate ($G{:}HCl{:}H_2O$),[26,27] guanine hydrochloride dihydrate ($G{:}HCl{:}2H_2O$),[28] the free acid of guanosine 5'-monophosphate (5'GMP(FA))[29] and guanine hydrobromide monohydrate ($G{:}HBr{:}H_2O$).[2] The radicals identified in these studies will be discussed in more detail in a later section.

### *5.3.2 Anion and Cation*

The adiabatic IP was calculated to be 171.8 kcal/mol (Table 5.10), which is in agreement with the experimental IP[15] (179.3 kcal/mol) and the value obtained with MP2[13] (176.6 kcal/mol). The EA, which has not been determined experimentally, was calculated to be -15.8 kcal/mol. This value is similar to that predicted from the vertical electron affinities through a best fit of the Koopman's EAs to experimental data of similar systems (-16.7 kcal/mol).[13] Both the guanine anion and cation were identified upon irradiation of a variety of guanine crystals. The anion was reported upon irradiation of 5'dGMP,[3] where the spin density at C8 was determined to be 0.11 (calculated value: C8 (0.08), C2 (0.57) and N2 (0.12)), which can be altered by the hydrogen bonding environment at N7.[3] The calculations indicate that the anion undergoes significant geometrical alterations upon formation, whereby the pyrimidine ring is distorted at C2 and the amino group is twisted such that one hydrogen is orientated directly perpendicular to the plane formed by the remainder of the guanine molecule and the other hydrogen is located at an angle of 104° with respect to it. Reorientation of the amino

Table 5.10: Calculated HFCCs (G) in the guanine anion and cation radicals.

| Radical | Atom | $A_{iso}$ | $T_{XX}$ | $T_{YY}$ | $T_{ZZ}$ |
|---|---|---|---|---|---|
| Anion | N2H | 1.6 | -2.1 | -1.1 | 3.2 |
| (EA = -15.8 kcal/mol) | N2H | 31.9 | -1.8 | -0.9 | 2.7 |
| | C8H | -2.5 | -1.6 | -0.1 | 1.6 |
| | N9H | -1.4 | -0.9 | -0.6 | 1.6 |
| $C_s$ Anion | N1H | -3.2 | -2.8 | -1.0 | 3.7 |
| | N2H | -2.5 | -2.2 | -1.0 | 3.2 |
| | N2H | -2.8 | -2.4 | -0.8 | 3.2 |
| | C8H | -3.5 | -2.0 | -0.2 | 2.2 |
| | N9H | -3.4 | -3.0 | -0.8 | 3.7 |
| Cation | N2H | -2.7 | -1.6 | -1.0 | 2.6 |
| (IP = 171.8 kcal/mol) | N2H | -3.1 | -2.5 | -0.7 | 3.2 |
| | C8H | -8.2 | -4.4 | -0.6 | 5.0 |

group may not be possible in the experiments due to hydrogen bonding possibilities in the crystals not accounted for in the calculations. To account for hydrogen bonding, the geometry of the anion was also optimized in a fixed $C_s$ symmetry which lies 17.9 kcal/mol higher in energy than the nonplanar radical.

Experimentally, a significant C8H isotropic coupling was obtained (-3.0 G, Table 5.9). This value is in good agreement with the calculated isotropic coupling in the nonplanar radical (-2.5 G, Table 5.10). However, the nonplanar anion (-1.6, -0.1, 1.6 G) and the experimental (-2.5, 0, 2.5 G) anisotropic tensors differ more than expected since this component can be calculated to a greater degree of accuracy than the isotropic HFCC. In addition, the calculations indicate that a large N2H isotropic coupling (31.9 G) would be observed due to the out-of-plane amino hydrogen. The HFCCs for the planar anion ($C_s$ anion, Table 5.10) improve the agreement with experiment. However, it is very difficult to conclude whether or not the anion is responsible for the observed spectrum. The C8H anisotropic HFCCs are in better agreement with experiment for the planar anion than the nonplanar form, but couplings of equal magnitude or larger were calculated for the two amino hydrogens, N1H and N9H, which were not reported experimentally. For a positive identification of the observed radical, additional experimental studies would be useful to determine the magnitude of the aforementioned couplings. Hole *et al.*[3] noted that the spectra assigned to the guanine anion in their study could possibly be due to the O6-hydrogenated radical. This option will be discussed in more detail below.

As previously mentioned, the guanine cation was observed in single crystals of G:HBr:$H_2O$,[2] G:HCl:$H_2O$[25,26] and 3'5'cGMP.[24] In crystals of G:HCl or G:HBr monohydrate, the parent guanine molecule is protonated at N7. Upon oxidation of these crystals, the N7-dehydrogenated radical is formed with respect to the initially protonated parent molecule and the net result is the guanine cation. The C8 spin density distributions in these crystals range from 0.14 to 0.182 (calculated value: 0.28). In G:HCl:$H_2O$ crystals, the N3 spin density was determined to be 0.28 (calculated value: 0.21). The experimental N2 spin density ranges from 0.15 to 0.17 in G:HCl:$H_2O$ and from 0.06 to 0.08 in G:HBr:$H_2O$ crystals (calculated value: 0.10). Unlike the guanine anion, the cation retains a planar conformation. The calculated isotropic C8H coupling (-8.2 G), along with the anisotropic component (largest tensor component: 5.0 G), is

larger in magnitude than the experimental results (average isotropic and largest anisotropic tensor components are -4.6 G and 2.8 G, respectively). In addition, two N2H coupling tensors were extracted in one study of guanine hydrochloride monohydrate crystals.[25] Once again, the experimental and calculated couplings differ although it is evident that the sign of the couplings should be negative. Thus, it is speculated that the guanine cation was probably not observed directly in these studies, but more likely a deprotonated radical is formed. The exact identity of the deprotonated cation is difficult to determine. Further experimental and theoretical work would be advantageous to determine which radical is responsible for the observed spectrum.

### *5.3.3 Net Hydrogen Addition Radicals*

Six net hydrogen addition radicals are possible of which the C8-hydrogenated radical is the lowest in energy (Table 5.11). The N7, C4, O6 and N3-hydrogenated radicals are 11.0, 14.8, 19.5, and 21.6 kcal/mol higher in energy, respectively. The C5-hydrogenated radical is the highest energy hydrogenated radical lying 35.8 kcal/mol above the corresponding C8 adduct. Considering that only the C8 and the C5 radicals have been observed in experimental studies, factors other than the thermodynamics considered here must affect the formation of the C5 addition product. The N3-hydrogenated product exhibits significant puckering in the pyrimidine ring, in particular at the C2 position with the amino group twisted such that one hydrogen is above the plane formed by the rest of the molecule and the second hydrogen below the plane. Distortion in the N7-hydrogenated radical occurs in both the five and six-membered rings. Neither of these net hydrogen atom addition radicals have been assigned in experimental studies.

The radical formed through net hydrogen addition to C5 was identified in detailed work on 5'dGMP.[3] The experimental study indicated that C5H has a very large isotropic coupling (54.0 G) and a very small anisotropic coupling tensor (-1.0, -0.7, 1.7 G). The C5-hydrogenated radical was calculated to be in a "butterfly" conformation identical to those described for hydrogenated and hydroxylated adenine radicals. The experimental anisotropic coupling tensor is in good agreement with the calculated tensor (-0.7, -0.5, 1.2 G). The calculated isotropic C5H coupling (49.5 G) also supports the experimental assignment of the observed spectrum to the C5-hydrogenated radical. The calculations

Table 5.11: Calculated HFCCs (G) in hydrogenated guanine radicals.

| Radical | Relative Energy | Atom | $A_{iso}$ | $T_{XX}$ | $T_{YY}$ | $T_{ZZ}$ |
|---|---|---|---|---|---|---|
| C8-hydrogenated | 0.0 | N2H | 1.6 | -0.8 | -0.4 | 1.2 |
| | | N2H | -0.3 | -0.9 | -0.4 | 1.3 |
| | | C8H | 36.9 | -1.1 | -0.7 | 1.8 |
| | | C8H | 37.2 | -1.1 | -0.7 | 1.8 |
| | | N9H | -2.9 | -2.6 | -0.9 | 3.5 |
| N7-hydrogenated | 11.0 | N7H | 11.3 | -4.3 | -2.3 | 6.6 |
| | | C8H | 25.1 | -7.6 | -1.1 | 8.7 |
| C4-hydrogenated | 14.8 | N2H | 1.0 | -0.3 | -0.2 | 0.5 |
| | | C4H | 42.7 | -0.9 | -0.6 | 1.5 |
| | | C8H | -7.1 | -4.1 | -0.7 | 4.7 |
| | | N9H | -3.4 | -3.3 | -1.2 | 4.5 |
| O6-hydrogenated | 19.5 | N1H | 7.1 | -2.0 | -1.9 | 3.9 |
| | | O6H | -2.8 | -3.9 | -2.4 | 6.3 |
| | | C8H | -2.7 | -1.6 | -0.1 | 1.7 |
| $C_s$ O6-hydrogenated | | N1H | -3.0 | -2.6 | -1.2 | 3.8 |
| | | O6H | -1.9 | -2.2 | -2.2 | 4.4 |
| | | C8H | -3.9 | -2.3 | -0.1 | 2.3 |
| N3-hydrogenated | 21.6 | N1H | -2.0 | -3.1 | -1.8 | 4.9 |
| | | N2H | 31.8 | -1.5 | -1.1 | 2.6 |
| | | N2H | 7.7 | -2.3 | -1.5 | 3.9 |
| | | C8H | -1.7 | -1.0 | -0.1 | 1.2 |
| C5-hydrogenated | 35.8 | N2H | -1.0 | -1.5 | -0.8 | 2.3 |
| | | N2H | 12.4 | -1.4 | -0.9 | 2.4 |
| | | C5H | 49.5 | -0.7 | -0.5 | 1.2 |

show that a hydrogen added to the C4 position in the corresponding C4-hydrogenated radical exhibits a slightly smaller, yet significant, isotropic coupling (42.7 G). The difference between the couplings in the C4 and C5-hydrogenated radicals is a significant isotropic coupling (12.4 G) calculated for one of the amino hydrogens in the C5-hydrogenated radical. This coupling might be useful for the clear identification of the C5-hydrogenated radical in future experimental studies.

The C8-hydrogenated radical was observed in two different studies of 2'-deoxyguanosine 5'-monophosphate.[3,23] In the earliest study,[23] the spin density was determined to reside mainly on N7 (0.43). The spin density was calculated to be located on N7 (0.51), N9 (0.11), C4 (0.13) and O6 (0.10). Experimentally,[23] two equivalent C8H isotropic couplings were resolved (37.8 G). In a more recent study,[3] two unique couplings were identified (39.3 and 37.2 G). The optimized C8-hydrogenated radical is mostly planar and two slightly different couplings were obtained for the C8 hydrogens (37.2 and 36.9 G). Difficulties in describing radical puckering have been discussed for thymine, cytosine and adenine. Consideration of these previous calculations and the

more accurate experimental techniques employed in the latter experimental studies indicates that the latter experimental results are more reliable. Through comparison of the anisotropic couplings obtained in both experimental studies to those obtained from the present calculations, the observed radical can confidently be assigned to the guanine C8-hydrogenated radical.

The substituents in the O6-hydrogenated radical are greatly affected by radical formation. The O6 position is displaced out of the molecular plane with a dihedral angle with respect to C4 of 33.2°. In addition, the relative location of the amino and N1 hydrogens is affected by this distortion, which is probably due to the large amount of spin density calculated to be located on C6 (0.64). Hole *et al.*[3] determined that the O6-hydrogenated radical was unlikely to give rise to a C8H coupling observed in the spectrum of 5'dGMP ($A_{iso}$ = -3.0 G; $T_{ii}$ = -2.5, 0, 2.5 G) and the coupling was assigned to the anion. However, comparison of the calculated and experimental couplings for the anion led to some concern. The calculated couplings for C8H in the O6-hydrogenated radical ($A_{iso}$ = -2.7 G; $T_{ii}$ = -1.6, -0.1, 1.7 G) are only in fair agreement with the experimental HFCCs. In addition, a larger N1H isotropic coupling (7.1 G) was calculated, but not detected in the experimental spectrum, which seems unlikely.

As discussed for the guanine anion and adenine radicals, crystal interactions may lead to a planar O6-hydrogenated radical rather than a puckered structure. An optimized radical constrained to $C_s$ symmetry lies only 3.8 kcal/mol above the distorted radical. The magnitude of the N1H HFCC in the planar radical (Table 5.12, $C_s$ O6-hydrogenated) is much smaller than that calculated for the nonplanar form. In addition, the C8H anisotropic couplings in the planar O6-hydrogenated radical (-2.3, -0.1, 2.3 G) are in very good agreement with the anisotropic couplings assigned experimentally to the guanine anion (-2.5, 0.0, 2.5 G). Thus, it is possible that the spectrum assigned to the guanine anion arises from the anion protonated at O6. More experimental work, such as the determination of the N1H HFCCs or searching for the O6H coupling through ENDOR spectroscopy, would be beneficial for the identification of the observed radical. The calculations indicate that the planar anion and O6-hydrogenated radicals can be distinguished through the amino hydrogen couplings, which could only be detected in the anion.

### *5.3.4 Net Hydrogen Abstraction Radicals*

The N9-dehydrogenated radical is the lowest energy species (Table 5.12), with the N1 and N2-dehydrogenated radicals lying 1.7 and 1.9 kcal/mol higher in energy, respectively. In full DNA samples, a sugar group replaces the N9 hydrogen and, thus, the N1 or N2-dehydrogenated products are expected. The C8-dehydrogenated radical was found to lie much higher in energy (24.1 kcal/mol) than the other radicals in this class providing a possible explanation for the absence of this radical in experimental spectra. Both the N1 and N9-dehydrogenated radicals remain planar upon formation, with very slight distortions occurring primarily at the amino group. The hyperfine coupling constants (Table 5.12) in these dehydrogenated radicals were also very similar, and consist of a C8H coupling (approximately -7 G) which has a considerable amount of anisotropy (largest component of the anisotropic tensor is approximately 4.5 G). In addition, small coupling tensors were calculated for both of the amino hydrogens. The optimized C8-dehydrogenated radical exhibits slight distortions, mainly at C8 which lead to a localization of the spin density at this position (0.82) and a small N9H isotropic coupling (-1.4 G). A significant anisotropic tensor (-3.1, -1.8, 4.9 G) calculated for this atom would aid in the experimental detection of this radical.

Table 5.12: Calculated HFCCs (G) in dehydrogenated guanine radicals.

| Radical | Relative Energy | Atom | $A_{iso}$ | $T_{XX}$ | $T_{YY}$ | $T_{ZZ}$ |
|---|---|---|---|---|---|---|
| N9-dehydrogenated | 0.0 | N2H | -2.1 | -1.5 | -0.9 | 2.4 |
| | | N2H | -2.0 | -2.2 | -0.6 | 2.8 |
| | | C8H | -6.6 | -3.7 | -0.7 | 4.4 |
| N1-dehydrogenated | 1.7 | N2H | -1.6 | -0.9 | -0.6 | 1.5 |
| | | N2H | -2.0 | -1.6 | -0.5 | 2.1 |
| | | C8H | -7.4 | -4.1 | -0.4 | 4.5 |
| N2-dehydrogenated | 1.9 | N2H | -7.6 | -6.6 | -1.2 | 7.7 |
| | | C8H | -6.0 | -3.4 | -0.3 | 3.7 |
| C8-dehydrogenated | 24.1 | N9H | -1.4 | -3.1 | -1.8 | 4.9 |

The only radical identified in nonprotonated guanine crystals formed through net hydrogen atom abstraction is the N2-dehydrogenated radical. This radical has been observed in 5'dGMP[3,22] and 3'5'cGMP.[17] The C8 and N2 spin density distributions in all samples were determined to be approximately 0.17 and 0.33 (calculated value: 0.19 and 0.37, respectively). The N3 spin density (0.31) was determined in the study of 3'5'cGMP crystals[17] (calculated value: 0.35). The experimental couplings for the N2-

dehydrogenated radical obtained in the various studies are remarkably similar (Table 5.9). The C8H coupling tensor consists of an average isotropic component of -4.9 G and an average anisotropic component of (-2.5, -0.2, 2.7 G), which are only in fair agreement with the calculated values ($A_{iso}$ = -6.0 G; $T_{ii}$ = -3.4, -0.3, 3.7 G). The remaining amino hydrogen was also observed in the experimental studies, where an isotropic HFCC, averaged between the three studies, of -9.6 G was obtained. The magnitude of this coupling is again larger than the N2H coupling obtained from DFT (-7.6 G). However, comparison of experimental (-6.9, -1.0, 7.8 G) and calculated (-6.6, -1.2, 7.7 G) anisotropic N2H coupling tensors supports the experimental assignment of the spectrum to the N2-dehydrogenated radical.

### *5.3.5 Net Hydroxyl Radical Addition Products*

Hydroxyl radical addition can occur at C4, C5 or C8 in guanine. The relative energies of these radiation products (Table 5.13) indicate that the C8-hydroxylated radical is the lowest in energy with the corresponding C4 and C5 radicals lying 14.2 and 19.0 kcal/mol higher in energy, respectively. This is identical to the relative energies calculated for the corresponding hydrogenated radicals, although the C5-hydroxylated radical is closer in energy to the other radicals than the C5-hydrogenated radical is to related species. The only hydroxylated product observed in experimental studies on neutral guanine crystals is that formed by addition to C4.

The calculated spin density distributions in hydroxylated radicals indicate that close to half of the spin density is located on a neighboring center (C5 (0.48), C4 (0.44) and N7 (0.47) in the C4, C5 and C8-hydroxylated radicals, respectively). Both the C4 and C5-hydroxylated radicals adopt a "butterfly" conformation previously discussed for the corresponding hydrogenated radicals and similar adenine radicals. Significant

Table 5.13: Calculated HFCCs (G) in guanine hydroxylated radicals.

| Radical | Relative Energy | Atom | $A_{iso}$ | $T_{XX}$ | $T_{YY}$ | $T_{ZZ}$ |
|---|---|---|---|---|---|---|
| C8-hydroxylated | 0.0 | C8H | 23.4 | -1.0 | -0.5 | 1.5 |
| | | N9H | -2.4 | -2.1 | -0.8 | 2.9 |
| C4-hydroxylated | 14.2 | C8H | -7.8 | -4.5 | -0.7 | 5.1 |
| | | N9H | -2.0 | -2.5 | -1.0 | 3.6 |
| C5-hydroxylated | 19.0 | N2H | 7.6 | -1.5 | -0.8 | 2.4 |
| | | N7H | -1.0 | -1.1 | -0.9 | 2.0 |
| | | C8H | -2.5 | -1.5 | -0.5 | 2.0 |

isotropic couplings were calculated for C8H (-7.8 G) and N2H (7.6 G) in the C4 and C5-hydroxylated radicals, respectively. The geometry of the C8-hydroxylated radical is not significantly different from the parent molecule with the hydrogen and the hydroxyl group orientated at C8 such that they are displaced equally on opposite sides of the molecular plane. This displacement results in a substantial C8H isotropic coupling (23.4 G).

The spectrum of the C4-hydroxylated radical was recorded in crystals of 3'5'cGMP.[17] The observed radical was determined to possess a C8 spin density of approximately 0.25 (calculated value: 0.26). The only coupling extracted from the experiments was for C8H, whose full coupling tensor is (-10.1, -6.9, -3.1 G). The calculated full tensor for the proposed radical is (-12.3, -8.5, -2.7 G). If the individual components of the coupling tensor are considered, then only fair agreement with experiment is obtained. Among the radicals investigated, the only couplings that match the experimental C8H isotropic (-6.7 G) and anisotropic results (-3.4, -0.2, 3.6 G) arise from the nonprotonated N2-dehydrogenated radical. The C8H calculated tensor in this radical is composed of a -6.0 G isotropic component and an anisotropic tensor of (-3.4, -0.3, 3.7 G). The N2-dehydrogenated radical also possesses a large N2H coupling (-7.6 G) while the C4-hydroxylated radical possesses a small N9H coupling (-2.0 G). These couplings would be useful for the full identification of this radical.

### *5.3.6 N7-Protonated Radicals*

A number of radicals have been identified in N7-protonated guanine derivatives (Table 5.14). Two hydrogenated radicals have been identified, the C8 and O6 adducts. The C8 hydrogen addition radical lies 18.8 kcal/mol lower in energy than the corresponding O6 radical (Table 5.15), which is close to the difference observed (19.5 kcal/mol) for the nonprotonated radicals. The C8-hydrogenated radical protonated at N7 was observed in studies on crystals of G:HCl:$H_2O$,[27] 5'GMP(FA),[29] G:HCl:$2H_2O$[28] and G:HBr:$H_2O$.[2] The average spin density distribution on N7 and N9 observed in these studies is 0.31 and 0.11, respectively (calculated values: 0.32 and 0.10). A coupling was assigned to N7H in all experimental studies which on average consists of an isotropic

Table 5.14: Experimental HFCCs (G) of N7-protonated guanine radicals.

| Radical | Molecule | Atom | $A_{iso}$ | $T_{XX}$ | $T_{YY}$ | $T_{ZZ}$ |
|---|---|---|---|---|---|---|
| O6-hydrogenated | G:HCl:$H_2O$[26] | "N1H" | -4.2 | -2.5 | -0.5 | 3.0 |
| | | "C8H" | -7.5 | -4.3 | 0.5 | 3.8 |
| | | "C8H" | -8.1 | -4.0 | -0.3 | 4.3 |
| | 5'GMP(FA)[29] | "N1H" | -3.7 | -2.6 | -0.6 | 3.2 |
| | | "O6H" | 0.4 | -1.6 | 0.1 | 1.5 |
| | | "N7H" | -3.3 | -1.6 | -1.0 | 2.6 |
| | | "C8H" | -7.2 | -3.5 | -0.4 | 3.9 |
| | G:HCl:2$H_2O$[28] | "N1H" | -2.2 | -1.7 | -0.1 | 1.7 |
| | | "N7H" | -1.7 | -1.7 | -0.8 | 2.5 |
| | | "C8H" | -7.7 | -4.7 | 0.6 | 4.1 |
| | | "N1H" | -4.1 | -2.9 | -0.6 | 3.4 |
| | | "N7H" | -3.5 | -2.2 | -0.7 | 2.9 |
| | | "C8H" | -7.6 | -3.8 | -0.4 | 4.2 |
| | | "N1H" | -3.5 | -2.5 | -0.5 | 3.0 |
| | | "N7H" | -3.1 | -1.8 | -0.9 | 2.7 |
| | | "C8H" | -7.8 | -4.1 | -0.2 | 4.3 |
| | | "N1H" | -3.2 | -2.4 | -0.6 | 3.0 |
| | | "N7H" | -2.9 | -1.6 | -0.9 | 2.5 |
| | | "C8H" | -8.3 | -3.6 | 0.0 | 4.7 |
| | G:HBr:$H_2O$[2] | "N1H" | -3.2 | -2.4 | -0.5 | 2.9 |
| | | "N7H" | -2.8 | -1.6 | -0.9 | 2.4 |
| | | "C8H" | -8.1 | -4.0 | -0.6 | 4.5 |
| C8-hydrogenated | G:HCl:$H_2O$[27] | "C8H" | 46 | | | |
| | | "C8H" | 25.8 | -1.6 | -0.3 | 1.7 |
| | | "N7H" | -8.3 | -6.6 | -0.6 | 7.3 |
| | 5'GMP(FA)[29] | "C8H" | 36.5 | -1.4 | -0.7 | 2.1 |
| | | "C8H" | 33.1 | -1.4 | -0.8 | 2.1 |
| | | "N7H" | -8.5 | -6.6 | -1.6 | 8.2 |
| | G:HCl:2$H_2O$[28] | "C8H" | 35.3 | -1.3 | 0.0 | 2.1 |
| | | "C8H" | 38.2 | -1.3 | -0.9 | 2.1 |
| | | "N7H" | -9.0 | -6.9 | -1.5 | 8.4 |
| | | "N9H" | -3.0 | -2.4 | -0.7 | 3.1 |
| | G:HBr:$H_2O$[2] | "N7H" | -8.6 | -7.2 | -1.6 | 8.5 |
| | | "N9H" | -3.2 | -2.6 | -0.8 | 3.0 |
| N9-dehydrogenated | G:HCl:$H_2O$[27] | "N7H" | -5.0 | -3.6 | -1.4 | 5.0 |
| | | "N2H" | -2.2 | -1.8 | -0.3 | 2.1 |
| | | "N2H" | -2.1 | -1.4 | -0.6 | 1.9 |
| | G:HCl:2$H_2O$[28] | "N2H" | -2.0 | -1.3 | -0.5 | 1.8 |
| | | "N2H" | -2.2 | -1.5 | -0.4 | 2.0 |
| | | "N7H" | -5.4 | -3.7 | -1.3 | 5.1 |
| C5-hydroxylated | G:HBr:$H_2O$[2] | "N2H" | -4.0 | -2.9 | -0.6 | 3.5 |
| | | "N2H" | -3.5 | -2.2 | -0.4 | 2.5 |
| | | "N7H" | -3.2 | -2.4 | -1.0 | 3.4 |
| | | "C8H" | -3.7 | -1.9 | -0.5 | 2.4 |
| C8-hydroxylated | G:HCl:2$H_2O$[28] | "N7H" | -8.5 | -6.5 | -1.5 | 8.0 |
| | | "C8H" | 20.2 | -1.1 | -0.6 | 1.6 |
| | | "N9H" | -2.2 | -1.8 | -0.7 | 2.5 |
| ring-opened | G:HBr:$H_2O$[2] | "C8H" | -4.9 | -2.6 | 0.1 | 2.4 |

Table 5.15: Calculated HFCCs (G) in various guanine N7-protonated radicals.

| Radical | Relative Energy | Atom | $A_{iso}$ | $T_{XX}$ | $T_{YY}$ | $T_{ZZ}$ |
|---|---|---|---|---|---|---|
| C8-hydrogenated | 0.0 | N2H | -1.3 | -0.9 | -0.5 | 1.4 |
| | | N2H | -1.6 | -1.1 | -0.4 | 1.5 |
| | | N7H | -8.1 | -6.5 | -1.8 | 8.3 |
| | | C8H | 29.1 | -1.1 | -0.7 | 1.7 |
| | | C8H | 29.1 | -1.1 | -0.6 | 1.7 |
| | | N9H | -3.0 | -2.5 | -0.9 | 3.4 |
| O6-hydrogenated | 18.8 | O6H | 22.0 | -1.5 | -1.2 | 2.7 |
| | | N7H | -2.4 | -1.5 | -1.2 | 2.7 |
| | | C8H | -11.0 | -6.2 | 0.3 | 5.9 |
| $C_s$ O6-hydrogenated | | N1H | -2.6 | -2.2 | -0.9 | 3.1 |
| | | O6H | -1.5 | -1.5 | -1.5 | 2.9 |
| | | N7H | -3.2 | -2.3 | -1.3 | 3.6 |
| | | C8H | -12.8 | -7.2 | 0.4 | 6.8 |
| N9-dehydrogenated | | N2H | -3.4 | -2.1 | -1.1 | 3.2 |
| | | N2H | -3.8 | -3.1 | -0.8 | 3.9 |
| | | N7H | -2.8 | -2.2 | -1.1 | 3.3 |
| | | C8H | -2.9 | -1.7 | -0.6 | 2.3 |
| C8-hydroxylated | 0.0 | N7H | -7.0 | -5.9 | -1.7 | 7.6 |
| | | C8H | 17.5 | -0.9 | -0.5 | 1.4 |
| | | N9H | -2.1 | -1.8 | -0.8 | 2.6 |
| C5-hydroxylated | 20.5 | N2H | -2.5 | -1.7 | -0.9 | 2.7 |
| | | N2H | -2.7 | -2.4 | -0.6 | 3.0 |
| | | N7H | -1.5 | -1.5 | -0.9 | 2.5 |
| | | C8H | -9.1 | -5.0 | -0.2 | 5.2 |
| ring-opened | 28.8 | N1H | -1.3 | -1.0 | -0.5 | 1.5 |
| | | N7H | -2.7 | -1.3 | 0.1 | 1.3 |
| | | C8H | -4.8 | -2.5 | -0.5 | 3.0 |
| | | O8H | -1.0 | -1.7 | -1.0 | 2.7 |
| | | N9H | -10.6 | -9.3 | -1.8 | 11.1 |

component of -8.6 G and a notable anisotropic tensor (-6.8, -1.3, 8.1 G). This is in very nice agreement with the calculated N7H HFCC in the protonated C8-hydrogenated radical ($A_{iso}$ = -8.1 G; $T_{ii}$ = -6.5, -1.8, 8.3 G). In two experimental studies,[2,28] a coupling tensor for N9H was observed ($A_{iso}$ = -3.1 G; $T_{ii}$ = -2.5, -0.8, 3.1 G), which is once again in agreement with the calculations ($A_{iso}$ = -3.0 G; $T_{ii}$ = -2.5, -0.9, 3.4 G).

The anisotropic C8H couplings in all experimental studies were virtually identical (-1.4, -0.7, 2.0 G) and in good agreement with the calculated tensor (-1.1, -0.7, 1.7 G). In contrast, the two isotropic C8H couplings vary between crystalline environments, where in some studies the difference between the two couplings is great[27] (approximately 20 G) and in other studies the difference is small[29,28] (3 G). The couplings with the small difference between the two values may be regarded as more reliable since the complete coupling tensors were determined using sophisticated ENDOR spectroscopy, whereas the

couplings that deviated by 20 G were determined only through ESR. However, differences in couplings extracted in each experiment may also arise due to the crystalline environment, the temperature, or the different time scales employed. The calculations indicate that the two C8 hydrogens have identical couplings, which are much smaller (29.1 G) than those observed in any of the ENDOR experiments (approximately 34 G and 37 G). The problem of calculating couplings smaller than recorded experimentally has previously been discussed for similar thymine and adenine radicals. Due to the good agreement between theory and experiment for all couplings besides the isotropic C8H component, the calculations support the experimental assignment of the protonated C8-hydrogenated radical. It should be noted that the isotropic C8H couplings calculated for the nonprotonated radical (36.9/37.2 G) are in excellent agreement with the couplings assigned to the corresponding protonated radical. However, due to the excellent agreement of the N7H HFCCs with experiment, it can be concluded that the radical is protonated and the poor agreement with experimental results is due to the model employed.

The N7-protonated O6-hydrogenated radical has been observed in studies on crystals of G:HCl:$H_2O$,[26] 5'GMP(FA),[29] G:HCl:$2H_2O$[28] and G:HBr:$H_2O$.[2] The geometry was calculated to exhibit distortions at C6, where O6H is located out of the molecular plane to result in a large isotropic O6H coupling which was not recorded experimentally. The calculated couplings for the hydrogen at O6 (22.0 G) and C8 (-11.0 G) are extremely large (Table 5.15), while the corresponding experimental couplings are small (Table 5.14). Not even the anisotropic couplings for this radical are in agreement. Thus, it seems unlikely that the N7-protonated O6 hydrogen addition radical is responsible for the spectra observed in these studies. Since hydrogen bonding interactions may result in a planar geometry, a $C_s$ radical was obtained through a full optimization, which possesses one imaginary frequency and lies 1.7 kcal/mol higher in energy than the nonplanar radical. Calculations on the planar radical yield a small O6H coupling which is expected experimentally and, thus, the agreement between calculated couplings and experiment could be considered to be improved over that observed for the nonplanar radical. A N1H coupling was calculated in the planar radical that was not obtained for the nonplanar form, however this coupling is still smaller than the experimental result. The

experimental and calculated couplings also disagree in the magnitude of the C8H coupling, where the HFCCs obtained from the calculations are far too large relative to those obtained in the experimental study.

The possibility that the observed radical is nonprotonated can be eliminated. In particular, the C8H HFCC for the planar O6-hydrogenated radical is different from that assigned to the N7-protonated O6-hydrogenated radical. Furthermore, clear couplings were observed experimentally for N7H. To ensure that differences in the calculated and experimental C8H couplings for the N7-protonated O6-hydrogenated radical do not arise due to differences in the hydrogen bonding environment at N7, a series of calculations were performed where the N7H bond was lengthened. The N1 and O6 hydrogen couplings did not change with variations in the N7H bond length. The C8H couplings (Table 5.16) also do not change substantially over the N7H bond lengths investigated. Alternatively, the N7H anisotropic couplings show a decrease in magnitude with an increase in bond length. Despite the great difference between the C8H couplings in the planar protonated and nonprotonated radicals, neither of these couplings match those assigned to the protonated O6-hydrogenated radical. However, the average of these couplings ($A_{iso}$ = -8.4 G; $T_{ii}$ = -4.8, 0.3, 4.6 G) is in good agreement with the experimental results ($A_{iso}$ = -7.8 G; $T_{ii}$ = -4.0, -0.1, 4.2 G). Moreover, the average calculated N1H couplings ($A_{iso}$ = -2.8 G; $T_{ii}$ = -2.4, -1.1, 3.5 G) are also in agreement with experiment ($A_{iso}$ = -3.4 G; $T_{ii}$ = -2.4, -0.5, 2.9 G). Any discrepancies between experimental and calculated N7H couplings can also be explained in terms of differences in the N7H bond

Table 5.16: Variation in the planar, N7-protonated O6-hydrogenated guanine radical's C8H and N7H HFCCs (G) with respect to the N7H bond length. (Å)

| Bond Length | C8H | | | | N7H | | | |
|---|---|---|---|---|---|---|---|---|
| | $A_{iso}$ | $T_{XX}$ | $T_{YY}$ | $T_{ZZ}$ | $A_{iso}$ | $T_{XX}$ | $T_{YY}$ | $T_{ZZ}$ |
| 0.908 | -13.1 | -7.3 | 0.4 | 6.9 | -3.1 | -2.9 | -1.1 | 4.0 |
| 1.008* | -12.8 | -7.2 | 0.4 | 6.8 | -3.2 | -2.3 | -1.3 | 3.6 |
| 1.108 | -12.8 | -7.1 | 0.4 | 6.7 | -3.2 | -1.9 | -1.4 | 3.3 |
| 1.208 | -12.6 | -7.0 | 0.4 | 6.6 | -3.5 | -1.6 | -1.4 | 3.0 |
| 1.308 | -12.4 | -6.9 | 0.4 | 6.5 | -4.0 | -1.4 | -1.3 | 2.7 |
| unprotonated† | -3.9 | -2.3 | -0.1 | 2.3 | | | | |
| experimental§ | -7.8 | -4.0 | -0.1 | 4.2 | -2.9 | -1.8 | -0.9 | 2.6 |

*The optimized bond length for the planar N7-protonated O6-hydrogenated radical.
†Calculated results for the $C_s$ O6-hydrogenated radical which is not protonated at N7.
§The experimental value was obtained as an average of the results presented in Table 5.14.

length. The experimental N7H HFCCs are in better agreement with the calculations performed at longer bond lengths than those performed at the optimized geometry. Thus, a possible explanation for the observed spectra is a recorded averaging where some of the O6-hydrogenated radicals are protonated at N7 and some exist as nonprotonated species or there exists a transfer between N7H and a neighboring Cl anion.

An additional explanation for the observed couplings is the guanine cation. The average C8H experimental full tensor components (-11.9, -8.0, -3.5 G) and those calculated for the guanine cation (-12.6, -8.8, -3.2 G) are in excellent agreement. In addition the experimentally assigned N1 (-5.9, -3.9, -0.6 G) and N7 (-4.8, -3.8, -0.3 G) tensors in the O6-hydrogenated radical are in excellent agreement with those calculated for the two N2 hydrogens (-5.6, -3.8, 0.1 G) and (-4.3, -3.7, -0.1 G), respectively. Hence, the experimentally assigned N7-protonated O6-hydrogenated radical has HFCCs remarkably similar to those calculated for the guanine cation, which could be formed through net N7 hydrogen removal from the parent molecule.

The only N7-protonated dehydrogenated radical reported experimentally is the N9 centered radical, which was observed in G:HCl:$H_2O$[27] and G:HCl:2$H_2O$.[28] On average the spin density was determined to be 0.19 and 0.08 on N7 and N2, respectively (calculated values: 0.10 and 0.13). Comparison of calculated (Table 5.15) and experimental (Table 5.14) HFCCs for the N9-dehydrogenated radical cation indicates that this radical is unlikely to be responsible for the observed spectrum. The variation in the HFCCs with respect to the N7H bond length for the protonated N9-dehydrogenated radical was investigated to account for differences in the hydrogen bonding scheme to N7 (not shown).[30] The amino and C8 hydrogen couplings do not change appreciably with variations in the N7H bond length. The variations in N7H HFCCs are greater, but the calculated results are still in poor agreement with experiment.

The experimental N7H anisotropic tensor (-3.7, -1.5, 5.1 G) is in much better agreement with that calculated for C8H in the nonprotonated radical (-3.7, -0.7, 4.4 G) than that calculated for N7H in the protonated radical (-2.2, -1.1, 3.3 G). In addition, the two experimental N2H anisotropic couplings (-1.4, -0.5, 1.9 G) and (-1.7, -0.4, 2.1 G) are in excellent agreement with the two N2H couplings calculated for the nonprotonated N9-dehydrogenated radical (-1.5, -0.9, 2.4 G) and (-2.2, -0.6, 2.8 G). The corresponding

anisotropic tensors for the N7-protonated radical are (-2.1, -1.1, 3.2 G) and (-3.1, -0.8, 3.9 G). Although mistaking a C8H coupling for an N7H coupling is highly unlikely, these results indicate that the experimentally assigned N7-protonated N9-dehydrogenated radical resemble couplings calculated for the corresponding nonprotonated radical more closely. No other possibilities can be put forth for the observed radical at this time through comparison of the experimental and calculated couplings.

Two N7-protonated hydroxylated radicals have been observed experimentally which involve net hydroxyl radical addition to C5 and C8. The C8-hydroxylated radical was calculated to be 20.5 kcal/mol lower in energy than the C5 radical. This is very similar to the energetics discussed for the nonprotonated radicals where the difference is 19.0 kcal/mol. The protonated C5-hydroxylated radical was assigned in G:HBr:$H_2O$.[2] The experimental spin density was determined to be 0.13, 0.11 and 0.12 on C8, N7 and N2, respectively, whereas the main components of the calculated spin density are 0.29, 0.12 and 0.37 on C8, C2 and C4, respectively. Clearly, the experimental and calculated spin density distributions are not in agreement. The agreement between experimental (Table 5.14) and calculated (Table 5.15) HFCCs is also poor. In particular, the calculated C8H anisotropic HFCC is approximately 3 G larger than that recorded in experiments and the other couplings also do not correspond.

Other possibilities were discussed for the radical assigned in the experimental study on G:HBr:$H_2O$,[2] including the C5-hydrogenated and N9-dehydrogenated radicals. The C5-hydrogenated radical was concluded to be unlikely since a large C5H coupling would be expected. The C5H HFCCs calculated for the nonprotonated C5-hydrogenated radical (49.5 G) confirmed that this radical is not responsible for the observed spectrum. The possibility that the recorded HFCCs are due to the N7-protonated N9-dehydrogenated radical was also dismissed in the experimental paper since the spectrum was different from that observed in other crystals (Table 5.14). However, since the previous experimental HFCCs for the N7-protonated N9-dehydrogenated radical were in poor agreement with the calculations, comparison of these couplings with those calculated for the N7-protonated N9-dehydrogenated radical is required. The experimental C8H isotropic (-3.7 G) and anisotropic (-1.9, -0.5, 2.4 G) couplings in question are in excellent agreement with the calculated C8H couplings in the N9-

dehydrogenated radical ($A_{iso}$ = -2.9 G; $T_{ii}$ = -1.7, -0.6, 2.3 G). The experimental ($A_{iso}$ = -3.2 G; $T_{ii}$ = -2.4, -1.0, 3.4 G) and calculated N7H couplings in the N9-dehydrogenated radical ($A_{iso}$ = -2.8 G; $T_{ii}$ = -2.2, -1.1, 3.3 G) are also in excellent agreement. Furthermore, both the experimental and the calculated radicals exhibit similar N2H HFCCs. Thus, it can be concluded that the observed radical originally assigned to the C5-hydroxylated radical is more than likely the N9-dehydrogenated radical. It should also be noted that much better agreement is obtained between the calculated N9-dehydrogenated HFCCs and the experimental C5-hydroxylated HFCCs than the experimental "N9-dehydrogenated" couplings discussed previously.

The radical formed by net hydroxyl radical addition to C8 has been observed in single crystals of G:HCl:2$H_2O$.[28] The observed spectrum consists of a large C8H isotropic coupling (20.2 G) and a very small anisotropic tensor (-1.1, -0.6, 1.6 G), which is in excellent agreement with the calculated values ($A_{iso}$ = 17.5 G; $T_{ii}$ = -0.9, -0.5, 1.4 G). Experimentally, another isotropic coupling was observed for N7H (-8.5 G) which also possesses great anisotropy (-6.5, -1.5, 8.0 G). The calculated N7H couplings ($A_{iso}$ = -7.0 G; $T_{ii}$ = -5.9, -1.7, 7.6 G) are in agreement with experiment considering the local environment has been shown to affect these couplings in other radicals (Table 5.16). A small N9H coupling was also noted for this radical (experimental and calculated isotropic HFCCs of -2.2 and -2.1 G, respectively). Experimentally, it was speculated that the observed spectrum could be due to the C8-hydrogenated radical where the additional hydrogen is added to an in-plane position and, thus, only one large C8H coupling is observed. This alternative seems very unlikely due to the excellent agreement between experimental and calculated HFCCs for the C8-hydroxylated radical cation.

One last radical observed experimentally was thought to have a molecular structure very similar to the N7-protonated C8-hydroxylated radical.[2] One experimental coupling was observed and assigned to C8H which has undergone significant reorientation. The proposed radical is the N7-protonated ring-opened radical (Figure 5.3), which was calculated to be 28.8 kcal/mol higher in energy than the corresponding ring-closed radical. The experimental coupling consists of an isotropic (-4.9 G) and an anisotropic (-2.6, 0.1, 2.4 G) C8H coupling. These results are in good agreement with the C8H couplings calculated for this radical ($A_{iso}$ = -4.8 G; $T_{ii}$ = -2.5, -0.5, 3.0 G). In

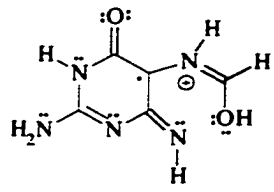

Figure 5.3: Structure of ring-opened, N7-protonated guanine radical cation.

addition to the C8H HFCC, the calculations indicate that couplings should be observed for the hydrogen attached to N9 and possibly N1, N7 and (the hydroxyl oxygen) O8. A more detailed experimental study is required for a definitive identification of this radical.

### *5.3.7 Experimentally Unassigned Guanine Radical*

In a study of 5'dGMP[3] crystals, a spectrum was left unassigned, although many possible radicals were discussed. The unassigned spectrum consists of a C8H coupling ($A_{iso}$ = -7.2 G, $T_{ii}$ = -3.7, -0.3, 4.0 G) and two couplings arising from hydrogens attached to nitrogen atoms. One NH coupling, proposed to be N1H or an amino hydrogen, possesses an isotropic component of -3.4 G and significant anisotropy (-2.6, -0.5, 2.9 G). The second NH coupling was suggested to arise from N2H, N3H or alternatively from a hydrogen atom involved in a hydrogen bond with N7. The couplings from this hydrogen are slightly smaller than those discussed for the first NH ($A_{iso}$ = -3.0 G; $T_{ii}$ = -1.9, -0.5, 2.4 G).

Two deprotonated radicals, formed via hydrogen removal from N1 or N2, were proposed to give rise to the unassigned spectrum. Comparison of the experimental couplings (Table 5.9) and those calculated for the N2-dehydrogenated radical (Table 5.11) indicates that this radical is unlikely to be responsible for the observed spectrum. In particular, only one NH coupling was calculated for this radical, which furthermore is significantly different from those discussed for the unidentified radical. The calculated couplings for the N1-dehydrogenated radical (Table 5.11) match those elucidated in the unassigned spectrum more closely, although the anisotropic couplings disagree more than expected for this component. It is interesting to note that the calculated anisotropic couplings for the N9-dehydrogenated radical are in excellent agreement with those of the unassigned radical. However, this radical is not expected in guanosine crystals since a sugar group replaces the hydrogen at N9.

The guanine cation was also proposed to have a spectrum similar to that unassigned experimentally and the calculated HFCCs (Table 5.10) support the hypothesis that the unassigned spectrum is similar to this radical. The calculated NH anisotropic couplings are in remarkable agreement with those obtained experimentally, whereas the calculated C8H anisotropic coupling is slightly larger than the recorded value. The guanine cation was not seriously considered to be responsible for the observed spectrum since it is unlikely that this radical would be observed at 200 K. The unassigned spectrum was also speculated to arise from an N7-protonated O6-hydrogenated radical.[3] The calculations (Table 5.15) yield different HFCCs than those obtained experimentally for both the planar and nonplanar geometries. However, the couplings extracted from the unassigned spectrum are very similar to the average of the protonated and nonprotonated O6-hydrogenated couplings discussed in the preceding section. This possibility offers the best explanation of the unassigned couplings to date.

Hole *et al.*[3] commented on the similarity of the unassigned spectra to that obtained for both the guanine anion and cation. In particular, they discussed the mandatory care required when interpreting the resonance patterns of the irradiated DNA bases, even for those spectra obtained from the sophisticated ENDOR technique. The calculations support their comments since many of the calculated HFCCs for the radiation products are very similar. Thus, even through the use of high-level calculations, interpretation of the observed spectra is very difficult. This example illustrates the great difficulties associated with the determination of DNA radiation products, even when the problem is reduced to examining the individual bases.

### *5.3.8 Summary of Guanine Results*

Disagreement between theoretical and experimental couplings for the guanine anion was exhibited which was improved upon through consideration of a planar radical. The calculated couplings for a planar O6-hydrogenated radical also match the experimental results. Only one coupling tensor was extracted in the experimental study and, thus, for positive identification of the observed radical more experimental couplings are required. In particular, the calculations indicate that the anion and its O6-protonated form can be distinguished through the identification of the amino hydrogen HFCCs.

Similarly, the couplings assigned to the guanine cation and the calculated couplings were not in good agreement.

The N9-dehydrogenated radical was determined to be the lowest energy radical in this class and the corresponding N1 and N2 radicals are very close in energy. Only the N2-dehydrogenated radical has been observed experimentally and the calculated HFCCs are in excellent agreement with experimental values. The C8 and C5-hydrogenated radicals are the lowest and highest energy radicals in their class. Both of these radicals have been observed experimentally and the calculations support their assignment. The C8-hydroxylated radical is the lowest energy radical formed via net hydroxyl radical addition. The couplings assigned to the C4-hydroxylated radical experimentally are in fair agreement with the calculated values if the principal components are considered. An alternate explanation for these observed couplings can be sought in the formation of the N2-dehydrogenated radical.

The good agreement obtained between theory and experiment for the nonprotonated radicals is not immediately transferable to the N7-protonated guanine radicals investigated in the present study. Among the protonated radicals, only the experimental assignment of the C8-hydrogenated and C8-hydroxylated radicals is supported by the calculations. The spectrum experimentally assigned to the protonated O6-hydrogenated radical was speculated to arise from an averaging of the planar forms of the protonated and nonprotonated O6-hydrogenated radicals. In addition, it was also noted that the spectrum experimentally assigned to the N7-protonated O6-hydrogenated radical contains HFCCs very similar to the guanine cation. The protonated N9-dehydrogenated radical was concluded to be unlikely responsible for the observed spectrum assigned experimentally to this radical. The only radical possessing couplings similar to those observed experimentally is the nonprotonated N9-dehydrogenated radical. No other possible product could be identified as leading to the experimental HFCCs. In addition, the observed HFCCs thought to arise from the C5-hydroxylated radical were determined to originate from an other guanine radical, most probably the N7-protonated N9-dehydrogenated radical. It was concluded that more experimental, as well as theoretical, studies are required for the full identification of N7-protonated radicals generated upon irradiation of guanine derivatives. It should be noted that no

environmental effects were included in the present study, which offers a possible explanation for discrepancies between theory and experiment.

Through comparison of experimental and calculated hyperfine coupling constants, it can be determined that the N2-dehydrogenated radical is the major dehydrogenated product formed in neutral guanine crystals. Formation of this radical produces a supply of hydrogen atoms which will add primarily to C5 and C8. In N7-protonated guanine crystals, the primary radiation products elucidated through comparison of experimental and calculated HFCCs are the C8-hydrogenated and C8-hydroxylated radicals. The identification of all other radicals is speculative. In addition, the O6-hydrogenated radical may be formed where the observed spectra exists as an average of that due to the protonated and nonprotonated radicals. Contrary to adenine, there exist differences in radical formation when N7-protonated crystals are considered. In particular, no dehydrogenated radicals were characterized in the protonated crystals. Thus, questions regarding how the hydrogen atoms are generated to form net hydrogenated radicals arise. However, all protonated crystals examined were hydrate derivatives. Thus, the most likely mechanism for damage in these hydrate crystals involves water, where net hydrogen atom and net hydroxyl radical addition occurs at C8 in guanine. The formation of the C8-hydroxylated radical in hydrate crystals of guanine derivatives provides further support for the proposed mechanism for damage in cytosine monohydrate crystals in Chapter Four.

### *5.4 Conclusions*

Similar to the thymine results discussed in Chapter Four, the calculated and experimental couplings obtained in adenine radicals are in very good agreement. The calculations indicate that the cation has been observed, but only in initially protonated crystals. In some instances, the calculated results were initially in poor agreement with experiment. However, upon consideration of crystal effects, improved results were obtained. For example, the calculated couplings in the N3-hydrogenated radical were different from the experimental results since a severely distorted radical was optimized. Once the extensive hydrogen bonding schemes in the crystals, which result in planar radicals, were taken into account, the calculated HFCCs were in much better agreement

with experimental results. Similar to the thymine C6-hydrogenated radical, the isotropic HFCCs in the C2 and C8-hydrogenated radicals were calculated to be of equal magnitude, while the radicals are slightly distorted at these positions in the experiments. The only radical assignment not supported by the calculations is the protonated C4-hydrogenated coupling. Experimentally, a small isotropic coupling was assigned to C4H in this radical, but the calculations indicate that this hydrogen should possess a large coupling. Consideration of the magnitude of the couplings obtained in other base derivatives when hydrogen is added perpendicular to the molecular plane supports the conclusions drawn from the calculations that the observed radical was misidentified.

The calculations on the guanine anion and cation indicate that the experimental assignment of these radicals is questionable. Alternatively, the calculations support the experimental assignment of all dehydrogenated and hydrogenated radicals identified in nonprotonated crystals. The C4-hydroxylated radical was identified in one experimental study, but the extracted couplings are only in fair agreement with the calculations indicating further studies are required to identify this radical. The identification of the C8-hydrogenated and hydroxylated radicals in protonated crystals was also supported by the calculations. The assignment of the O6-hydrogenated radical in protonated crystals can be defended by the calculations if an averaging between protonated and nonprotonated radicals is considered. However, the assignment of the other radicals in protonated crystals can be questioned through comparison to the calculations. In particular, the results for the N9-dehydrogenated and C5-hydroxylated radicals are in poor agreement. The couplings in these radicals were similar to the nonprotonated and protonated N9-dehydrogenated radicals, respectively. Complete assignment of these radicals is not possible without the resolution of more experimental HFCCs.

Through comparison of the calculated and experimental HFCCs the identity of one radical in each of adenine and guanine derivatives was assigned to a net hydroxyl radical addition product. In particular, the calculations support the experimental assignment of the C4 and C8-hydroxylated radicals in frozen aqueous solutions of deoxyadenosine 5'-monophosphate and crystals of guanine hydrochloride dihydrate. If the full coupling tensors are considered then the calculations also support the experimental assignment of the C4-hydroxylated radical in crystals of guanosine 3',5'-

cyclic monophosphate. These conclusions support the hypothesis put forth in Chapter Four that net hydroxyl addition to the cytosine base may occur in cytosine monohydrate crystals. The reactions of water with cytosine, as well as uracil and thymine, will be considered in Chapter Seven.

### *5.5 References*


1. Nelson, W. H.; Sagstuen, E.; Hole, E. O.; Close, D. M. *Radiat. Res.* **1998**, *149*, 75.
2. Hole, E. O.; Sagstuen, E.; Nelson, W. H.; Close, D. M. *Radiat. Res.* **1991**, *125*, 119.
3. Hole, E. O.; Nelson, W. H.; Sagstuen, E.; Close, D. M. *Radiat. Res.* **1992**, *129*, 119.
4. Close, D. M. *Radiat. Res.* **1993**, *135*, 1.
5. Hole, E. O.; Sagstuen, E.; Nelson, W. H.; Close, D. M. *Radiat. Res.* **1995**, *144*, 258.
6. Close, D. M.; Nelson, W. H.; Sagstuen, E.; Hole, E. O. *Radiat. Res.* **1994**, *137*, 300.
7. Lichter, J. J.; Gordy, W. *Proc. Natl. Acad. Sci., USA* **1968**, *60*, 450.
8. Zehner, H.; Flossmann, W.; Westhof, E. *Z. Naturforsch.* **1976**, *31C*, 225.
9. Zehner, H.; Westhof, E.; Flossmann, W.; Müller, A. *Z. Naturforsch.* **1977**, *32C*, 1.
10. Close, D. M.; Nelson, W. H. *Radiat. Res.* **1989**, *117*, 367.
11. Kar, L.; Bernhard, W. A. *Radiat. Res.* **1983**, *93*, 232.
12. Nelson, W. H.; Sagstuen, E.; Hole, E. O.; Close, D. M. *Radiat. Res.* **1992**, *131*, 272.
13. Colson, A.-O.; Sevilla, M. D. *Int. J. Radiat. Biol.* **1995**, *67*, 627.
14. Sevilla, M. D.; Besler, B.; Colson, A. O. *J. Phys. Chem.* **1995**, *99*, 1060.
15. Orlov, V. M.; Smirnov, A. N.; Varshavsky, Y. M. *Tet. Lett.* **1976**, *48*, 4377.
16. Colson, A.-O.; Sevilla, M. D. *J. Phys. Chem.* **1996**, *100*, 4420.
17. Hole, E. O.; Sagstuen, E.; Nelson, W. H.; Close, D. M. *Radiat. Res.* **1992**, *129*, 1.
18. Wetmore, S. D.; Boyd, R. J.; Eriksson, L. A. *J. Phys. Chem. B* **1998**, *102*, 10602.

19. Gregoli, S.; Olast, M.; Bertinchamps, A. *Radiat. Res.* **1974**, *60*, 388.

20. Box, H. C.; Budzinski, E. E. *J. Chem. Phys.* **1976**, *64*, 1593.

21. Sagstuen, E.; Hole, E. O.; Nelson, W. H.; Close, D. M. *Radiat. Res.* **1996**, *146*, 425.

22. Hole, E. O.; Nelson, W. H.; Close, D. M.; Sagstuen, E. *J. Chem. Phys.* **1987**, *86*, 5218.

23. Hole, E. O.; Sagstuen, E. *Radiat. Res.* **1987**, *109*, 190.

24. Kim, H.; Budzinski, E. E.; Box, H. C. *J. Chem. Phys.* **1989**, *90*, 1448.

25. Close, D. M.; Sagstuen, E.; Nelson, W. H. *J. Chem. Phys.* **1985**, *82*, 4386.

26. Close, D. M.; Nelson, W. H.; Sagstuen, E. *Radiat. Res.* **1987**, *112*, 283.

27. Close, D. M.; Sagstuen, E.; Nelson, W. H. *Radiat. Res.* **1988**, *116*, 379.

28. Nelson, W. H.; Hole, E. O.; Sagstuen, E.; Close, D. M. *Int. J. Radiat. Biol.* **1988**, *54*, 963.

29. Sagstuen, E.; Hole, E. O.; Nelson, W. H.; Close, D. M. *Radiat. Res.* **1988**, *116*, 196.

30. Wetmore, S. D.; Boyd, R. J.; Eriksson, L. A. *J. Phys. Chem. B* **1998**, *102*, 9332.

# *CHAPTER SIX*

# Sugar Radicals in Irradiated DNA Components

## *6.1 Introduction*

The formation of sugar radicals in irradiated DNA is of great interest since it is widely accepted that single-strand breaks occur via these intermediates.[1,2] Sugar radicals can be formed through direct mechanisms, in which alkoxyl or base radicals are formed and radical character is transferred to the sugar group, and indirect mechanisms, where hydrogen or hydroxyl radicals generated from water radiolysis attack the sugar group. In an important study of D-glucose, Schuchmann and von Sonntag[3] concluded that hydroxyl radicals attack the six carbon atoms in this sugar to an equal extent. However, ESR techniques have been unable to detect sugar radicals in irradiated DNA.[4] As mentioned in Chapter One, Hole *et al.*[5] were the first to observe a large variety of sugar radicals in their ENDOR study of 2'-deoxyguanosine 5'-monophosphate, where nine sugar radicals were characterized. This provides a nice example of the power of the ENDOR technique since ESR did not easily detect these radicals. A subsequent ENDOR study of single crystals of deoxyadenosine[6] supported the hypothesis that many sugar radicals are generated upon irradiation.

Theoretical investigations of carbon-centered sugar radicals have appeared in the literature.[7,8] In these studies, geometries, relative energies, spin density distributions and hyperfine coupling constants were calculated at the HF level. Both studies were very complete and carefully performed at the level of theory chosen. However, as discussed in Chapter Two, Hartree-Fock overestimates the hyperfine coupling constants considerably and electron correlation yields important contributions to this property.

It is of interest to calculate the HFCCs of possible radicals in the DNA sugar moiety in order to assign the experimental spectra to specific radicals with confidence. Once the radicals formed in single crystals are fully characterized, experimentalists will have a better understanding of how to recognize these radicals in full DNA and be able to answer an important question, namely whether sugar radicals are formed upon irradiation of DNA.[4]

The structure and standard atomic numbering of a DNA nucleotide unit is presented in Figure 6.1 (structure I). Due to the number of atoms involved in the nucleotides, a model system must be used. The model chosen represents phosphate groups with hydroxyl groups and the DNA base with an amino group (Figure 6.1, structure II). From previous studies it is known that in order to correctly describe ring puckering an amino group must be present at C1', although geometrical effects generated by replacing the amino group with cytosine are small.[8] The use of hydroxyl groups rather than phosphate groups in the chemical model may also lead to some geometrical differences, although these will not be discussed in the present work. The model sugar used within differs from those previously employed by the inclusion of a hydroxyl group at the C5' position[7] and phosphate groups have been implemented in the past rather than hydroxyl groups.[8]

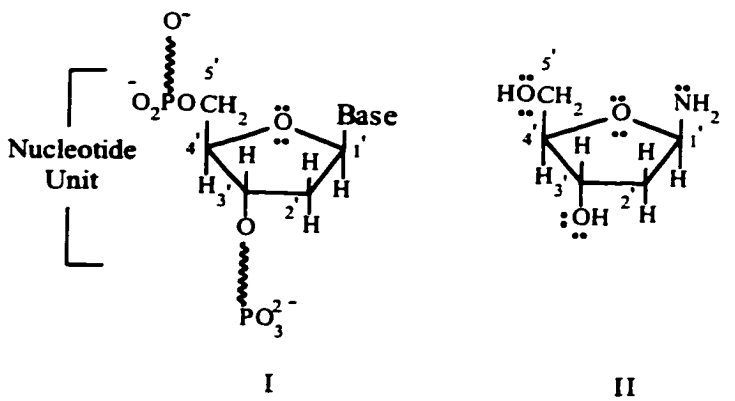


Figure 6.1: Structure and numbering of the sugar group present in DNA (I) and the model system used for the calculations presented herein (II).

In the present chapter, the geometry and HFCCs of possible sugar radicals generated through irradiation of DNA are examined with density-functional theory. The sugar radicals to be contemplated include hydrogen abstraction radicals formed by removal of hydrogen from all carbon and oxygen atoms, radicals formed via removal of either of the hydroxyl groups in the model system, as well as a variety of radicals which lead to significant sugar ring alterations. Computational techniques applied to these systems are identical to those previously discussed for the DNA bases in Chapter Four and a discussion of the methods employed will not be repeated here.

### *6.2 Background Discussion of Sugar Radical Properties*

Two different puckering modes were examined for each possible radical corresponding to north (N) and south (S) radicals, which are defined according to where the radical is located on the pseudorotation cycle.[9] It is convenient to analyze the puckering amplitudes in the sugar molecules through the use of the pseudorotational phase angle[9] defined as

$$\tan P = \frac{(\upsilon_4 + \upsilon_1) - (\upsilon_3 + \upsilon_0)}{2\upsilon_2 (\sin 36^\circ + \sin 72^\circ)} \tag{6.1}$$

where the $\upsilon_j$ are the ring dihedral angles: $\upsilon_0$ = C4'O1'C1'C2', $\upsilon_1$ = O1'C1'C2'C3', $\upsilon_2$ = C1'C2'C3'C4', $\upsilon_3$ = C2'C3'C4'O1', and $\upsilon_4$ = C3'C4'O1'C1'. The puckering amplitude[7] ($\tau_m$), which is defined as

$$\tau_m^2 = \frac{2}{5}\sum_{j=0}^{4}\upsilon_j^2 \tag{6.2}$$

is also a useful parameter to indicate the degree of puckering in the sugar ring where a low value of $\tau_m$ indicates a relatively flat ring. Figure 6.2 depicts the pseudorotation cycle and the relation of $P$ to this cycle.[9]

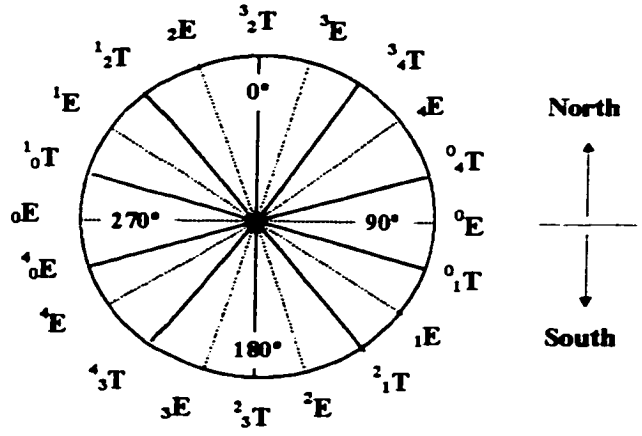


Figure 6.2: The pseudorotation cycle for deoxyribose depicting the pseudorotational phase angle, the puckering modes and the location of the north and south conformers.

The puckering in the sugar molecules can be considered to be either an envelope (E) form, where four atoms define a plane and the fifth atom is located out of this plane, or a twist (T) form, where three atoms define a plane and the other two atoms are displaced on opposite sides of this plane.[9] Displaced atoms are categorized as *endo* or

*exo* according to whether they are located on the same side or opposite side of C5', respectively. A superscript (subscript) on the left side of the puckering symbol (E or T) is used to represent *endo* (*exo*) puckering. For example, the C3'-*endo* and C2'-*endo* forms which are observed in nonradical sugar molecules in A-DNA and B-DNA are both envelope conformations and can be represented as $^{3}E$ and $^{2}E$, respectively. Pictorial descriptions of sugar ring distortion are displayed in Figure 6.3. In general, E or T can only approximately describe sugar ring puckering and intermediate levels of the twist mode can be obtained. Intermediate twist modes correspond to the area between divisions on the pseudorotation cycle and, thus, this cycle depicts all possible puckering amplitudes for the sugar group.

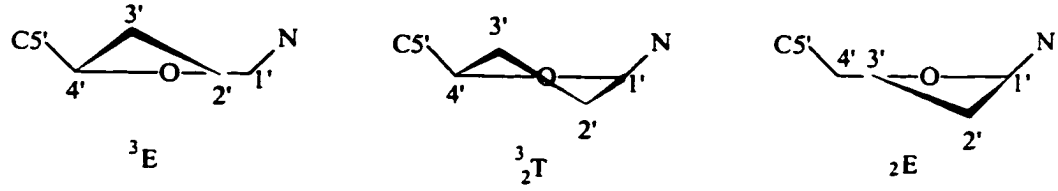


Figure 6.3: Examples of the puckering modes exhibited in the DNA sugar group: $^{3}E$ represents C3' *endo* puckering, $^{3}_{2}T$ represents a twist conformation and $_{2}E$ represents C2' *exo* puckering.

### *6.3 Energetics and Geometrical Parameters*

The relative energies of the hydrogen abstraction sugar radicals are displayed in Table 6.1. From the results it can be seen that the C4'(S) and C2'(S) radicals are the lowest and highest energy radicals among those formed by hydrogen abstraction from a carbon, respectively. The north and south type conformers for each of the C1', C2', C3' and C5' radicals are energetically separated by less than 2 kcal/mol. A larger difference is observed for the C4' pair, where the north conformer is 3.3 kcal/mol higher in energy than the south counterpart. Alkoxyl radicals, formed via hydrogen removal from a hydroxyl group in the model sugar, are very high in energy lying on average 10.2 and 12.9 kcal/mol above the C4'(S) radical for the O3' and O5' hydrogen abstraction radicals, respectively. Radicals formed through removal of a hydroxyl radical in the model system correspond to breakage of a phosphoester bond in DNA. The C3' centered radical is approximately 3.5 kcal/mol lower in energy than the corresponding C5' radical, identifying this as a possible site for strand-breaks in DNA.

Table 6.1: Relative energies (kcal/mol), puckering mode, pseudorotational phase angle (deg.) and puckering amplitude ($\tau_m$) of hydrogen and hydroxyl abstraction sugar radicals.

| Radical | R. Energy +ZPE | R. Energy | P | $\tau_m$ |
|---|---|---|---|---|
| | Hydrogen Removal Radicals | | | |
| C4'(S) | 0.0 | 0.0 | $^{2}_{1}T$ | 135.3 | 31.9 |
| C5'(N) | 1.4 | 1.6 | $^{1}_{0}T$ | -64.3 | 35.9 |
| C3'(S) | 1.8 | 2.3 | $^{0}E$ | 103.0 | 33.0 |
| C1'(S) | 2.3 | 3.1 | $^{2}E$ | 163.9 | 30.8 |
| C1'(N) | 2.3 | 3.2 | $^{4}E$ | 58.7 | 35.7 |
| C3'(N) | 2.5 | 2.8 | $_{2}E$ | -32.4 | 31.1 |
| C5'(S) | 3.0 | 3.2 | $^{2}_{3}T$ | 174.4 | 37.6 |
| C4'(N) | 3.3 | 4.1 | $_{2}E$ | -13.1 | 27.3 |
| C2'(N) | 8.3 | 9.5 | $^{3}_{2}T$ | -1.4 | 33.5 |
| C2'(S) | 8.7 | 9.7 | $_{3}E$ | 206.4 | 23.7 |
| O3'(S) | 10.2 | 10.4 | $^{2}E$ | 152.1 | 38.1 |
| O3'(N)* | | 12.2 | $^{3}E$ | 29.1 | 42.3 |
| O5'(N) | 12.9 | 13.9 | $^{3}_{4}T$ | 42.1 | 38.3 |
| O5'(S) | 12.9 | 14.1 | $^{2}_{1}T$ | 141.0 | 34.3 |
| | Hydroxyl Removal Radicals | | | |
| C3'(S) | 0 | 0 | $_{1}E$ | 113.5 | 30.0 |
| C3'(N) | 0.7 | 0.5 | $^{1}_{2}T$ | -46.0 | 28.1 |
| C5'(S) | 3.2 | 4.1 | $^{2}E$ | 154.2 | 39.3 |
| C5'(N) | 3.7 | 4.5 | $^{3}_{4}T$ | 45.5 | 41.4 |

*The MP2 geometry was used for single-point calculations (see text for further details).

The lowest energy product determined differs from that reported when HF geometries were obtained and energetic studies performed with higher-level single-point calculations.[7,8] However, all products were reported to have small relative energies and the C2' carbon centered radicals were determined to be the highest lying products. Due to the relatively small stabilization energy of one radical over another, it is not surprising that differences arise in the results once electron correlation is included in the geometry optimizations and slight modifications in the model systems are implemented. Furthermore, in the previous studies it is not clear whether corrections were made for the zero-point vibrational energy. Table 6.1 indicates that when the ZPE is not taken into account, the magnitude of the energy difference between radicals increases and the relative order of the radicals may change. For example, without ZPE the C3'(S) radical is lower in energy than the two C1' radicals, but inclusion of the ZPE indicates that the C1' radicals are lower in energy.

The sugar puckering modes for C2'(N), C2'(S) and C4'(S) hydrogen abstraction radicals differ from those obtained in a previous study.[7,8] On the contrary, the puckering

modes for the C1', C3' and C4'(N) radicals and the magnitude of the pseudorotational phase angle are in good agreement with previous work. Miaskiewicz and Osman[7] assigned the C3' radical with $P$ = 84.4° to a south type $^0$E envelope form. From the results in Table 6.1, it can be seen that this radical indeed possess an $^0$E form with $P$ = 103.3°. C2'(S) and C5'(S) have the smallest and largest $\tau_m$ values (Table 6.1). These results are in agreement with previous studies,[8] which used phosphate rather than hydroxyl groups, indicating that only small effects are generated by using hydroxyl groups in the model system. It has been suggested that the relatively flat structure for the C2' radicals occurs since an oxygen atom is not present next to the radical center. The other carbon centered radicals with oxygen next to the radical site are more pyramidal due to interactions between the lone pairs and the unpaired electron.[7] The net C3' hydroxyl abstraction radicals have lower puckering amplitudes relative to the similar C5' radicals and are nearly planar in structure. This indicates that the C3' center is $sp^2$ hybridized after radical formation.

For all hydrogen and hydroxyl abstraction radicals, the major geometrical alterations that occur upon radical formation involve the bonds and angles in which the radical center is involved.[10] The bonds between the radical center and surrounding atoms are generally contracted between 0.04 and 0.07 Å. The bond angle in which the radical center is the central atom changes between 2 and 8°. The remainder of the sugar ring geometry is relatively unaffected. This is in agreement with results obtained at the HF level.[7]

### *6.4 Hyperfine Coupling Constants*

#### *6.4.1 Dehydrogenated Carbon Centered Radicals*

It has been argued in the past that all sugar radicals can be generated from alkoxyl radicals and, thus, no sugar radicals can be formed in DNA due to the lack of hydroxyl groups.[11] However, due to the number of sugar radicals generated in 5'dGMP,[5] which contains only one hydroxyl group, it was suggested that other mechanisms for the formation of these radicals must be considered. For example, carbon centered radicals have been proposed to be formed via hydrogen abstraction by hydroxyl or hydrogen

radicals. In addition, it has been suggested that carbon centered radicals can possibly be formed through excitation followed by homolytic cleavage of CH bonds.[5] Experimental HFCCs for dehydrogenated carbon centered radicals are displayed in Table 6.2.

Table 6.2: Experimental HFCCs (G) for sugar radicals generated through hydrogen abstraction from a ring carbon.

| Radical | Molecule | Atom | $A_{iso}$ | $T_{XX}$ | $T_{YY}$ | $T_{ZZ}$ |
|---|---|---|---|---|---|---|
| C1' | 5'dGMP[5] | "C2'H" | 28.0 | -2.1 | -1.8 | 3.9 |
| | | "C2'H" | 16.1 | | | |
| | rA:HCl[12] | "C2'H" | 25.8 | -1.8 | -0.5 | 2.3 |
| | dAm[6] | "C2'H" | 17.2 | -1.9 | -1.7 | 3.6 |
| | | "C2'H" | 25.4 | -1.7 | -0.7 | 2.3 |
| | 5'CMP[13] | "C2'H" | 19.6 | -1.4 | -0.8 | 2.2 |
| | | "C2'H" | 19.6 | -2.0 | -1.4 | 3.3 |
| C2' | 5'dGMP[5] | "C2'H" | -23.1 | -12.2 | 1.0 | 11.1 |
| | | "C1'H" | 32.4 | -2.1 | -0.3 | 2.4 |
| C3' | 5'dGMP[5] | "C2'H" | 16.7 | -1.6 | -0.9 | 2.5 |
| | | "C2'H" | 38.1 | -2.1 | -1.4 | 3.4 |
| | | "C4'H" | 27.5 | -1.7 | -0.9 | 2.7 |
| | | unassigned* | | (16) | (~22) | (29) |
| C4' | 5'UMP[14] | "βH" | 36 ± 2 | | | |
| | | "βH" | 25 ± 3 | | | |
| | | "βH" | 24 ± 3 | | | |
| | rI[15] | "C3'H" | 34.7 | | | |
| | | "C5'H" | 33.4 | | | |
| | | "C5'H" | 3.4 | | | |
| | rA:5BrU[16] | "C3'H" | 21.0 | | | |
| | | "C5'H" | 10.0 | | | |
| C5' | 5'dGMP[5] | "C5'H" | -22.2 | -8.7 | 0.8 | 7.9 |
| | | "C5'H" | -20.9 | -8.6 | 0.6 | 8.0 |
| | | "C5'H" | -20.8 | -8.8 | 0.8 | 8.0 |
| | | "C5'H" | -19.6 | -8.7 | 0.5 | 8.2 |
| | | "C4'H" | 2.5 | | | |
| | | "O5'H"* | | (16.3) | (20.2) | (28.1) |
| | dA[17] | "C5'H" | -14.7 | -7.9 | -1.7 | 9.7 |
| | | "C4'H" | 7.0±1 | | | |
| | dAm[6] | "C5'H" | -17.5 | -11.8 | 0.8 | 11.0 |
| | 3'CMP[13] | "C5'H" | -22.7 | -9.3 | 0.7 | 8.5 |
| | | "C4'H" | 4.5 | -3.0 | 0.1 | 3.0 |
| | | "O5H" | 20.8 | -4.3 | -1.5 | 5.8 |
| | 5Cl and | "C5'H" | -20.7 | -12.5 | 2.9 | 9.6 |
| | 5BrdU[13] | "O5'H" | 8.6 | -3.1 | -1.0 | 4.2 |
| | | "C4'H" | 18.9 | -1.6 | -0.2 | 1.9 |

*Principal tensor components.

The couplings present in the spectra of a number of irradiated DNA molecules have been assigned to the C1' radical.[5,6,12,13] In addition to hydrogen abstraction and CH bond cleavage resulting from excitation, another mechanism for radical formation is deprotonation of a parent sugar radical cation at the C1' position. This mechanism was

suggested for the corresponding C4' radical.[14] In particular, it was proposed that if the electron vacancy is primarily located on O1', then the positively charged radical is most likely stabilized through deprotonation at positions close to O1' (i.e., C4' or C1').

Hole *et al.*[5] determined that the $\pi$-spin density at C1' is 0.64, which is smaller than the calculated value (0.75). Comparison of experimental (Table 6.2) and theoretical (Table 6.3) HFCCs indicates that the calculations support the experimental assignment of the C1' radical. In particular, the experimental results agree more closely with those calculated for the N-type radical. One of the C2'H couplings calculated for the S-type C1' radical is significantly smaller (9.1 G) than the experimental results (approximately 18 G). This is a nice example of the effects of the puckering amplitude on the HFCCs. It should be noted that although the C2'H isotropic components differ between N and S-type radicals, the anisotropic values are almost identical.

Table 6.3: Calculated HFCCs (G) for dehydrogenated sugar radicals.

| | | North | | | | South | | | |
|---|---|---|---|---|---|---|---|---|---|
| Radical | Atom | $A_{iso}$ | $T_{XX}$ | $T_{YY}$ | $T_{ZZ}$ | $A_{iso}$ | $T_{XX}$ | $T_{YY}$ | $T_{ZZ}$ |
| C1' | C2'H | 18.5 | -1.4 | -1.0 | 2.4 | 29.3 | -1.4 | -1.1 | 2.5 |
| | C2'H | 22.7 | -1.9 | -1.6 | 3.4 | 9.1 | -1.9 | -1.4 | 3.3 |
| C2' | C2'H | -21.3 | -13.1 | -0.2 | 13.4 | -20.7 | -13.0 | -0.2 | 13.3 |
| | C1'H | 30.9 | -2.0 | -1.0 | 3.0 | 31.6 | -1.9 | -0.9 | 2.9 |
| | C3'H | 38.2 | -2.3 | -0.9 | 3.2 | 7.9 | -2.2 | -1.0 | 3.2 |
| | O3'H | 1.9 | -1.4 | -0.6 | 2.0 | -2.4 | -3.5 | -0.5 | 4.0 |
| C3' | C2'H | 18.9 | -1.7 | -1.5 | 3.2 | 12.4 | -1.6 | -1.1 | 2.7 |
| | C2'H | 34.0 | -1.5 | -1.1 | 2.6 | 31.2 | -1.9 | -1.5 | 3.5 |
| | O3'H | -2.8 | -4.3 | -3.1 | 7.4 | -2.3 | -4.5 | -3.3 | 7.7 |
| | C4'H | 22.5 | -1.6 | -1.3 | 2.8 | | | | |
| C4' | C5'H | 27.9 | -1.8 | -1.1 | 2.8 | | | | |
| | C5'H | 2.8 | -2.1 | -1.4 | 3.5 | 6.2 | -2.4 | -1.1 | 3.5 |
| | C4'H | 22.1 | -1.8 | -1.1 | 2.8 | 31.4 | -1.9 | -1.2 | 3.2 |
| | O5'H | | | | | 5.6 | -1.6 | -0.8 | 2.5 |
| C5' | C5'H | -9.4 | -11.2 | -0.8 | 12.0 | -10.4 | -10.9 | -0.7 | 11.7 |
| | C4'H | 33.6 | -1.7 | -0.8 | 2.5 | 35.3 | -1.6 | -0.8 | 2.4 |
| | O5'H | -4.3 | -5.1 | -3.4 | 8.5 | -3.9 | -5.0 | -3.3 | 8.3 |
| O5' | C5'H | 20.4 | -2.6 | -1.6 | 4.1 | 17.5 | -2.5 | -1.5 | 4.0 |
| | C5'H | 92.5 | -3.2 | -1.4 | 4.6 | 90.3 | -3.1 | -1.5 | 4.5 |
| | C1'H | 4.8 | -0.3 | -0.2 | 0.5 | 2.1 | -0.3 | -0.3 | 0.6 |
| O3' | C3'H | 3.2* | -2.1 | -1.5 | 3.6 | 12.5 | -2.0 | -1.7 | 3.7 |
| | C1'H | 5.9 | -0.7 | -0.3 | 1.0 | 2.7 | -1.0 | -0.7 | 1.7 |

*MP2 geometry was used in single-point calculations (see text for further details).

The C2' hydrogen abstraction radical has appeared in experimental studies only as a minor product,[5] which is not surprising since it was predicted to be the highest energy radical among carbon hydrogen abstraction adducts. From the experimental study, an $sp^2$

configuration at the C2' center was suggested, which would involve rehybridization at this position upon radical formation and explain the relatively flat structure of this species. An experimental spin density of 0.89 was obtained for C2' (calculated value: 0.96). The experimental HFCCs for the C2' radical are in qualitative agreement with the calculated values. The C2'H HFCC exhibits a great deal of anisotropy in the experimental results which is supported by the calculations. The C2'(S) and C2'(N) calculated HFCCs differ mainly in the C3'H coupling since a larger isotropic HFCC was obtained for the north conformer (38.2 G) relative to the south conformer (7.9 G). Experimentally, no C3'H coupling was detected, and thus the radical observed in the experiment is most likely to be in a south conformation.

The C3' dehydrogenated radical was observed in an investigation of irradiated 5'dGMP and the results indicated that C3' remains $sp^3$ hybridized rather than rehybridizing as discussed for the C2' radical.[5] Through comparison of the two calculated C2'H couplings in the N and S-type conformers with experimental results, the nature of the observed radical is difficult to predict. However, the calculated HFCCs for the N and S-type C3' radicals differ through the absence of a C4'H coupling in the latter conformation. Since a large C4'H coupling was recorded experimentally, the calculations predict this radical to be present in the north conformation. The calculated values indicate that O3'H has a small isotropic coupling and a relatively large anisotropic contribution which were not detected in the experimental study. However, experimentally there was another coupling observed for which only the principal components were resolved and assignment to a particular atom was not made. The unassigned couplings are not unlike those of a C2' hydrogen and could possibly be due to a C2'H in a ring with another conformation. The difference between the experimental and the calculated isotropic hyperfine coupling constants in this radical could be due to the presence of a phosphate group at the C5' position in the experimental study since it has been previously determined that the phosphate groups affect the HFCCs in the C3' radical.[8]

Radicals formed through hydrogen abstraction from the C4' position have been observed in three different crystals: uridine 5'-monophosphate (5'rUMP),[14] inosine (rI,

which can be derived from adenosine by replacing the amino group at C6 with a hydroxyl group)[15] and adenosine:5-bromouracil (rA:5BrU).[16] As previously discussed, the net C4' hydrogen abstraction radical can be formed via deprotonation of the parent sugar radical cation. Alternatively, it could arise through abstraction of a hydrogen at C5' followed by a 4',5'-hydrogen atom transfer. The C4'(N) radical exhibits two C5'H couplings, one of substantial magnitude (27.9 G), and no O5'H coupling, while the south conformer has a significant O5'H coupling (5.6 G) and only one small C5'H coupling (6.2 G). Experimentally, three substantial couplings of 36, 25 and 24 G were recovered in crystals of 5'rUMP,[14] and two small couplings were observed at certain orientations for which accurate HFCCs could not be evaluated. In rI,[15] large C3'H (34.7 G) and C5'H (33.4 G), as well as a small C5'H (3.4 G), couplings were obtained. In rA:5BrU, two couplings were resolved corresponding to the C3' and C5' hydrogens (21.0 and 10.0 G, respectively). Overall poor agreement between theoretical and experimental HFCCs for this radical indicates that either better data must be obtained or other radical possibilities must be considered. In particular, no anisotropic components, which are important for comparison to theoretical work, were isolated. Differences between theory and experiment could arise due to alterations experienced when phosphates groups replace the hydroxyl model group.[8]

The C5' hydrogen abstraction radical has been assigned in studies of various DNA constituents,[5,6,13,17] and differing results have been obtained for the HFCCs. In some cases, ring-breaking or ring-opened radicals were believed to be present rather than this carbon centered radical.[18] Early studies which identified the C5' radical include experiments performed on cytosine 3'-monophosphate (3'CMP), 5-chlorodeoxyuridine (5CldU) and 5-bromodeoxyuridine (5BrdU).[13] The C5'H isotropic HFCCs obtained in these studies are similar while the anisotropic C5'H components and the C4'H and O5'H HFCCs depend on the crystal examined. Hole *et al.*[5] assigned four parallel lines in the spectrum of irradiated 5'dGMP to C5' hydrogens in different conformers of the C5' hydrogen abstraction radical. The magnitude of the isotropic C5'H coupling agrees with those obtained in earlier studies, but once again the C5'H anisotropic, C4'H and O5'H HFCCs differ from those discussed above. The same group observed evidence of the

formation of this radical in irradiated dAm.[6] From Table 6.2, it is evident that the C5'H isotropic coupling recovered in dAm agrees well with those previously discussed, but the anisotropic components resemble those obtained in earlier studies rather than those obtained in 5'dGMP crystals. The calculated C5'H anisotropic coupling indicates that this center should possess a large degree of anisotropy, which is in agreement with experiment. However, the calculated isotropic C5'H and C4'H couplings are smaller and larger than those observed in the above experimental studies, respectively.

Alexander and Franklin observed a radical upon irradiation of deoxyadenosine debated to be either the C5' radical or a radical formed through breakage of the C4'O1' bond within the sugar ring.[17] The radical was concluded to be the C5' radical and a considerable degree of anisotropy, as seen in other experimental studies and in the calculations, was recorded. However, the isotropic couplings are much smaller in magnitude than those previously assigned indicating that reexamination of this radical is necessary. These experimental results will be discussed in more detail below.

The experimental systems discussed above differ from the model radical used in the present study by a phosphate group at the C5' position. However, it was suggested that a similar radical with the phosphate group replaced by a hydroxyl group was also observed in the experimental spectrum of 5'dGMP.[5] Principal values typical of $\beta$(OH) couplings ($A_{XX}$ = 16.3, $A_{YY}$ = 20.2, $A_{ZZ}$ = 28.1 G) were elucidated. The calculated values for this coupling are however much smaller in magnitude.

Due to discrepancies between experimental and theoretical results, an in-depth investigation of the couplings assigned to the C5' hydrogen abstraction radical is required. Since significant effects on the HFCCs can be observed with changes in geometry, an investigation of the dependence of the HFCCs on rotation about the C5'C4' bond was undertaken. The XC5'C4'C3', X = O5' or H5', dihedral angles in the north conformer were varied by increments of 15° starting from the optimized geometry (289.3° and 144.4° for X = H5' and O5', respectively) and single-point calculations performed at each step. The results for the variation in C4'H, C5'H and O5'H HFCCs as a function of rotation angle are displayed in Figure 6.4. It is interesting to note that upon rigid rotation, the isotropic component of the HFCCs changes considerably, while the

anisotropic components (not shown) do not differ more than twenty percent from the values displayed in Table 6.3. On average, the rotation barrier about the C4'C5' bond is 8.6 kcal/mol, with maximum and minimum values occurring at 90° (14.4 kcal/mol) and 15° (1.4 kcal/mol), respectively.

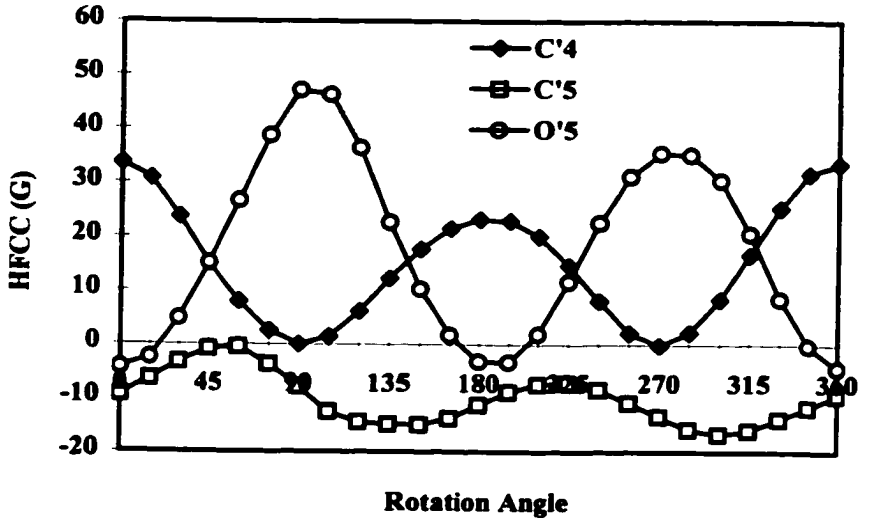


Figure 6.4: The C4', C5' and O5' hydrogens' HFCCs (G) versus the rotation angle (deg.) about the C5'C4' bond for the C5'(N) radical.

The results in Figure 6.4 shed some light on the dependence of the HFCCs on rotation about the C5'C4' bond. The calculated C5'H isotropic HFCC does not reach the experimental value (-22 G) obtained in 5'dGMP, but comes close to the value obtained in dAm (-17 G) upon a 300° rotation (-16.7 G). The variation between O5'H and C4'H results obtained for 3'CMP and 5Cl or 5BrdU can also be understood from these results. For 3'CMP, the calculated values which satisfy both the C4' and O5' experimental couplings occur at a 130° rotation, where $A_{iso}$(O5'H) = 22.6 G and $A_{iso}$(C4'H) = 8.1 G (experimental values are 20.8 and 4.5 G, respectively). Similarly, results in agreement with 5Cl and 5BrdU experimental HFCCs occur upon a 150° rotation, where $A_{iso}$(C4'H) = 17.7 G and $A_{iso}$(O5'H) = 10.3 G (experimental values: 18.9 and 8.6 G, respectively). Hence, the calculated results agree very well with the HFCCs obtained experimentally in these studies.

At 130° rotation, the C5'H and C4'H HFCCs (-14 G and 7 G, respectively) obtained by Alexander and Franklin in dA are also in good agreement with the calculated values (-16.7 G and 8.4 G). However, at this degree of rotation, a large O5'H HFCC is also calculated (30.5 G) which was not detected in the experiment. Thus, the results of Alexander and Franklin[17] cannot be understood through this rotation analysis and other radical possibilities must be considered.

### *6.4.2 Alkoxyl Radicals*

Alkoxyl radicals can be formed through abstraction of a hydrogen from O5' and O3', both of which have been assigned to experimental spectra.[5,13,19,20] In full DNA, these radicals would be formed by breaking a bond within the phosphate group and, hence, would lead to strand breaks. Bernhard and co-workers[19] examined O5' alkoxyl radicals and noted that these species are relatively unstable, decaying between 4 and 120 K. The experimental results (Table 6.4) indicate that the magnitude of the two C5'H couplings varies with the compound considered, although the sum of the two couplings fluctuates between a small range (134 to 145 G). The calculated results for both the north and south type O5' radicals (Table 6.3) are very similar which is not surprising since the radical center is outside the sugar ring and, hence, puckering effects on the HFCCs are expected to be small. The calculated HFCCs consist of two large C5'H couplings (on average 91 and 19 G) and a smaller C1' coupling (approximately 3 G). The relative magnitude of the two C5'H couplings differs from the experimental results.

Table 6.4: Experimental HFCCs (G) for sugar alkoxyl radicals.

| Radical | Molecule | Atom | $A_{iso}$ | $T_{XX}$ | $T_{YY}$ | $T_{ZZ}$ |
|---|---|---|---|---|---|---|
| O5'-alkoxyl | rT[13] | "C5'H" | 80.4 | -3.1 | -1.7 | 4.8 |
| | | "C5'H" | 71.3 | -3.1 | -1.7 | 4.8 |
| | Uβaf[13] | "C5'H" | 90.0 | -1.0 | -1.0 | 2.0 |
| | | "C5'H" | 47.3 | -1.3 | -0.3 | 1.7 |
| | rA:HCl[19] | "C5'H" | 93.5 | -3.3 | -2.0 | 5.3 |
| | | "C5'H" | 48.0 | -2.7 | -1.9 | 4.5 |
| | 5CldU[19] | "C5'H" | 83.3 | -4.1 | -1.9 | 5.9 |
| | | "C5'H" | 85.6 | -3.5 | -0.9 | 4.3 |
| | 5BrdU[19] | "C5'H" | 58.5 | -3.3 | -0.3 | 3.7 |
| | | "C5'H" | 57.3 | -2.6 | -2.1 | 4.6 |
| | 3'CMP[19] | "C5'H" | ~ 82 | | | |
| | | "C5'H" | ~ 59 | | | |
| | dAm[19] | "C5'H" | ~ 100 | | | |
| | | "C5'H" | ~ 53 | | | |
| O3'-alkoxyl | 5'dGMP[5,20] | "C3'H" | 20.3 | -4.7 | -0.5 | 5.1 |

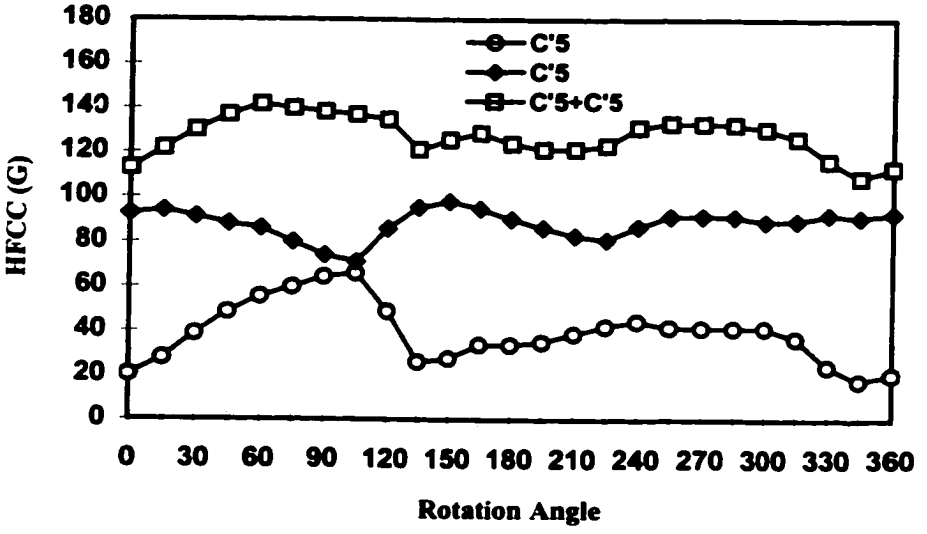


Figure 6.5: The C5' hydrogens' HFCCs (G) versus the rotation angle (deg.) about the C5'C4' bond and the sum of these couplings in the O5'(N) radical.

Due to the differences between experimental and calculated HFCCs, the effects of rotation about the C5'C4' bond on the HFCCs were examined in the north-type radical (Figure 6.5). Results are displayed as a function of the O5'C5'C4'C3' angle with respect to the optimized value (193.2°). The average (2.7 kcal/mol) and maximum (7.0 kcal/mol) rotational barriers are much smaller than those observed for the C5' hydrogen abstraction radical. The HFCCs vary greatly upon rotation, although not in the smooth manner observed for the C5' centered radical. In some instances, the rotation study clarifies discrepancies between experiment and theory. For example, the C5'H experimental couplings observed in uracil-β-D-arabinofuroside (Uβaf)[13] (90.0 G and 47.3 G) and adenosine:HCl[19] (93.5 and 48.0 G) are in better agreement with the results obtained upon a 45° rotation (88.2 and 48.6 G) than the values calculated at the optimized geometry. In other instances, the rotation study does not explain the experimental results. For example, the two C5'H couplings in 5CldU[19] (83.3 and 85.6 G) and 5BrdU[19] (58.5 and 57.3 G) are equal in magnitude. However, although the calculated C5'H couplings come close in value upon a 105° rotation (66.0 G and 71.0 G), the couplings are different from those observed experimentally. It should be noted that there exists an extensive

hydrogen-bonding scheme with respect to O5' in these crystals[19] not accounted for theoretically which offers a possible explanation for the disagreement between experiment and theory. Although the calculated values for the sum of the C5'H couplings (Figure 6.5) are on average slightly smaller than those obtained experimentally,[19] the calculated sum varies over a small range of 25 G (experimental range: 22 G). Furthermore, the ratios of the two calculated couplings vary between 1:1 and 1:5 (experimental ratios: 1:1 and 1:6). The above information leads to the conclusion that the calculations support the assignment of the O5' alkoxyl radical.

Significant isotropic (20.3 G) and anisotropic (-4.7, -0.5, 5.1 G) couplings observed in irradiated 5'dGMP were assigned to the O3' alkoxyl radical.[5,20] The calculated results for the south conformer are in poor agreement with experiment where the magnitude of both the isotropic (12.5 G) and anisotropic components (-2.0, -1.7, 3.7 G) were calculated to be too small. Unfortunately, the north conformer has not been detected upon optimization with DFT, but it has been isolated at the HF and MP2 levels. Since MP2 and DFT geometries are comparable, the MP2 optimized geometry was used to study the HFCCs in the O3'(N) radical through B3LYP single-point calculations. The calculated C3'H isotropic HFCC is much smaller in magnitude (3.2 G) than that obtained for the south conformer (12.5 G) or the experimentally observed radical (20.3 G). In addition, the anisotropic couplings are nearly identical to those obtained for the south conformer, which are in poor agreement with experiment. A possible explanation for the poor agreement between experiment and theory for the O3' alkoxyl radicals can also be sought in hydrogen bonding effects not accounted for in the calculations.

### *6.4.3 Radicals Formed Through Breakage of a Phosphoester Bond*

Radicals formed through breakage of a phosphoester bond have been observed experimentally (Table 6.5). In the sugar model system, these radicals would be formed through net removal of a hydroxyl radical from C5' or C3'. These radicals would lead to single-strand breaks in DNA. Hole *et al.*[5] observed the C5' radical in 5'dGMP crystals at temperatures below 10 K indicating that this radical is unlikely to arise from a base radical, but is probably formed via direct reduction or excitation. The C3' centered radical is approximately 3 kcal/mol lower in energy relative to the C5' centered radical,

however it has not been assigned in any experimental spectra.

Table 6.5: Experimental HFCCs (G) for the radical formed through breakage of the C5'–$OPO_3^{-2}$ bond in experimental crystals.

| Molecule | Atom | $A_{iso}$ | $T_{XX}$ | $T_{YY}$ | $T_{ZZ}$ |
|---|---|---|---|---|---|
| 5'dCMP[13] | "C5'H" (2) | -21.4 | -8.3 | 1.0 | 7.4 |
| | "C4'H" | 36.0 | | | |
| 5'dGMP[5] | "C5'H" | -15.5 | -8.9 | -1.2 | 10.2 |
| | "C5'H" | -17.3 | -9.7 | -0.2 | 9.9 |
| | "C4'H" | 6 | | | |
| | "C5'H" | -18.0 | -9.8 | -0.4 | 10.2 |
| | "C4'H" | 6 | | | |

The calculated HFCCs (Table 6.6) for the C5' centered radical consist of large isotropic C5'H couplings of equal magnitude which possess a high degree of anisotropy. The N and S conformers of this radical can be identified through the C4'H isotropic coupling. Experimentally, this radical has been observed in 5'dCMP[13] and 5'dGMP,[5] where two conformers have been identified in the later crystals. The experimental C5'H couplings in both crystals are comparable in magnitude (Table 6.5). The calculated isotropic C5'H couplings in both the N and S conformers are similar to those experimentally assigned, although the calculated anisotropic components are larger in magnitude (Table 6.6). The experimentally observed C4'H couplings differ in the two crystals. Comparison to the calculated results indicates that the radical observed in 5'dCMP (36.0 G) is probably in a south-type conformation (31.8 G). Alternatively, the radical observed in 5'dGMP (6 G) is probably in a north-type conformation (12.8 G). More detailed experimental work which identifies full anisotropic tensors for C4'H would be beneficial.

Table 6.6: Calculated HFCCs (G) for sugar radicals resulting from a breakage of a phosphoester bond.

| | | North | | | | South | | | |
|---|---|---|---|---|---|---|---|---|---|
| Radical | Atom | $A_{iso}$ | $T_{XX}$ | $T_{YY}$ | $T_{ZZ}$ | $A_{iso}$ | $T_{XX}$ | $T_{YY}$ | $T_{ZZ}$ |
| C5' | C5'H | -21.7 | -13.4 | -0.1 | 13.5 | -22.6 | -13.9 | 0.1 | 13.8 |
| | C5'H | -21.6 | -13.6 | 0.0 | 13.6 | -21.4 | -13.8 | -0.2 | 14.0 |
| | C4'H | 12.8 | -2.0 | -1.4 | 3.4 | 31.8 | -1.8 | -1.4 | 3.3 |
| C3' | C4'H | 36.3 | -1.7 | -1.1 | 2.8 | 33.9 | -1.8 | -1.4 | 3.1 |
| | C3'H | -20.0 | -13.1 | 0.0 | 13.2 | -21.4 | -13.4 | 0.0 | 13.4 |
| | C2'H | 23.5 | -1.7 | -1.3 | 3.0 | 23.5 | -1.6 | -1.6 | 2.9 |
| | C2'H | 49.0 | -1.8 | -1.1 | 2.9 | 47.4 | -1.8 | -1.8 | 3.0 |

### *6.4.4 Ring-Breaking Radicals*

Radicals involving more extensive damage to the ring than sole removal of a hydrogen atom or breakage of a phosphoester bond have been identified experimentally (Table 6.7).[5,17,18,20,21] These radicals include those generated through breaking bonds to the sugar ring oxygen (Figure 6.6). A C4' radical, generated through breaking the C4'O1' bond, has been proposed experimentally[5,18,21] and HFCCs have been assigned to this radical in 5'dGMP and 5'rUMP crystals.[5,21] The experimental results (Table 6.7) exhibit differences in the magnitude of the couplings. However, it is interesting to note that the sum of the C5'H couplings is very similar in both studies (61 and 64 G) indicating that alternative conformers may be responsible for the differences. Calculations (Table 6.8) reveal a large isotropic C4'H coupling (-21.3 G) possessing significant anisotropy (-13.0, 0.0, 13.0 G), not unlike that assigned in 5'rUMP.[21] Substantial C3'H and C5'H couplings were also obtained from the calculations (32.4 and 32.8 G, respectively) which do not correspond to those observed experimentally. Experimental studies of this radical with partially deuterated samples would aid in the determination of the entire coupling tensor to a greater degree of accuracy, whereby the deviations in experimental assignments could possibly be unveiled. However, the C3', C4' and C5' hydrogens are not easily replaced.

As previously mentioned Alexander and Franklin[17] accredited observed couplings to the C5'-dehydrogenated radical, which was an assignment not supported by the calculations. The ring-opened radical was also suggested as a precursor to the observed spectrum. Comparison of the results assigned to the C5' hydrogen abstraction radical (Table 6.2) with the experimental and calculated values for the ring-opened radical, suggests that this radical is also unlikely responsible for the observed couplings.

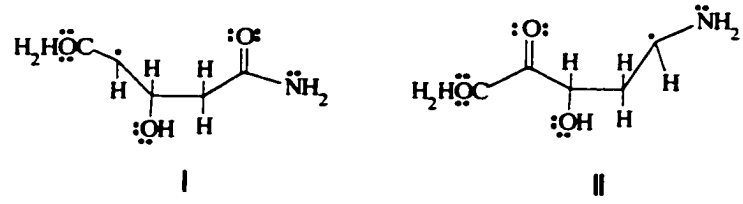

I II

Figure 6.6: The structure of model C4' (I) and C1' (II) centered radicals formed through opening the sugar ring.

Table 6.7: Experimental HFCCs (G) for a variety of ring altering radicals.

| Radical | Molecule | Atom | $A_{iso}$ | $T_{XX}$ | $T_{YY}$ | $T_{ZZ}$ |
|---|---|---|---|---|---|---|
| C4' ring-opened | 5'dGMP[18] | "C5'H" | 27 | | | |
| | | "C5'H" | 37 | | | |
| | | "C4'H" | 32.2 | | | |
| | 5'rUMP[21] | "C4'H" | -18.8 | -9.8 | -0.2 | 10.0 |
| | | "C5'H" | 48 | | | |
| | | "C5'H" | 13 | | | |
| ring-breaking | 5'GMP[5] | | -15.5 | -11.0 | 1.1 | 9.8 |
| | | | 4.0 | -1.4 | -0.2 | 1.5 |
| | 5'GMP[20] | | -16.9 | -8.0 | 0.2 | 7.8 |
| | | | 3.8 | -1.6 | -0.2 | 1.9 |
| $H_2O$ + H removal | 5'GMP[20] | "αH" | -16.0 | -11.7 | 1.9 | 9.8 |
| | | "βH" | 25.0 | -3.8 | 0.8 | 3.0 |
| | | "βH" | 23.0 | -6.7 | -0.2 | 7.0 |
| | | "βH" | 12.9 | -3.3 | -0.7 | 4.1 |

Principal components.

A corresponding C1' centered ring-opened radical (Figure 6.6) can also be considered, although this radical has not been proposed in experimental studies. B3LYP/6-311G(2df,p) single-point calculations indicate that the C4' centered radical lies 16.2 kcal/mol lower in energy than the corresponding C1' radical, providing an explanation for the lack of detection of the C1' centered radical. The calculations predict a large C1'H isotropic coupling (-11.9 G) which has considerable anisotropy. In addition, both C2' hydrogens have large isotropic HFCCs. Some of the spin density was calculated to be located on N1 (0.17), indicating that the unpaired spin density could be distributed throughout the base to stabilize this radical. It is interesting to note that the magnitudes of these couplings are not unlike those isolated in 5'rUMP and assigned to different atoms in the corresponding C4' centered radical.

The second series of ring breaking radicals is formed through removal of a portion of the sugar ring (Figure 6.7). The radical depicted in structure I has been proposed to be formed in nucleotides by abstraction of a hydrogen atom from the C5' position by a base radical, followed by breakage of the sugar ring and reorientation about the C4'O1' bond.[5] A very similar radical appears in structure II, where this radical was observed only after irradiation at room temperature.[20] The coupling constants in these radicals were calculated using a model system (structure III) that represents either the phosphate[5] or the carbon[20] group (II) with a hydroxyl group. The experimental results (Table 6.7) include a large C5'H isotropic coupling (approximately -17 G) and a small

Table 6.8: Calculated HFCCs (G) for ring-altering radicals.

| Radical | Atom | $A_{iso}$ | $T_{XX}$ | $T_{YY}$ | $T_{ZZ}$ |
|---|---|---|---|---|---|
| C4' ring-opened | C2'H | 2.2 | -0.9 | -0.7 | 1.6 |
| (Figure 6.6, I) | C3'H | 32.4 | -1.9 | -1.0 | 3.0 |
| | C4'H | -21.3 | -13.0 | 0.0 | 13.0 |
| | C5'H | 32.8 | -2.3 | -0.8 | 3.1 |
| | C5'H | 3.8 | -2.1 | -1.5 | 3.5 |
| | O5'H | 3.4 | -1.5 | -0.7 | 2.1 |
| C1' ring-opened | C1'H | -11.9 | -11.4 | -0.4 | 11.8 |
| (Figure 6.6, II) | C2'H | 12.5 | -1.7 | -1.4 | 3.1 |
| | C2'H | 33.0 | -1.5 | -1.1 | 2.6 |
| ring-breaking | C4'H | -2.8 | -1.8 | -1.3 | 3.0 |
| (Figure 6.7, III) | C5'H | -14.1 | -7.6 | -1.1 | 8.8 |
| | O5'H | -4.2 | -4.4 | -3.0 | 7.4 |
| ring-breaking with phosphorus | C5'H | 0.0 | -0.8 | -0.7 | 1.5 |
| (Figure 6.7, V) | O5'P | -21.1 | -2.2 | 1.0 | 1.2 |
| $H_2O$ + H removal | C2'H | -12.7 | -7.8 | 0.0 | 7.8 |
| (Figure 6.8) | C1'H | 27.3 | -1.0 | -0.4 | 1.5 |
| | C5'H | 11.2 | -1.3 | -0.7 | 2.0 |

C4'H isotropic coupling (4 G). The major difference in the two data sets is the magnitude of the largest component of the anisotropic tensor. The C5'H couplings calculated using the model system (Table 6.8) are in good agreement with the experimental results. However, the anisotropic results agree more closely with those obtained from more recent experiments.[20] The C4'H and the hydrogen in the hydroxyl group also exhibit notable couplings, however the latter coupling is not possible experimentally since a hydroxyl group was used to model a phosphate or carbon group.

Hole *et al.*[20] proposed that an alternative explanation for the couplings observed in 5'GMP is the radical displayed as structure IV (Figure 6.7) where a large experimental coupling (-17 G) was suggested to arise from the phosphate group. The model system displayed in structure V, was used to test this hypothesis. The calculated results indicate that the phosphorus yields a similar coupling (-21 G) to that observed experimentally. However, the calculated phosphorus anisotropic and experimental C5'H couplings do not concur. Thus, due to the better agreement obtained for the ring-breaking radical modeled by structure III, it can be concluded that the most likely structure for the observed radical is that displayed as structure I.

An explanation for the results obtained by Alexander and Franklin can also be sought in the calculated couplings for structure III (Figure 6.7). Recall that couplings assigned in their work were in poor agreement with results obtained for the C5' hydrogen

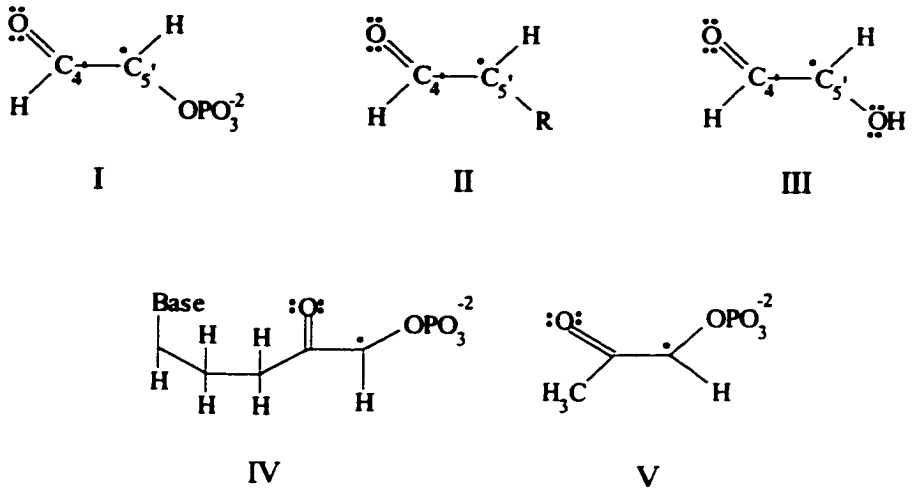


Figure 6.7: Model systems used for various ring-breaking sugar radicals: radicals observed experimentally (I and II), model ring-breaking radical (III), C5' centered radical proposed experimentally (IV) and the model ring-breaking radical with a phosphate group (V).

abstraction radical and the C4' centered ring-opened radical. Comparison of the results obtained by Alexander and Franklin (Table 6.2) and the calculated results for structure III leads to the conclusion that a radical similar to that depicted in structure I is most likely to be responsible for the observed couplings. In addition, their results resemble the values obtained in other experiments for the ring-breaking radicals (Table 6.7).

The radical displayed in Figure 6.8 can be formed either through abstraction of hydrogen from C2' followed by removal of water (C3'–OH and C4'H) or through abstraction of a hydrogen from C4' followed by removal of water (C3'–OH and C2'H). This radical would lead to single-strand breaks in DNA and has been proposed to be the precursor of four large couplings observed in 5'dGMP[20] (Table 6.7, $H_2O$ + H removal radical). The optimized geometry of this radical is planar and only three large couplings were obtained from the calculations (Table 6.8). The experimentally assigned $\alpha$ coupling (-16.0 G) is not unlike that calculated for C2'H (-12.7 G), although the magnitude of the anisotropic couplings differ. Two of the experimentally assigned $\beta$ couplings (12.9 G and 25.0 G) are similar in magnitude to C5'H and C1'H HFCCs, respectively (11.2 G and 27.3 G). The fourth large coupling exhibited in the experiments (23.0 G) cannot be accounted for in the calculations. It is possible that DFT has incorrectly predicted this radical to be planar as discussed in Chapter Four and Five for select base radicals.

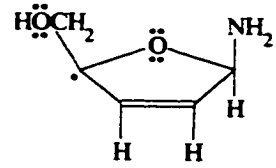

Figure 6.8: Radical formed via $H_2O$ elimination from products formed by hydrogen abstraction at C2' or C4'.

Another possible explanation could be that the third large $\beta$ coupling arises from the other C5'H. This coupling may not be observed in the calculations due to a fixed orientation of the groups attached to C5', while experimentally rotation of this group could be observed. Further insight into discrepancies between experimental and theoretical results is not available without more detailed experimental and theoretical studies.

### *6.5 Conclusions*

In this chapter, possible sugar radicals formed upon irradiation of DNA were examined with DFT. The radicals discussed include hydrogen abstraction radicals, radicals formed via breakage of a phosphoester bond, and different radicals arising from significant alterations to the sugar ring. The energetics indicate that the C4' and C3' south-type radicals are the lowest lying species for radicals formed via removal of a hydrogen or a hydroxyl group, respectively. The C2' hydrogen abstraction radical is higher in energy than any other carbon centered radical and has a relatively flat ring structure. In all radicals, the sugar-ring geometry is primarily altered at the radical center.

The calculated hyperfine couplings in the dehydrogenated radicals support the experimental assignment of these radicals in most cases. The only carbon hydrogen abstraction radical for which poor results were obtained is the C4' centered radical. However, only the isotropic HFCCs are available experimentally and elucidation of the full coupling tensors for this radical is mandatory for the positive identification of this species. For all other carbon-centered radicals, the agreement between experiment and theory is extremely good despite the fact that crystal interactions were not accounted for in the theoretical model. In particular, the couplings in the C5' radical were initially in

poor agreement with experiment. A study of the isotropic couplings versus rotation about the C5'C4' bond was required to confidently support the experimental assignment of this radical. The HFCCs obtained from this rotation study agree well with the experimental couplings and information about the radical conformation in the crystalline environment can be obtained.

Through the calculations, differences in the couplings of north and south-type radicals, arising from distinct puckering amplitudes, can be studied. Comparison of calculated and experimental HFCCs led to some speculations about which radical forms were present in the experiments. For example, the C3' radical was determined to be observed in a north conformation since this was the only conformer to possess a large C4'H coupling comparable to the experimental value. Information about the radical's conformation is not directly attainable from the experiments.

The calculated couplings for alkoxyl radicals were in poorer agreement with experiment relative to the carbon-centered radicals. This was speculated to be due to crystal interactions, since extensive hydrogen bonding schemes in the crystals are known to affect the HFCCs in alkoxyl radicals. These effects were not accounted for in the calculations and thus differences between experimental and theoretical couplings were evident for the O3' centered radicals. A rotation study analogous to that performed for the C5' centered radical was required to support the experimental assignment for the O5' centered radical.

The radical formed through breakage of the C5'–O bond was also investigated and the calculated results were in fair agreement with the experimental data. More specifically, differences in the experimental couplings elucidated from unique studies were determined to arise due to different ring conformations in each study. Various ring-altering radicals were also discussed and attempts to clarify experimental discrepancies were made. The calculations support the experimental identification of one ring-breaking radical, which indicates that disruption of the ring is a possible side effect of radiation damage. However, since the experimental spectra for these radicals were often weak, it was determined that more detailed experimental data would be beneficial, including the identification of more coupling tensors.

The calculations presented within this chapter provide support for experimental data which speculates that many different sugar radicals are formed upon irradiation of DNA base derivatives. In fact, the calculations even defend the possibility of the formation of damaging ring-altering radicals. This is very important information since sugar radicals have not been assigned in the spectra of full DNA. Positive identification of sugar radicals in single crystals will aid in the detection of these radicals in irradiated DNA. Understanding whether these radicals are formed in full DNA or whether they react to form other radicals will lead to significant information about the effects of radiation on DNA.

### *6.6 References*

1. von Sonntag, C. In *The Chemical Basis of Radiation Biology*; Taylor and Francis: New York, 1987.

2. Becker, D.; Sevilla, M. D. In *Advances in Radiation Biology*; Academic Press: New York, 1993.

3. Schuchmann, M. N.; von Sonntag, C. *J. Chem. Soc., Perkin Trans.* **1977**, *2*, 1958.

4. Close, D. M. *Radiat. Res.*, **1997**, *147*, 663.

5. Hole, E. O.; Nelson, W. H.; Sagstuen, E.; Close, D. M. *Radiat. Res.* **1992**, *129*, 119.

6. Close, D. M.; Nelson, W. H.; Sagstuen, E.; Hole, E. O. *Radiat. Res.* **1994**, *137*, 300.

7. Miaskiewicz, K.; Osman, R. *J. Am. Chem. Soc.* **1994**, *116*, 232.

8. Colson, A.-O.; Sevilla, M. D. *J. Phys. Chem.* **1995**, *99*, 3867.

9. Saenger, W. In *Principles of Nucleic Acid Structure*; Springer-Verlag: New York, 1984.

10. Wetmore, S. D.; Boyd, R. J.; Eriksson, L. A. *J. Phys. Chem. B* **1998**, *102*, 7674.

11. Hüttermann, J. *Ultramicroscopy*, **1982**, *10*, 25.

12. Nelson, W. H.; Sagstuen, E.; Hole, E. O.; Close, D. M. *Radiat. Res.* **1992**, *131*, 272.

13. *Effects of Ionizing Radiation on DNA*; Hüttermann, J., Köhnleif, W., Teoule, R.,

Bertinchamps, A. J., Eds.; Springer: Heidelberg, 1978.

14. Sagstuen, E. *J. Mag. Res.* **1981**, *44*, 518.

15. Hole, E. O.; Nelson, W. H.; Sagstuen, E.; Close, D. M. *Radiat. Res.* **1992**, *130*, 148.

16. Kar, L.; Bernhard, W. A. *Radiat. Res.* **1983**, *93*, 232.

17. Alexander, Jr., C.; Franklin, C. E. *J. Chem. Phys.* **1971**, *54*, 1909.

18. Rakvin, B.; Herak, J. N. *Radiat. Res.* **1981**, *88*, 240.

19. Bernhard, W. A.; Close, D. M.; Hütterman, J.; Zehner, H. *J. Chem. Phys.* **1977**, *67*, 1211.

20. Hole, E. O.; Sagstuen, E. *Radiat. Res.* **1987**, *109*, 190.

21. Sagstuen, E. *Radiat. Res.* **1980**, *84*, 164.

# *CHAPTER SEVEN*

## Reactions Between Water and the DNA Bases

### *7.1 Introduction*

Many studies have appeared in the literature which attempt to answer questions regarding the role water plays in the formation of DNA radicals (to be discussed in more detail in Chapter Eight). It is believed that water molecules in the hydration layer surrounding DNA can lead to radical formation through two possible pathways. The first (the direct pathway), involves reactions between hydroxyl radicals or hydrogen atoms generated from irradiation of water and the DNA strand. The second (the indirect pathway), involves transfer of the charge imposed on the water molecules by irradiation to the DNA strand. The mechanism for radiation damage in hydrate crystals of base derivatives is believed to follow an indirect damage pathway where water radicals do not play a straightforward role in radical formation.

The calculations presented in Chapter Four provide new evidence that net hydroxyl radical addition adducts are possible radiation damaged products in cytosine monohydrate crystals. Additionally, comparison of theoretical and experimental HFCCs obtained in monohydrate crystals of the purines, adenine and guanine, led to the conclusion that net hydroxyl radical addition products are formed. The only logical mechanisms for the formation of net hydroxylated radicals in monohydrate crystals of base derivatives involve water molecules. Additionally, in cytosine monohydrate crystals and in protonated monohydrate crystals of guanine derivatives the major radical products were determined (Chapters Four and Five) to be formed through net addition of hydrogen and hydroxyl radicals. More specifically, no net dehydrogenated products were identified. If water is not a participant in the radiation damage pathway and no net dehydrogenated radicals are formed, questions arise about the origin of the hydrogens adding to base derivatives to yield net hydrogenated species. These results indicate that in hydrate crystals direct damage imposed by water radicals may be important. However, the mechanism of radical formation is not well understood.

There exists a lot of interest in reactions between water and the DNA bases for a variety of reasons. For example, primary products of hydroxyl radical addition have been

shown to result in sugar radicals.[1] Additionally, bond formation between DNA and proteins (a DNA-protein cross-link) occurs due to hydroxyl radical addition to the DNA bases, where the hydroxyl radicals are formed upon irradiation of the samples involving water.[2] In the present chapter, the reactions between water and various DNA bases will be discussed to obtain more information about possible reaction mechanisms in monohydrate crystals and the preferred site for hydroxyl radical addition to the nucleobases.

## *7.2 Reactions Between Cytosine and Water*

Many different radiation products have been identified which could be formed by reactions between cytosine and water. Net hydroxyl radical addition to cytosine has been shown to lead to the formation of two main products: the C5 and C6-hydroxylated radicals.[3,4] Evidence exists that cross-links between cytosine and the amino acid tyrosine are generated after the formation of the C5-hydroxylated cytosine radical.[2a] It is well known that when DNA is exposed to hydroxyl radicals, a deamination reaction can occur at cytosine which converts this base into uracil.[4] Alternative products resulting from hydroxyl radical attack at cytosine include 5-hydroxycytosine and 3-carbamoyl-4-hydroxyhydantoin.[5] Uracil glycol and urea have also been identified as byproducts of radicals formed through hydroxyl radical addition to the C5 or C6 positions in cytosine. Additionally, products in which a bond is formed between the sugar moiety and the cytosine base have been suggested to arise from net cytosine hydroxylated products.[4] These few examples illustrate the range in the nature of radical products that can be formed through reactions of cytosine and water. Thus, it is very important to understand the underlying mechanisms for the formation of hydroxylated cytosine radicals. Initially, hydroxyl radical addition to the C5 position in cytosine will be discussed where a systematic study has been carried out to determine the most appropriate computational method to study these reactions.

### *7.2.1 The Reaction Profile for Hydroxyl Radical Addition to C5 in Cytosine*

#### *7.2.1.1 Computational Details*

The B3LYP/6-31G(d,p) potential energy surface was scanned by increasing the C5O bond length from that present in the C5-hydroxylated radical. The energy along this

reaction coordinate continues to rise until the energy of the separated reactants is obtained. This indicates that the reaction between cytosine and the hydroxyl radical characterized by the B3LYP/6-31G(d,p) level is barrierless. Similar scans were also performed with the B3P86 and B3PW91 functional combinations and the 6-31G(d,p) basis set and similar results were obtained. The phenomena of barrierless reactions for hydroxyl radical addition have been observed previously at this level of theory.[6] It is well known that the barrier heights predicted with DFT are often much lower than those obtained with other *ab initio* methods.[7] However, DFT techniques based on Becke's hybrid functional usually compensate for the faults of other exchange functionals through the inclusion of HF exchange.

Due to the flat potential energy surfaces predicted by DFT, an alternative method is required to study these reactions. Møller-Plesset perturbation theory would be the next desirable level at which to investigate the potential energy surface under consideration. MP2 has been used in the past with a great deal of success to study hydroxyl radical addition and abstraction reactions.[8,9,10,11,12,13] However, due to limitations imposed by computer resources, especially when a frequency analysis is required for a system of the size under consideration, lower levels of theory must be implemented.

The geometries for the species along the reaction profile were calculated at the UHF/6-31G(d,p) level. Correlation has been shown to be important for the calculation of transition state (TS) geometries.[8,9,10] In some instances, differences between HF and MP2 TS geometries are small, where the bond lengths and angles vary by less than 0.1 Å and a few degrees, respectively.[8,9] However, in other cases the geometries are not comparable[10] and differences in the conformation (for example, staggered versus eclipsed groups) exist between geometries obtained at the HF and MP2 levels.[9] Another problem with HF is that it overestimates barrier heights. Therefore, subsequent single-point calculations must be performed. A variety of computational methods (MP2 and DFT based methods) and a larger basis set (6-311G(2df,p)) were used to obtain better estimates of the transition barrier heights. The zero-point vibrational energy calculated at the HF/6-31G(d,p) level was used to correct the energetics calculated at higher levels. Transition barrier heights comparable to those calculated at geometries obtained with higher levels of theory have been calculated with high-level single-point calculations on

HF geometries.[9] These results indicated that the barrier heights are more dependent on the level of correlation included in the single-point calculation than the explicit geometry implemented. Therefore, the optimization of the geometries at the HF level followed by higher-level single-point calculations will yield satisfactory results for a preliminary study of the reactions between the DNA bases and water.

An additional problem associated with the UHF level is that the unrestricted HF wave function is not a spin eigenfunction. Therefore, the calculations often suffer from a great deal of spin contamination. This is also true, in particular, for MP2 single-point calculations on TSs. This problem can be remedied through the use of spin projection with the PUHF and PMP2 methods. PMP2 single-point calculations at UHF geometries have previously been shown to yield activation barriers in good agreement with experiment.[9] Calculations were performed with the GAUSSIAN 94 program package.[14]

#### *7.2.1.2 Geometries*

The conformations of the reactant complex (RC), the transition state (TS) and the product (P) for the addition of a hydroxyl radical to C5 in cytosine are displayed in Figure 7.1, along with select geometrical parameters. The reactant complex is a configuration of the initial reactants that results in a lowering of the energy relative to that of the reactants at infinite separation (R). From Figure 7.1, it is evident that the energy of the addition complex is lowered relative to that of separated reactants due to the formation of hydrogen bonds between the hydroxyl hydrogen and N3 in cytosine (r(N3H) = 2.050 Å) and the hydroxyl oxygen and an amino hydrogen (r(N4H-O) = 2.248 Å). Interactions between the two reactants are also evident in the RC since the OH bond length is 0.01 Å longer than that in an isolated hydroxyl radical. The addition complex is planar, including the amino group. The spin contamination exhibited for this structure at the UHF/6-31G(d,p) level is very small ($<S^2>$ = 0.755 compared to 0.750 for a pure doublet).

The transition state exhibits slight puckering, where the C5 position is located 13.3° out of the plane formed by the remainder of the ring atoms. This distortion is due to the interactions between the hydroxyl radical and the base moiety at this position. The C5O distance is 1.870 Å and the hydrogen in the hydroxyl radical is pointed towards N3. This orientation of the hydroxyl radical provides an explanation for the configuration of

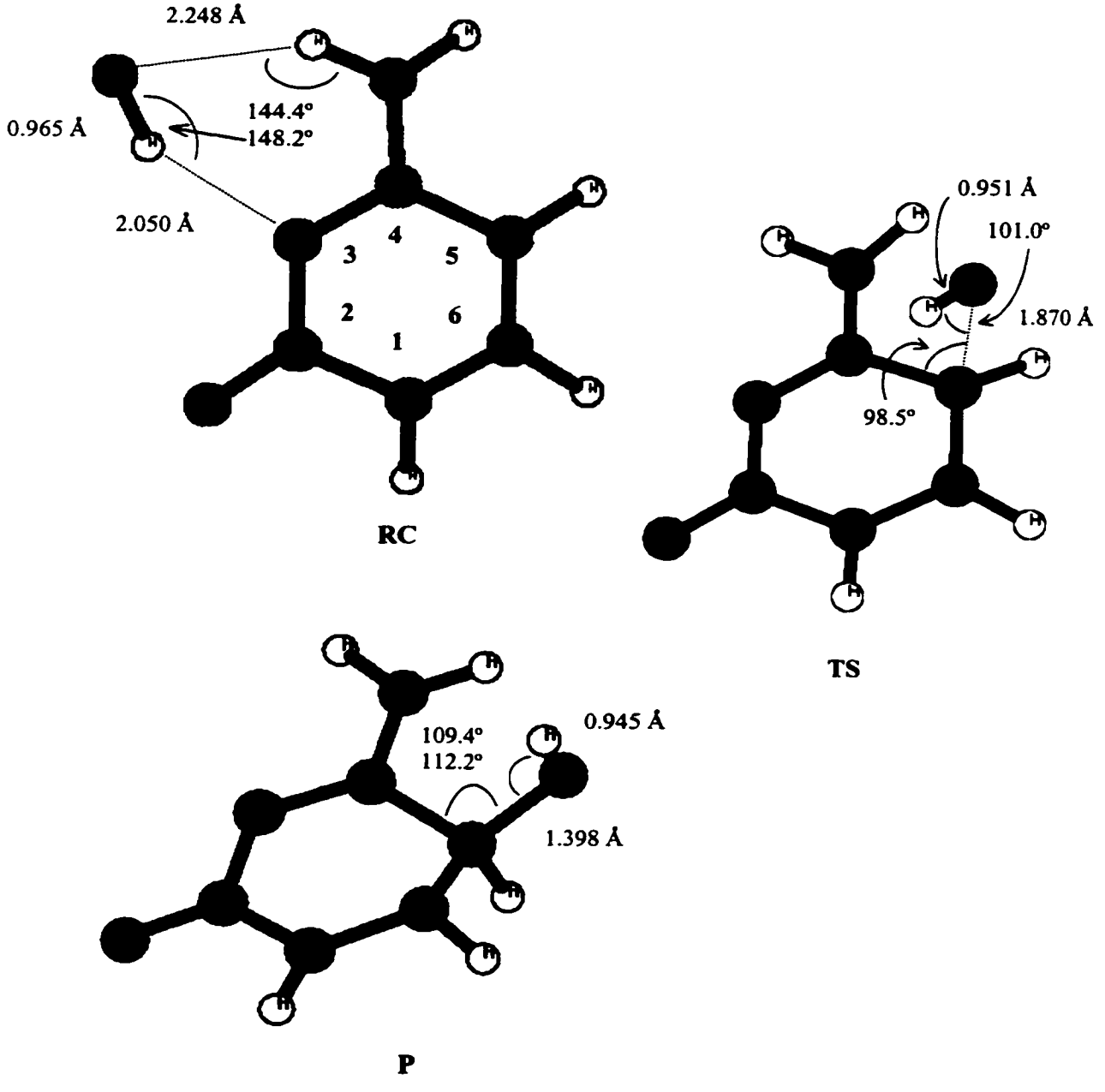


Figure 7.1: Select geometrical parameters in the RC, TS and P for hydroxyl radical addition to C5 in cytosine.

the reactant complex. As expected, the degree of spin contamination observed in the calculation of the TS geometry is quite large ($\langle S^2 \rangle$ = 0.958). This geometry was confirmed to be a TS by a frequency calculation, where the Hessian matrix was calculated to possess only one negative eigenvalue corresponding to an imaginary frequency of 689 $cm^{-1}$. This imaginary frequency eigenvector corresponds primarily to

motion of O and C5 towards each other. The r(C5O) value in the final product is 1.398 Å and the C5 position is located farther out of the molecular plane (∠(C5C6N1C2) = -27.6°). The hydroxyl group has reoriented slightly such that the hydrogen is directed towards the center of the molecular ring. The geometry optimization performed for P also suffers from a small amount of spin contamination ($<S^2> = 0.765$).

#### *7.2.1.3 Reaction Barrier Height*

Figure 7.2 displays the reaction profile for hydroxyl addition to cytosine at C5 obtained through single-point calculations (on UHF/6-31G(d,p) geometries) with the 6-311G(2df,p) basis set and the UHF, MP2 and B3LYP methods. The barrier heights calculated, relative to the RC at the respective level of theory, are also given in the figure. Table 7.1 displays the relative energy for the geometries along the reaction path (with respect to the isolated reactants at the same level of theory) and the degree of spin contamination in the single-point calculations.

Figure 7.2 conveys that the energy of the RC is 7.5 kcal/mol lower than that of the separated reactants at the UHF level. Despite the fact that little spin contamination is exhibited in the UHF single-point calculation (0.756), the projection of contaminating spin states through the PUHF method leads to a greater lowering of the energy (9.5 kcal/mol). MP2, PMP2 and B3LYP all predict an even greater lowering in the energy of the RC relative to the isolated reactants (approximately 10.5 kcal/mol). The stability imposed by the configuration involving hydrogen bonds relative to the isolated reactants is clearly seen.

The transition barrier predicted by HF theory (25.8 kcal/mol) is extremely large relative to the other barriers, as expected since this method is well known to drastically overestimate barrier heights. The barrier calculated with MP2 (13.5 kcal/mol) is approximately half of the value obtained with UHF, which clearly displays the importance of electron correlation. The spin contamination in the TS energy calculations at these levels of theory is quite large (0.957), which is not surprising due to the implementation of the unrestricted formalism. PUHF lowers the UHF barrier from 25.8 to 16.0 kcal/mol, while the barrier predicted with PMP2 (4.7 kcal/mol) is also much smaller than that obtained with MP2 (13.5 kcal/mol). The difference between the MP2

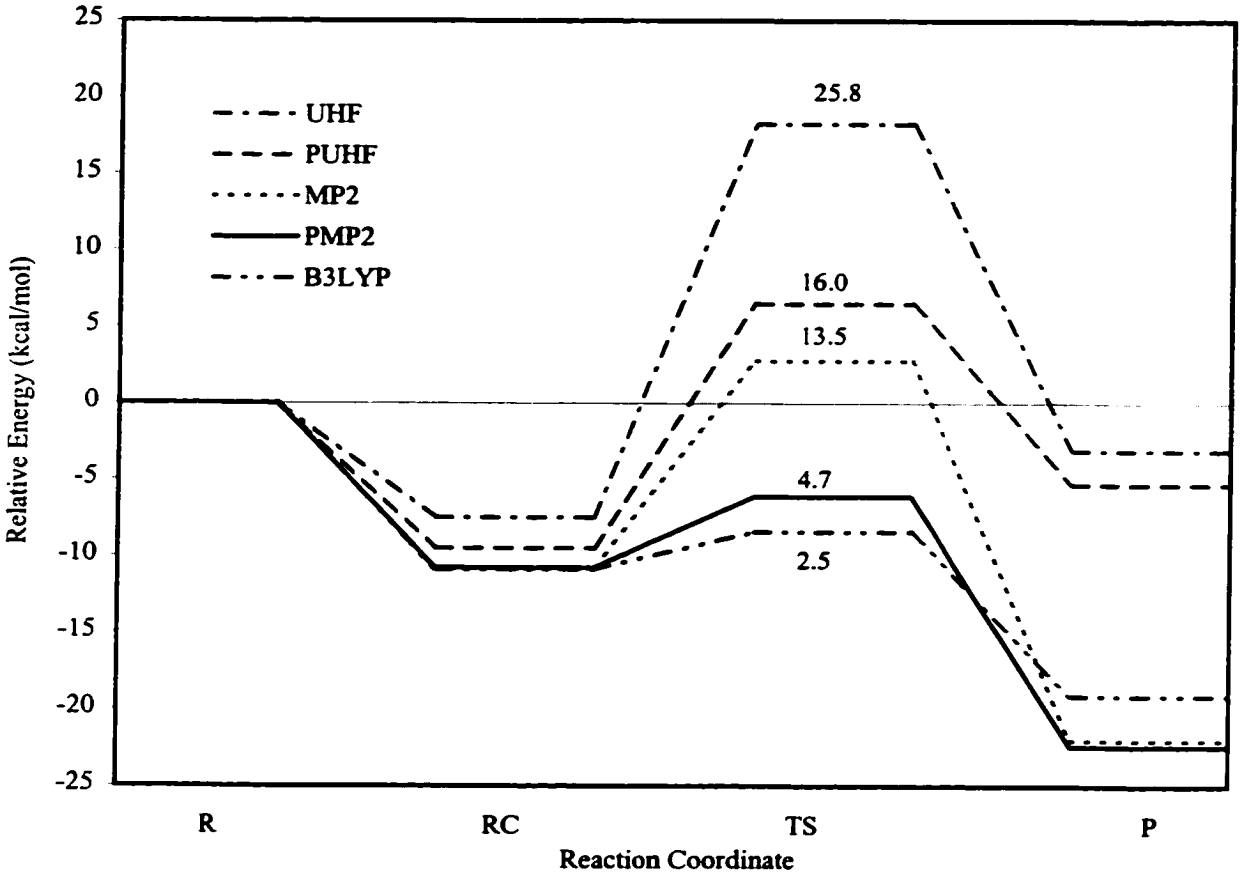


Figure 7.2: Energetics for hydroxyl radical addition to cytosine at C5.

and PMP2 barrier heights is in agreement with previous suggestions that spin contamination leads to an overestimation of MP2 barriers by up to 10 kcal/mol.[15] PMP2 practically eliminates any spin contamination in the transition state ($<S^2> = 0.759$). The B3LYP barrier (2.5 kcal/mol) is half the size of the value predicted by PMP2 and the spin contamination of the TS (0.769) is relatively small.

Although B3LYP is the most widely used DFT functional combination in recent theoretical studies, it is of interest to examine the barrier heights predicted with alternative functionals. The UHF/6-31G(d,p) surface was used to perform single-point calculations on the RC and TS with a variety of functionals and these results are displayed in Table 7.2. Barrier heights were calculated with the LYP, P86 and PW91 correlation functionals in combination with the B and B3 exchange functionals. From Table 7.2, it can be seen that all "pure" DFT functionals examined predict negative

Table 7.1: Relative energies (kcal/mol) with respect to the energy of the separated products obtained for hydroxyl radical addition to C5 in cytosine with a variety of methods, the 6-311G(2df,p) basis set and the HF/6-31G(d,p) geometries.

| | UHF | PUHF | MP2 | PMP2 | B3LYP |
|---|---|---|---|---|---|
| R (ΔE) | 0.00 | 0.00 | 0.00 | 0.00 | 0.00 |
| $<S^2>$ | 0.756 | 0.751 | 0.756 | 0.751 | 0.752 |
| RC (ΔE) | -7.47 | -9.48 | -10.73 | -10.77 | -10.86 |
| $<S^2>$ | 0.756 | 0.750 | 0.756 | 0.750 | 0.752 |
| TS (ΔE) | 18.29 | 6.50 | 2.76 | -6.10 | -8.40 |
| $<S^2>$ | 0.957 | 0.759 | 0.957 | 0.759 | 0.769 |
| P (ΔE) | -3.09 | -5.31 | -22.03 | -22.41 | -19.11 |
| $<S^2>$ | 0.766 | 0.750 | 0.766 | 0.750 | 0.755 |

barriers for the reaction under consideration. That is, the transition structures are lower in energy than the reactant complex. The spin contamination for these single-point calculations is also very small. Conversely, all hybrid DFT functionals predict small (positive) barriers. The spin contamination observed from these methods is slightly higher than observed from the "pure" functionals due to the inclusion of HF exchange. It is interesting to note that the relative DFT barrier heights are predicted by the correlation functional, where the barrier increases in size according to P86 < PW91 < LYP regardless of the exchange functional implemented. The inclusion of HF exchange increases the barrier heights by between 6 and 10 kcal/mol.

Another exchange functional, G96, developed by P. Gill,[16] is becoming popular due to its inclusion in GAUSSIAN 98.[17] This functional has also been implemented in the present study in conjunction with the three correlation functionals previously mentioned (Table 7.2). Once again, it is apparent that the correlation functional determines the relative magnitude of the barrier heights. Additionally, similar to the other "pure" DFT functionals, these three functional combinations predict negative transition barriers and the degree of spin contamination is small.

The results obtained with a variety of DFT functionals indicate that B3LYP yields results in most satisfactory agreement with PMP2 data. PMP2 energetics are used as a reference since, as previously mentioned, it has been shown that barrier heights obtained with PMP2 single-point calculations on HF geometries can reproduce experimental activation barriers[8] and no experimental data is available for the present system. Thus, among the functionals investigated in the present study, the B3LYP combination is the

Table 7.2: Barrier heights (kcal/mol) for the reaction of cytosine with the hydroxyl radical obtained with a variety of DFT functionals, the 6-311G(2df,p) basis set and the HF/6-31G(d,p) geometries.

| Functional | Barrier Height | TS $\langle S^2 \rangle$ |
|---|---|---|
| BLYP | -3.7 | 0.756 |
| BP86 | -9.4 | 0.756 |
| BPW91 | -4.8 | 0.756 |
| B3LYP | 2.5 | 0.769 |
| B3P86 | 0.5 | 0.768 |
| B3PW91 | 1.6 | 0.769 |
| G96LYP | -3.7 | 0.756 |
| G96P86 | -6.0 | 0.756 |
| G96PW91 | -4.9 | 0.756 |
| HF | 25.8 | 0.957 |
| MP2 | 13.5 | 0.957 |
| PMP2 | 4.7 | 0.759 |

most appropriate for the examination of reactions between water and various DNA bases. The small barrier for the addition of a hydroxyl radical to C5 in cytosine and the fact that this reaction is predicted with high-level calculations to be exothermic should be noted. In order to obtain more information about the possible reaction mechanism upon irradiation of single crystals of cytosine monohydrate, alternative mechanisms must also be considered.

### *7.2.2 Mechanism for Radiation Damage in Cytosine Monohydrate Crystals*

In Chapter Four, three mechanisms for radiation damage in cytosine monohydrate crystals were discussed. In summary, the first mechanism, which involved hydrogen transfer between two cytosine units and generated the N1-dehydrogenated and N3-hydrogenated radicals, was eliminated since the calculated HFCCs for these products did not match the experimentally reported values. Instead, the calculated HFCCs predicted the formation of a net C5-hydroxylated cytosine radical and therefore the damage mechanisms that were subsequently discussed involved the surrounding water molecules in the cytosine monohydrate crystals. The second mechanism discussed in Chapter Four (summarized by Equation 7.1) costs 207 kcal/mol in the first step and gains 149 kcal/mol in the second step.

$$\mathbf{H_2O + C + C \rightarrow H_2O + C^{+\bullet} + C^{-\bullet} \rightarrow C(}\textit{C5-hydroxylated}\mathbf{) + C(}\textit{N3-hydrogenated}\mathbf{)} \quad (7.1)$$

The third possible mechanism (summarized by Equation 7.2) costs 298 kcal/mol in the

first step and releases 240 kcal/mol in the second step.

$$H_2O + C + C \rightarrow H_2O^{\bullet+} + C + C^{\bullet-} \rightarrow C(\textit{C5-hydroxylated}) + C(\textit{N3-hydrogenated}) \quad (7.2)$$

It was determined in Chapter Four that the mechanism portrayed in Equation 7.1 is most likely to occur since cytosine is much larger than water and therefore a majority of the ionizations are expected to occur on the cytosine moiety. Additionally, this reaction has a lower energy cost for the first step. However, it was also noted that hydroxyl radical addition has been speculated to lead to strand breaks[18] and the lack of detection of hydroxyl radicals in the DNA hydration layer has been postulated to be due to radical addition to the bases.[19] The small barrier heights predicted at the highest level of theory employed in the present study for hydroxyl radical addition to C5 indicate that this reaction is feasible. However, more work must be performed in order to eliminate the possibility that the reaction outlined in Equation 7.1 occurs. As a first approximation to investigate this damage mechanism, the reaction between water and a cytosine cation was investigated.

#### *7.2.2.1 Water Addition to the Cytosine Cation*

Figure 7.3 displays the geometries calculated at the UHF/6-31G(d,p) level for the RC, TS and product complex (PC) for water addition to C5 in the cytosine cation. In the RC, the water oxygen is involved in hydrogen bonding with one of the amino hydrogens where r(N4H-O) equals 1.939 Å. At this arrangement, the water oxygen is 3.431 Å away from the C5 position. The spin contamination in the calculation of this structure is quite large ($<S^2> = 0.917$).

The C5O (1.626 Å) and OH bond distances (0.956 Å) are lengthened in the TS from those expected in an isolated C5-hydroxylated cytosine radical (1.398 Å) and a water molecule (0.943 Å), respectively. The second OH bond length is stretched from that calculated for an isolated water molecule to 1.438 Å in the transition state for water addition. Due to the interaction between the oxygen and the C5 position in the cytosine cation, slight puckering is exhibited at the C5 position in the transition state and the hydrogen at C5 is notably displaced from the molecular plane. The spin contamination observed in the UHF/6-31G(d,p) calculation of the transition state ($<S^2> = 0.89$) is smaller than that observed in the calculation of the transition state for hydroxyl radical

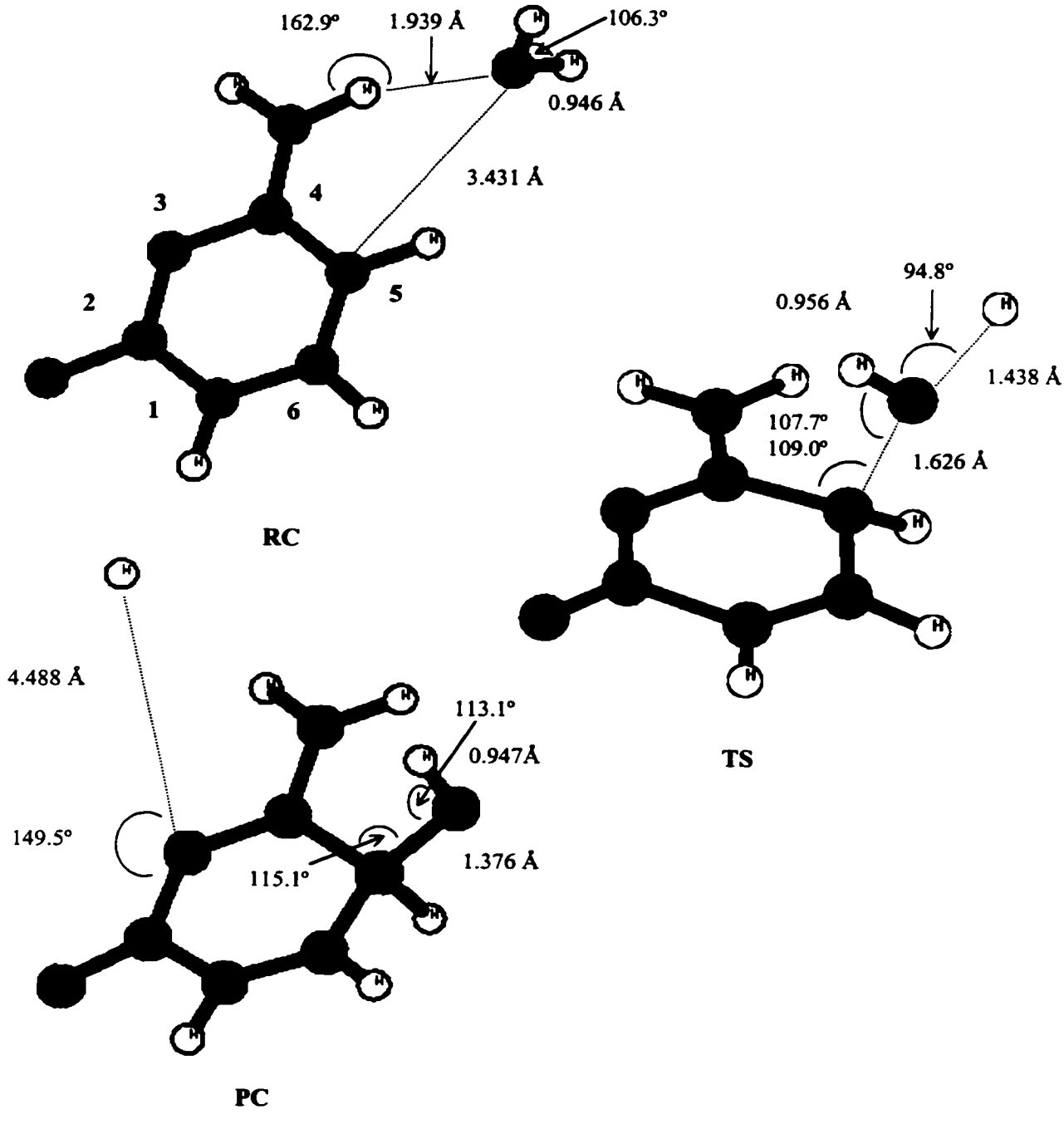


Figure 7.3: Select geometrical parameters in the RC, TS and PC for water addition to the cytosine cation at C5.

addition to a neutral cytosine molecule ($<S^2> = 0.958$). The geometry was confirmed to be a TS through a frequency analysis, which predicted one imaginary frequency (2310 $cm^{-1}$), primarily corresponding to motion of H away from OH and O towards C5.

The optimized structure for the product complex (PC, Figure 7.3) obtained through a HF calculation, which does not suffer from spin contamination, places the hydrogen nucleus 4.488 Å from the cytosine N3 nucleus, where the HN3C2 angle equals 149.5°. The C5O and OH bond lengths in the product complex (1.376 and 0.947 Å) differ slightly from those obtained for an isolated C5-hydroxylated radical (1.398 and 0.945 Å). These differences may reflect variances in the molecular environment, such as charge. Examination of the charge distribution in the PC indicates that the positive charge resides exclusively on the cytosine portion of the complex. This indicates that the hydrogen nucleus removed from the cytosine by-product is in reality a hydrogen atom. This is further confirmed by the spin distribution, which through high-level (B3LYP and PMP2) calculations was determined to reside solely at the hydrogen nucleus. Re-examination of the TS reveals that a hydrogen atom is leaving as a hydroxyl radical adds to the cytosine cation. A B3LYP/6-311G(2df,p) single-point calculation indicates that the spin and charge on the leaving hydrogen in the TS is 0.53 and 0.19, respectively. Some spin was also calculated to reside on the water oxygen (-0.07) and C5 in cytosine (0.23). A PMP2 single-point calculation using the same basis set indicates that the spin and the charge on the leaving hydrogen are 0.80 and 0.08, respectively. Spin was also calculated to be located at the water oxygen (-0.31) and the cytosine C5 position (0.42), which is quite different from that obtained with B3LYP. The PMP2 calculations clearly indicate that as water adds to the cytosine cation, a concerted process occurs where a bond is formed between the hydroxyl oxygen and C5 in cytosine and the water OH bond breaks yielding a hydrogen atom. Thus even in the TS, the leaving group is a hydrogen atom, rather than a proton, and net hydroxyl radical addition to the cytosine cation is occurring. From this discussion, it could be argued that since a hydrogen atom is generated rather than a proton, the reaction between water and the cytosine cation is unlikely to occur.

An explanation for why a hydrogen atom rather than a proton is leaving the cytosine by-product in the reaction under examination can be found through consideration of the ionization potentials of the species involved. In particular, the IP of a hydrogen atom (calculated at the B3LYP/6-311G(2df,p) level) is 315.1 kcal/mol. Alternatively, the IP of the cytosine C5-hydroxylated radical (calculated at the same level

of theory with the HF/6-31G(d,p) geometries) is 148.0 kcal/mol. Therefore, a proton cannot be expected as one of the products in the gas-phase reaction between the cytosine cation and water, since the IP of a hydrogen atom is over twice the size of the IP of the remaining radical. Therefore, in order to form the net C5-hydroxylated radical from water addition to the cytosine cation, an additional step must occur which involves electron capture by the cytosine by-product.

The reaction between water and the cytosine cation emphasizes the importance of hydroxyl radical attack, since in reality net hydroxyl radical addition to the cytosine cation was observed in the reaction discussed above. The barriers calculated through B3LYP and PMP2 single-point calculations (66.5 and 65.6 kcal/mol, respectively) for the reaction between water and the cytosine cation are much larger than those determined at the same levels of theory for hydroxyl radical addition to neutral cytosine (2.5 and 4.7 kcal/mol). Therefore, these results hint that hydroxyl radical addition to neutral cytosine is a more favorable and simplistic pathway for the formation of the net C5-hydroxylated radical than water addition to the cytosine cation, which involves hydrogen atom loss followed by electron gain. It is important to stress that the results presented within correspond to a gas-phase reaction between water and the cytosine cation. The more complex problem of the reaction that occurs in single crystals has not been solved. In single crystals, the situation is quite different due to complex hydrogen bonding schemes. Therefore, in single crystals proton transfer can occur which may assist the reaction between water and the cytosine cation. Thus, although the results presented within indicate that hydroxyl radical addition is the most favorable reaction out of the two considered, this preliminary study cannot be taken as an accurate prediction of results expected in the solid state. More complex calculations that include a larger part of the crystal environment, for example additional water and/or cytosine molecules, are required in order to eliminate the reaction between water and a cytosine cation as a radiation damage pathway in cytosine monohydrate crystals.

### *7.2.3 The Reaction Profile for Hydroxyl Radical Addition to C6 in Cytosine*

Since it appears that hydroxyl radical addition to neutral cytosine is a feasible means to generate the net C5-hydroxylated cytosine radical, it is of interest to investigate hydroxyl radical attack at the C6 position. This is important since hydroxyl radical

addition is believed to predominantly occur across the C5C6 double bond and investigating both reactions will lead to information about the favored site for hydroxyl radical addition to cytosine. Additionally, an experimental coupling left unassigned in single crystals of cytosine monohydrate was noted to be not unlike that calculated for the C6-hydroxylated adduct, indicating that perhaps this radical is also formed. Early studies concluded that hydroxyl radical addition to cytosine, as well as to uracil, predominantly occurs at C5.[20] More recent ESR spin-trapping studies determine the production ratio of these two radicals through investigating the ratio of the C5 to C6 radical spin-trapped products via computer simulations. It was determined that the ratio of C5:C6 products is 1:1.3 in a neutral solution of 2'-deoxycytidine.[3] However, this ratio may not accurately reflect the initial ratio of attack since the trapping rate of the two radicals may be different. Questions also arise in the use of computer simulations to determine the relative abundance of two radicals whose spectra are highly similar, since changing the relative abundance of each radical may have little effect on the appearance of the spectra. An alternative technique to determine the ratio of C5 to C6-hydroxylated base radicals involves monitoring the rate at which the generated radicals oxidize NNN'N'-tetramethyl-*p*-phenylenediamine or reduce tetranitromethane.[21] This method is favorable since the C5-hydroxylated product is strongly reducing, while the C6-hydroxylated radical is strongly oxidizing. Thus, the oxidizing and reducing rates can be used to determine the relative abundance of these radicals. With this technique, the C5:C6 ratio was predicted to be 8.7:1 for cytosine. The results obtained from the calculations will primarily be compared to those obtained from the reduction and oxidation properties of the hydroxylated radicals since these were specifically obtained for cytosine (the computational model system), rather than species that include a sugar group.

#### *7.2.3.1 Geometries and Reaction Barrier Heights*

The reactant complex for hydroxyl radical addition to C6 in cytosine is identical to that discussed for addition to the C5 position. The corresponding TS and P, calculated at the UHF/6-31G(d,p) level, are displayed in Figure 7.4. The majority of the molecular ring is planar in the TS with the exception of the C6 position, which lies 10.2° out of the plane formed by N1, C2 and N3. This distortion is similar to that observed in the corresponding transition state for addition to C5, where the C5 position was displaced by

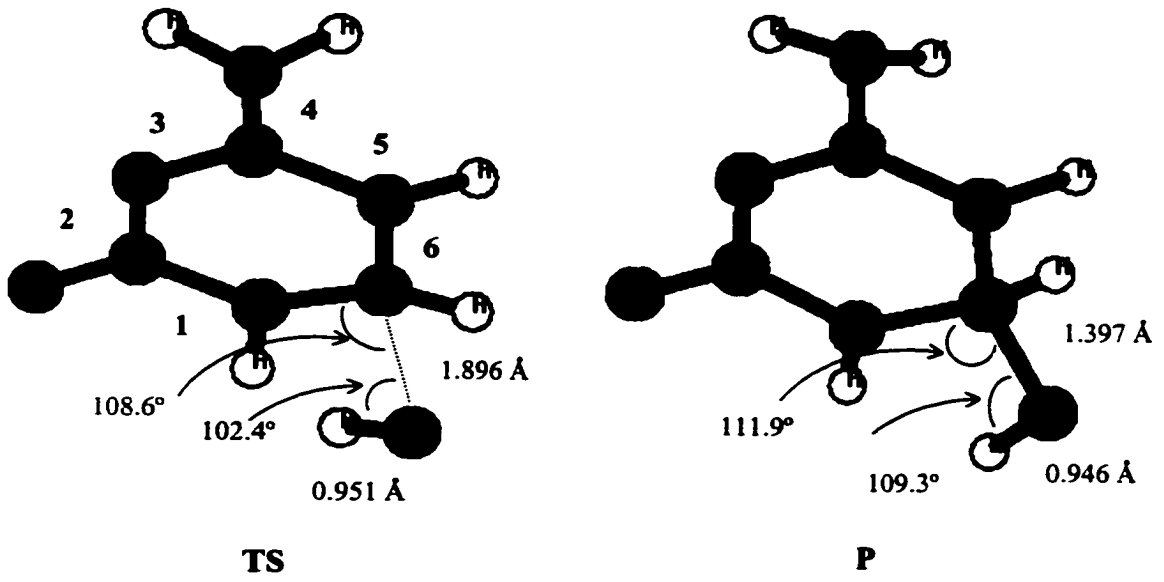


Figure 7.4: Select geometical parameters in the TS and P for hydroxyl radical addition to C6 in cytosine.

13.3°. The C6O bond length in the transition state is equal to 1.896 Å, which is 0.026 Å longer than that calculated for the equivalent C5 centered transition state. Significant spin contamination is exhibited in the calculation which optimized the TS geometry ($<S^2>$ = 0.889). The hydrogen in the hydroxyl group is orientated towards the N3 position in cytosine, providing a possible explanation for the similar addition complex between the C5 and C6 centered transition states. One imaginary frequency was obtained for this geometry of 801 $cm^{-1}$, which is larger than that calculated for the C5 TS (689 $cm^{-1}$).

The hydroxyl hydrogen remains directed towards N3 in the C6-hydroxylated radical and the C6O bond length is 1.397 Å, which is identical to the bond length in the corresponding C5 adduct. Similar to the TS, considerable spin contamination is present in the calculation of this geometry ($<S^2>$ = 0.868). Unlike the optimized geometry for the C5-hydroxylated radical, all of the ring atoms in the C6 adduct remain in the same plane and the hydrogen and hydroxyl group at C6 are evenly distributed on either side.

Single-point calculations were performed on the TS and P with the 6-311G(2df,p) basis set and the MP2 and B3LYP methods. As discussed for the previous reactions, the MP2 method involves a high degree of spin contamination in calculations on transition

states, where the eigenvalue of $<S^2>$ was determined to be 0.981 for the TS under discussion. Therefore, only the PMP2 and B3LYP barrier heights will be discussed, where the eigenvalues of $<S^2>$ were calculated to be 0.767 and 0.774 in the TS calculations, respectively. The PMP2 and B3LYP barriers for hydroxyl radical addition to C6 in cytosine are 6.2 and 4.4 kcal/mol, respectively.

#### *7.2.3.3 Comparison of Hydroxyl Addition to C5 and C6 in Cytosine*

Figure 7.5 compares the energetics for hydroxyl radical addition to the C5 and C6 positions in cytosine relative to the energy of the isolated reactants. A more complete search of the potential energy surface for this reaction may reveal different RCs for these two processes. The barrier heights calculated with PMP2 are both higher than the corresponding heights calculated with DFT (B3LYP). However, the relative energies for C5 versus C6 addition are in agreement for both levels of theory. PMP2 predicts hydroxyl radical addition to the C6 position to have a larger barrier than addition to C5

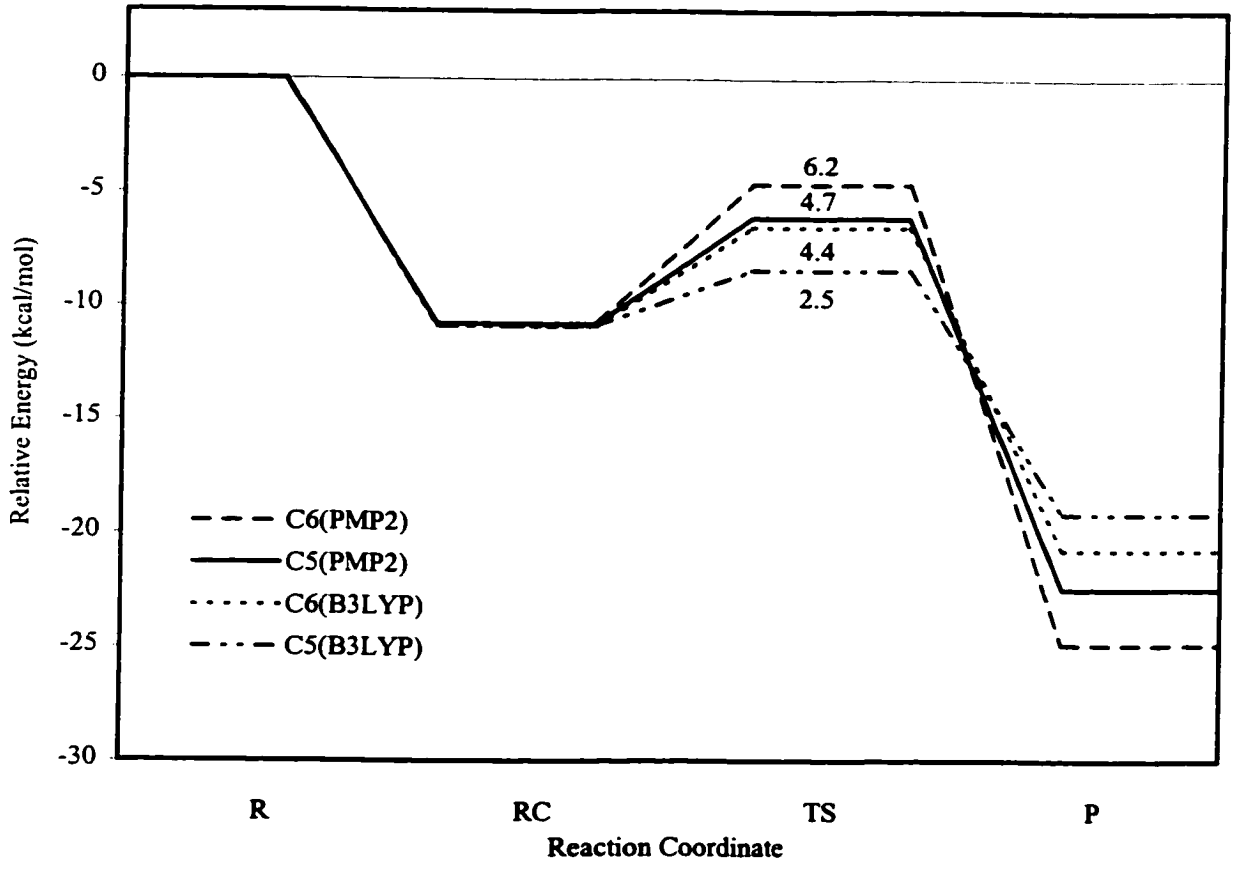


Figure 7.5: Energetics for hydroxyl radical addition to cytosine calculated with MP2 and B3LYP

by 1.5 kcal/mol. B3LYP predicts the C6 addition barrier to be 1.9 kcal/mol higher than the C5 barrier. This illustrates the predictive power the B3LYP functional possesses despite the fact that the barriers are estimated to be lower than the PMP2 values. Additionally, both B3LYP and PMP2 predict the C6-hydroxylated product to be lower in energy (by 1.5 and 2.5 kcal/mol, respectively). Thus, both PMP2 and B3LYP single-point calculations indicate that the C5-hydroxylated radical is favored kinetically and the C6-hydroxylated product is favored thermodynamically.

Due to the magnitude of the transition barrier heights and the relative stability of the products, a mixture of the C5 and C6-hydroxylated radicals is expected, which was observed experimentally. However, since the barrier for formation of the C5-hydroxylated radical is approximately 2 kcal/mol lower in energy than that for formation of the C6-hydroxylated barrier, a predominant attack at the C5 position can be understood.

### *7.2.4 Summary of Cytosine Reactions*

The present section discussed the reactions between products generated by the irradiation of cytosine and water. Investigations of hydroxyl radical addition to cytosine and water addition to the cytosine cation provided information about the mechanism of radiation damage to cytosine in the gas phase. In particular, preliminary results indicate that in the gas phase, net hydroxyl radical addition to neutral cytosine is the most feasible reaction mechanism for formation of the cytosine C5-hydroxylated product. Comparison of theoretical and experimental HFCCs (Chapter Four) determined that the cytosine C5-hydroxylated radical is formed in these crystals. However, it was also speculated that addition might occur at the C6 position since one experimental coupling left unassigned was similar to that calculated for the C6-hydroxylated radical. Comparison of the calculated barrier heights and the relative stability of the products led to the conclusion that the C5-hydroxylated product is favored kinetically, while the C6-hydroxylated product is favored thermodynamically. Thus, the calculations support predictions that both hydroxylated products can be formed when hydroxyl radicals attack neutral cytosine.

### *7.3 Hydroxyl Radical Addition to Uracil*

It is of interest to investigate the barriers for hydroxyl radical addition in other DNA bases to obtain more information about the effects of the surrounding water on the entire DNA strand. Additionally, it is intriguing to determine whether theoretical techniques can reproduce differences observed experimentally regarding the site specificity of hydroxyl radical addition. Reactions between uracil and products generated from irradiated water have been investigated to a great extent. In particular, many studies have investigated the subsequent reactions of these by-products such as the formation of sugar radicals[22] and subsequent strand breaks.[23,24] The reactivity between uracil and hydroxyl radicals is expected to be similar to cytosine, where hydroxyl radicals add to the C5C6 double bond. ESR spin-trapping studies predict the ratio of C5 to C6 addition products to be 1:2 for 2'-deoxyuridine, compared to the value of 1:1.3 previously discussed for 2'-deoxycytidine.[3] Through examination of redox properties, other studies have indicated that addition to the C5 position dominates in uracil, 1,3-dimethyluracil and poly(U) in a 4.5:1, 4:1 and 3:1 ratio, respectively.[20] Recall from Section 7.2.4 that the C5:C6 ratio for cytosine was determined to be 8.7:1, which indicates an increase in the production of the C6-hydroxylated radical in uracil relative to cytosine. Hydroxyl radical addition to uracil will be discussed in the following section to determine if these differences can be explained and to reveal more information about hydroxyl radical addition to the nucleobases.

#### *7.3.1 Geometries*

Unlike the cytosine hydroxyl addition reactions, different reactant complexes were obtained at the HF/6-31G(d,p) level for uracil depending on the addition site. The RC for hydroxyl radical addition to C5 in uracil (Figure 7.6) involves interactions between the hydrogen and oxygen in the hydroxyl radical and the O4 and N3H positions in uracil, respectively. The HO4 and O-HN3 bond lengths are 1.997 and 2.267 Å, respectively, indicating stronger interactions between the hydroxyl group and the O4 position in uracil. The reactant complex for hydroxyl radical addition to C6 (Figure 7.7) involves interactions between the hydrogen and oxygen in the hydroxyl group and the O2 and N1H positions in uracil, respectively. The HO2 and O-HN1 bond lengths in this complex are equal to 2.013 and 2.193 Å, respectively. The calculated eigenvalue of $\langle S^2 \rangle$

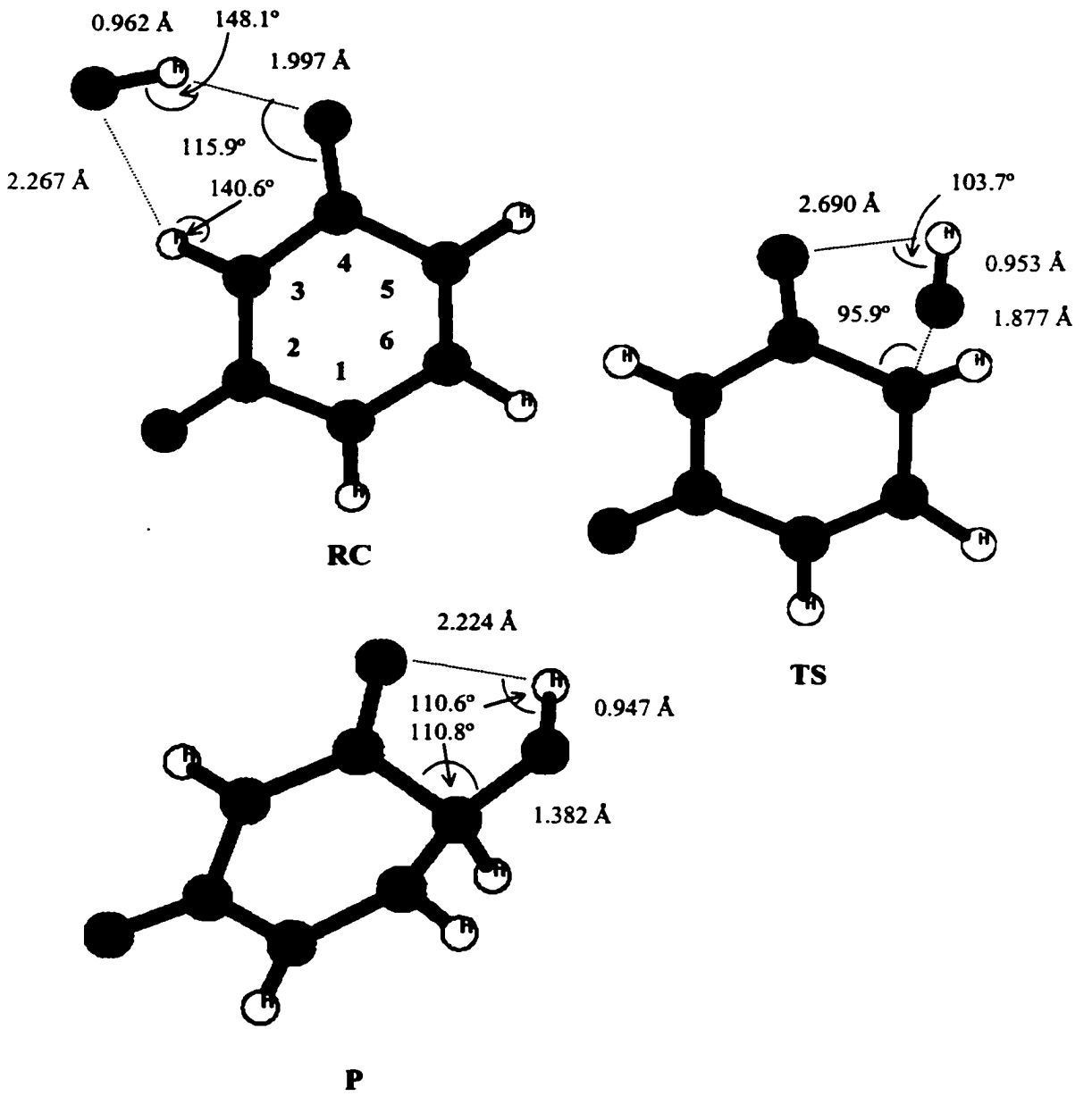


Figure 7.6: Select geometrical parameters for the RC, TS and P for hydroxyl radical addition to C5 in uracil.

is 0.755 for both addition complexes, and both are planar. Additionally, the bond length in the hydroxyl radical in both complexes (0.962 Å) is slightly elongated from that found in an isolated hydroxyl radical (0.955 Å) due to the interactions with uracil.

The transition states for hydroxyl radical addition to the C5 and C6 position in uracil explain the observed differences in the reactant complexes. The C5 centered TS possesses a C5O bond length of 1.877 Å and the hydrogen is directed away from the

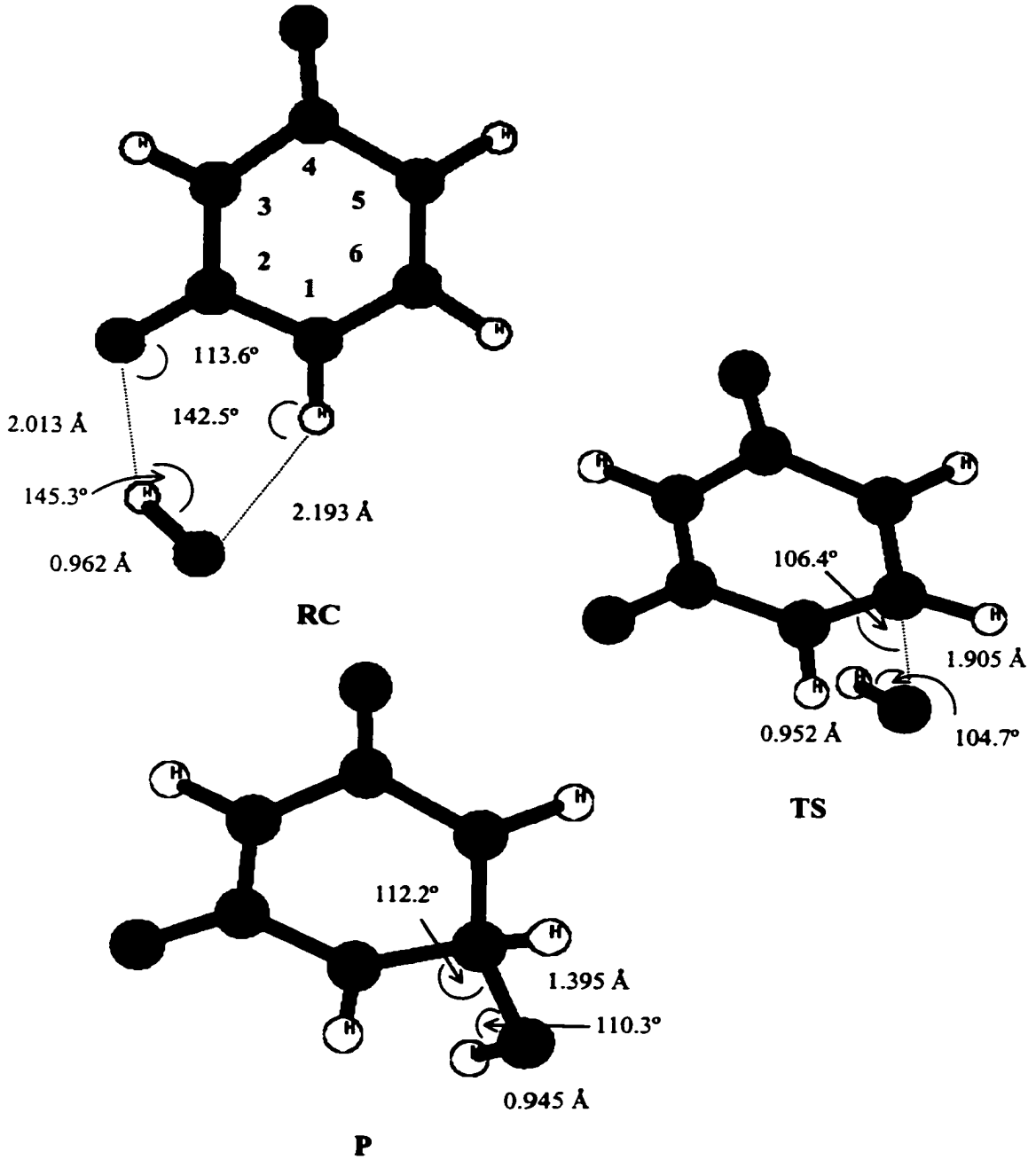


Figure 7.7: Select parameters for the RC, TS and P for hydroxyl radical addition to C6 in uracil.

molecular ring towards the O4 center. This orientation and the relatively close proximity of O4 and the hydroxyl hydrogen (2.690 Å) explain interactions observed in the addition complex between these two atoms. The C5 position is displaced slightly (12.4°) from a molecular plane formed by C4, N3 and C2. The C6 centered TS possesses a C6O bond length of 1.905 Å, which is longer than that observed for the C5 TS. This trend is similar

to that observed for cytosine. The C6 position in the uracil TS is located out of the molecular plane formed by the other ring atoms (by approximately 11°). A greater degree of spin contamination was obtained in the calculations of the C5 TS ($<S^2>$ = 0.998) than the C6 TS ($<S^2>$ = 0.883). Both geometries were confirmed to be TSs through a frequency analysis where the imaginary frequencies were determined to be 696 (C5 addition) and 731 $cm^{-1}$ (C6 addition).

The C5-hydroxylated radical is distorted to a greater extent than the corresponding TS, where the C6 and C5 positions are located on either side of the molecular plane formed by N1, C2, N3 and C4. The C5O bond length is 1.382 Å and the hydroxyl hydrogen is directed towards O4 where these two atoms are separated by 2.224 Å. The orientation of the hydroxyl group at C5 is slightly different from that observed in the TS, but illustrates the interaction between the hydrogen in this group and O4. A small degree of spin contamination was exhibited in this geometry optimization ($<S^2>$ = 0.763). The C6-hydroxylated product exhibits less puckering than the C5 product, as observed for the cytosine radicals. The C6 position is displaced slightly out of the molecular plane (by 7.4° with respect to the plane formed by N1, C2 and N3), the C6O bond length is 1.395 Å and the eigenvalue of $<S^2>$ is 0.813, which is larger than that calculated for the C5 product.

### *7.3.2 Reaction Barrier Heights*

Figure 7.8 compares the transition state barriers for hydroxyl radical addition to the C5 and C6 positions in uracil obtained through B3LYP/6-311G(2df,p) single-point calculations on the HF/6-31G(d,p) geometries. At this level of theory, the C5 and C6 RCs lead to a lowering of the energy by 9.1 and 9.9 kcal/mol with respect to the energy of the isolated reactants. The activation barriers for the two uracil addition reactions are very similar, where the barrier for C6 addition is 1 kcal/mol larger than that for C5 addition. Figure 7.8 also illustrates that the C6-hydroxylated product is 2.7 kcal/mol lower in energy than the corresponding C5 radical at this level of theory. The spin contamination in the energy calculations was relatively small, where the largest degree of contamination was observed for the transition states ($<S^2> \approx 0.77$).

The reaction profiles for hydroxyl radical addition to uracil can be compared to

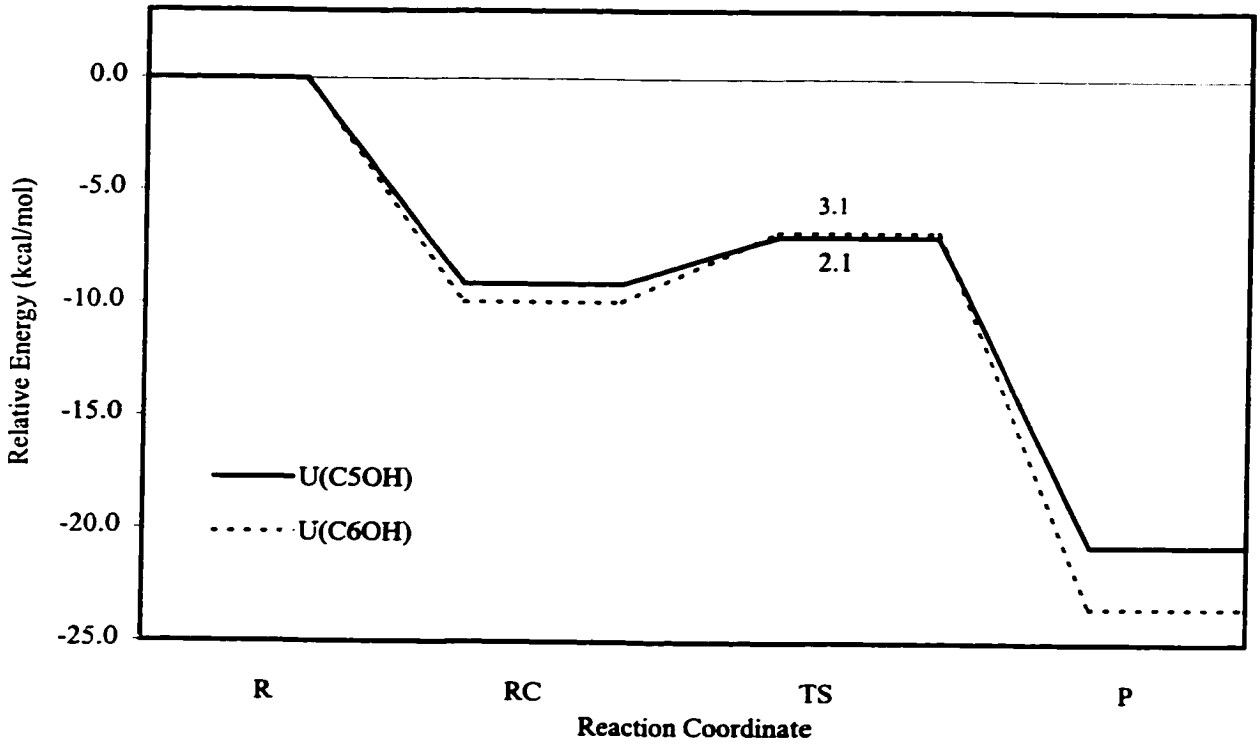


Figure 7.8: Relative energetics for hydroxyl radical addition to uracil calculated with B3LYP.

those calculated for cytosine (Figures 7.8 and 7.5, respectively). One of the major differences in the two sets of profiles is that two different addition complexes were found for hydroxyl radical addition to uracil, while only one was found for addition to cytosine. However, as previously mentioned, a more complete search may also reveal two different RCs for the cytosine reactions. Similarities in the two reaction profiles also exist. First, the RCs calculated for both uracil and cytosine lead to a lowering of the energy relative to the isolated reactants by approximately 10 kcal/mol. Secondly, the barrier for addition to the C6 position was determined to be higher in both cytosine and uracil (by 1.9 and 1.0 kcal/mol, respectively). Finally, the C6-hydroxylated product was determined to be lower in energy than the corresponding C5 radical in both cytosine and uracil (by 1.5 and 2.7 kcal/mol, respectively). Thus, the difference in the transition barriers for the formation of the two products formed by hydroxyl radical addition is smaller for uracil than for cytosine and the energy difference between the products is greater. This implies that there is a greater preference for addition to C6 in uracil than in cytosine, which is

clearly seen by comparing the ratio of product formation determined experimentally for uracil (C5:C6 4.5:1) and cytosine (8.7:1) by examining the redox properties of the radical products.

The trend of an increase in the production of the C6-hydroxylated product in uracil relative to cytosine is also observed from the C5:C6 ratio predicted from ESR spin-trapping studies for 2'-deoxyuridine (1:2) and 2'-deoxycytidine (1:1.3), although the relative yield is reversed. One possible explanation for the difference in the predominant site of attack determined for ESR spin-trapping studies (C6) and for the calculations (C5) is the model system employed. For example, the ESR spin-trapping studies were performed on 2'-deoxyuridine, but the calculations were performed on uracil. The discrepancy arises since a hydrogen bond was calculated to exist in the RC between the hydroxyl radical and the O2 and the hydrogen at the N1 position in uracil. This is problematic since in 2'-deoxyuridine, a sugar group replaces the hydrogen at N1. Thus, hydrogen bonding of the hydroxyl radical to the N1 hydrogen cannot occur. Additionally, the bulky sugar group may prohibit the hydroxyl radical from hydrogen bonding to the O2 position. More work must be performed in order to transfer conclusions obtained in the present study to full DNA, for example, finding alternative RCs and/or adding substituents to the N1 position of uracil.

### *7.3.3 Summary of Uracil Reactions*

Hydroxyl radical addition to the C5 and C6 positions in uracil was discussed in the current section. The geometries of the RC, TS and P were compared to those previously considered for cytosine. Similar to cytosine, the activation barrier for the formation of the uracil C6-hydroxylated radical is larger than that for the C5 adduct, while this product is lower in energy than the C5 analog. However, it is noted that the barrier for addition to C6 in uracil is closer to the barrier for C5 addition, than the corresponding barriers in cytosine. Additionally, the C6-hydroxylated uracil radical is more stable with respect to the C5 uracil radical, than the C6-hydroxylated cytosine radical is to the corresponding C5 adduct. This information was used to conclude that there exists a greater preference for C6 addition in uracil than in cytosine. This conclusion is supported by experiments that studied the redox properties of the radical products, as well as ESR spin-trapping investigations.

### *7.4 Hydroxyl Radical Addition to Thymine*

Hydroxyl radical addition to thymine has been noted to be different than addition to either uracil or cytosine. The replacement of a hydrogen at the C5 position in uracil with a methyl group in thymine results in two main differences. First, hydroxyl radicals can abstract hydrogen atoms from the methyl group in thymine to form the methyl-dehydrogenated radical product. The formation of this allylic radical has been shown to lead to cross-links between thymine and the amino acid tyrosine.[2b] Secondly, it has been noted that the preference of radical attack on the C5 and C6 centers is altered relative to the attack observed in cytosine and uracil. ESR spin-trapping studies predict that the ratio of C5:C6 products will be 2:1 in thymidine, compared to 1:2 for 2'-deoxyuridine, indicating an increase in the number of attacks at the carbon to which the methyl group is attached.[3] Other studies predict that the methyl group leads to a decrease in the number of attacks at the C5 position. For example, the C5:C6 ratio determined by studying the redox properties of the radical products changes from 4.5:1 to 2:1 when a methyl group is added to C5 in uracil to form thymine.[24] Thus, it is of interest to investigate hydroxyl radical addition in attempts to clarify some of these discrepancies and to determine if differences exist between uracil and thymine due to the replacement of a hydrogen by a methyl group.

#### *7.4.1 Geometries*

Similar to the uracil addition reactions, unique reactant complexes were found for the thymine C5 and C6 hydroxyl radical addition reactions (Figures 7.9 and 7.10). These reactant complexes possess very similar geometrical properties to those observed for the uracil RCs. For example, the RC related to C5 addition involves interactions between the hydroxyl hydrogen and oxygen and the thymine O4 and N3H positions. Additionally, the RC related to C6 addition involves interactions between the hydroxyl hydrogen and oxygen and the thymine O2 and N1H positions. These hydrogen bond lengths are indistinguishable from those discussed for the corresponding uracil RCs.

The C5 addition TS exhibits slight puckering at the C5 position, while the remainder of the ring atoms are in the same plane. The C5O bond distance is 1.906 Å, which is slightly larger than the C5O distances observed in the corresponding uracil and cytosine transition states. The hydrogen in the hydroxyl group is orientated towards O4

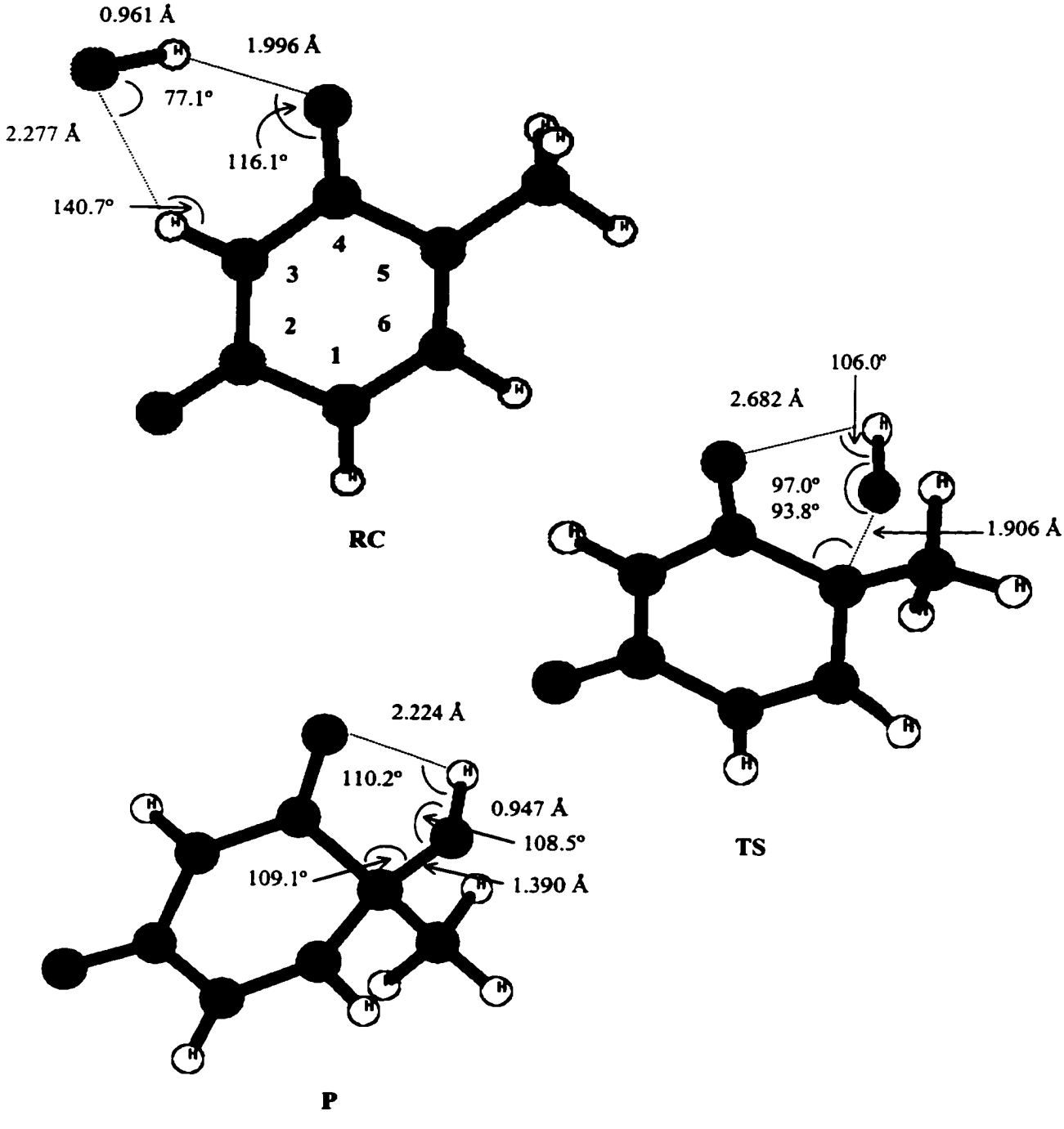


Figure 7.9: Select geometrical parameters in the RC, TS and P for hydroxyl radical addition to C5 in thymine.

as predicted from the RC, where the HO4 distance is 2.682 Å. The methyl group is reoriented slightly from an eclipsed conformation with respect to the C5C6 bond in the TS due to interactions with the hydroxyl group. The C6O distance in the C6 related

transition state is 1.929 Å, which is longer than that observed for the C5 TS and slightly longer than those observed for the C6 TS in uracil and cytosine. It is interesting to note that for all three bases, the CO bond length for the C6 addition TS is longer than that in the C5 addition TS. The hydroxyl hydrogen is directed towards the center of the

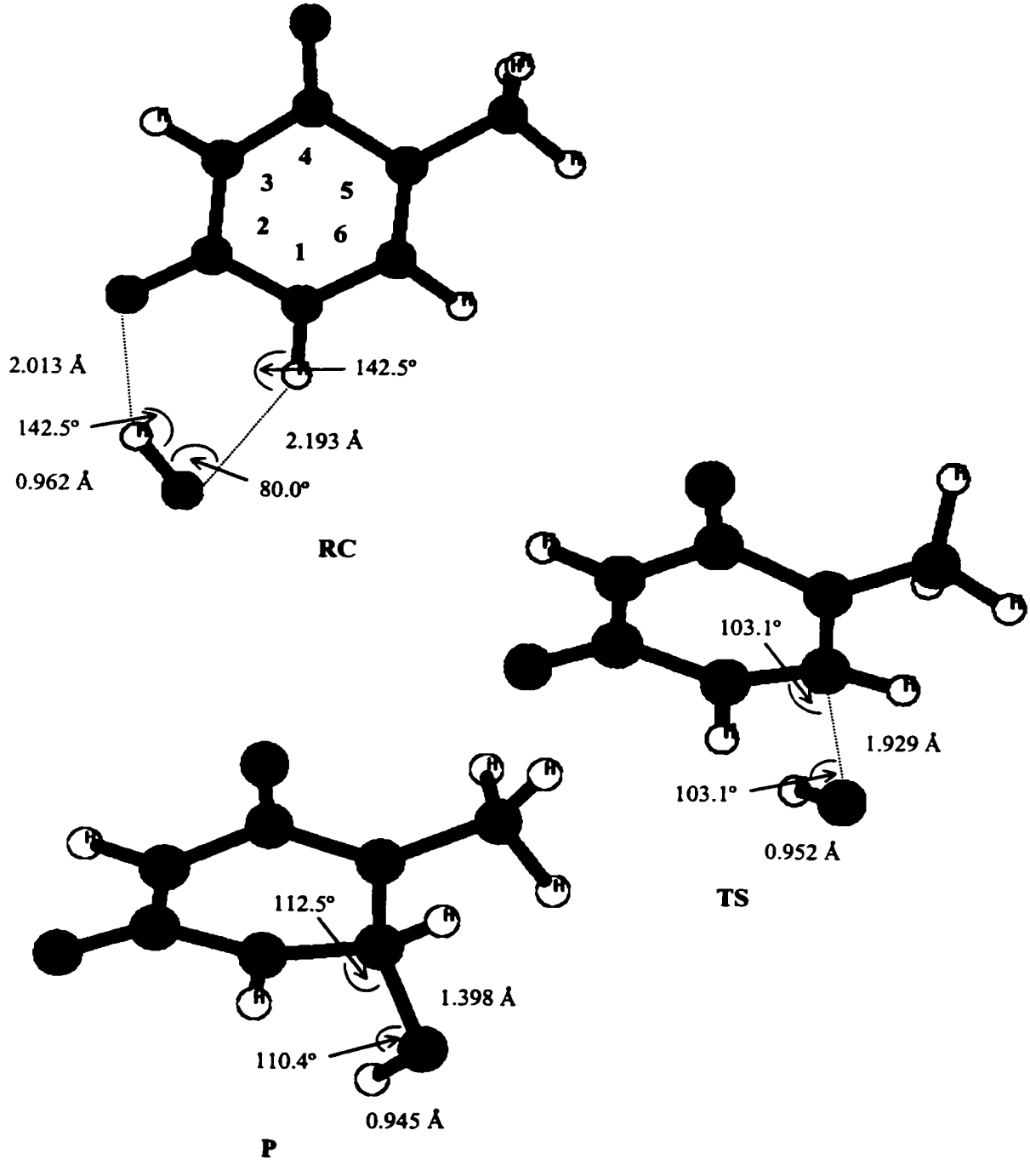


Figure 7.10: Select geometrical parameters in the RC, TS and P for hydroxyl radical addition to C6 in thymine.

molecular ring in the C6 related TS and the C6 position is approximately 10° out of the molecular plane formed by the remainder of the ring atoms. The spin contamination exhibited for the thymine transition states is the largest discussed thus far for hydroxyl radical addition, where the eigenvalues of $<S^2>$ equal 1.024 and 1.018 for the C5 and C6 related transition states, respectively. These geometries were concluded to be TSs through examination of the Hessian matrix which possesses one negative eigenvalue corresponding to an imaginary frequency of 654 and 683 $cm^{-1}$ for the C5 and C6 related TSs, respectively.

The thymine C5-hydroxylated radical possesses an orientation of the hydroxyl group very similar to that discussed for the corresponding uracil radical. In particular, the hydroxyl hydrogen is directed towards O4, where the HO4 distance is 2.224 Å. The C5O bond length (1.390 Å) is also very similar to that discussed for the uracil product. The C6-hydroxylated thymine radical exhibits puckering at the C6 position, where this atom is approximately 12.5° out of the plane formed by the remainder of the ring atoms. The corresponding uracil radical is planar. The deviation of the thymine radical from planarity could be due to the methyl group at C5. The hydroxyl hydrogen is directed towards the center of the ring in the C6-hydroxylated product and the C6O distance is 1.398 Å. The spin contamination in the optimization of the C6 product ($<S^2> = 0.805$) is greater than that observed previously for both the related uracil and cytosine products and for the thymine C5 adduct ($<S^2> = 0.763$).

### *7.4.2 Reaction Barrier Heights*

Figure 7.11 displays the reaction barrier heights predicted by B3LYP/6-311G(2df,p) single-point calculations on the HF/6-31G(d,p) geometries. The energy of the isolated reactants is lowered upon consideration of the RC by 8.9 and 9.9 kcal/mol for the C5 and C6 addition profiles, respectively. B3LYP predicts the transition barrier for hydroxyl radical addition to C5 in thymine to be 2.4 kcal/mol, while the barrier is only 1.8 kcal/mol for C6 addition. Additionally, the C6-hydroxylated product is predicted to be 6.2 kcal/mol lower in energy than the C5 adduct.

Despite the fact that the stability observed for the RCs relative to the isolated reactants is similar in all systems, several differences between the thymine reaction

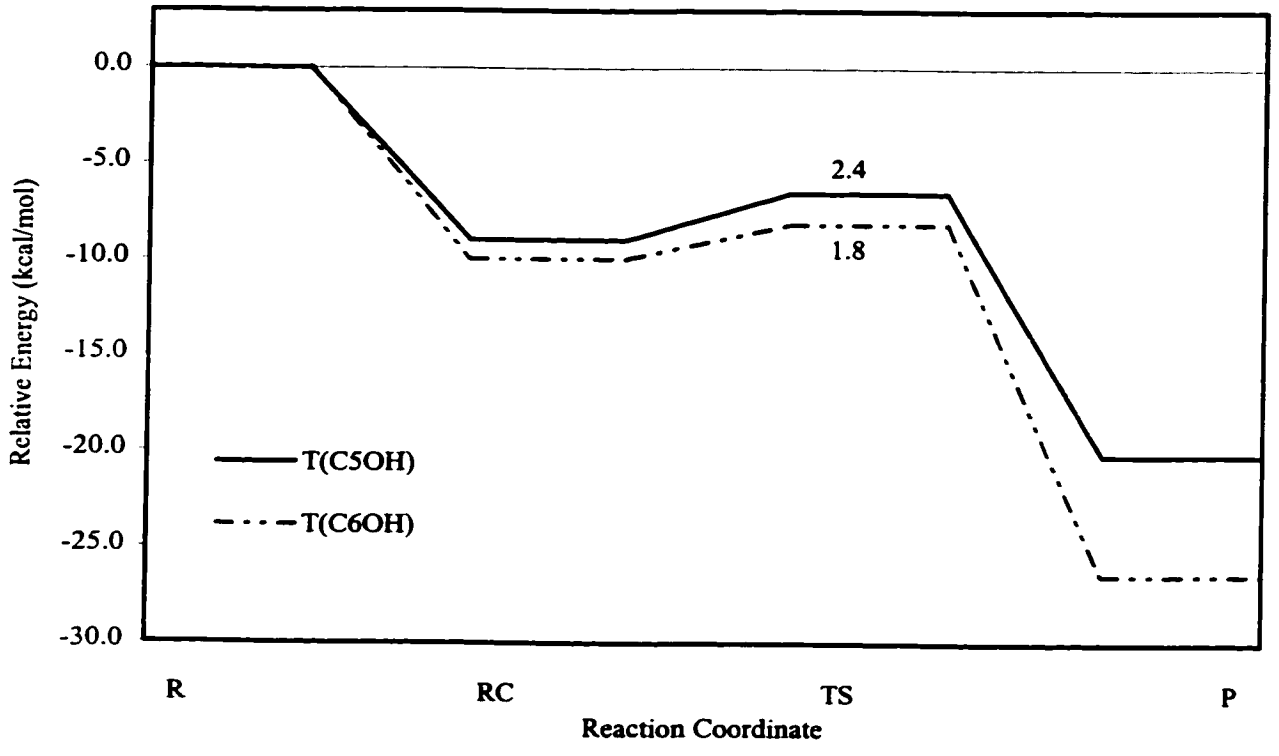


Figure 7.11: Relative energetics for hydroxyl radical addition to thymine calculated with B3LYP.

profiles and those discussed for uracil and cytosine exist. First, the transition barriers for C5 addition were determined to be smaller than the C6 barrier for uracil and cytosine, but the converse was obtained for thymine. Thus, from a kinetic point of view the C6-hydroxylated product is favored rather than the C5 species as determined for uracil and cytosine. For all three bases, the C6-hydroxylated radical was determined to be lower in energy than the C5 product, indicating this product is favored thermodynamically. However, for uracil and cytosine this energy difference was much smaller (2.7 and 1.6 kcal/mol, respectively) than the difference calculated for thymine (6.2 kcal/mol). These differences in the uracil, cytosine and thymine reaction profiles indicate that there exists an even greater preference for addition to C6 in thymine, as predicted by examination of the redox properties of the hydroxylated radicals.

As for uracil, the conclusions within contradict ESR spin-trapping studies, which predicted the C5 and C6 products to be formed in a 2:1 ratio in thymidine, compared to 1:2 for 2'-deoxyuridine.[3] Once again, discrepancies may arise due to the geometries

calculated for the RCs, where the hydrogen bonding observed in the calculations cannot occur in the experiments due to the presence of a sugar group. A more complete investigation of substituent effects on the reaction between hydroxyl radicals and thymine and complete characterization of reactant complexes are required to clarify these discrepancies.

### *7.4.3 Summary of Thymine Reactions*

In the present section, the reactions involving hydroxyl radical addition to the thymine C5C6 double bond were investigated. The geometries of the RC, TS and P were discussed and compared to those calculated for uracil. Great similarities were observed in the uracil and thymine geometries along the reaction pathway. Comparison of the reaction barriers for C5 and C6 hydroxyl radical addition to thymine leads to conclusions different from those reached for uracil and cytosine. For thymine, the C6-hydroxylated product is favored both kinetically (due to the lower barrier height) and thermodynamically (due to the 6.2 kcal/mol greater stability of this product relative to the C5 adduct). The differences in the reaction profiles of thymine, uracil and cytosine indicate that the methyl group stabilizes the TS involved in hydroxyl radical addition to the C6 position and, therefore, addition to this position in favored. This trend is in agreement with studies investigating the redox properties of hydroxylated base radicals.

## *7.5 Conclusions*

The present chapter investigated reactions between water (or products generated from irradiation of water) and the DNA bases. Initially a study was performed on reactions involving cytosine in order to obtain more information about the mechanism of radiation damage in cytosine monohydrate crystals. Hydroxyl radical addition to neutral cytosine and water addition to the cytosine cation were investigated in terms of addition to the C5 position. It was determined that for the gas-phase reactions, hydroxyl radical addition to neutral cytosine appears to be the most feasible mechanism for the formation of the C5-hydroxylated cytosine radical. These results are not directly transferable to cytosine monohydrate crystals due to detailed hydrogen bonding in the crystals. More complex model systems must be used in order to determine the radiation damage mechanism in these crystals.

Once hydroxyl radical addition was determined to be the main pathway for hydroxylated radical formation, alternative hydroxylated products were investigated. Foremost hydroxyl radical addition to the C6 position in cytosine was investigated to determine if addition to this position is also feasible. The C5-hydroxylated product was determined to be favored kinetically (by approximately 1.9 kcal/mol) and the C6-hydroxylated product favored thermodynamically (by approximately 1.6 kcal/mol). Therefore, it was concluded that hydroxyl radical addition will occur to a greater extent at the C5 position, due to the 2 kcal/mol lower transition barrier, but addition will also occur at the C6 position due to the greater thermodynamic stability of this product.

Hydroxyl radical addition to the C5 and C6 positions in uracil and thymine were also investigated and the results were compared to those obtained for cytosine. In uracil, as in cytosine, it was determined that the C5-hydroxylated product is favored kinetically (by 1.0 kcal/mol), while the C6-hydroxylated product is favored thermodynamically (by 2.7 kcal/mol). Due to energetics differences, relative to the cytosine reactions, it was concluded that the C6-hydroxylated product will be formed to a greater extent in uracil than in cytosine. This trend was observed experimentally where the C5:C6 ratio was determined to be 8.7:1 and 4.5:1 when cytosine and uracil were examined, respectively, in terms of the radical's redox properties. Alternatively, the thymine C6-hydroxylated product was calculated to be favored both kinetically and thermodynamically. Since the barrier heights were reversed relative to uracil and cytosine and the thymine C6-hydroxylated adduct has a greater stability over the C5 radical than observed for the cytosine and uracil products, it was concluded that the methyl group in thymine leads to favored addition to the C6 position. This conclusion is once again supported by the experimental ratios for C5:C6 hydroxyl radical addition which were determined to be 4.5:1 and 2:1 for uracil and thymine, respectively. Discrepancies between these conclusions and those obtained in alternative experimental studies were determined to be due to differences in the model systems employed and more detailed studies were proposed.

It should be noted that these calculations were performed as an initial investigation of the reactions between water and the DNA bases, in terms of an optimization at a low level of theory followed by higher level single-point calculations.

Despite this fact, the relative energetics of the C5 and C6-hydroxylated products are in good agreement with those calculated in Chapter Four through optimization of the geometries with DFT followed by higher level DFT single-point calculations. This indicates that although this work represents an initial study, the results appear to be trustworthy. More work remains to be done, however, including calculations which confirm the relationship between the reactant complexes, the TSs and the products.

### *7.6 References*


1. Catterall, H.; Davies, M. J.; Gilbert, B. C. *J. Chem. Soc. Perkin Trans.* **1992**, *2*, 1379.

2. (a) Gajewski, E.; Dizdaroglu, M. *Biochem.* **1990**, 29, 977; (b) Dizdaroglu, M.; Gajewski, E.; Reddy, P.; Margolis, S. A. *Biochem.* **1989**, 28, 3625.

3. Davies, M. J.; Gilbert, B. C.; Hazlewood, C.; Polack, N. P. *J. Chem. Soc. Perkin Trans.* **1995**, *2*, 13.

4. Hiraoka, W.; Kuwabara, M.; Sato, F.; Matsuda, A.; Ueda, T. *Nucleic Acid Res.* **1990**, *18*, 1217.

5. Téoule, R. *Int. J. Radiat. Biol.* **1987**, 51, 573.

6. Llano, J.; Eriksson, L. A. *J. Phys. Chem. B* **1999**, *in press.*

7. Johnson, B. G.; Gonzales, C. A.; Gill, P. M. W.; Pople, J. A. *Chem. Phys. Lett.* **1994**, *221*, 100.

8. Sekušak, S.; Güsten, H.; Sabljic, A. *J. Chem. Phys.* **1995**, *102*, 7504.

9. Melissas, V. S.; Truhlar, D. G. *J. Phys. Chem.* **1994**, *98*, 875.

10. Gonzalez, C.; McDouall, J. J. W.; Schlegel, H. B. *J. Phys. Chem.* **1990**, *94*, 7467.

11. McKee, M. L. *J. Phys. Chem.* **1993**, *97*, 10971.

12. Alvarez-Idaboy, J.; Díaz-Acosta, I.; Vivier-Bunge, A. *J. Comp. Chem.* **1998**, *19*, 811.

13. (a) Martell, J. M.; Mehta, A. K.; Pacey, P. D.; Boyd, R. J. *J. Phys. Chem.* **1995**, *99*, 8661; (b) Martell, J. M.; Boyd, R. J. *J. Phys. Chem.* **1995**, *99*, 13402.

14. Frisch, M. J.; Trucks, G. W.; Schlegel, H. B.; Gill, P. M. W.; Johnson, B. G.; Robb, M. A.; Cheeseman, J. R.; Keith, T. A.; Petersson, G. A.; Montgomery, J. A.;

Raghavachari, K.; Al-Laham, M. A.; Zakrzewske, V. G.; Ortiz, J. V.; Foresman, J. B.; Cioslowski, J.; Stefanov, B. B.; Nanayakkara, A.; Challacombe, M.; Peng, C. Y.; Ayala, P. Y.; Chen, W.; Wong, M. W.; Andres, J. L.; Replogle, E. S.; Gomperts, R.; Martin, R. L.; Fox, D. J.; Binkley, J. S.; Defrees, D. J.; Baker, J.; Stewart, J. P.; Head-Gordon, M.; Gonzalez, C.; Pople, J. A. *Gaussian 94* (Revision B.2); Gaussian, Inc.: Pittsburgh, PA, 1995.

15. Gonzales, C.; Soza, C.; Schlegel, H. B. *J. Phys. Chem.* **1989**, *93*, 2435.

16. Gill, P. M. W. *Mol. Phys.* **1996**, *89*, 433.

17. Frisch, M. J.; Trucks, G. W.; Schlegel, H. B.; Scuseria, G. E.; Robb, M. A.; Cheeseman, J. R.; Zakrzewski, V. G.; Montgomery, J. A., Jr.; Stratmann, R. E.; Burant, J. C.; Dapprich, S.; Millam, J. M.; Daniels, A. D.; Kudin, K. N.; Strain, M. C.; Farkas, O.; Tomasi, J.; Barone, V.; Cossi, M.; Cammi, R.; Mennucci, B.; Pomelli, C.; Adamo, C.; Clifford, S.; Ochterski, J.; Petersson, G. A.; Ayala, P. Y.; Cui, Q.; Morokuma, K.; Malick, D. K.; Rabuck, A. D.; Raghavachari, K.; Foresman, J. B.; Cioslowski, J.; Ortiz, J. V.; Stefanov, B. B.; Liu, G.; Liashenko, A.; Piskorz, P.; Komaromi, I.; Gomperts, R.; Martin, R. L.; Fox, D. J.; Keith, T.; Al-Laham, M. A.; Peng, C. Y.; Nanayakkara, A.; Gonzalez, C.; Challacombe, M.; Gill, P. M. W.; Johnson, G.; Chen, W.; Wong, M. W.; Andres, J. L.; Gonzalez, C.; Head-Gordon, M.; Replogle, E. A.; Pople, J. A. *Gaussian 98* (Revision A.4),Gaussian, Inc., Pittsburgh PA, 1998.

18. Wala, M.; Bothe, E.; Görner, H.; Shulte-Frohlinde, D. *J. Photochem. Photobiol. A, Chemistry* **1990**, *53*, 87.

19. (a) Becker, D.; La Vere, T.; Sevilla, M. D. *Radiat. Res.* **1994**, *140*, 123; (b) LaVere, T.; Becker, D., Sevilla, M. D. *Radiat. Res.* **1996**, *145*, 673.

20. Hayon, E.; Simic, M. *J. Am. Chem. Soc.* **1973**, 95, 1029; Simic, M.; Hayon, E. *Int. J. Radiat. Biol.* **1972**, 22, 507.

21. von Sonntag, C.; Schuchmann, H.-P. *Int. J. Radiat. Biol.* **1986**, *49*, 1 *and references therein.*

22. Hildenbrand, K.; Behrens, G.; Schulte-Frohlinde, D.; Herak, J.N. *J. Chem. Soc. Perkin Trans* **1989**, *2*, 283.

23. Catterall, H.; Davies, M. J.; Gilbert, B. C. *J. Chem. Soc. Perkin Trans* **1992**, *2*, 1379.

24. Hildenbrand, K.; Schulte-Frohlinde, D. *Int. J. Radiat. Biol.* **1989**, *55*, 725.

# CHAPTER EIGHT

## DNA Radiation Products

### *8.1 Introduction*

The previous four chapters have discussed the effects of radiation on individual DNA components in relation to experimental results obtained from single crystals of base derivatives at low temperatures. Issues can now be addressed which question the relevance of these studies to the identification of the radiation products in full DNA. Early ESR work on DNA revealed that the classification of radiation products is a difficult task. In particular, the first derivative of the absorption of DNA closely resembles an extremely broad singlet, which indicates that there exists overlapping of the spectra for each radical. This occurs since the DNA radicals are extremely similar and therefore the hyperfine couplings and g-factors are not sufficient to separate their spectra. This chapter will discuss some of the trials and tribulations confronted by experimental attempts to study the full DNA strand. This discussion will include a background of the methods available to study the radiation effects on a molecule as complex as DNA. In addition, the products identified in both early and more recent experimental work will be analyzed and the effects of water on DNA radiation damage will be considered. All of this information, in addition to results obtained from single-crystal studies and calculations, will be used to develop a picture of the effects of radiation on the entire DNA strand.

### *8.2 Experimental Methods Available to Study DNA*

Studies have been performed on DNA both in the dry state and in aqueous solutions.[1] Frozen aqueous solutions are often investigated and the effects of radiation on these samples are quite complicated. Specifically, in addition to the formation of DNA radicals upon exposure to radiation ("direct" effects), solvent (water) radicals can be generated. These solvent radicals can also give rise to base or sugar radicals by attacking the DNA strand ("indirect" effects). Thus, the spectrum of an irradiated frozen aqueous solution is a superposition of the spectra of DNA and water radicals (primarily hydroxyl radicals, hydrogen atoms and aqueous electrons). Since the hydroxyl radical is unstable

at temperatures above 110 K, the spectrum of frozen aqueous solutions can be simplified by annealing. Low temperature glasses have also been employed on occasion to investigate full DNA. Typically these glasses are produced using saturated solutions of LiCl or $BeF_2$ in $H_2O$. The advantage of using low temperature glasses is that reactive radicals can be stabilized and the specificity of a reaction can be studied by carefully selecting the glass-forming agent. For example, hydroxyl radicals are known to be abundant in $BeF_2$ glasses, electrons in LiCl glasses or in the presence of strong bases (NaOH) and hydrogen atoms in strong acids ($H_2SO_4$). Lyophilized (freeze-dried) powders are often used to study the effects of radiation on the DNA strand, where the powders have been prepared completely dry or with varying degrees of hydration. The relative humidity (typically 76%) or the number of water molecules per nucleotide (typically 2.5 to 11) characterize the level of hydration.

The methods discussed thus far yield a random orientation of the DNA molecules and therefore the resulting spectrum is composed of an overlap of the spectrum of each radical in all directions. These "powder" spectra are very broad and lack distinguishing features. If the individual spectrum of each radical is nearly isotropic, then information can be obtained from the powder spectra. However, if anisotropy exists in the hyperfine couplings, then the resulting fine features will be smeared in the powder spectrum and information will be lost. Ideally, single-crystal studies would be beneficial, but it is not possible to prepare these samples for an entire DNA strand. A common approach to these problems is to use orientated fibers to study irradiated DNA, which are normally equilibrated at 76% relative humidity. Orientated fibers have an advantage over other methods since the spectra can be monitored at two orientations of the fiber (perpendicular and parallel) relative to the magnetic field. This allows for the identification of some species that may not be observable in randomly orientated samples.

Additional tactics used by experimentalists investigating DNA include implementing deuterated samples, for example replacing $H_2O$ with $D_2O$, to improve spectral resolution or identify radical products. Alternatively, additives can be included in the sample to improve the spectra. For example, electron scavengers, most commonly $FeCl_3$ or $K_3[Fe(CN)_6]$, have been used to obtain valuable information about electron loss centers. In addition, the spectrum with and without scavengers can be subtracted to yield

information about products formed through electron gain. Thermal annealing is also a very useful tool to differentiate between products. Annealing experiments provide information about lines which decay together and therefore represent one or more related species. Alternatively, information can be obtained about the relationship between the decay of one product and the growth of another. In addition, the spectrum of DNA can be compared to the spectra of base derivatives to identify products. Once a product has been identified, its spectrum can be subtracted from the spectrum of full DNA for further simplification. Computer simulations are often performed that use experimentally derived parameters (for example, HFCCs) for the speculated radical products to model the full DNA spectrum. Information is obtained by adjusting the parameters until a best fit is obtained between the simulated and experimental spectra.

Through all of these techniques, information about the radicals generated in irradiated DNA can be obtained. The implementation of a variety of experimental conditions allows for the determination of the dependence of radical formation on the environment (for example, strand conformation, hydration level, $O_2$ content). Despite great efforts put forth by experimentalists, the exact identity of most radical products is still unknown. However, advances have been made in the last few years and some products have been confidently identified. The next section will be dedicated to a discussion of the radicals identified thus far in studies on the full DNA strand.

## *8.3 Initial Characterization of Radicals Generated in DNA*

### *8.3.1 Electron Gain and Loss Centers*

The first experimental work on full DNA emphasized the formation of a radical speculated to be derived from thymine.[2,3] In these studies, the similarity between the recorded spectra of DNA and thymine or thymidine was used to predict the formation of a thymine radical. Salovey *et al.* postulated that the detected radical possesses a fragment of the form $-^{\bullet}C(CH_3)-CH_2-$, which would correspond to a thymine centered radical since only thymine possesses a methyl group.[3] Work performed on DNA irradiated by ultraviolet light confirmed that the recorded octet pattern arises from a radical formed through hydrogen atom addition to C6 in thymine [**T(C6H)**, Figure 8.1].[4] Studies performed on orientated fibers also predicted that considerable amounts of **T(C6H)** is

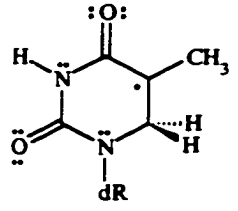

**T(C6H)**

Figure 8.1: The first radical identified in irradiated DNA: the thymine C6-hydrogenated radical.

formed.[5] The definitive identification of a thymine radical product led to the conclusion that the thymine anion ($T^{\bullet-}$) must be initially formed in irradiated DNA, which was proven shortly thereafter.[6] Following these studies identifying thymine as a damage site, little progress was made to classify additional radiation products in full DNA for years, although work continued on single crystals of base derivatives and other DNA subunits.

The model of radiation damage to DNA was greatly enhanced through work performed on orientated fibers by Gräslund and coworkers.[7,8,9] Radicals identified in these studies were determined to have ionic character with delocalized π-spin density, and therefore were most probably base centered radicals. The radical mixture generated in DNA was suggested to be composed of thymine (and/or cytosine) anions and guanine (and/or cytosine) cations.[7] The initial assumption that cytosine may also be damaged was discarded[9] and the picture of radiation damage in DNA resulting in $T^{\bullet-}$ and guanine cations ($G^{\bullet+}$) became known as the "two-component" model (Figure 8.2). Primarily, the facts that the anionic radical converts to **T(C6H)** and that products generated from cytosine anions were not observed were used to favor $T^{\bullet-}$ as the primary anion. The two-

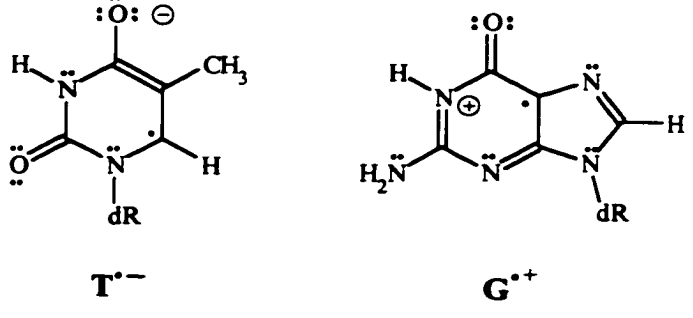

$T^{\bullet-}$ $G^{\bullet+}$

Figure 8.2: The primary radical products generated according to the two-component model for DNA radiation damage.

component model was often criticized since it was believed that insufficient proof was available to support this mechanism for DNA radiation damage.[10,11] Alternatively, the evidence supporting the model continued to grow.[12]

Cullis and coworkers[13] alluded that the two-component model for damage to DNA seems surprising since ionizing radiation damages indiscriminately. Thus, initial electron gain and loss centers should include water, the phosphate group, the sugar moiety and all four bases. Major criticism of the two-component model for radiation damage in DNA arose since the spectrum assigned to $\mathbf{T}^{\bullet-}$ is in poor agreement with that obtained from single-crystal studies.[10] In addition, the cytosine anion ($\mathbf{C}^{\bullet-}$, Figure 8.3) yields a doublet with couplings approximately equal to those of $\mathbf{T}^{\bullet-}$. This indicates that it will be difficult to distinguish between these two species and perhaps cytosine is also a site for radiation damage.

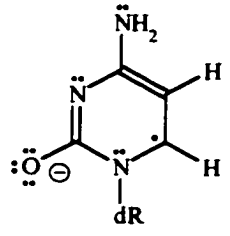


$\mathbf{C}^{\bullet-}$

Figure 8.3: The third radical identified as a major radiation damage product: the cytosine anion.

Additional support for a wider range of damage to DNA than the sole production of $\mathbf{T}^{\bullet-}$ and $\mathbf{G}^{\bullet+}$ began to appear in the literature. Bernhard and coworkers determined that $\mathbf{C}^{\bullet-}$ is the predominant electron gain radiation product in low temperature glasses of oligonucleotides[14] and that it may also be the major anion generated in DNA.[15] Sevilla *et al.*[16] investigated the products in irradiated DNA through the use of computer analysis and determined that $\mathbf{C}^{\bullet-}$ is generated to a greater extent (77% of all anions) than $\mathbf{T}^{\bullet-}$ (23%) at 100 K. The use of computer simulations was later cautioned, however, since the spectra of these two species are so similar that slight changes in the simulation input can yield very different percentages.[13] More evidence to support the favored formation of $\mathbf{C}^{\bullet-}$ in DNA was obtained in a study of the one-electron reduction potentials of the bases in aqueous solutions.[17] Since the rate of reduction of $\mathbf{T}^{\bullet-}$ was dependent on the pH and that

of $C^{\bullet-}$ was not dependent on the pH, it was determined that $C^{\bullet-}$ is protonated. This indicates that $C^{\bullet-}$ has a greater tendency to be protonated by its base pair guanine than thymine by adenine. This can be understood since the cytosine-guanine base pair takes part in three hydrogen bonds, while the thymine-adenine base pair involves only two hydrogen bonds. Thus, cytosine has the ability to accept one net proton and cytosine should be the most easily reduced base in DNA. In addition, the spectrum assigned to $T^{\bullet-}$ in nondeuterated DNA samples did not change upon deuteration (specifically at C5-$CH_3$ and C6H), indicating that some other species must be responsible for the spectrum,[18] possibly $C^{\bullet-}$.

Cullis *et al.*[13] examined strand-breaks in DNA in order to determine if they occur to a greater extent at positions next to thymine or guanine as predicted by the two-component model. It was concluded that strand-breaks are not site-specific and therefore all possible sites are damaged in DNA. More importantly, this indicates that $T^{\bullet-}$ and $C^{\bullet-}$ should be initially present in comparable amounts. Additional evidence suggesting that cytosine is the predominant electron gain center was obtained from studies on frozen samples of both single and double-stranded DNA.[19] It was determined that in single-stranded DNA $T^{\bullet-}$ slightly prevails whereas in double-stranded DNA the production of $C^{\bullet-}$ predominates. The explanations for this difference include interstrand base-pairing and base-stacking effects, which allow electrons to travel to more stable positions in double-stranded DNA.

A debate over the site of electron loss in DNA has also appeared in the literature. This controversy was initiated when it was noted that the spectra of $G^{\bullet+}$ recorded in solid-state studies of nucleotides and nucleosides did not correspond to the spectrum recorded in full DNA.[20] From computer analyses, Sevilla *et al.*[16] determined that over 90% of the cations generated in DNA are centered on guanine implying that hole transfer from adenine to guanine is complete in double-stranded DNA. Through investigations of the strand-break specificity, Cullis *et al.*[13] determined that some adenine cations could be generated. In a more recent study, guanine end products accounted for 90% of the electron loss products indicating that if holes are initially formed on adenine, or even thymine or cytosine, they are quickly transferred to guanine.[21] These studies support the two-component model in that the vast majority of the cations formed in irradiated DNA

are guanine centered. However, the results add the new dimension that it is also possible for other (adenine, $A^{\bullet+}$, Figure 8.4) cations to be formed.

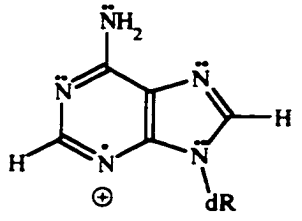


$A^{\bullet+}$

Figure 8.4: The adenine cation, which may also be a product in irradiated DNA.

From the above studies, it can be concluded that radiation damage in DNA is less specific than initially assumed by the two-component model. More precisely, radical centers on all four DNA bases can be expected upon irradiation of full DNA. The relative abundance of $C^{\bullet-}$, $T^{\bullet-}$, $G^{\bullet+}$ and $A^{\bullet+}$ in double-stranded DNA at 100 K is approximately 42, 17, 38 and 3%, respectively, with no substantial amounts of the pyrimidine cations or the purine anions.[19] It is interesting to note that base anion formation is favored over base cation formation in a 1.4:1 ratio. This is realistic since although equal numbers of cations and anions must be initially formed upon irradiation, the relative degrees of radical stabilization do not have to be equivalent. However, it can be speculated that this could also indicate that positive centers are formed elsewhere and have been left undetected (for example, on the sugar phosphate backbone as to be discussed in a later section).

### *8.3.2 Theoretical Predictions of Electron Gain and Loss Centers*

More information about the specificity of electron gain and loss in DNA can be obtained by calculating the ionization potentials and the electron affinities of the bases. The ionization potentials have been previously calculated with MP2 single-point calculations on HF geometries.[22] Table 8.1 compares the IPs for the nucleobases obtained experimentally, with MP2 and with DFT (B3LYP calculations presented in Chapters Four and Five). It can be seen that the theoretical data is in good agreement with the experimental results. In particular, all three sets of data predict the magnitude of the ionization potential to follow the trend T > C > A > G. This indicates that an electron is most easily removed from guanine. Additionally, a significant difference in the IP of

Table 8.1: The adiabatic IPs and EAs (kcal/mol) of the DNA bases obtained at various levels of theory and experimentally.

| | IP | | | EA | |
|---|---|---|---|---|---|
| | DFT | MP2 | Exp. | DFT | Estimated |
| T | 196.0 | 204.2 | 204.6 | -14.8 | 7.2 |
| C | 194.2 | 201.5 | 200.1 | -13.8 | 4.8 |
| A | 182.3 | 188.6 | 190.5 | -17.7 | -7.2 |
| G | 171.8 | 176.6 | 179.3 | -15.8 | -16.7 |

guanine and the other three bases is noted. These results agree with experimental predictions that the guanine cation is the major oxidation product in irradiated DNA.

Table 8.1 also displays adiabatic EAs calculated for the bases, since no experimental data is available for this property. The DFT results were presented previously in Chapters Four and Five. The "estimated EA" values were obtained by correcting the HF Koopmanns EA by the calculated nuclear relaxation energy.[22] The "estimated EAs" predict negative values for the EA of adenine and guanine and positive values for cytosine and thymine. The EA is defined as the energy required to add an electron to a neutral molecule and calculated as the energy of the neutral molecule minus the energy of the anion. Therefore, a negative value for the EA indicates that the anion is higher in energy than the corresponding neutral molecule and therefore energy is released upon anion formation. A negative EA cannot be measured experimentally due to the dissociation of the anion into an electron and the neutral molecule before nuclear relaxation. The trend in the "estimated EAs" is T > C > A > G, which is in agreement with early studies on DNA which predicted that the thymine anion is the major reduction product after irradiation. DFT predicted EAs were obtained by directly comparing the energy of the neutral base with the respective base anion, which is expected to be more reliable than the "estimated values". DFT predicts all bases to possess a negative EA. Additionally, the trend predicted with DFT (C > T > G > A) is in contrast to that obtained from the "estimated EAs". However, the DFT results support experimental data that predicts cytosine to be the major reduction site in irradiated DNA. Contrary to the difference between the IP of guanine and the IPs of the other bases, a very small difference was calculated between the EA of cytosine and that of the other bases, in particular thymine.

It should be noted that diffuse functions can be important for the calculation of anion geometries and EAs and, thus, negative EAs may not be obtained through calculations performed with larger basis sets. However, preliminary calculations performed on cytosine indicate that the cytosine anion geometry does not change considerably upon inclusion of diffuse functions in the basis set for the heavy atoms. In addition, through single-point calculations on this geometry with the 6-311+G(2df,p) basis set, the EA was determined to be -1.4 kcal/mol. Thus, even with large basis sets DFT predicts the EA of cytosine to be negative. It can be speculated that the trend calculated with DFT is however correct and therefore the DFT results support the possibility that both cytosine and thymine anions are formed, while the guanine cation is the major oxidation product.

### *8.3.3 The Formation of Secondary Radicals*

The discussion thus far has focussed on the formation of ionic centers as the primary radiation effects in DNA at low temperatures. At higher temperatures, or more specifically those of biological systems, these ionic radicals are not expected to be stable, but rather secondary species must be formed, which evolve from the ionic radical products. The first clues to support this statement were obtained in early ESR investigations of DNA which assigned an observed octet pattern to **T(C6H)**. Concrete evidence for the mechanism of formation of this radical was obtained by recognizing a relationship between its growth and the decay of $\mathbf{T}^{\bullet-}$.[8] It was concluded that these species are related by

$$\mathbf{T}^{\bullet-} + \mathbf{XH}^{+} \rightarrow \mathbf{T(C6H)} + \mathbf{X} \qquad (8.1)$$

where **X** represents an unknown proton source and is not restricted to only one species.[8,12] The **T(C6H)** radical has been monitored in other studies as well.[13,19,23] Despite the evidence for the formation of **T(C6H)**, critics still speculated that $\mathbf{C}^{\bullet-}$ is a predominant damage site and perhaps a transfer of the anionic character from cytosine to thymine, followed by protonation, can account for the high yield of **T(C6H)** in irradiated DNA.[19] Evidence for this phenomenon has been obtained in co-crystals of 1-methylcytosine and 5-fluorouracil (a thymine derivative). The primary radicals were identified to be the cytosine anion and the uracil centered cation. However no cytosine

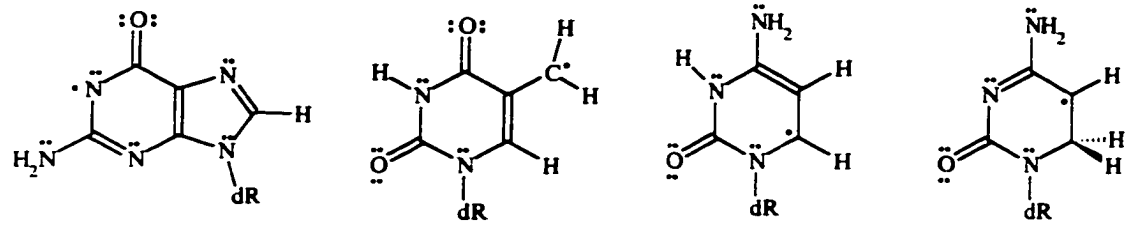

**G(N1)** **T(CH2)** **C(N3H)** **C(C6H)**

Figure 8.5: The secondary radicals identified in ESR studies on DNA in addition to **T(C6H)**.

radicals formed by proton addition to C5 or C6 were observed, but rather uracil products evolving from the uracil anion were identified.[24] In addition, it was later speculated that the decay of the guanine cation is related to the growth of the product formed by deprotonation at N1 [**G(N1)**, Figure 8.5].[12,23]

The radical formed via net loss of a hydrogen atom from the thymine methyl group [**T(CH2)**] has also been observed in highly hydrated DNA samples.[23] This radical could be a proton source, but no relationship between this radical and **T(C6H)** was found. In samples prepared with $D_2O$, the concentration of this radical was determined to be between 10 and 15%, although in nondeuterated samples its spectrum is less pronounced.[25] Evidence also exists that at 77 K, the cytosine anion is stabilized by protonation at N3 [**C(N3H)**] by its guanine base pair.[26] Additionally, in thymine deuterated DNA samples, a deuteron has been determined to add to the C6 position of the cytosine anion [**C(C6H)**].[23] These secondary radicals are displayed in Figure 8.5.

### *8.4 A Closer Look at DNA Radiation Products*

As discussed above, progress in the identification of the radiation products in DNA has been slow. Despite great advances in experimental techniques, only a few products were initially identified. More specifically, the only component not under debate is the octet assigned to the thymine C6-hydrogenated radical. Advances have been made in the past few years, however, to identify more than two or three products in one DNA sample. The most promising results were obtained by Hüttermann and coworkers, in both orientated fibers[27] and in randomly orientated DNA.[28,29] The primary conclusions from these studies will be summarized in the subsequent sections.

### *8.4.1 Results From Orientated Fibers*

Perhaps the most complete study of the radiation products in orientated fibers was performed with a sophisticated pulsed ESR technique on double-stranded DNA upon irradiation at 77 K.[27] Through the use of the field-swept electron spin-echo technique, the ESR spectrum of DNA could be reproduced as spectra of spin packets with the same relaxation parameters and nine clear patterns were identified. Despite the fact that a radical structure was proposed for seven of these patterns (Figure 8.6), only one of these assignments was conclusive and the others were based on additional arguments including

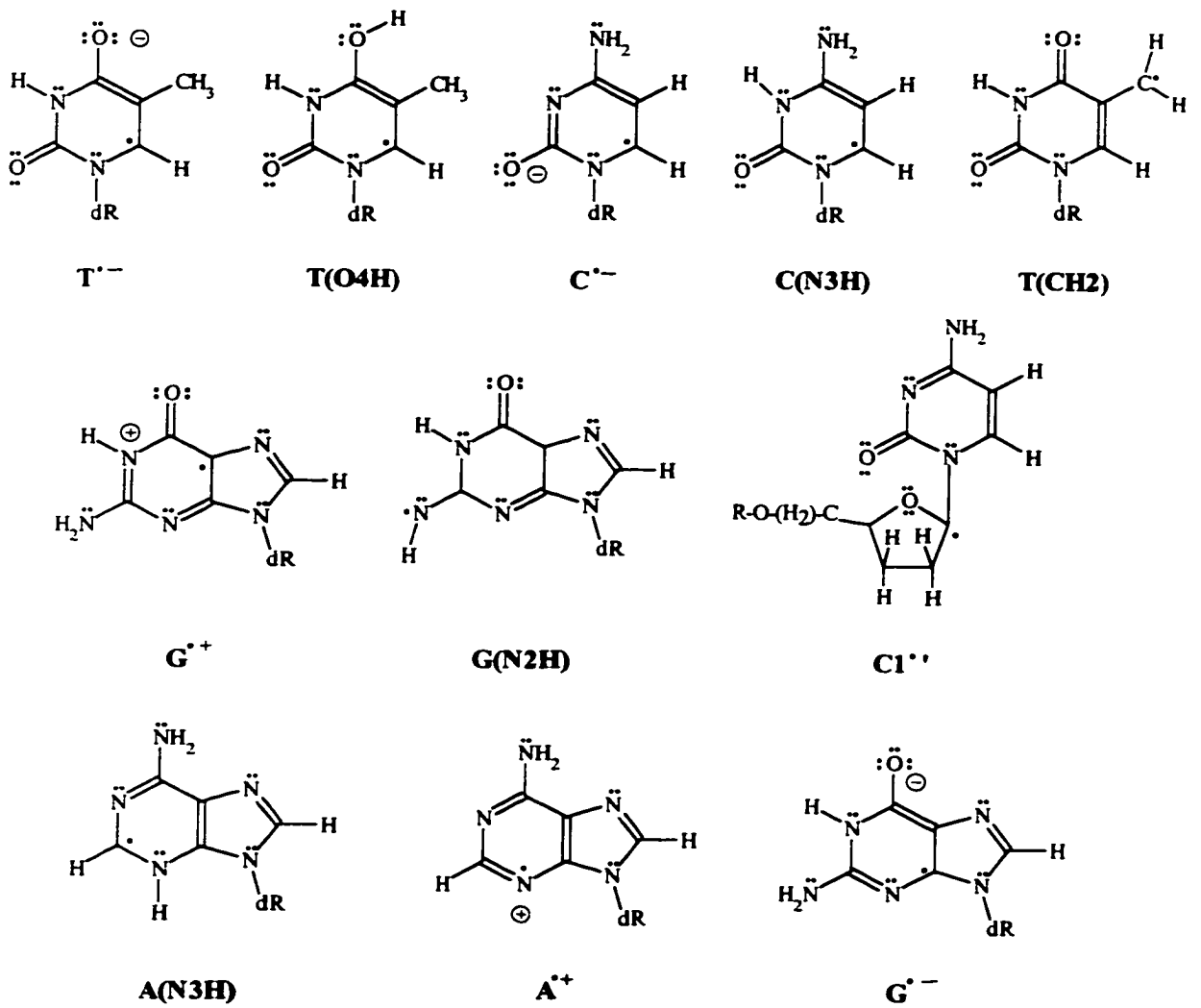


Figure 8.6: Radicals predicted to be formed in orientated samples of DNA.

simulations and mechanistic assumptions. The proposed radiation products will now be discussed.

An observed "doublet" (or rather, a group of related patterns differing with water content and H/D exchange) was confidently assigned to $\mathbf{T}^{\bullet-}$, although whether the anion was protonated at O4 [**T(O4H)**] could not be determined. Another component, previously assigned to $\mathbf{T}^{\bullet-}$,[7,12] was reassigned to $\mathbf{C}^{\bullet-}$, possibly protonated at N3 [**C(N3H)**]. This new assignment seems plausible since it rationalizes large, previously unexplainable couplings as nitrogen interactions. $\mathbf{G}^{\bullet+}$ was also determined to be present, although it seemed unlikely that a charged species would be stable thermally. The assignment to $\mathbf{G}^{\bullet+}$ was supported since the amino-deprotonated guanine radical [**G(N2H)**] possesses a different spectrum from that observed in DNA. These species were all discussed previously in the literature as possible damage products.

The first newly proposed radical product for orientated fibers was the radical formed via net hydrogen atom removal from the methyl group in thymine [**T(CH2)**]. A sugar radical was also speculated for this spectrum, but this postulation was discarded since the tensors are typical for a base radical and the spectrum of a deuterated sample supported the assignment to **T(CH2)**. A spectrum with features typical of an electron interacting with a single nitrogen nucleus was tentatively assigned to a radical formed via proton loss at C1' in the sugar moiety. In this sugar radical, the main part of the spin density is restricted to interactions with the glycosidic nitrogen in a cytosine unit due to the orientation of the base, the sugar moiety and the orbital at C1' possessing the unpaired electron. The possibility of net hydrogen loss occurring at a sugar next to the other bases was not ruled out, although the radical assignment was made based on a spectrum previously observed from cytidine. An assignment was made to the adenine radical formed via hydrogen addition to N3 [**A(N3H)**] based on comparison with previous experimental results. However, the spectrum of this radical was not clear in full DNA and differs from that obtained in the copolymer poly(A:U). Therefore, the assignment is uncertain. The final spectrum addressed was for a "singlet" previously assigned to $\mathbf{G}^{\bullet+}$ for which little direct information could be obtained. Since $\mathbf{G}^{\bullet+}$ was already assigned in the study under discussion, caution was advised and suggested assignments include the guanine anion ($\mathbf{G}^{\bullet-}$) or the adenine cation ($\mathbf{A}^{\bullet+}$), since the adenine anion is related to a

species already identified [**A(N3H)**]. As previously mentioned, two more components could not be assigned due to insufficient information. Thus, this study on orientated fibers clearly indicates that the damage to DNA is broader that initially expected since products on all four bases and the sugar moiety were proposed. In addition, more work is required in order to determine the exact identity of the radical products since structural information is difficult to obtain through the methods implemented.

### *8.4.2 Results from Randomly Orientated DNA Samples*

The first study performed on randomly orientated fibers, which detected more than two or three ionic species, was performed on DNA equilibrated at various levels of hydration, as well as on frozen aqueous solutions.[28] This experimental study was initially proposed to clarify discrepancies in the literature and unconditionally identify the primary radiation products in DNA by comparison with nucleotide patterns. In lyophilized powders, $G^{\bullet+}$, $C^{\bullet-}$ and $T^{\bullet-}$ were identified without any uncertainty for the first time. The spectra obtained for frozen aqueous solutions were very different from those equilibrated at 76% relative humidity. In particular, the amount of $G^{\bullet+}$ is reduced considerably in frozen aqueous solutions. This is in agreement with previous work which found that $G^{\bullet+}$ does not play a dominant role in the radiation chemistry of DNA in frozen aqueous solutions at 77 K.[30] **T(C6H)** and **T(CH2)** were also assigned in this study.

A continuation of the study discussed above examined lyophilized DNA powders in dry environments and equilibrated at 76% relative humidity. The goal of this work was to directly analyze the DNA spectrum. More specifically, electron scavengers were implemented rather than using results obtained from model systems. This approach avoids questions associated with transferring results obtained from single crystals to full DNA and problems establishing near identical experimental conditions in the model systems and in full DNA samples. As a result, many new radicals were identified besides **T(C6H)** (Figure 8.7). A "triplet", previously discussed to be composed of more than one individual spectrum and partially assigned to $G^{\bullet+}$, was assigned to the cytosine radical formed via net hydrogen atom addition to the amino group [**C(N4H)**]. This is the first time this radical has been proposed for DNA. However, the triplet assigned to **C(N4H)** has been identified in aqueous solutions of cytosine derivatives at 77 K, where it was determined that protonation at N3 is more important for oligomers and therefore probably

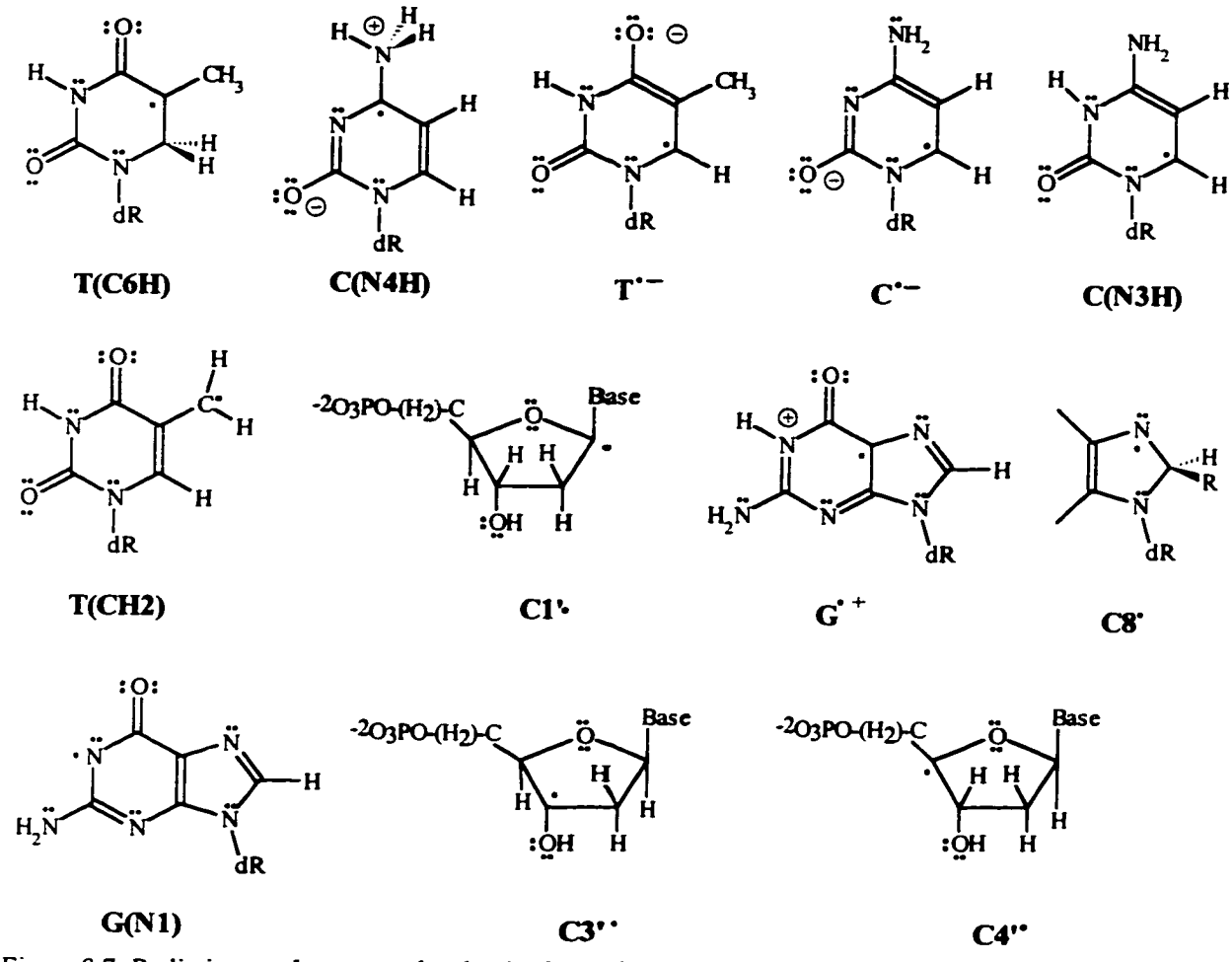


Figure 8.7: Radiation products speculated to be formed in randomly orientated samples of DNA.

more important for DNA as well.[31] Despite the fact that the spectrum did not change upon deuteration of the sample, this assignment was determined to be practical since full exchange of hydrogens is difficult to achieve in DNA samples.

A "doublet" was observed for a species formed via one electron gain. This was speculated to arise from two very similar doublets, one of $\mathbf{T}^{\bullet-}$ and one of $\mathbf{C}^{\bullet-}$ or **C(N3H)**. A "quartet" component was observed which contained features very similar to that previously assigned to **T(CH2)**. Other features of the quartet component were noted to be very similar to that assigned to the C1' hydrogen abstraction deoxyribose radical in cytosine and adenine containing nucleotides. Therefore it was deemed likely that a C1' radical (**C1'**), formed through an oxidation pathway, is generated in full DNA.

Assignment to this radical was supported since the experimental conditions favored electron loss products and the spectrum was not observed in RNA.

A commonly observed "singlet" pattern was assigned to $\mathbf{G^{\bullet+}}$. An additional "broad doublet" was observed which contained typical nitrogen interactions. This was the first study to acknowledge this pattern and it was speculated to be due to radical addition at the C8 position of one of the purines (**C8'**). The concentration of this radical was too small for an assignment to be conclusive and it was only observed in certain dry DNA samples. A "sharp singlet" was recorded for the first time and accredited to the guanine radical formed via net hydrogen atom removal from N1 [**G(N1)**]. One additional spectrum, denoted as "doublet/ox", was also observed and speculated to be due to the C4' or C5' hydrogen abstraction sugar radical, but a definitive assignment could not be made. At high doses of radiation, it was noted that the "quartet" and "octet" patterns provided a stronger contribution to the DNA spectrum. An additional spectrum also appeared at high doses which gave strong indications to be due to the C3' or C4' net hydrogen abstraction radicals (**C3''** or **C4''**).

These studies on orientated fibers and randomly orientated DNA are very important to the field of radiation chemistry. Specifically, these papers were the first to demonstrate the great variety of radicals that can be identified in irradiated DNA. The next section will discuss how the surrounding medium can influence the formation of DNA radicals.

### *8.5 Effects Of Water On Radical Formation In DNA*

Since full DNA has been investigated in numerous environments (varying degrees of relative humidity, frozen aqueous solutions, prepared in $D_2O$), it is possible to gain some information about the effects of water on radical formation. Upon irradiation of water, many different products can be formed:

$$\mathbf{^{\bullet}OH + e^{-}_{(aq)} + {}^{\bullet}H + H_2O^{\bullet+} + H^{+} + H_2O_2 + H_2}$$

The first 14 water molecules (per nucleotide) in the hydration layer surrounding DNA have approximately the same mass as DNA[32] and, therefore, will endure the same number of ionizations as the DNA strand. In addition, the hydration layer of DNA is known to affect the DNA conformation, base stacking and hydrogen bonding between

base pairs.[32] For example, by changing the level of hydration, the conformation of DNA can be converted between A and B forms. The level of DNA hydration has also been shown to affect the ability of electrons to move throughout the hydration layer and, thus, ultimately affect how they react with DNA.[33] Thus, it seems reasonable that the damage to DNA due to water will exist in a variety of forms. However, separating the effects due to $H_2O$ and effects $H_2O$ imposes on the DNA strand (for example, changes in conformation) is difficult.[34,35]

The primary hydration layer of DNA is composed of approximately 20 or 21 water molecules per nucleotide and is commonly referred to as "bound water". Approximately 11 to 15 of these water molecules are bound very tightly to DNA. The remainder are involved in hydrogen bonding to these 11 to 15 water molecules rather than being directly bonded to the DNA strand. Due to the hydrogen bonding scheme, the water molecules in the primary hydration layer exhibit properties different from crystalline ice upon freezing. The secondary hydration layer is composed of water molecules that cannot be distinguished from bulk water upon crystallization and are therefore denoted as "bulk water".

The exact effect of ionizing radiation on the water of hydration and, thus, the formation of DNA damage in an aqueous environment is still under debate. More specifically, it is unknown how the water molecules in the primary hydration layer are affected by radiation. Theories exist which imply that upon the application of ionizing radiation, water cations and electrons are formed, which in turn transfer their ionic character to the DNA strand (Equations 8.2 to 8.4).

$$H_2O \rightarrow H_2O^{\bullet+} + e^{-} \quad (8.2)$$

$$e^{-} + DNA \rightarrow DNA^{-} \quad (8.3)$$

$$H_2O^{\bullet+} + DNA \rightarrow DNA^{\bullet+} + H_2O \quad (8.4)$$

The damage resulting from these reactions is identical to that resulting from direct effects (or direct ionization of the DNA strand) and, thus, damage formed via this pathway is known as quasi-direct effects. However, it is also possible to imagine that the water cation transfers a proton to a neighboring water molecule in the hydration layer, which would result in hydroxyl radicals (Equation 8.5).

$$H_2O^{\bullet+} + H_2O \rightarrow {}^{\bullet}OH + H_3O^{+} \quad (8.5)$$

This mechanism implies that hydroxyl radicals could react with DNA and the resulting damage is said to arise from indirect effects. The primary water radicals which can yield indirect effects include hydroxyl radicals, hydrogen atoms and aqueous electrons.

Many studies have investigated the effects of the relative degree of hydration on the production of DNA radiation damage. Perhaps the first indication of the dependence of DNA damage on hydration was reported for frozen aqueous solutions.[36] It was determined that the radical yield in wet DNA is twice the yield obtained in dry DNA. In lyophilized DNA, it was instead noted that radical yield increases with hydration to a certain extent, but then a plateau is reached that cannot be surmounted by increasing the level of hydration.[23] Additionally, the yield of radical ions at 77 K was found to increase by a factor of four upon inclusion of the primary DNA hydration layer.[37] In this experimental study, it was suggested that hydroxyl radicals are not generated in the primary hydration layer, but are observed in the "bulk" water where they do not interact with the DNA strand. Examination of the effects of hydration on radical yield at 4 K speculated that damage transfer from water to DNA could be a reason for the lack of detection of hydroxyl radicals or hydrogen atoms in this layer at 77 K.[35] Alternatively, it was suggested that the primary hydration layer could be less efficient at trapping free radicals since radicals could quickly recombine in this area.[35]

In addition to the dependence of the relative radical yields on the hydration level, the absolute yields of the individual ion radicals have been determined.[26] In dry DNA, the radical composition was determined to be approximately 12% $\mathbf{A}^{\bullet-}$, 15% **C(N3H)**, 32% $\mathbf{T}^{\bullet-}$ and 41% $\mathbf{G}^{\bullet+}$. Upon hydration at 77 K and the application of low radiation doses, radical yield became 27% **C(N3H)**, 35% $\mathbf{T}^{\bullet-}$ and 38% $\mathbf{G}^{\bullet+}$, which upon annealing to 130 K became 37% **C(N3H)**, 22% $\mathbf{T}^{\bullet-}$ and 40% $\mathbf{G}^{\bullet+}$. At 77 K, high radiation doses changed the yield to 52% **C(N3H)**, 5% $\mathbf{T}^{\bullet-}$, 24% $\mathbf{G}^{\bullet+}$, 1% **T(C6H)** and 18% of an unknown radical related to $\mathbf{G}^{\bullet+}$ (possibly a sugar radical). Results obtained at high doses and high temperatures indicate that $\mathbf{T}^{\bullet-}$ converts to $\mathbf{C}^{\bullet-}$, which is speculated to be driven by a greater stabilization obtained by protonation of cytosine at N3 by its guanine base pair. Preference of $\mathbf{T}^{\bullet-}$ in dry DNA is speculated to occur since *ab initio* calculations

predict that thymine possesses a higher electron affinity than cytosine, which becomes nearly equal to that of cytosine upon hydration.[22] Weiland *et al.*[28] also determined that the importance of the thymine anion decreases at high levels of hydration and cytosine becomes the primary reduction site.

Damage caused by the release of unaltered DNA bases has been determined to be equivalent whether ionization of the primary hydration layer or only direct ionization is considered, but increases when ionization of the secondary hydration layer is also considered.[34] The damage was determined to be caused by charge transfer from water cations formed in the primary hydration layer and by attack of hydroxyl radicals formed in the loosely bound water.[34] A more complete investigation of the effects of hydration on base damage from electron loss centers also indicates that the yields of unaltered bases and base damage products (14 detected in total) in DNA including the primary hydration level and dry DNA are equivalent, but the yield increases with the inclusion of the secondary hydration layer.[21] The efficiency of strand breaks in DNA including the primary hydration layer was also determined to be equivalent to dry DNA, but less than when bulk water radicals are considered.[38] These studies indicate that quasi-direct and direct effects cause damage by similar mechanisms and therefore provide comparable yields of damage. In addition, once water molecules are included beyond the primary hydration level, hydroxyl radicals are formed which increase the amount of damage.

The preliminary ESR investigations discussed above did not detect hydroxyl radicals, hydrogen atoms or free electrons in the primary hydration layer of DNA. This evidence has been used to speculate that primary effects of the hydration layer must occur via the quasi-direct pathway (Equations 8.3 and 8.4). This implies that holes are transferred to DNA to form cationic and anionic base radicals faster than the water cation can transfer a proton to a neighboring water molecule. However, it is possible that hydroxyl radicals are formed, but are not detected or they rapidly react with the DNA strand. Conversely, it appears to be accepted that hydroxyl radicals can be formed in the secondary hydration layer, where water molecules are more loosely bound. Questions addressing which process predominates in the primary hydration layer of DNA are important since the damage by hole transfer or by hydroxyl radicals is very different.

A major revelation in the effects of the hydration layer on DNA radiation damage was obtained in a study of γ-irradiated DNA where hydroxyl radicals were observed in low yields in the primary hydration layer.[39] The direct detection of hydroxyl radicals was used, as well as the yield of $H_2O_2$ formed via recombination of hydroxyl radicals, despite the fact that hydroxyl radicals in the primary hydration layer have very broad ESR spectra and therefore are difficult to detect. It was concluded that since only a low yield of hydroxyl radicals could be detected, most of the oxidative damage in the hydration layer is transferred to DNA. This is the first direct evidence for hydroxyl radical formation in the hydration layer, as well as for charge transfer to DNA. It was later noted that over the levels of hydration examined, some water molecules could be more loosely bound and therefore these molecules could be resulting in the observed hydroxyl radicals.[21] This issue was reinvestigated by the same group in a more recent study.[40] It was determined that the hydration layer of DNA can be separated into three partitions: (1) the first 9 water molecules which do not form significant amounts of hydroxyl radicals, but transfer their charge upon irradiation to DNA; (2) an additional 12 water molecules completing the primary hydration layer which predominantly form hydroxyl radicals, but unsubstantial charge transfer may also occur; and (3) bulk water which forms hydroxyl radicals. No trapped electrons were found in the first two levels indicating all free electrons transfer to DNA, however no electrons are transferred to DNA from the bulk water. It is still possible that hydroxyl radicals were not detected in the first 9 water molecules since they quickly react with DNA or they are ESR silent. Alternatively, since these water molecules are tightly bound to the DNA phosphate groups, a charge transfer mechanism seems more plausible.

Perhaps the most convincing evidence to support hydroxyl radical attack on the DNA bases comes from a study on aqueous $BeF_2$ glasses of base derivatives, where products resulting from water reacting with the bases were observed.[41] Hydroxyl radicals were found to add to the C5C6 double bond in cytosine and uracil, abstract a hydrogen from the methyl group in thymine and add to C2 in adenine. These results are different from those obtained in the liquid state where hydroxyl radicals add to the C5C6 double bond in all pyrimidines[42] and to C4, C5 and C8 in purines.[43] In addition, it has been

determined in the liquid state that rather than direct attack of hydroxyl radicals at the sugar moiety, hydroxyl radicals add to the bases and the radical center is transferred to the sugar.[44] Thus, differences exist between glasses and liquids. Differences also exist between low temperature glasses and frozen aqueous solutions where indirect and direct or quasi-direct pathways are thought to predominate in the former and latter, respectively. In particular, it has been shown that the relative concentration of the primary ions ($\mathbf{T}^{\bullet-}$, $\mathbf{C}^{\bullet-}$ and $\mathbf{G}^{\bullet+}$) did not change upon the inclusion of hydroxyl radical scavengers in fully hydrated frozen DNA at 77 K. This indicates that hydroxyl radicals are not an important source of DNA damage in this environment and no hydroxyl radical addition or abstraction products are formed.[45] One study of full DNA speculated that a C1' sugar radical forms via hydroxyl abstraction of the relevant hydrogen, although it was also noted that it could be formed from a cationic radical.[27] Formation of a radical left unidentified in frozen DNA could also be due to hydroxyl radicals.[26]

Hüttermann *et al.*[46] proposed a new mechanism for radiation damage in frozen aqueous solutions. It was postulated that electrons primarily attack DNA and oxidation primarily occurs at water. In thymidine 5'-monophosphate at 77 K, the primary radicals formed were $\mathbf{T}^{\bullet-}$ and hydroxyl radicals (from oxidation of water). Thus, direct oxidation of thymine seems negligible as does hole transfer from the water cations to thymine. Stable radicals were subsequently formed through addition of hydroxyl radicals [**T(C6OH)**] and hydrogen atoms to C6 and abstraction of a hydrogen atom from the methyl group by hydroxyl radicals. This is the first indication that in frozen aqueous solutions hydroxyl radicals can take part in the radiation damage to DNA components. This mechanistic pathway is different from that previously suggested, but it still explains experimental observations.[47] The quintet spectra assigned to **T(C6OH)** is under debate since any ESR silent group added to this position will yield a similar spectrum. For example, an allyl radical could attack a neighboring thymine at C6 (dimer radical) or its own sugar group (cyclic radical).[48] However, none of these mechanisms are supported by more recent work which determined that the allylic radical could be formed via a base cation and indicates that hydroxyl radicals may not be directly related to its formation as previously speculated.[25]

Work on single crystals of DNA components has also suggested that water can be involved in the initial ionization process. Studies on single crystals of guanine derivatives determined that it is necessary to consider ionization of the surrounding water molecules in order to account for the formation of the identified radicals.[49] Since all of these crystals were initially protonated at N7, it was speculated that if water cations are formed, repulsion between the cationic base and the water cation leads to dissociation of the latter resulting in protons and hydroxyl radicals. However, the work presented in Chapter Four provides support that water may also be the primary site for oxidative damage in cytosine monohydrate crystals. Additionally, investigation of the relevant reaction mechanisms (Chapter Seven) indicates that hydroxyl radical addition to cytosine occurs with very small barrier heights. This is important information since it indicates that rather than direct transfer of the positive charge to the base, water radicals may directly play an important role in the damage of single crystals even if the crystals are not originally protonated. This also has important implications for full DNA, since the bases are not necessarily protonated, but products generated from reactions with water molecules may be formed.

Despite the efforts put forth, the influence of water on the formation of DNA radicals can still be disputed. In particular, from the above studies, the direct role of water on the formation of DNA radicals remains unknown. The transfer of these results to the effect water has on radiation damage in cells can also be questioned. In particular, within cells many organic molecules exist which can react with water radicals.[45] Additionally, molecules could be packed differently within cells making little room for water and hence water damage may become less important. Alternatively, living systems are composed mostly of water and thus one would expect ionization to occur in the surrounding medium. Thus, it is important to learn more about how hydration affects DNA damage in order to apply results from model systems to damage generated in living entities.

### *8.6 Formation of Sugar or Phosphate Radicals in DNA*

As previously stated, ionizing radiation does not discriminate. Thus, since 50% of DNA is composed of bases and 50% is composed of the sugar and phosphate

backbone, it seems strange that sugar and phosphate radicals were initially not observed upon irradiation of full DNA.[16] It was originally suggested that in DNA the damage is shifted from the sugar (where alkoxyl radicals are often observed in nucleotides but cannot be formed without a strand break in DNA) to the bases.[50] The rationale for the lack of sugar radicals in irradiated DNA was that all sugar radicals are generated from alkoxyl radicals, but no hydroxyl groups are present in DNA to form these radicals. However, Hole *et al.* were able to identify at least nine different sugar radicals in irradiated single crystals of 2'-deoxyguanosine 5'-monophosphate,[51] which possesses only one hydroxyl group, and the calculations presented in Chapter Six support these experimental assignments. Despite experimental efforts, it was discouraging and very curious that no sugar radicals were identified in full DNA samples.[52] Possible explanations offered for the lack of detection of sugar radicals include a small abundance of such radicals, multiple conformations for each radical and the similarity of the spectrum of each radical.[52] In addition it was noted that the sole use of ESR to examine full DNA is inadequate for the detection of sugar radicals or, as mentioned, these radicals could lead to base radicals upon annealing.[53] Through simulations, it was resolved that the spectrum due to C1' can be observed in DNA since the outer lines should be visible, while the spectra of the C4' and C5' centered radicals are doublets hidden by the DNA spectrum and the C2' and C3' radical signals should be barely visible. Thus, it is possible that these radicals are formed, but are left undetected.

Despite the problems associated with the identification of sugar radicals, indications that these radicals are formed in full DNA have appeared. For example, evidence for the formation of formyl and peroxyl radicals in DNA samples with 66% relative humidity lead to the conclusion that oxidation of the sugar-phosphate backbone may influence the radiation damage mechanism.[23] Hüttermann and coworkers[28,29] provided the first direct evidence that these radicals are formed in full DNA samples. Through their careful analysis, it was possible to characterize the spectra of select sugar radicals in DNA. In particular, the C1' and the C3', C4' or C5' radicals were proposed as possible radiation products in DNA. In addition, studies performed with heavy ion beam irradiation of DNA noted the resemblance between the simulated spectra of the C4' and C3' radicals and the spectrum obtained for DNA.[54]

In addition to sugar radicals, little evidence for the formation of phosphate centered radicals has appeared in the literature. Studies on model systems show that electron capture at the phosphate group would result in cleavage of the phosphoester bond.[55,56] Additionally, sugar radicals of the form –C4'–˙C5'$H_2$ have been observed (**C5'(H2)**, Figure 8.8) and the most likely mechanism for their formation is through capture of an electron at a phosphate group.[51] It has been assumed that electrons transfer to the DNA bases if they are captured on the phosphates.[56] Evidence to support transfer of the radical site away from the phosphate groups was obtained by Steenken and Goldbergerova,[57] who showed that oxygen centered phosphate radicals efficiently abstract hydrogen from C4'. The resulting C4' centered radical (**S**, Figure 8.8) undergoes rapid elimination of the phosphate-ester group. Thus, the ease of the hydrogen transfer

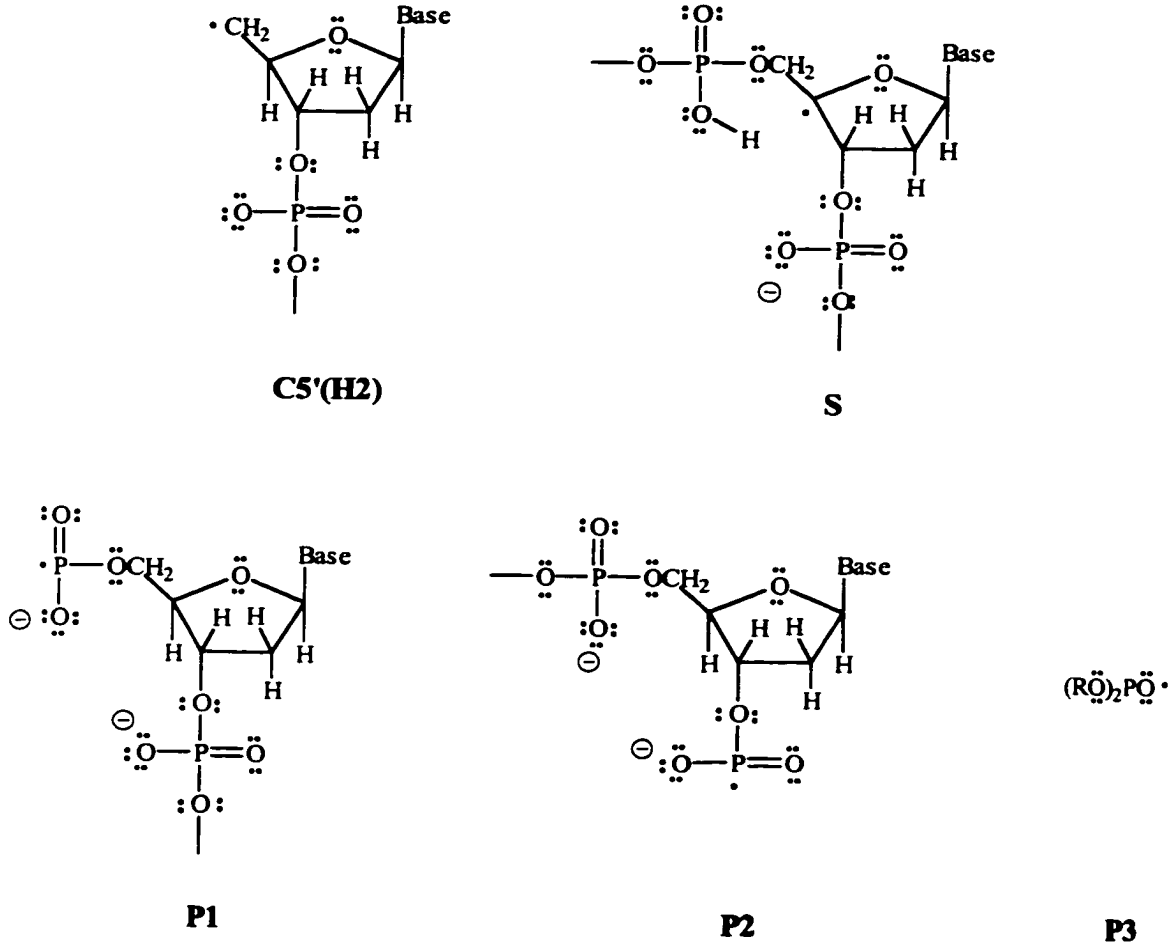


Figure 8.8: The first phosphate radicals observed in DNA.

removes the phosphate centered radicals quickly and therefore they cannot be detected. The only indication that phosphate centered radicals are formed in DNA was obtained through irradiation by a heavy ion beam.[54] Large couplings were obtained in this experimental study and assigned to phosphorus atoms in radicals displayed in Figure 8.8 (**P1** and **P2**). **P1** and **P2** lead to a prompt DNA strand break. Radicals of the type **P3** (Figure 8.8) could not be eliminated in the experimental study under discussion.

Thus, despite early failures to detect radicals in the backbone of the DNA double helix, recent experimental advances prove to be invaluable for the determination of the radiation damage mechanism in DNA samples.

### *8.7 Major Radical Products Formed in Irradiated DNA*

As mentioned previously, ionizing radiation damages indiscriminately and the number of initial damage products formed on a particular center is proportional to the mass of the center under consideration. Therefore, upon irradiation of a DNA strand, cationic and anionic centers will be formed at each base, the sugar moiety and the phosphate group. These radicals are denoted primary radicals since they have no observable precursors. Studies investigating the effects of the hydration layer on the yield of damage to the DNA strand (production of unaltered bases, base damage products and strand breaks) have determined that the yield of damage increases upon consideration of the hydration layer.[21,34,38] This information indicates that the water surrounding DNA plays a role in the formation of radiation damaged products. More specifically, since living entities are largely composed of water, a model of the radiation damage to DNA must also encompass the ionization of water molecules, which generates water cations and electrons. These initial radiation products can transform into alternative products or secondary radicals by protonation or deprotonation.

Due to the nature of the DNA double helix, it is possible for the initial damage to be transferred through the DNA strand to produce more stable intermediate radical products. Electron transfer has been reported to occur over as few as three base pairs to as many as one hundred.[58] The consensus in the literature regarding radicals initially formed upon irradiation of DNA is that the primary electron loss center is guanine and the primary electron gain centers are cytosine and thymine. The formation of these

primary products is also supported by *ab initio*[22] and DFT calculations (Section 8.3.2). Thus, if an adenine anion is formed initially, the electron can be transferred throughout the DNA strand to produce either a thymine or cytosine anion. Interbase electron transfer is possible in DNA due to the small distance between base pairs, which results in an overlap of the π-systems, and hydrogen bonding of the bases.[43] Evidence for charge transfer through the DNA strand can be obtained from a study that predicted thymine anions to be present in slightly larger yields in single-stranded DNA, while the cytosine anion clearly predominates in double-stranded DNA.[19] This phenomenon is also supported by *ab initio* calculations which determined that base-pairing raises the EA of cytosine relative to that of the isolated base.[22]

Alternatively, long range hole transfer in DNA is considered to be more difficult. However, evidence supporting hole transfer in some crystals does exist, which provides evidence that hole transfer may also occur in DNA.[58] For example, positive holes formed on thymine, cytosine or adenine can be transferred to guanine. Additional evidence for hole transfer exists since it has been determined that the guanine-cytosine and adenine-thymine base pairs have lower IPs than guanine or adenine, respectively.[59] The redox properties of the base pairs suggest that the initial stabilization of base radicals may also depend on proton transfer reactions.[60]

The radiation products generated in DNA will be discussed in terms of how the primary cation and anion radicals decay to form secondary radical products. This discussion will encompass results from single crystals,[53] the aqueous state,[43,60] the calculations presented in the previous chapters, as well as those obtained from *ab initio* studies,[22] and studies on orientated and randomly orientated DNA.[27,29]

### *8.7.1 DNA Cations and Secondary Radicals*

As previously remarked, cations can be formed via direct ionization of the DNA strand. Base cations can also be generated through transfer of the positive charge from irradiated water molecules in the hydration layer. Alternatively, sugar radicals can be formed via transfer of the radical character from the base cations. Once formed, cations can recapture an electron, generated from either ionization of water or the DNA strand, to

heal the damage. In addition, if a cation is formed on a site different from guanine, transfer of the positive hole to guanine can occur.

At low temperatures, it is realistic to expect cations to be stabilized. However at higher temperatures, or more specifically those of biological systems, the presence of neutral radicals is more probable. Thus, if cations are stabilized for a sufficient period of time on any DNA center, deprotonation is likely. However, in experimental studies on DNA, it is difficult to determine the deprotonation state of the primary radical products. This is clearly seen from the calculations performed on model systems presented in the previous chapters, which illustrate that there exists very little difference in, for example, the spin densities of cations and their deprotonated counterparts.

The thymine cation has not been identified in experiments on single crystals[53] and *ab initio* calculations predict that this base has the largest IP.[22] However, the radical formed through net hydrogen atom removal from the methyl group [**T(CH2)**] has been identified in all thymine derivatives,[53] an assignment which was supported by HFCCs calculated with DFT (Chapter Four). Thus, assuming that the thymine cation is stabilized for a sufficient period of time in DNA to allow for deprotonation, the most abundant secondary thymine radical would be formed via loss of a methyl proton. This hypothesis is supported by the fact that **T(CH2)** has been identified in the most complete studies on both orientated fibers[27] and randomly orientated DNA.[28,29] Studies of the redox properties of base pairs indicate that one-electron oxidized thymine in DNA should be characterized by both $\mathbf{T}^{\bullet+}$ and **T(N3)**, the radical formed by net hydrogen removal from N3, implying proton transfer from T(N3) to A(N1) can occur.[60] The **T(N3)** radical has not been identified in single crystals through comparison of calculated and experimental HFCCs, even in studies on base pairs. Additionally, this radical has not been suggested to be formed in full DNA. This indicates that proton transfer cannot compete with deprotonation at the methyl group.

Little experimental evidence has been obtained for the formation of the cytosine cation. Early ESR studies predicted that the cytosine cation is formed in cytosine monohydrate crystals, however, through the use of the ENDOR technique this assignment was determined to be unlikely.[53] In single crystals of deoxycytidine 5'-monophosphate, the cytosine cation was also postulated, but the HFCCs did not match

those calculated with DFT (Chapter Four). The only direct successor of this cation discussed in the literature is that formed via net hydrogen loss at N1. In cytosine monohydrate crystals, this radical product was postulated, but through comparison with calculated HFCCs, a new mechanism was proposed involving oxidation at water rather than at cytosine (Chapter Four). The N1-deprotonated cytosine radical is irrelevant when DNA is considered since the hydrogen at N1 is replaced with deoxyribose. Alternatively, sugar radicals have been observed in some cytosine derivatives.[53] These radicals could be formed from the cytosine cation, where the cationic nature is transferred to deoxyribose and deprotonation subsequently occurs at the sugar moiety. The instability of the cytosine cation in single crystals indicates that upon irradiation of DNA, the formation of the cytosine cation, or its secondary radical products, is unlikely. This is in agreement with results obtained from the redox properties of the base pairs which determined that the cytosine cation will not deprotonate since guanine is such a weak base.[60] In addition, since cytosine is base paired with guanine, which is well accepted to be the ultimate cationic site in irradiated DNA, transfer of the positive charge from cytosine to guanine (or the sugar moiety) is more likely than the formation of a cytosine radical by deprotonation.

The adenine cation has not been confidently assigned through comparison of calculated HFCCs and those obtained from single crystals of nonprotonated adenine derivatives which are not co-crystallized with another base derivative (Chapter Five). However, a study performed on the co-crystals of 1-methyluracil and 9-ethyladenine detected the adenine cation at 10 K[61] and the HFCCs agree well with those presented in Chapter Five. Additionally, the cation can be observed in protonated crystals.[53] The extreme conditions at which the adenine cation was observed in these studies are not evident in full DNA.

Deprotonation of the adenine cation is expected to occur primarily at the amino group [**A(N6H)**]. In single crystals it has been determined that this radical is formed if one of the amino hydrogens is involved in a hydrogen bond to a site which can transfer the damage further away from the initial adenine molecule.[62] Alternatively, in some crystals it has been determined that the hydrogen not involved in a hydrogen bond is lost. In DNA, the proton could be transferred through the hydrogen bond formed with the

base-pair thymine, although further transfer through a hydrogen bond network is not possible. In co-crystals of 1-methylthymine and 9-methyladenine, no products formed via deprotonation of the adenine cation were detected, which was believed to indicate that proton transfer between adenine and thymine is unlikely.[63] Additionally, although the adenine cation and the amino-deprotonated counterpart were observed in co-crystals of 1-methyluracil and 9-ethyladenine,[61] uracil and adenine acted as if they were isolated from one another. These results indicate that stacking and hydrogen bonding effects are not sufficient for radical stabilization. In solution, it has been determined that although the adenine cation is a strong acid, thymine is a poor base and therefore will not abstract a proton from adenine.[60] *Ab initio* calculations also predict that proton transfer is not favorable in adenine and thymine ion pairs.[22] These results indicate that the effects of base pairing on the formation of the adenine cation or its secondary radicals in DNA are unknown and hydrogen transfer between base pairs cannot be used to justify the most abundant adenine deprotonated radical. An alternative possibility for the formation of **A(N6H)** in DNA is that the hydrogen not involved in the base-pair hydrogen bonding could be removed. In some adenine crystals, the C1' sugar radical (**C1'**) was detected and postulated to be formed from the adenine cation.[53] Thus, if an adenine cation is stabilized for a time longer than that required to transfer its cationic character to guanine, either deprotonation at the amino group or transfer of the cationic character to the sugar moiety is expected.

As discussed, it is agreed in the literature that guanine is the major oxidation site in DNA. *Ab initio* calculations on base pairs indicate that the IP of the guanine-cytosine base pair lowers to a greater extent than the IP of the adenine-thymine base pair relative to guanine and adenine, respectively.[59] This lends even more support to guanine being the major positive center in DNA. Despite this fact, the HFCCs calculated with DFT did not support the experimental assignment to the guanine cation in single crystals (Chapter Five). Deprotonation of the guanine cation is also expected in solution, however the equilibrium constant was determined to be small. The primary product formed via deprotonation of this cation in single crystals is the amino-dehydrogenated radical [**G(N2H)**]. Alternatively, in solution, deprotonation primarily occurs at N1 [**G(N1)**].[43] In DNA, deprotonation at N1 or the amino group are both possible due to transfer

through a hydrogen bond with cytosine. However, since N3 has been determined to be the most likely site for protonation in cytosine (to be discussed), transfer from N1 may be favored in DNA. *Ab initio* calculations have determined that the guanine-cytosine base pair cation can readily undergo proton transfer along the C(N3)–G(N1H) bond, where the activation barrier was calculated to be 0.9 kcal/mol and the products are only 1.6 kcal/mol higher in energy.[59] Alternatively, if transfer does not occur through the hydrogen bonds, but rather protons are released into the surrounding environment as proposed for adenine, then the amino hydrogen not involved in a hydrogen bond can be deprotonated. Only the **G(N1)** deprotonated product has been identified thus far in studies of randomly orientated DNA.[29]

It has been suggested that since the predicted total yield of anions is larger than the total yield of cations in DNA, some cations may have been left undetected. This provides evidence that oxidation may also occur on the sugar moiety in DNA. Deoxyribose has an IP larger than the bases, but smaller than the phosphate group,[22] indicating that cation formation could occur on this center. It should also be noted however that calculations accounting for the phosphate hydration layer indicate that the IP of the sugar and the phosphate groups are more similar to one another.[22] In single crystals, direct oxidation of the sugar moiety is expected to result in alkoxyl radicals, which are commonly observed in various base derivatives.[53] Other sugar radicals can be formed directly from alkoxyl radicals. Alternatively, hydrogen atoms can be abstracted by neighboring molecules in the single crystals. Besides direct ionization of the sugar group, oxidation of a base followed by transfer of the radical character to the sugar moiety can result in deoxyribose radicals. However, transfer of radical character from the sugar to the base was observed at 200 K in single crystals of 2'-deoxyguanosine 5'-monophosphate. Thus, this pathway for sugar radical formation may not be relevant to radiation effects on living systems. Additionally, it should be clearly noted that the mechanism of hole transfer from the sugar moiety to the bases will be competing with the formation of neutral sugar radicals.

Any of the mechanisms discussed for the formation of sugar radicals can be expected to lead to deprotonation at any of the carbons (C1' to C5'). In studies on single crystals of base derivatives,[51,53] the C1' position appears to be the favored site for

deprotonation. It is speculated that thymine and guanine derivatives are more likely to deprotonate at the base rather than transfer character to the sugar group due to the abundant formation of alternative deprotonated radicals. The C1' centered radical has been suggested as a product in orientated fibers[27] and randomly orientated DNA.[28,29] The formation of the C3', C4' and C5' centered radicals was also postulated in DNA samples.[29] On the contrary, the C2' radical has not been suggested to be formed in DNA. This is supported by both *ab initio*[22] and DFT (Chapter Six) calculations, since both predicted the C2' radical to be much higher in energy than the other carbon centered radicals which are all very close in energy. Additional sugar radicals have been observed in single-crystal studies (Chapter Six), which involve considerably more damage to the sugar ring than breakage of one bond. The relevance of these structures to DNA is unknown at this time since none of these products have been observed in irradiated samples.

Products formed by loss of an electron from the phosphate group have not been identified in single-crystal studies of base derivatives or studies on full DNA. Experiments and calculations indicate that the IP of the phosphate group in DNA or outside the helix is low.[22] However, if an environment which is more relevant to biological systems is considered (for example, inclusion of solvation or counterion effects), then the IP increases by a factor of 2 to 2.5.[22] Thus, products generated by loss of an electron from the phosphate groups are unexpected in DNA. It is postulated that these radicals are quickly repaired by capture of an electron.

The role the water encompassing the DNA strand plays in radiation damage appears to be unsettled. However, it is agreed that water is primarily involved in the radiation process through an oxidation type mechanism. Oxidation of water leads to free electrons and $H_2O^+$, which can dissociate to form protons and hydroxyl radicals. The hydroxyl radicals can subsequently react with any of the undamaged bases or the sugar group. Aqueous[42,43] and solid state[40] results predict that the primary sites for hydroxyl radical addition is across the C5C6 double bond in the pyrimidines and at C8 in the purines, as well as C2 in adenine. In a study of randomly orientated DNA,[29] a secondary product was identified to be generated through radical addition to C8 in one of the purines. This species could be accredited to hydroxyl radical addition to C8 in guanine or

adenine. Alternatively, hydroxyl radicals can abstract a hydrogen atom to form, for example, the thymine methyl-dehydrogenated radical or carbon centered radicals in deoxyribose. Whether hydroxyl radicals prefer to abstract hydrogen from the sugar moiety or add to the bases remains to be determined.

In addition to products formed via ionization of water, the close contact between water molecules in the hydration layer of DNA and the bases can lead to protonation of base anions and the formation of hydroxyl anions. For example, Steenken suggested that upon formation of the adenine anion, proton transfer from T(N3) to A(N1) occurs, forming the thymine anion, which is subsequently protonated by a nearby water molecule to form hydroxyl anions.[60] Thus, initial reduction of adenine could lead to an abundance of negative charge in the hydration layer. Alternatively, the adenine cation could transfer non-hydrogen bonded amino-hydrogens to a neighboring water molecule. Thus, these experimental results indicate that the charge can be transferred from bases in the DNA strand to the hydration layer where it can be stabilized or additional water radicals can be formed to attack the base and the sugar moiety.

It should be noted that although the secondary radicals mentioned in the present section were discussed in terms of formation from the primary cationic centers, other pathways can lead to the equivalent species. For example, upon irradiation of DNA it is possible to generate excited species. The excess energy on these centers can be relieved by dissociation of an X-H bond which would result in radical products equivalent to those discussed above. Excitation could occur at the bases to yield for example **T(CH2)** or at the sugar group to yield any of the net hydrogen atom removal radicals (**C1'** to **C5'**).

### *8.7.2 DNA Anions and Secondary Radicals*

The generation of cations through irradiation of DNA and its surrounding water molecules yields a supply of electrons which can add to the DNA strand to generate anionic centers. Similar to the cations, these anions may be stable under extreme conditions, but they can be expected to rapidly protonate at elevated temperatures. The protons can be obtained from deprotonation of the base, sugar or water cations. The protonation state of the anions in DNA is difficult to determine. In particular, if the added proton lies in the molecular plane, which is often the case, the resulting HFCCs are

very small and extremely difficult to detect even with the sophisticated ENDOR technique.

Through comparison of data from single crystals[53] and DFT calculations (Chapter Four), it can be determined that at 10 K the thymine and cytosine anions are protonated in many different crystals. Since radicals formed through net hydrogen atom addition have been observed with ENDOR spectroscopy even at low temperatures in single crystals, it seems likely that thymine and cytosine radicals should also exist as neutral species in irradiated DNA. The most probable sites for protonatation are O4 and N3 in thymine [**T(O4H)**] and cytosine [**C(N3H)**], respectively. These protonation sites are even more likely in full DNA samples due to the hydrogen bonding interactions between the base pairs. In particular, the ease of proton transfer along the C(N3)–G(N1H) bond in the guanine-cytosine base pair cation has already been discussed and proton transfer has been determined through *ab initio* calculations to be favorable in guanine-cytosine ion pairs.[22] Furthermore, if the cytosine anion is formed, which is a strong base, it is base paired with guanine, which is a strong acid, and proton transfer is very favorable.[60] Both **T(O4H)** and **C(N3H)** have been speculated to be formed in full DNA.[27,29]

It is also possible to protonate along the C5C6 double bond in both pyrimidines. The thymine C6-hydrogenated radical was observed in the first ESR studies on irradiated DNA[4] and has been identified with more advanced methods.[27,29] It is expected that this radical is predominant since adenine is a weak acid. Therefore adenine cannot donate a proton to its thymine base pair at the O4 position. *Ab initio* calculations have shown that proton transfer ability across the T(N3H)–A(N1) bond in the adenine-thymine base pair cation is poor.[59] Although transfer between T(O4H) and the adenine amino group was not investigated, other calculations have shown that proton transfer is not favorable in adenine-thymine ion pairs.[22] Additionally, single-crystal studies indicate that transfer across a hydrogen bond where the acceptor is a ketyl oxygen (=O) represents less favorable conditions for a successful proton transfer.[62] Thus, evidence exists suggesting that proton transfer across the T(O4)–A(N6H) hydrogen bond may be slow. Therefore, other proton donating agents (such as water or free protons generated from deprotonation of base cations) have an opportunity to react with the thymine anion. In particular, protonation is expected to occur at C6 (or C5) in thymine [**T(C6H)** or **T(C5H)**].

In addition to the **C(N3H)** product, the cytosine N4 protonated radical [**C(N4H)**] has been proposed experimentally for full DNA samples.[29] This radical has been observed in single crystals of cytosine hydrochloride[64] and couplings calculated with DFT for this radical are in good agreement with experiment even though the chlorine counterions were not included in the model system.[65] If protonation from a neighboring guanine molecule is slow, then there exists the possibility for the formation of the N4-hydrogenated radical. Moreover, the radicals formed by protonation across the C5C6 double bond [**C(C5H)** or **C(C6H)**] could be generated, both of which have been observed in single crystals and the assignment is supported by DFT calculations (Chapter Four). The **C(C6H)** product has also been observed in deuterated DNA samples, where a deuteron adds to C6. However, as indicated by *ab initio* calculations, proton transfer is favorable in the guanine-cytosine base pair ions and **C(N3H)** is probably the most predominant cytosine net hydrogen addition radical product.[22] It is interesting to note that cytosine has one more probable protonation product than thymine, which could offer an explanation for the experimentally observed higher yield of the cytosine anion, since it is difficult to detect the differences between the cytosine anion and its protonated analogs with ESR.

The adenine anion has also been determined to be protonated in single crystals at very low temperatures. The main protonation site in single crystals is N3 [**A(N3H)**], which is supported by DFT calculations (Chapter Five). Additionally, protonation can occur at both C2 [**A(C2H)**] and C8 [**A(C8H)**], where these sites are favorable under conditions where N3 is not involved in a hydrogen bond in single crystals.[53] In the aqueous state, the adenine anion has been determined to be able to accept a proton from N3 in thymine at the N1 position.[60] This can be followed by a 1,2-shift to form the **A(C2H)** product.[43] Only the **A(N3H)** product has been assigned in orientated DNA.[27] However, a product has been identified in randomly orientated DNA and assigned to a net radical addition product at C8 in one of the purines,[29] which could be associated with **A(C8H)**.

The guanine anion has been suggested as a product in some single crystals, but since the other three bases were determined to be protonated even at low temperatures and the anion and its protonated form possess similar characteristics, it is unlikely that the

guanine anion will be observed directly in irradiated DNA samples. Through comparison of single crystal and calculated results, the primary protonation site for the guanine anion is O6 [**G(O6H)**]. In full DNA, this position is hydrogen bonded to the amino group of its base-pair cytosine. However, the amino-dehydrogenated cytosine radical has not been observed in either single crystals or irradiated DNA. Furthermore, from studies in aqueous solutions it is known that cytosine is a weak acid.[60] Thus, a simple proton transfer mechanism seems unlikely. Comparison of single crystal results and calculations (Chapter Five) indicates that alternative sites for protonation include C8 and C5.

Electron capture at the sugar group is not expected to occur. This is primarily due to the fact that the electron affinities of the bases are much larger than that of the sugar group and therefore they shield deoxyribose. However, a radical formed by a rupture of the phosphoester bond at C5' was determined to be formed at 10 K in 2'-deoxyguanosine 5'-monophosphate (**C5'(H2)**, Figure 8.8).[51] Since this radical was formed at such low temperatures, it must be generated through a reductive pathway at the sugar group rather than through transfer of character from the base. Thus, although products generated from electron capture at the sugar were not expected in the past, a reductive mechanism involving deoxyribose cannot be ruled out for radical formation. In addition, a similar radical could be formed at the C3' position (**C3'(H)**). If these radicals are generated in irradiated DNA, then a prompt strand break will occur. Alternatively, it has been proposed that net hydrogen abstraction sugar radicals observed in 2'-deoxyguanosine 5'-monophosphate could occur as a result of reduction at the sugar moiety,[51] since hydrogen abstraction radicals have been shown to be products of reduction pathways in related sugars.[66]

The phosphate group is also a possible site for electron capture. Two phosphate-centered radicals were discussed in a previous section and speculated to be due to electron gain on the phosphates at either C3' or C5' (**P1** or **P2**, Figure 8.8).[54] Radical character could also be transferred to the sugar moiety. Alternatively, as discussed in a previous section, electron capture at the phosphate group could lead to elimination of this group, or strand breaks in DNA, by the formation of the **C5'(H2)** or **C3'(H)** sugar products. This is thought to occur mainly through abstraction of hydrogen from C4' which forms a radical at this center.[51,57]

It should be noted that the products discussed within could also be formed via hydrogen atom addition. These hydrogen atoms can be generated via recombination of an electron and a proton or as products following excitation of the bases or sugar moiety. For example, in randomly orientated DNA a radical product was identified as being formed by radical addition to C8 in one of the purines (adenine or guanine).[29]

### *8.7.3 Summary of DNA Radiation Damage*

Figure 8.9 summarizes the explanation provided in the previous sections for the effects of radiation on the entire DNA strand and the surrounding water molecules. The diagram depicts the formation of the primary radicals (cation and anion radicals) on all bases (**T**, **C**, **A**, **G**), the phosphate group (**P**), the sugar moiety (**S**) and the surrounding water molecules (**W**). The transformation of each primary radical to secondary radicals is also displayed. It should be noted that the (de) protonation of (cations) anions is in strict competition with electron transfer throughout the DNA strand. However, the electron transfer mechanisms are not shown in the diagram for simplification. Thus, the formation of secondary radical products is dependent on whether or not the (cation) anion is stabilized for a sufficient period of time to allow for (de) protonation. Alternatively, as mentioned, hydrogen atoms or hydroxyl radicals can attack the undamaged bases to form the radical products included in the model.

The model presented in Figure 8.9 indicates that a primary product could directly result in the formation of a secondary radical. For example, the thymine cation can deprotonate to form the methyl-dehydrogenated product. An alternative pathway could be that the primary radicals react to form radical products on another center. For example, the cytosine cation was determined not to deprotonate, but rather it results in a sugar cation (indicated by a horizontal line in the figure), which subsequently forms a sugar deprotonated radical. Another example is water cations form hydroxyl radicals that can abstract a hydrogen atom from the thymine methyl group or from deoxyribose. The protons formed from the water cations, in addition to the hydroxyl radicals, can add to any of the base anions to form protonated products (these processes are also indicated by horizontal lines in the figure).

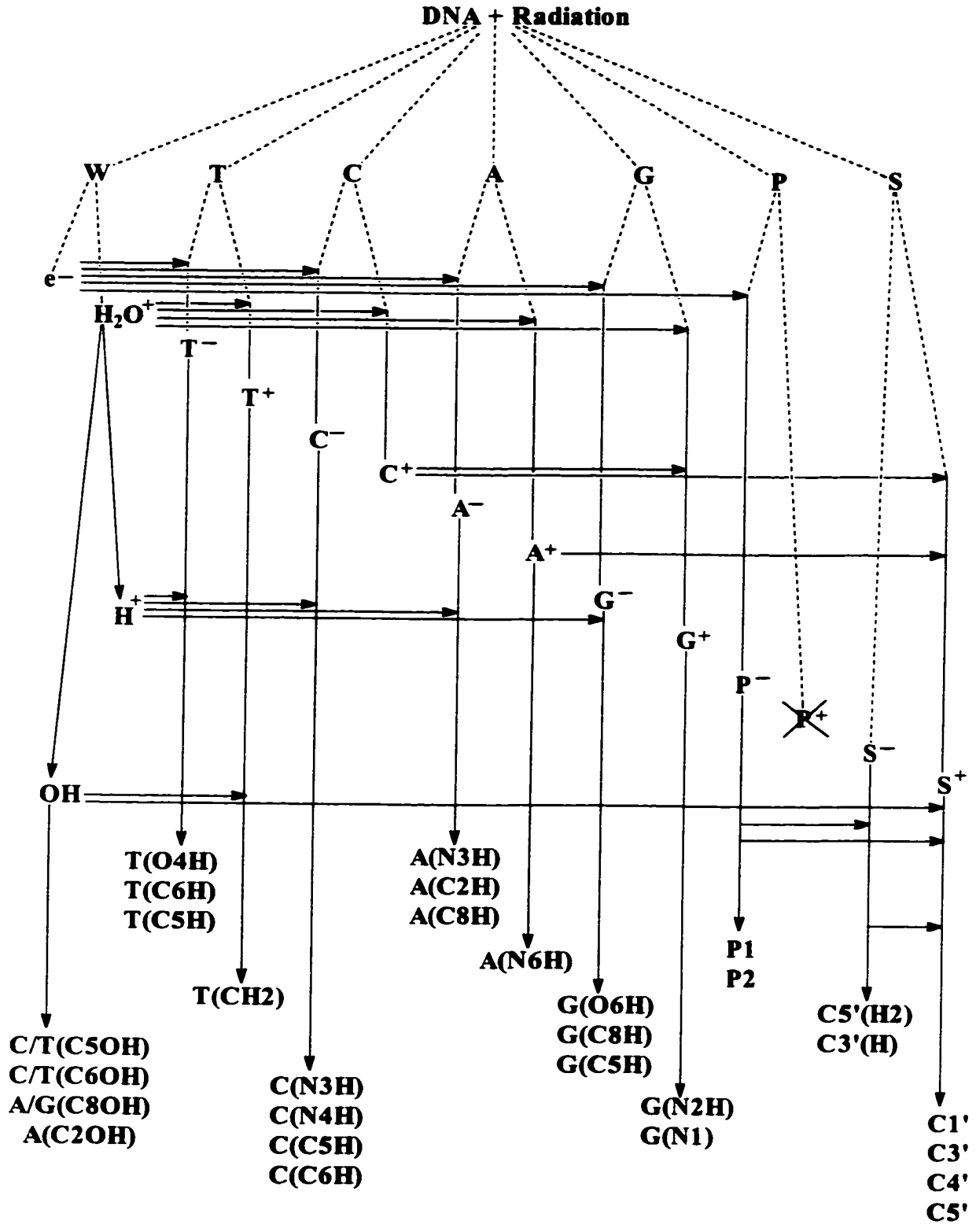


Figure 8.9: A model for radiation damage to DNA which includes damage to the bases, the sugar moiety, the phosphate group and the surrounding water molecules.

From the model developed in the present chapter and displayed in Figure 8.9, it can be seen that the possibilities of radical formation in irradiated DNA are extremely abundant. Since these are the most probable radical products in irradiated DNA, this model may be useful when attempting to characterize the ESR spectra of DNA. In order to narrow the formation of radical products further, more experimental work must be performed to rule out each product. For example, many experimental studies have shown that the formation of a specific radical cannot be eliminated solely due to the fact that its signal is not observed with ESR, since often a strong ENDOR signal will be obtained with the same sample. It is postulated that as experimental techniques become more advanced and are able to characterize more products, evidence will be obtained to support the current working model for radiation damage to DNA.

### *8.8 Conclusions*

The discussion presented in the present chapter illustrates the diversity of radical products generated in irradiated DNA samples. The knowledge of which radicals are formed has important consequences for determining the type of damage exhibited (for example, strand-breaks, tandem lesions, DNA-protein cross-links, unaltered base release). The model outlined above is extensively more complex than the original two-component model which speculated that initial radiation damage centers on the formation of only two ionic radicals. Moreover, early researchers have claimed on occasion that the "complexity of the DNA radical population" can be explained by the formation of four radicals.[36] From the discussion within, it can be determined that this is clearly not true. The determination of the radicals generated upon irradiation of DNA leads to a broader area of research which can investigate how these radicals are formed or, more importantly, how they subsequently react to result in more permanent damage to the DNA strand.

### *8.9 References*

1. *Effects of Ionizing Radiation on DNA*; Hüttermann, J., Köhnleif, W., Teoule, R., Bertinchamps, A. J., Eds.; Springer: Heidelberg, 1978.

2. Ehrenberg, A.; Ehrenberg, L.; Löfroth, G. *Nature* **1963**, *200*, 376.

3. Salovey, R.; Shulman, R. G.; Walsh, W. M., Jr. *J. Chem. Phys.* **1963**, *39*, 839.

4. Pershan, P. S.; Shulman, R. G.; Wyluda, B. J.; Eisinger, J. *Science* **1964**, *148*, 378.

5. Ehrenberg, A.; Rupprecht, A.; Ström, G. *Science* **1967**, *157*, 1317.

6. Ormerod, M. G. *Int. J. Radiat. Biol.* **1965**, *9*, 291.

7. Gräslund, A.; Ehrenberg, A.; Rupprecht, A.; Ström, G. *Biochim. Biophys. Acta* **1971**, *254*, 172.

8. Gräslund, A.; Ehrenberg, A.; Rupprecht, A.; Tjälldin, B.; Ström, G. *Radiat. Res.* **1975**, *61*, 488.

9. Gräslund, A.; Ehrenberg, A.; Rupprecht, A.; Ström, G.; Crespi, H. *Int. J. Radiat. Biol.* **1975**, *28*, 313.

10. Bernhard, W. A. *Adv. Radiat. Biol.* **1981**, *9*, 199.

11. Kar, L.; Bernhard, W. A. *Radiat. Res.* **1983**, *93*, 232.

12. Hüttermann, J.; Voit, K.; Oloff, H.; Köhnlein, W.; Gräslund, A.; Rupprecht, A. *Faraday Discuss. Chem. Soc.* **1984**, *78*, 135.

13. Cullis, P. M.; McClymont, J. D.; Malone, M. E.; Mather, A. N.; Podmore, I. D.; Sweeney, M. C.; Symons, M. C. R. *J. Chem. Soc., Perkin Trans* **1992**, *2*, 1695.

14. Bernhard, W. A. *J. Phys. Chem.* **1989**, *93*, 2187.

15. Barnes, J.; Bernhard, W. A.; Mercer, K. R. *Radiat. Res.* **1991**, *126*, 104.

16. Sevilla, M. D.; Becker, D.; Yan, M.; Summerfield, S. R. *J. Phys. Chem.* **1991**, *95*, 3409.

17. Steenken, S.; Telo, J. P.; Novais, H. M.; Candeias, L. P. *J. Am. Chem. Soc.* **1992**, *114*, 4701.

18. Zell, I.; Hüttermann, J.; Gräslund, A.; Rupprecht, A.; Köhnlein, W. *Free Radical Res. Commun.* **1989**, *6*, 105.

19. Yan, M.; Becker, D.; Summerfield, S.; Renke, P.; Sevilla, M. D. *J. Phys. Chem.* **1992**, *96*, 1938.

20. (a) Close, D. M.; Sagstuen, E.; Nelson, W. H. *J. Chem. Phys.* **1985**, *82*, 4386; (b) Hole, E. O.; Nelson, W. H.; Close, D. M.; Sagstuen, E. *J. Chem. Phys.* **1987**, *86*, 5218.

21. Swarts, S. G.; Becker, D.; Sevilla, M.; Wheeler, K. T. *Radiat. Res.* **1996**, *145*, 304.

22. Colson, A. -O.; Sevilla, M. D. *Int. J. Radiat. Biol.* **1995**, *67*, 627.

23. Hüttermann, J.; Röhrig, M.; Köhnlein, W. *Int. J. Radiat. Biol.* **1992**, *61*, 299.

24. Close, D. M.; Bernhard, W. A. *Bull. Am. Phys. Soc.* **1980**, *25*, 416.

25. Lange, M.; Weiland, B.; Hüttermann, J. *Int. J. Radiat. Biol.* **1995**, *68*, 475.

26. Wang, W.; Yan, M.; Becker, D.; Sevilla, M. D. *Radiat. Res.* **1994**, *137*, 2.

27. Gatzweiler, W.; Hüttermann, J.; Rupprecht, A. *Radiat. Res.* **1994**, *138*, 151.

28. Weiland, B.; Hüttermann, J.; van Tol, J. *Acta Chem. Scan.* **1997**, *51*, 585.

29. Weiland, B.; Hüttermann, J. *Int. J. Radiat. Biol.* **1998**, *74*, 341.

30. Lange, M.; Weiland, B.; Hüttermann, J. *Int. J. Radiat. Biol.* **1995**, *68*, 475.

31. Podmore, I. D.; Malone, M. E.; Symons, M. C. R.; Cullis, P. M.; Dalgarno, B. G. *J. Chem. Soc. Faraday Trans* **1991**, *2*, 3647.

32. Saenger, W. *Principles of Nucleic Acid Structure*, Cantor, C. R., Ed.; Springer-Verlag: New York, 1984.

33. van Lith, D.; de Haas, M. P.; Warman, J. M.; Hummel, A. *Biopolymers* **1983**, *22*, 807.

34. Swarts, S. G.; Sevilla, M. D.; Becker, D.; Tokar, C. J.; Wheeler, K. T. *Radiat. Res.* **1992**, *129*, 333.

35. Mroczka, N.; Bernhrad, W. A. *Radiat. Res.* **1993**, *135*, 155.

36. Gregoli, S.; Olast, M.; Bertinchamps, A. *Radiat. Res.* **1982**, *89*, 238.

37. Wang, W.; Becker, D.; Sevilla, M. D. *Radiat. Res.* **1993**, *135*, 146.

38. Ito, T.; Baker, S. C.; Stickley, C. D.; Peak, J. G.; Peak, M. J. *Int. J. Radiat. Biol.* **1993**, *63*, 289.

39. Becker, D.; La Vere, T.; Sevilla, M. D. *Radiat. Res.* **1994**, *140*, 123.

40. La Vere, T.; Becker, D.; Sevilla, M. D. *Radiat. Res.* **1996**, *145*, 673.

41. Ohlmann, J.; Hüttermann, J. *Int. J. Radiat. Biol.* **1993**, *63*, 427.

42. von Sonntag, C.; Schuchmann, H.-P. *Int. J. Radiat. Biol.* **1986**, *49*, 1.

43. Steenken, S. *Chem. Rev.* **1989**, *89*, 503.

44. Davies, M. J.; Gilbert, B. C.; Hazlewood, C.; Polack, N. P. *J. Chem. Soc. Faraday Trans* **1995**, *2*, 13.

45. Cullis, P. M.; Langman, S.; Podmore, I. D.; Symons, M. C. R. *J. Chem. Soc. Faraday Trans* **1990**, *86*, 3267.

46. Hüttermann, J.; Lange, M.; Ohlmann, J. *Radiat. Res.* **1992**, *131*, 18

47. Gregoli, S.; Olast, M.; Bertinchamps, A. *Radiat. Res.* **1974**, *60*, 388; *ibid* **1976**, *65*, 202; *ibid* **1977**, *72*, 201.

48. Malone, M.; Symons, M. C. R.; Parker, A. W. *J. Chem. Soc. Perkin Trans.* **1993**, *2*, 2067.

49. (a) Close, D. M.; Nelson, W. H.; Sagstuen, E. *Radiat. Res.* **1987**, *112*, 283; (b) Close, D. M.; Sagstuen, E.; Nelson, W. H. *Radiat. Res.* **1988**, *116*, 379; (c) Nelson, W. H.; Hole, E. O.; Sagstuen, E.; Close, D. M. *Int. J. Radiat. Biol.* **1988**, *54*, 963; (d) Hole, E. O.; Sagstuen, E.; Nelson, W. H.; Close, D. M. *Radiat. Res.* **1991**, *125*, 119.

50. Hüttermann, J. *Ultramicroscopy* **1982**, *10*, 25.

51. Hole, E. O.; Nelson, W. H.; Sagstuen, E.; Close, D. M. *Radiat. Res.* **1992**, *129*, 119.

52. Close, D. M. *Radiat. Res.* **1997**, *147*, 663.

53. Close, D. M. *Radiat. Res.* **1993**, *135*, 1.

54. Becker, D.; Razskazovskii, Y.; Callaghan, M. U.; Sevilla, M. D. *Radiat. Res.* **1996**, *146*, 361.

55. Sanderud, A.; Sagstuen, E. *J. Chem. Soc. Faraday Trans.* **1996**, *92*, 995.

56. Nelson, D. J.; Symons, M. C. R.; Wyatt, J. L. *J. Chem. Soc. Faraday Trans.* **1993**, *89*, 1955.

57. Steenken, S.; Goldbergerova, L. *J. Am. Chem. Soc.* **1998**, *120*, 3928.

58. Sevilla, M. D.; Becker, D. In *A Specialists Periodical Report Electron Spin Resonance, Vol. 14*, Atherton, N. M.; Davis, M. J.; Gilbert, B. C.; Eds.; Royal Society of Chemistry: Cambridge, 1994, p. 130.

59. Hutter, M.; Clark, T. *J. Am. Chem. Soc.* **1996**, *118*, 7574.

60. Steenken, S. *Free Radical Res. Commun.* **1992**, *16*, 349.

61. Sagstuen, E.; Hole, E. O.; Nelson, W. H.; Close, D. M. *Radiat. Res.* **1998**, *149*, 120.

62. Nelson, W. H.; Sagstuen, E.; Hole, E. O.; Close, D. M. *Radiat. Res.* **1998**, *149*, 75.

63. Sagstuen, E.; Hole, E. O.; Nelson, W. H.; Close, D. M. *Radiat. Res.* **1996**, *146*, 425.

64. Hole, E. O.; Nelson, W. H.; Sagstuen, E.; Close, D. M. *Radiat. Res.* **1998**, *149*, 109.

65. Wetmore, S. D.; Boyd, R. J.; Himo, F.; Eriksson, L. A. *J. Phys. Chem. B* **1999**, *103*, 3051.

66. Sagstuen, E.; Lindgren, M.; Lund, A. *Radiat. Res.* **1991**, 128, 235.

# CHAPTER NINE

## Global Conclusions and Future Work

This thesis provides an in-depth investigation of the calculation of the main property used to characterize radicals, namely the hyperfine coupling constant. The focus of the work included within can be divided into two main categories. The first category is a survey of how accurately different quantum chemical methods can calculate hyperfine coupling constants for oxygen nuclei. The second category is the application of methods that are known to provide reliable properties to an important chemical problem. This chapter summarizes the results obtained for these two topics separately in terms of global conclusions and avenues for future research.

### *9.1 Peroxyl and Hydroxyl Radicals*

#### *9.1.1 Conclusions*

The properties of oxygen centered radicals were systematically studied for the first time. Large peroxyl radicals were investigated through the use of density-functional theory. The hyperfine coupling constants were examined as a function of both the DFT functional and the basis set. It was shown for alkyl peroxyl radicals, as well as the hydroxyl radical, that the best agreement with experiment was obtained with the B3LYP functional and the IGLO-III basis set. Other basis sets yielded similar results, although decontraction of the *s*-space was often necessary. Through these calculations, it was determined that the terminal oxygen in peroxyl radicals possesses the main fraction of the unpaired electron. This information clarifies discrepancies in the literature regarding the location of the unpaired spin in these molecules.

Despite the fact that results obtained with DFT were comparable to experiment, the deviation between the two sets of data was larger than expected from studies of the HFCCs in other radicals. A similar DFT investigation of the fluoroperoxyl radical did not reproduce the experimental results. Explanations for the deviations between experiment and theory included multi-reference, vibrational and matrix effects. The former was investigated with multi-reference configuration interaction. MRCI calculations on the hydroxyl radical, chosen for its small size, with a basis set that had

previously proven to be very good for $NH_2$, failed to improve upon the DFT results. Attempts were made to further improve the MRCI results by adjusting the basis set (adding more functions) and the reference space (using natural orbitals and/or using additional criteria, such as the spin density matrix, to choose the reference configurations). All of these attempts failed to improve upon the initial MRCI results.

Due to the surprisingly poor agreement between MRCI and experimental HFCCs, other high-level *ab initio* methods were also examined. The methods employed include coupled-cluster and quadratic configuration interaction, both of which provided results superior to those obtained with MRCI. In addition, the difference between implementing an ROHF or UHF reference determinant was investigated with the CC method to determine if MRCI failed due to the use of an ROHF reference determinant. Through these calculations it was determined that once a high enough level of electron correlation is included in CC or QCI techniques (usually triple excitations), results in good agreement with experimental $^{17}O$ data can be obtained regardless of the choice of reference data. This implies that the MRCI method has difficulties improving upon the ROHF reference determinant for the hydroxyl radical. This was concluded to be mainly because each additional reference configuration only contributes a small amount to the isotropic HFCC. Thus, to improve upon DFT results either the CC or QCI methods should be implemented. MRCI appears to work very well in some cases (for example, $NH_2$), but choosing the appropriate reference space is not always easy or practical under constraints of computer resources.

The poor agreement between the experimental and theoretical couplings for the fluoroperoxyl radical could be due to geometrical changes imposed by the experimental matrix or vibrational effects. These issues can be addressed through the use of combined quantum mechanics and molecular dynamics techniques, where the radical is placed in a cavity of a matrix consisting of rare gas atoms and the temperature is adjusted to match the experimental conditions. Both MP2 and B3LYP were implemented as the QM method and simulations were performed on HOO and FOO in an argon matrix at 4 K. The simulations did not drastically alter either the geometry or the HFCCs from those obtained in static gas phase calculations. This indicates that neither the matrix nor vibrational effects are to blame for the poor agreement between theory and experiment,

and suggests that contemporary DFT methods cannot adequately describe the HFCCs in radicals such as HOO and FOO.

The HOO and FOO radicals were also examined with the QCISD method. The agreement with experiment is comparable with that observed for other oxygen centered radicals. This indicates, once again, that QCISD must be relied upon if an accurate description of oxygen couplings is desired. Additionally, the geometry calculated with QCISD is in poor agreement with the experimental geometry for FOO, despite the fact that both sets of HFCCs are in good agreement. This fact, in addition to discrepancies observed for the related ClOO molecule, was used to conclude that more accurate studies must be performed to determine the exact geometry of these radicals.

### *9.1.2 Future Work*

The work outlined above concentrating on the hyperfine coupling constants of peroxyl and hydroxyl radicals can be extended in several directions. Primarily, it is evident that more work elucidating the optimal DFT functional and basis set combination for the calculation of HFCCs is necessary. Design of special basis sets and/or functionals to calculate this property would be extremely beneficial. The former is important due to the demands imposed on the types of basis functions required to accurately calculate HFCCs (Chapter Two) and the latter may be achieved through examination of the electron density. Secondly, small inorganic peroxyl radicals must be examined more closely. Discrepancies arise in the theoretical and experimental geometries for FOO and ClOO despite the fact that the corresponding HFCCs are in good agreement and this property is sensitive to the molecular geometry. Through careful examination of DFT, QCI and CC (including up to triple excitations), more information about the bond lengths in these interesting radicals may be obtained.

## *9.2 DNA Radiation Products*

### *9.2.1 Conclusions*

The majority of the work in the present thesis was dedicated to the investigation of the effects of radiation on the DNA strand with an emphasis on the calculation of the hyperfine coupling constants of the individual DNA components. Close agreement between the DFT values and the results of experimental studies on single crystals of base

derivatives provided strong support for the assignment of the spectra to specific radicals. Alternatively, discrepancies between the experimental and computed HFCCs were used to propose alternate assignments of the spectra. In addition to the four DNA bases, as well as the RNA base uracil, the sugar moiety in the DNA strand was also investigated through the implementation of a model system. Previous theoretical studies of DNA base and sugar radicals have concentrated on properties such as the ionization potentials and electron affinities. The work presented within was the first to investigate radiation effects through the calculation of accurate hyperfine coupling constants, the most important property for the experimental identification of DNA radicals.

The calculated HFCCs obtained for thymine are in very good agreement with experimentally derived parameters. This indicates that the level of theory chosen to investigate the DNA components is adequate and reliable. The important observation for thymine was that the calculations support the experimental prediction that the thymine anion is protonated at O4 in single crystals. The hypothesis that a proton adds to this position was supported by the calculation of a large coupling for the corresponding hydrogen atom, which was determined to be located out of the molecular plane.

Upon comparison of the calculated HFCCs for cytosine with experimental results obtained from cytosine monohydrate crystals, discrepancies in the data were observed. In particular, the calculations do not support the experimental assignment to a net dehydrogenated product formed via oxidation of a cytosine unit. On the contrary, the only explanation for the observed HFCCs is that the radical product should instead be assigned to the product formed via net hydroxyl radical addition. The formation of this product (the net C5-hydroxylated radical) and the other major product (the net N3 hydrogen atom addition radical) indicates that water is involved in the radiation damage in these crystals. This is a very important discovery for the radiation chemistry of DNA since it has previously been speculated that water plays a minor role in radical formation in single crystals of base derivatives and, thus, in DNA.

Investigation of adenine and guanine was important since many different crystals of these bases have been studied which contain water. Therefore, species formed by hydroxyl radical addition, similar to those proposed for cytosine monohydrate crystals, may be observed. Additionally, in order to obtain a complete working model for the

radiation effects on DNA, the purines must also be examined. An important conclusion drawn from the work on the purines is that all anions and cations generated in single crystals are quickly protonated or deprotonated to form neutral radicals. Only under extreme conditions, such as crystals which are initially protonated or temperatures below 10 K, could the cations of these bases be observed. Thus, since ionic radicals are believed to form neutral radicals at low temperatures in single crystals, this is also expected to be true in biologically relevant circumstances. Furthermore, in some crystals the calculated HFCCs support the identification of net hydroxyl radical addition products and the newly proposed mechanism for radiation damage in cytosine monohydrate crystals is supported.

Chapter Six examined the sugar moiety in DNA. The radicals examined include those formed by net hydrogen atom and hydroxyl radical abstraction from a model sugar group, as well as more complex radicals involving, for example, breakage of the sugar ring. The calculations provide clear evidence that numerous radicals generated in single crystals of base derivatives are centered on the sugar group. This is an important observation since for a long time it was speculated that sugar radicals are not formed in DNA. However, since concrete evidence exists that such radicals can be formed in single crystals, it is reasonable to assume that these radicals can also be generated in DNA. More experimental work can now be performed which searches for deoxyribose radicals in full DNA samples.

Chapter Seven discussed the reactions between small nucleobases and water. The transition barriers for hydroxyl radical addition to neutral cytosine and water addition to the cytosine cation were examined. The gas-phase reaction for water addition to the cytosine cation was concluded to be more complex and less feasible than hydroxyl radical addition to neutral cytosine. Additionally, consideration of kinetic and thermodynamic arguments led to the conclusion that hydroxyl radical addition to the C6 position in cytosine is also practical. Comparison of the results obtained for the C5 and C6 addition reactions indicates that the conclusion that hydroxyl radicals more favorably add to the C5 than the C6 position, in agreement with experimental studies on cytosine.

Hydroxyl radical addition to uracil and thymine was also investigated. Experimentally, it was previously determined that hydroxyl radical addition to C6 is

more favorable for uracil than cytosine. The smaller transition barriers and the greater product stability calculated for the uracil C6-hydroxylated radical support this trend. For thymine, however, the C6-hydroxylated product was calculated to be favored both kinetically and thermodynamically. Thus, hydroxyl radical addition is expected to occur to a greater extent at the C6 position in thymine than in uracil and cytosine. This conclusion is supported by speculation that the methyl group in thymine leads to an increase in the product formed by addition to the C6 site.

Through comparison of theoretical and experimental couplings a complete picture of the radicals formed in irradiated single crystals of base derivatives is now available. In addition, this information in conjunction with that obtained from studies on aqueous solutions and full DNA samples was used to develop a model for the radiation damage in DNA. This model includes damage to all four bases, the sugar moiety, the phosphate groups and the surrounding water molecules. Through the use of the model presented in Chapter Eight experimentalists studying full DNA samples will know which products are most likely to be present in irradiated DNA and thus aid in the assignment of the spectra.

### *9.2.2 Future Work*

From an experimental point of view, many different routes can be taken in order to broaden our knowledge of the effects of radiation on DNA. More work on single crystals can be performed to clarify the discrepancies between experiment and theory outlined in the present thesis. Investigation of $^{13}C$ or $^{17}O$ labeled crystals would yield more information about the various radical products and allow for further comparison with theoretically determined couplings. This is important since many of the hydrogen couplings are very similar in the DNA radical products. Thus, investigation of couplings for other nuclei may allow for a clearer differentiation between products. Experimental work on base pairs, which represent more realistic models for the bases present in DNA, would also be advantageous. Work has appeared in the literature investigating co-crystals of adenine and thymine (or uracil) derivatives[1] and interesting information has been obtained about radical formation when the bases are paired. Examination of the co-crystals of guanine and cytosine derivatives would yield more information about the products generated from these bases. Finally, more detailed experimental work on full DNA would be the best approach to identify radiation products in this complex molecule.

ESR and ENDOR studies seem to be insufficient for the clear identification of products. Thus, the development of more advanced ESR based methods would aid experimentalists attempting to study the effects of radiation on the entire DNA strand. It is postulated that once more complete studies are performed, many more radical products will be identified and the complexity of the effects of radiation on DNA will be better understood.

Another interesting experimental research topic would be to examine differences in damage caused by ultraviolet light versus that caused by ionizing radiation. Some work has been performed using UV light and different products have been identified relative to those discussed for ionizing radiation.[2] Additionally, some similarities in the damage caused by these two irradiation methods have been found to exist. However, reasons for these differences and similarities are not well understood. This research would have important implications for understanding the effects of ozone depletion on the increase in skin cancer, for example.

Theoretically, more work is required to determine the radiation damage processes that occur in cytosine monohydrate crystals. In particular, improved agreement between experimental and theoretical hyperfine coupling constants would be advantageous to conclusively determine the radiation products in these crystals. Furthermore, the results presented within represent gas-phase reactions, which may not accurately describe the processes occurring in single crystals, where hydrogen bonding effects may be important. Investigation of a more substantial part of the crystal can be used to model possible reaction mechanisms, as well as to examine crystal effects on the cytosine radical coupling constants. These calculations will aid in the determination if, for example, hydrogen bonding increases the importance of the reaction between water and the cytosine cation.

Additionally, the results presented in Chapter Seven are preliminary in both the level of theory employed and the fact that calculations must be performed in order to verify the relationship between the reactant complex, the transition states and the products. Further calculations at the HF level have isolated unique reactant complexes for the cytosine reactions and different RCs, than those reported in Chapter Seven, for hydroxyl radical addition to C5 in uracil and thymine. DFT single-point calculations on these RCs indicate that the barriers for hydroxyl radical addition to the C5 position in all

three bases are negative. However, the trends in the relative barrier heights remain the same as those reported in Chapter Seven and thus the conclusions remain unchanged. A more complete investigation of these reactions is required, including geometry optimizations at the MP2 level, in order to gain a greater understanding of the mechanism for hydroxyl radical addition to the pyrimidines.

In addition to a more extensive investigation of the radiation damage mechanism for cytosine monohydrate crystals, future work can also aim to clarify discrepancies between experiment and theory when comparing hydroxyl radical addition to the C5 and C6 positions in the small nucleobases. In particular, it was discussed in Chapter Seven that experimental studies on 2'-deoxyuridine and thymidine reached conclusions different from those obtained from the calculations. Discrepancies were believed to arise due to the model system employed in the calculations, where the sugar group present in the experiments was replaced with a hydrogen, since some of the RCs involved hydrogen bonding to this position in uracil. Thus, for example, as a first approximation, the reactions between a hydroxyl radical and 1-methyluracil could be investigated to determine if alternative RCs are observed which alter the barrier heights for these reactions from those determined for uracil.

Future work should also concentrate on the mechanisms associated with the formation of the main radical products and how these radicals subsequently yield nonradical products (more permanent forms of radiation damage). The work presented in the present thesis provides a basis for understanding which radicals are formed in irradiated DNA. Equally important questions remain regarding how these products are generated and how they react once they are formed. For example, base radicals are known to attack other bases to form dimers in solution and perhaps in single crystals. The thymine dimer is the most well known product, however, the mechanism for dimer formation or dimer repair is not well understood in terms of reaction intermediates.[3] Alternatively, tandem lesions are often formed in irradiated DNA. In oxygen environments, these lesions include hydroxyl radical addition to guanine, degradation of the pyrimidines to a formyl group and conversion of the methyl group in thymine to a formyl group.[4] Under anoxic conditions, covalent linkages are formed between adjacent

bases.[5] The mechanism for formation of these products is unknown and the dependence of product formation on the environment is not well understood.

Another extremely interesting topic which stems from the work presented is related to the formation of sugar radicals. Sugar radicals play an important role in DNA radiation damage since it is believed that strand breaks occur through the formation of these radicals. If a double-strand break occurs in DNA, that is a break in both sides of the double helix is generated, then the DNA molecule is not repaired, but rather the cell loses its reproductive activity and eventually is destroyed. Strand breaks have been shown to develop from both direct (direct formation of DNA radicals) and indirect (formation of solvent radicals followed by attack of these radicals on the DNA strand) radiation damage mechanisms.

Strand breaks resulting from indirect effects are speculated to occur through base radicals, formed via attack of hydroxyl radicals, which subsequently result in sugar radicals. Experimental studies exist in the literature examining the attack of hydroxyl radicals on RNA components[6,7] and discussing possible mechanisms for damage transfer to the sugar and mechanisms for strand breaks.[8] Although it has been postulated that base radicals abstract hydrogen from the sugar moiety, which hydrogen and the radical transfer mechanism are not clear. Different mechanisms exist which involve net hydrogen abstraction from C4' or C2'. Evidence that similar transfer reactions occur in DNA has also been observed experimentally.[9] However, not all of the RNA products are observed in DNA and explanations for these differences (besides removal of a hydroxyl group) are vague.

Strand breaks formed via direct effects have also been documented and postulated to be generated through base radical cations.[10,11] These cations can subsequently undergo a variety of reactions including hydrogen abstraction from the sugar, deprotonation at the sugar or deprotonation at the base followed by abstraction from the sugar. Some of the postulated reactions disrupt the DNA strand through breaking phosphoester bonds in the DNA backbone and others result in breakage of the bond between the base and the sugar group, which results in unaltered base release. The relative importance of these mechanisms and the mechanistic differences from indirect damage pathways are poorly understood.

Studying the mechanism for DNA strand breaks will provide valuable information about the radiation effects on this complex molecule. Additionally, information may be obtained which would aid in the understanding of repair mechanisms for radiation damage. Thiols are expected to provide an efficient means to protect against radiation damage in biological systems.[12] In this respect, thiols react with hydroxyl molecules to prevent attack on the DNA strand. Alternatively, thiols can react with the target molecule to inhibit strand breaks. Some *ab initio* calculations have been performed on model thiol systems, in order to obtain information about the ionization potentials and/or electron affinities in these systems.[12] However, the detailed mechanisms for damage repair have not been investigated and are very important in order to understand how a DNA strand that has been affected by ionizing radiation can be restored.

Through the work discussed within and that proposed for future research, a greater understanding of the effects of radiation on DNA and on the population will be obtained. The work presented in this thesis provides a foundation from which to investigate the primary effects of radiation on DNA since the identities of the radicals generated in DNA are now known. The work proposed for future research provides a means to study the second important area related to the effects of radiation on DNA, namely how these free radicals react to form stable products. Lastly, once these processes are well understood, research examining the effects of these products on biologically active species can be undertaken and information on how to protect organisms from radiation damage will be obtained.

### *9.3 References*

1. (a) Sagstuen, E.; Hole, E. O.; Nelson, W. H.; Close, D. M. *Radiat. Res.* **1998**, *149*, 120; (b) Sagstuen, E.; Hole, E. O.; Nelson, W. H.; Close, D. M. *Radiat. Res.* **1996**, *146*, 425.

2. Doetsch, P. W.; Zastawny, T. H.; Martin, A. M.; Dizdaroglu, M. *Biochem.* **1995**, *34*, 737.

3. (a) Katz, H.; Stallings, W.; Glusker, J. P.; *Photochem. Photobiol.* **1993**, *57*, 609; (b) Podmore, I. D.; Heelis, P. F.; Symons, M. C. R.; Pezeshk, A. *J. Chem. Soc., Chem. Commun.* **1994**, 1005; (c) Pezeshk, A.; Podmore, I. D.; Heelis, P. F.; Symons, M. C.

R. *J. Phys. Chem.* **1996**, *100*, 19714; (d) Aida, M.; Inoue, F.; Kaneko, M.; Dupuis, M. *J. Am. Chem. Soc.* **1997**, *119*, 12274.

4. (a) Budzinski, E. E.; Dawidzik, J. D.; Wallace, J. C.; Freund, H. G.; Box, H. C. *Radiat. Res.* **1995**, *142*, 107; (b) Budzinski, E. E.; Maccubbin, A. E.; Freund, H. G.; Wallace, J. C.; Box, H. C. *Radiat. Res.* **1993**, *136*, 171; (c) Schroder, E.; Budzinski, E. E.; Wallace, J. C.; Zimbrick, J. D.; Box, H. C. *Int. J. Radiat. Biol.* **1995**, *68*, 509.

5. (a) Box, H. C.; Budzinski, E. E.; Dawidzik, J. B.; Gobey, J. S.; Freund, H. G. *Free Rad. Bio. Med.* **1997**, *23*, 1021; (b) Box, H. C.; Budzinski, E. E.; Dawidzik, J. D.; Wallace, J. C.; Evans, M. S.; Gobey, J. S. *Radiat. Res.* **1996**, *145*, 641; (c) Box, H. C.; Budzinski, E. E.; Dawidzik, J. B.; Wallace, J. C.; Iijima, H. *Radiat. Res.* **1998**, *149*, 433.

6. Catterall, H.; Davies, M. J.; Gilbert, B. C. *J. Chem. Soc. Perkin Trans.* **1992**, *2*, 1379.

7. Hildenbrand, K.; Behrens, G.; Schulte-Frohlinde, D., Herak, J. N. *J. Chem. Soc. Perkin Trans.* **1989**, *2*, 283.

8. Hildenbrand, K.; Schulte-Frohlinde, D. *Int. J. Radiat. Biol.* **1989**, *55*, 725.

9. Davies, M. J.; Gilbert, B. C.; Hazlewood, C.; Polack, N. P. *J. Chem. Soc. Perkin Trans.* **1995**, *2*, 13.

10. Malone, M. E.; Cullis, P. M.; Symons, M. C. R.; Parker, A. W. *J. Phys. Chem.*, **1995**, 99, 9299.

11. Melvin, T.; Botchway, S. W.; Parker, A. W.; O'Neill, P. *J. Am. Chem. Soc.*, **1996**, 118, 10031.

12. Colson, A. O.; Sevilla, M. D. *Int. J. Radiat. Biol.* **1995**, 67, 627 *and references therein.*